BYG·DTU

Lone Hedegaard Mortensen

Hygrothermal Microclimate on Interior Surfaces of the Building Envelope

DANMARKS
TEKNISKE
UNIVERSITET

DTU

PhD thesis
BYG·DTU
R-163
2007
ISSN 1601-2917
ISBN 97887-7877-237-4

Preface

This PhD thesis is part of the project *Hygrothermal Performance of Whole Buildings* that was initiated by Associate Professor, Carsten Rode and Assistant Professor, Ruut Peuhkuri at the Department of Civil Engineering, Technical University of Denmark. The project was carried out at the section of Building Physics and Services with financial funding by STVF, Technical Research Council of Denmark, which is gratefully acknowledged. The thesis is a synopsis based on 5 papers.

During the project it was possible to be part of the International Energy Agency's (IEA), Annex 41, which is a research project of *Whole Building Heat, Air and Moisture Response*. The international collaboration and academic discussions with other members are highly appreciated and have certainly contributed to improve the current project. Within this group special thanks go to Associate Professor Monika Woloszyn and co-workers at CETHIL (the Thermal Science Centre of Lyon) for hosting my 5 month research stay with fruitful supervising. The research stay was supported by private funds *Otto Mønsteds Fond*, *Knud Højgaards Fond* and *Larsen & Nielsen Fonden* and their funding is thankfully appreciated.

This big task could not have been completed without help from a number of people, and I want to express my gratitude to all who in one way or another have contributed. Special thanks go to my supervisor team Associate Professor Carsten Rode and Ruut Peuhkuri, who guided and encouraged me and always generously shared both time and knowledge with me. Our small group of building physicists collaborated with the International Centre of Indoor Environment and Energy and of those I especially want to thank Associate Professor, Arsen Meilikov for valuable discussions of airflow measurement techniques, guidance and loan of equipment.
I will also express my gratitude to all my colleagues at the Department of Civil Engineering and particularly the section of Building Physics and Services for they have always made work and life more enjoyable not least during the traditional coffee breaks. For practical help and guidance I will mention and thank Associate Professor, Kurt Kielsgaard Hansen, Ulla Gjøl Jacobsen and Michael Ramskov. My thanks also go to Jeff Mertens, a Belgian master student, who spent 6 months with our building physics' group, for the collaboration, hard work, new perspective and deeply appreciated experimental work.
At last I want to thank all my friends and my family for support - especially, Kristina Hansel, for editorial help. My wonderful husband Peter, who is always there for me and my daughter Louisa, who ensures my daily share of laughter, the pair of you made all the difference by your love and support.

Lyngby, marts 2007

Lone Hedegaard Mortensen

Abstract

This thesis describes *hygrothermal microclimate on interior surfaces of the building envelope.* Moisture plays a significant role in the development of many processes that are harmful to both the indoor air quality and the building envelope. So the thesis topic was to obtain fundamental understanding of the moisture transfer between indoor air and building materials with special focus on the rate of moisture transfer. The purpose of the project was to establish a model that can predict the hygrothermal microclimate on the interior surfaces of the building envelope and to perform measurements that reveal the influence of airflows in rooms. Both modelling and experimental work have been based on a selected case study of a piece of furniture placed near a poorly insulated external wall, which represents a hygrothermal microclimate.

The report includes: a numerical model with a method to embrace moisture transport in rooms, both in air and constructions, by a Computational Fluid Dynamics (CFD) approach, literature survey on humidity impacts on indoor air quality and moisture buffering, and investigations of moisture surface resistances and the influence of furniture on airflows near wall surfaces.

The numerical model is an extension of an existing CFD model. Normally, solids in CFD models are impervious to moisture transport and hence an approach of using immobile fluids as walls has been developed. The advantage of this approach is that vapour diffusion is already included so merely a transport across the boundary between the wall and the room air must be programmed. A macro-modelling approach that neglects surface resistance was used. The results seem reasonable but need further validation.
To gain further knowledge about the moisture surface resistances, these were investigated by sorption experiments based on an inverted dry cup method. The study was extended with numerical CFD simulations to reveal the surface heat transfer coefficients and airflow patterns. Furthermore the experiments lead to development of a Petri dish cup method for field measurements of surface resistances. The results showed that it is possible to determine the moisture surface resistance by the inverted dry cup method, but the measured resistances were smaller than theoretically estimated, but higher than values estimated from the CFD simulation. The measured and simulated results show the same pattern. The Petri dish experiments are promising but need further development and testing.
The experimental work was further extended to include 2D Particle Image Velocimetry (PIV) measurements on the case study. The purpose of the measurements was to investigate the influence of different furniture positions. It was anticipated that the furniture would limit the airflow in the air gap between the furniture and the external wall. Even the lowest measured maximum velocity is high enough to cause draught, if it is experienced by people, so the airflow is not negligible. The results showed that elevation of the furniture by legs will increase the airflow behind the furniture and the flow rate will be even higher if the distance between the wall and the furniture is increased. Numerical simulation of the measured cases replicated the results for a 50 mm gap but lower velocities were predicted for a 25 mm air gap.

Keywords: Boundary conditions, PIV measurements, CFD simulation, surface resistances, moisture modelling, natural convection, airflow velocity.

Resumé

Denne afhandling beskriver *hygrotermisk mikroklima på indvendige overflader af klimaskærmen*. Fugt er en af de hyppigste årsager til skader på bygninger, og fugt i luften påvirker luftkvaliteten i bygninger. Hovedemnet i projektet har derfor været at skaffe ny viden om mekanismerne bag fugttransporten i mikroklimaer på indvendige overflader i rum med særlig fokus på den transporterede fugtmængde. Formålet med projektet er at opstille en model, der kan forudbestemme de hygrotermiske mikroklimaer på den indvendige side af klimaskærmen. Dette arbejde skal kombineres med eksperimentelle undersøgelser af luftstrømninger i rum og deres indflydelse på fugttransporten. Både det eksperimentelle arbejde og den numeriske modellering tager udgangspunkt i udvalgt *case study*, som repræsenterer et hygrotermisk mikroklima. Det valgte *case study* udgøres af et skab placeret foran en dårlig isoleret ydervæg.

Afhandlingen indeholder; en numerisk model som kan regne detaljeret på fugtforholdene i såvel rumluften som i de omgivende konstruktioner ved brug af en CFD (Computational Fluid Dynamics) model, en litteratur gennemgang af fugts betydning for luftkvaliteten, fugtbuffervirkning af materialer, og undersøgelse af fugtovergangsmodstande og indvirkning af møblers placering på luftstrømninger.

CFD modeller bruges normalt kun til forudsigelse af fugtfordelingen i fluider (ofte luft) og medregner derfor ikke fugt i materialer. CFD modellen, som er benyttet i dette projekt, er derfor udvidet med en metode, hvor man implementer fugtfordeling i materialer/konstruktioner ved at opbygge dem som ubevægelige fluider. Fordelen ved denne metode er, at fluider som standart indeholder en fugtdiffusionsmodel. Der skal dog programmeres en fugttransport henover overfladen af de to fluider (luft og vægge). Ved transporten blev der set bort fra overflademodstande. Resultaterne er lovende, men yderligere undersøgelser er nødvendige.
For at skaffe viden om fugtovergangsmodstande blev der udført en række sorptionsforsøg baseret på tør-kop's metoden. Undersøgelsen blev udvidet med numerisk CFD simulering af luftstrømningsforholdene over kopperne. Modellen beregner varmeoverførselskoefficienterne, og disse kan omregnes til fugtovergangsmodstande. Resultaterne viste at metoden kan benyttes, men undersøgelsen viste også at de teoretisk beregnede modstande var større end de målte. Omvendt blev det fundet at de numeriske simuleringer estimerede for lave fugtovergangsmodstande. Forsøgene førte til udvikling af en Petriskåls metode som kan benyttes til eksperimentelle feltundersøgelser af fugtovergangsmodstande. Metoden er ligeledes baseret på tør-kop's forsøgsmetoden. Resultaterne af de første Petriskåls forsøg er lovende men yderligere undersøgelser er nødvendige.
2D (to-dimensionale) Particle Image Velocimetry (PIV) forsøg af det valgte case study er også blevet udført. Formålet med PIV forsøgene var at undersøge luftstrømningerne i spalten mellem møblet og væggen som en funktion af møbelplaceringen. Det var forventet, at møblet ville begrænse luftstrømningen i spalten, men selv den lavest målte max hastighed er stor nok til at give problemer med træk for mennesker, så hastigheden er betydelig. Resultaterne viste, at luftstrømmen i spalten bag møblet bliver større, hvis møblet hæves fra gulvet ved hjælp af møbelben, og volumenstrømmen forøges yderligere, hvis spaltebredden øges.

Nøgleord: Græselag, PIV målinger, CFD simuleringer, fugtovergangsmodstande, fugtmodellering, naturlig konvektion, luftstrømningshastigheder.

Contents

This PhD thesis is a synopsis which includes the chapters presented above, and it is based on the following 5 research papers.

Paper I: Moisture buffer performance of a fully furnished room

Paper II: Determination of moisture surface resistance using cup experiments.

Paper III: Investigation of microclimate by CFD modelling of moisture interactions between air and constructions.

Paper IV: Investigation of airflow patterns in a microclimate by Particle Image Velocimetry (PIV).

Paper V: Numerical simulation of natural convection behind furniture compared to PIV measurements.

Chapter 1

Introduction

In buildings and dwellings humidity is present in the indoor air as well as in all hygroscopic materials in the indoor environment. The humidity in the air will interact with the moisture in the surface materials by sorption processes. This process is called moisture buffering. The humidity in the room air is important for the occupants' perception of the indoor air quality, which is closely related to the moisture level in the material surfaces. The main purpose of building design is to assure comfort for the occupants with high indoor air quality. In the past, thermal comfort was the main consideration for building designers, but today hygrothermal impact on the indoor environment also needs to be taken into account. However, there are still moisture problems in dwellings. These are mainly related to critical areas where the microclimatic conditions can lead to condensation and maybe even mould growth. Therefore, it is important to investigate the hygrothermal conditions in microclimates.

The objective of this thesis is to study the hygrothermal microclimate on interior surfaces, which is important for both the building envelope and the indoor air. The aim is to comprehend some of the risk factors in critical microclimatic areas.

1.1 Background

A topic of general interest, for both researchers and public, is the indoor environment. People spend up to 90 % of their lives indoors at day-care institutions, schools, work or at home, so it is essential for humans to have a good indoor environment. The indoor humidity levels have been found to affect the indoor air quality (Toftum & Fanger, 1999). Unfortunately, the resent years have also shown an increase in the number of illnesses, and there are indications that moist buildings may play a role (Bornehag et al. 2001).

It is a well known fact that moisture is the most important reason for damage in buildings. In the yearly reports from The Building Damage Fund in Denmark, it is clear that most reported damages are moisture related e.g. rot decay in outdoor wooden constructions, wetting from thermal bridges and lack of ventilation. Generally, the list of damages clearly points out that moisture plays an important role.

It is acknowledged that there might be many circumstances where moisture is damaging like leakage e.g. in attics due to leaking from roof valleys, built-in moisture in newly completed buildings etc. These effects have not been studied in this project, where the main focus is on internal surfaces that interact with the indoor environment.

Mould growth is an indicator of moisture problems and it is often seen in critical microclimatic areas. A microclimate can be defined as; a local area within a room where the climate varies from that of surrounding areas due to a variety of influencing factors. The critical microclimates are often found near thermal bridges, like corners or behind furniture placed close to poorly insulated walls. Critical areas in buildings typically have high humidity levels or condensation and it is often combined with lower surface temperature.

The effect of humidity in dwellings can be observed in the moisture content of building materials. As an example, the changes in moisture contents can be seen in especially older buildings with wooden floors, where tiny cracks or small gaps may appear in winter and go unnoticed during summer. The effect is connected to moisture buffering of the open hygroscopic wood, which for wood also has an effect on the dimensions. Building materials, constructions and furnishing surfaces exposed to indoor air, will reduce daily peak variation of the indoor humidity by moisture buffering. This effect has been studied experimentally by numerous people (Künzel 1960, Harderup 1998, Padfield 1998, Mitamura *et al.* 2001, Simonson 2001, Svennberg 2003, Peuhkuri 2003, Ojanen *et al.* 2003, Mortensen et al. 2005, Rode et al. 2005, and Holm and Künzel 2006).

These investigations show that the moisture buffering effect of internal surfaces should not be neglected. Platner and Woloszyn (2002) showed that a much better prediction of the indoor relative humidity was obtained, when the sorption of internal surfaces was included. This points out that moisture modelling is very important.

In past decades, considerable progress has been made in the application of numerical simulation models to assess the heat, air and moisture behaviour of building components, building zones and whole buildings. The hygrothermal modelling of building components addresses Heat, Air and Moisture in single building parts and the models are known as HAM modelling tools. The HAM tools are used to investigate durability in terms of moisture safety of e.g. roof constructions. The model tool for building zones includes computational fluid dynamics (CFD), which focus on air and heat (and moisture) transport. The CFD tools are often applied in studies of human comfort, which is largely affected by local airflow velocities. Finally, whole building tools aim at predicting heat and air (and moisture) transport in entire buildings. These whole building tools can be based on development of building energy simulations tools that can predict the energy use for a building, which is mostly governed by conduction, ventilation and radiation.

Whole building simulation models that include moisture interactions have been developed and presented by e.g. Rode & Grau (2003) and Holm et al. (2003).
Even though building physicists are very interested in the hygrothermal effects on building envelopes and indoor environment, it is still not common practice to use the developed building simulation models in the design phase.

These whole building simulations tools can calculate temperatures and vapour content in walls whereas the room air is represented by just one node. For overall energy performance this simplification is reasonable but for microclimatic investigations more details are needed. The local airflow patterns will influence the microclimate due to changes in the surface heat transfer coefficient and temperature differences. Hence, at present it is impossible to use whole building simulation tools for hygrothermal predictions in microclimates like corners because sophisticated analysis is required in order to resolve the special airflow conditions and surface heat transfer coefficients.

An available tool that can predict the local airflows in rooms are CFD models. These models can predict the room airflows accurately but usually the boundary conditions, in form of surrounding walls, are described as constant or by very simple conditions.

The critical microclimates occur in a small part of room and their complexity requires more accurate modelling tools to include both moisture in the building envelope and the room air. This means that hygrothermal investigations of microclimates could be an integration of CFD and whole building simulation models.

Some researchers have already tried to use the advantages of CFD for building simulation. Negrão, 1998; Bartak et al., 2002; Zhia et al., 2002; Zhia and Chen, 2003 have all attempted to couple CFD and energy simulations of building envelopes but they did not include moisture transport. However, in relation to moisture interactions Clarke et al. (1999) developed a model that could predict conditions leading to mould, and recently Hohota (2003) has shown that CFD models can be used to predict condensation on surfaces. Their works present the potential for combined tools to investigate hygrothermal microclimates.

Integration of different tools like CFD and HAM is fairly new and therefore modelling of hygrothermal microclimates needs to be validated to experimental data. It is a difficult task to measure airflow velocities especially if it is near a surface. Luckily, the experimental techniques have also progressed, so today sophisticated equipment for airflow measurements is available like Particle Image Velocimetry (PIV). The PIV technique is based on digital images where tracer particles follow the fluid flow. The tracer particles are recorded by a camera, which uses a laser light sheet as a flash. When two images are recorded with minute intervals the particles in the first image can be rediscovered in the second. This can basically provide vector images of the airflow.

This thesis work is therefore a combination of experimental and modelling work.

1.2 Hypothesis and scope

The hypothesis of the current work is that comprehensive moisture modelling can make it possible to predict the hygrothermal microclimatic conditions of surfaces in specific microclimates in buildings like heat, air and moisture conditions behind furniture in bedrooms.

There are two scopes of this thesis; one is to establish a model that can predict the hygrothermal microclimate on the interior surfaces of the building envelope and another is to perform measurements that reveal airflow velocities near surfaces.

1.3 Scientific method

The extensive interactions in a building are shown in Figure 1.1. The figure visualizes the factors that influence the moisture transport in a building. The focus of this investigation will be on the multi-dimensional moisture interactions between constructions and the room air. A minimal airflow velocity is found in the vicinity of surfaces, where a thin air layer (boundary layer) occurs. The airflow conditions in the room influence the thickness of the boundary layer. Thus, it will be important to investigate the airflows carefully and to estimate their influence on the moisture transport

The scopes will be examined by use of two allied case studies that will represent critical microclimates. Both modelling and experimental work will be based on the selected case studies, where a piece of furniture is placed near a poorly insulated external wall, which represents a hygrothermal microclimate.
The model work will try to incorporate airflow modelling in the form of CFD and moisture distributions in constructions. The experimental investigation will involve Particle Image Velocimetry (PIV) in a full-scale set-up.

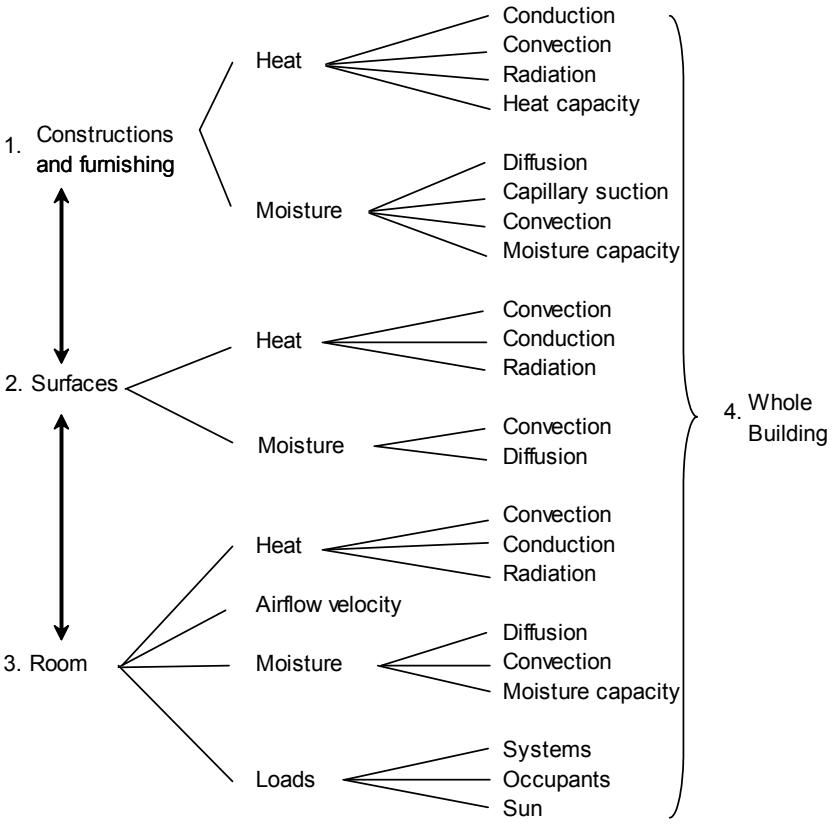

Figure 1.1 *Factors that influence moisture interactions in a building*

1.4 Thesis outline

The structure of the current thesis is briefly summarized here.

The thesis begins by describing the background (Chapter 1, Introduction), and includes literary reviews on humidity impacts within indoor environments, as they relate to the performance of building materials, construction and furnishing as moisture buffers (Chapter 2, Humidity impacts).The findings of **Paper I** and part of **Paper III** are also presented here, followed by the influence of boundary layers (Chapter 3, Boundary layers). The content of **Paper II** is an experimental investigation of the moisture surface resistance, which is also introduced here.

This is followed by a description of the investigated case studies (Chapter 4, Case studies), where **Papers III, IV and V** are included. **Paper III** contains a method to include a detailed investigation of heat and moisture distribution in walls in a CFD code, which is illustrated by a numerical simulation of a room with a piece of furniture placed near a cold external wall. The local airflow in the gap between furniture and a cold external wall is investigated experimentally by Particle Image Velocimetry in **Paper IV**. **Paper V** describes a numerical simulation that examines the same case as the experimental investigation. This can help further the understanding of the measurements.

At the end of the thesis the major findings of the different investigations are discussed and recommendations for future work are given (Chapter 5, Discussion), which is rounded up by a presentation of the final conclusion of the thesis work (Chapter 6, Conclusion).

Paper I:	Moisture buffer performance of a fully furnished room
Paper II:	Determination of moisture surface resistance using cup experiments.
Paper III:	Investigation of microclimate by CFD modelling of moisture interactions between air and constructions.
Paper IV:	Microclimate investigation of airflow patterns by Particle Image Velocimetry (PIV).
Paper V:	Numerical simulation of natural convection behind furniture compared to PIV measurements.

Chapter 2

Humidity in indoor environments

It is important to investigate moisture transport mechanisms in microclimates in order to gain knowledge about hygrothermal transfers in full size rooms or on a building scale. The importance lies within the microclimatic conditions that influence the indoor environment.
It is essential for humans to have a good indoor environment, since humans spend most of the time indoors at work, day-care institutions, schools or in homes. The primary purpose of building design is thus to ensure a good indoor environment for the occupants. This is obtained by interactions between the outdoor conditions, the building envelope and the occupants. The thermal conditions are already recognized as being important as opposed to moisture, which is not as integrated in building design.

This chapter presents a literary review of the influence of humidity in the indoor environment. Humidity is important for both the direct influence on the perception of indoor air quality (IAQ) and the indirect impact due to biological growth like mould and house dust mites or emission from materials. The emission from materials is closely related to the moisture levels in building materials, constructions and furnishing. Moisture permeable surfaces in the indoor environment can act as moisture buffers that try to even out daily variations in humidity levels. The significance of moisture buffering of materials and constructions is therefore also reviewed in the current chapter. The literary reviews point out that humidity has a huge impact on the indoor environment, but to gain more knowledge, it is important to investigate moisture transport mechanisms in microclimates. The reason is that the microclimatic conditions will influence the indoor environment and that the understanding of hygrothermal transfers in microclimates can help to comprehend the interactions in full size room or at a building scale.

2.1 Humidity impact on indoor air

There seems to be clear evidence that air humidity has an impact on the perception of indoor air quality, and experimental studies have found indications that the perception is connected with cooling of the mucous membrane. Air humidity also effects the pollutant emissions and biological growth in the indoor environment and therefore it

is related to the productivity, which is very important in schools and offices and it may even pose health risks. A minor literary review on the topic has been conducted. Visible mould and condensation are common characteristic signs of high relative humidity combined with cold interior surfaces of the building envelope especially near thermal bridges. Several studies have discovered that relative humidity (RH) has an impact of the growth of dust mites. Periods of low relative humidity (<35 %) are an efficient way of reducing the number of dust mites in the indoor environment (Korsgaard, 1979; Fanger, 1983; Clausen *et al.*, 1999). Mould spores and dust mites are unwanted in the indoor environment, because they can lead to Sick Building Syndrome, which cover symptoms like irritation of the mucous membranes, skin rashes, headaches etc. A review study by Bornehag *et al.* (2001) on dampness and health confirms that moist buildings are to be avoided.

A set of summer and winter comfort zones are provided by ASHRAE (2005) with restrains on both temperature and humidity. Originally, this was based purely on studies of thermal comfort, and the thermal comfort zones specify conditions that will be thermally acceptable for 80 % of sedentary persons. The humidity levels are given as a lower limit at dew-point temperature of 2°C and two upper limits of 18 and 20°C wet bulb temperature for winter and summer, respectively. The lower limit should avoid uneasiness due to dry eyes, nose, throat and skin while the upper limits should prevent warm discomfort due to insufficient cooling of the mucous membrane.

The limits of the comfort zones have been widely investigated. An investigation by Fang *et al.* (1998b) found that the air quality perception decreases with lowered respiratory cooling effect whether the air is clean or polluted. This indicates that an upper limit for humidity can be established for comfort. Furthermore, it was found that the perception of air quality is very sensitive to temperature and humidity, but they do not influence the perception of odour intensity of materials. The study was based on facial exposure only. These results are not coherent with the study by Reinikainen and Jaakola (2003), where the humidity was found to influence the odour intensity in a real office wing. Another study by Fang et al. (1998a) with whole body exposure gave different results and supported Reinikainen and Jaakola's (2003) findings. In the study the temperature and humidity levels had a strong impact on the perceived air quality and little impact on the odour sensitivity. It was assumed that the changed result for the odour sensitivity was due to the changed procedure from facial exposure, where the occupants were allowed to compare the air to a reference sample. The main results were that sufficient cooling of the mucous membrane by the inhaled air is essential for an acceptable perception of air quality. In the study it was also found that human acclimatization is insignificant to air polluted by building materials. Moreover, prior exposure was found to have limited influence on immediate perception. Therefore, it was concluded that first impressions of air quality can be used as an indication of the perceived air quality. Another interesting result of the study was that perception of air quality is better for cold and dry polluted air, than more humid and warmer clean air, which suggests that the ventilation rate can be lowered if the air is dried and cooled. Work by Toftum and Fanger (1999) also found that at lower relative humidity, the air is perceived as being fresher, which increases the IAQ. They suggest that this effect is obtained from increased cooling of the mucous membrane.

The skin humidity is also influenced by relative humidity in the air. The skin humidity is found to have an impact on the perception of comfort, since high levels of skin

humidity will make the clothing cling more to the skin and this will feel uncomfortable while moving (Toftum *et al,* 1998; Berglund, 1998). However, the results indicate that there is no need for upper humidity comfort limit due to skin humidity, which is only vaguely dependant on the relative humidity of the air.

An investigation by Fang et al. (1999) showed an impact of temperature and humidity on chemical and sensory emissions from building materials. It was found that after an initial ventilation period, the emission rate was only slightly dependent on the temperature but, the humidity still influences both chemical and sensory emission rate of waterborne floor varnish and acrylic wall paint.

The perception of low air humidity has also been investigated. In a study by Wyon et al. (2002) 5 hours of exposure to low humidity (5, 15, 25 and 35 % RH) levels resulted in only little discomfort. But medical examinations showed that exposure to humidities of 5 or 15 % RH gave measurable more dry mucous layers and eye films than if exposed to 25 % RH. The dryness symptoms increased if the air was polluted. The blink rate was also found to increase at low humidities. An earlier long (78 hours) study of exposure to 9 % RH at 23°C by Andersen et al. (1974) showed no effect on the nasal mucous flow, which indicates that the humidifying capacity of the nose is sufficient to compensate for dry air. Hence, they concluded that there is no physiological need for humidifying clean air. However, in Fanger (1983) it is suggested that the dryness of the mucous membrane is caused by irritation from pollutants in the air.

Fanger (2006) suggests that one way to improve the IAQ so also the most sensitive 15-30 % of the population will be satisfied, is by providing cool and dry air. He suggests drying the air but only to 20 % RH, since below this level the dry air may have a negative effect on blink rate and productivity.

Based on this review, it is clear that an upper limit of humidity should be defined, since this will also improve the IAQ sensation because high humidity creates an effect of stuffy air. Low humidity is found to provide a better air quality than a higher one, and it is anticipated that this is due to decreased cooling of the mucous membrane. Furthermore, humidity impacts the emissions from building materials, so to reduce the pollutant levels the humidity should be kept low. This will also decrease the number of dust mites, and the number of allergens in the air. However, it is also found that too dry air will increase the blink rate, which could reduce productivity. Some find that even at a low humidity occupants do not perceive the air as being dry, and their mucous membrane in the nose do not seem to be damaged by low humidity. It is therefore considered unnecessary to humidify the indoor air artificially. However, it has been reported that occupants feel dryness even at times when the air is not dry, but this may be related to the pollutant level.

2.2 Building materials and furnishing as moisture buffers

Humidity and moisture also affects the building constructions and furnishing. Moisture is the most frequent cause of damages to buildings. This fact alone makes moisture unwanted in buildings but it should be avoided for several reasons, of which the most important are deterioration and mould growth. Moist buildings are often referred to as damp buildings in indoor environment investigations. Here a brief

introduction to moisture buffering is provided, followed by a short literature review of the topic.

Moisture buffer capacity of building materials and furnishing can be used to minimise daily variations of relative humidity in indoor air. Materials capable of functioning as moisture buffers have open permeable surfaces where sorption interactions occur with the indoor air. The peak reductions can be useful in e.g. an office where the humidity will rise during the day when the office is occupied, whereas the humidity will decrease during night due to ventilation. A moisture buffer in the office will be able to reduce these variations. Figure 2.1 shows an example of how the main humidity in an office can be reduced by use of wall surfaces as moisture buffers. The Figure demonstrates that the daily humidity variation can be reduced significantly by moisture buffers.

Moisture buffer capacity can also be beneficial in bedrooms, kitchens and other indoor spaces that are exposed to peaks in humidity production. It must be kept in mind that a high ventilation rate will lower the effect of the moisture buffering. On the other hand, there might not be the same demand for ventilation if the humidity can be kept lower by using interior materials as moisture buffers. There are great advantages of avoiding periods with both very high and very low relative humidity. The benefit of avoiding high relative humidity is to prevent biological growth on cold surfaces where there will be a risk of condensation. To reduce the number of dust mites, it is often recommended to keep the RH below a certain level (species dependant), but to be effective the peak humidities must be avoided (Cunningham, 1996). There will also be a reduction in the number of spores from mould growth because of the reduction of possible condensation. Because of this, a lower maximum relative humidity will benefit people who are allergic to these allergens.

Ventilation rate will direct the mean RH, but peak variation, due to building occupancy, may be reduced by moisture buffering. A vast amount of the total heat loss from a building is due to ventilation. The ventilation serves to ensure the physiological necessary supply of fresh air and removal of moisture, produced by the indoor activities and pollutant emission from occupants and materials (Clausen *et al.,* 1999). Therefore, it is important to know the exactly minimum necessary ventilation rate in order to save energy but, without compromising a good IAQ.

The interest in moisture buffering has lead to a number of studies. In past studies the moisture buffer capacities of several materials have been investigated in small scale (Padfield 1998, Mitamura *et al.* 2001; Svennberg & Harderup 2002; Peuhkuri 2003, and Ojanen *et al.* 2003).

Full scale measurements of moisture buffering have also been performed. In Finland a full scale investigation concerning the moisture buffer capacity of a bedroom in an ecological building without vapour retarder was conducted (Simonson 2000). It was found that daily variations of high peak humidity in the bedroom, could be reduced by up to 20% RH. A similar investigation concerned simulation of the same room when exposed to weather data from four different cities. There, buffer materials was found to have most impact in a moderate climate like in Scandinavia, and the buffer effect of hygroscopic thermal insulation was strongly reduced when it was not directly exposed (Simonson *et al.*, 2001). Mortensen et al. (2005) reported a study of full scale

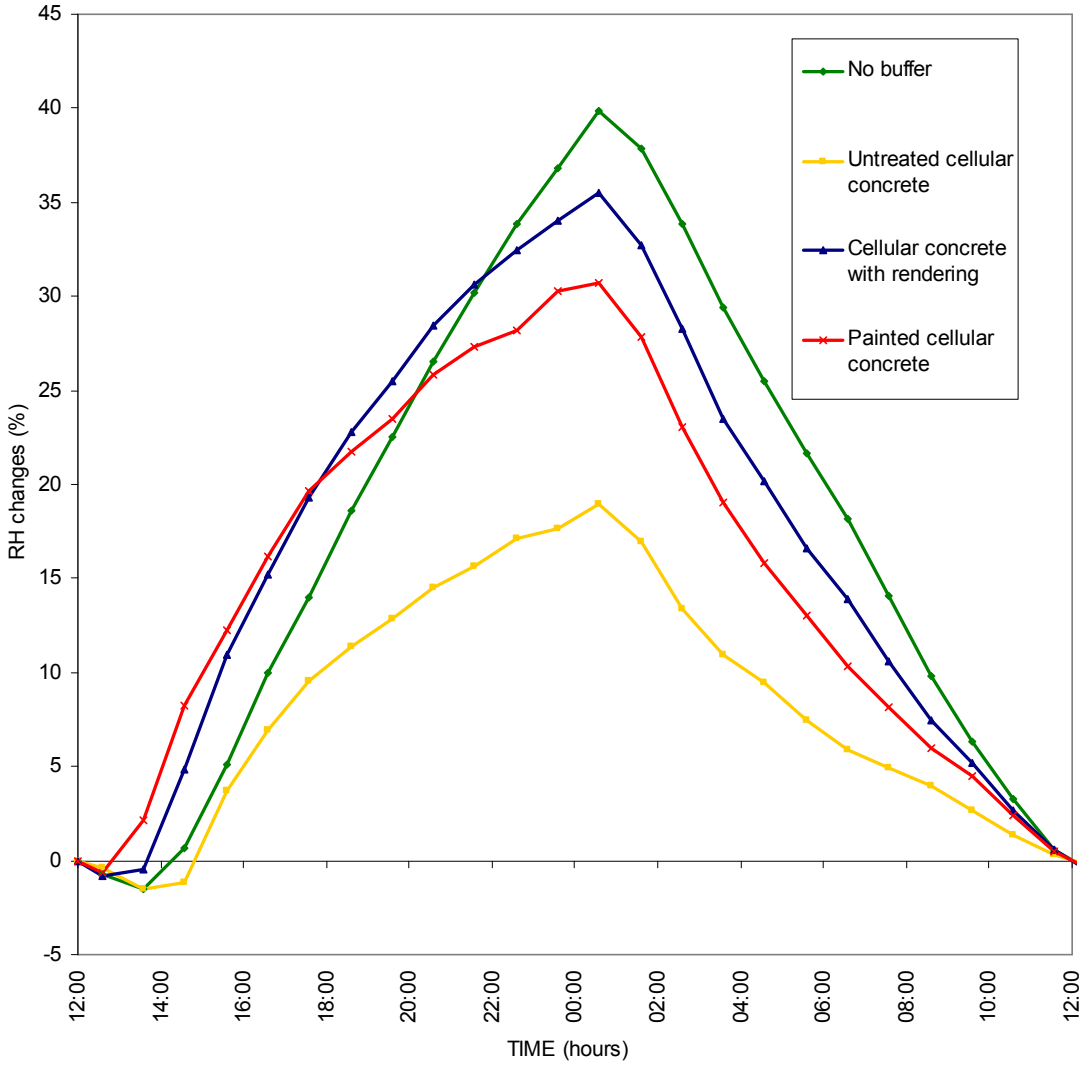

Figure 2.1 *The curves show the main daily humidity variation in a single office where two of the wall surfaces acts as buffers. The moisture load is equivalent to occupancy of a single person (Mortensen et al. 2005)*

moisture buffer capacity of internal wall materials, where it was found that surface treatments strongly reduce buffering effects. Holm and Künzel (2006) investigated the buffer performance of wood based panels and found that wooden fibreboard panels can reduce peak humidity by as much as 80 % RH but they also point out that in dwellings fibreboards are surface treated which will reduce the effect.

Building constructions are not the only buffers in dwellings. Furnishing, textiles and paper are hygroscopic materials that are often found in dwelling in form of e.g. drapes, carpets, upholstery and books. Therefore, the moisture buffer performance of a fully furnished room was investigated in **Paper I, Moisture buffer performance of a fully furnished room**.

The paper describes a series of experiments that show the moisture buffer performance of various furnishing elements. The experiments were carried out in a climatic test cell, which imitates an ordinary office. The objects were exposed to cyclic humidity variations like in an inhabited indoor environment, and the response

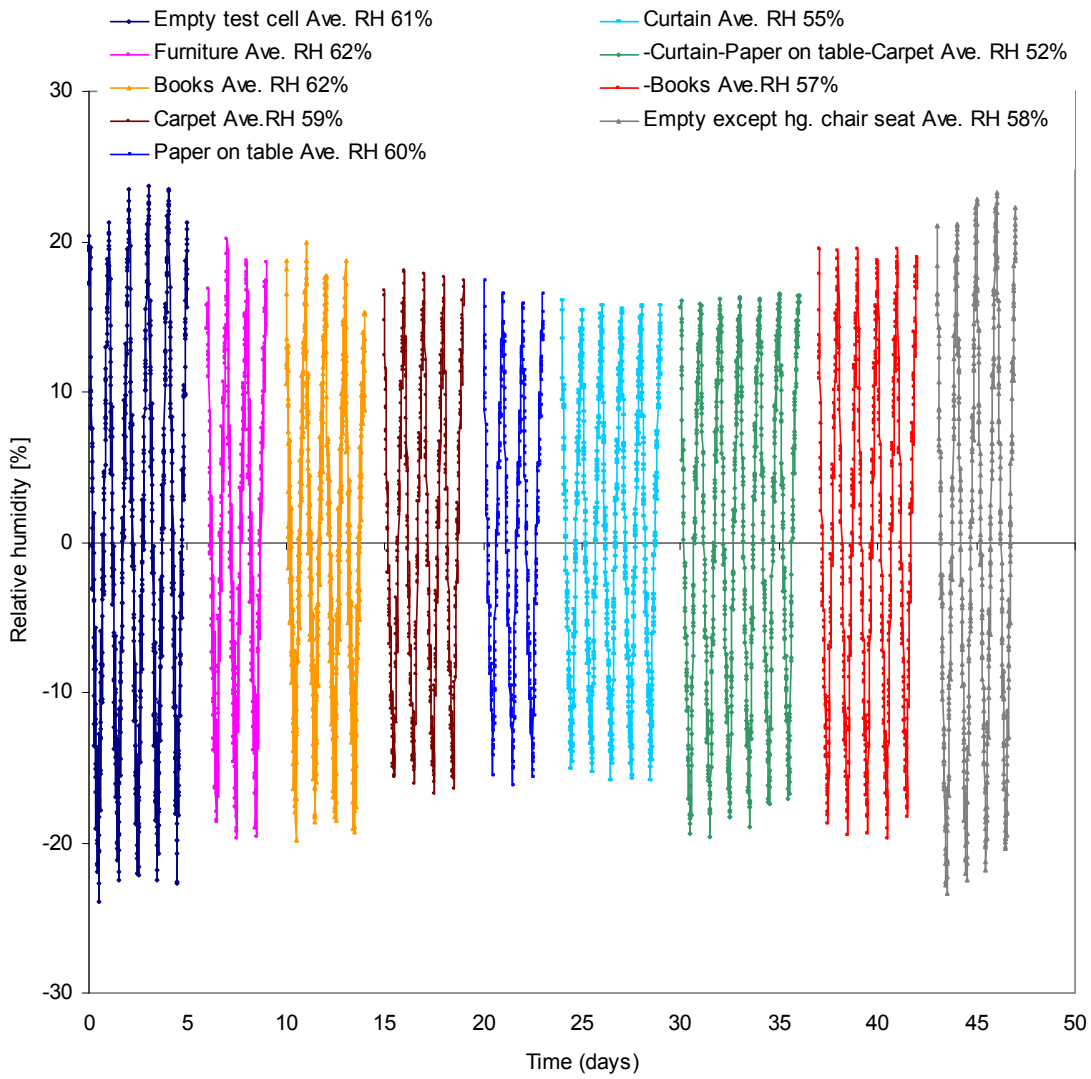

Figure 2.2 *Main variations in RH for the nine different cases for the furnished room experiments. In the first 6 sequences objects are added in the room and in the last 3 the furnishing elements are removed again*

of the indoor humidity was followed over time. It was a step-by-step investigation starting with an empty room and going towards a fully furnished room. The moisture variation was studied in detail inside a single chair seat at different depths.
The buffer performance result is shown in Figure 2.2 for the room.

By full-scale measurements it was shown that the imposed daily humidity variation in a fully furnished room could be reduced by ~25% RH compared to an empty room. The chair seat reacts almost instantly to changes of the humidity level in the room. The numerical whole building simulation model (Rode & Grau, 2003) estimates bigger changes in relative humidity and this may be explained by some hygroscopic absorption of moisture in the paint.

The main conclusions of **Paper I** were that the fully furnished room has shown that moisture buffering needs to be more carefully studied since it has a notable impact on the moisture conditions in rooms. Calculation tools need to be modified to be able to

handle all kinds of materials and there is a lack of moisture property data for many materials. There is also a lack of; moisture property data and description of different surface materials present in normal indoor environments. Alongside the task to find better descriptions of the materials, a better understanding and greater knowledge of the microclimate indoors is necessary.

A review study by Svennberg et al. (2007) retrieve studies of indoor surface materials from 1960-2000 in Sweden and Germany, which include both building materials and textiles.

The great interest in moisture buffering led to a NORDTEST Workshop on *Moisture Buffer Capacity* initiated by Rode (2003). The outcome of the workshop was that there was a need for definition of a stringent term for moisture buffer capacity. This workshop was followed up by a NORDTEST project by Rode et al. (2005), which developed a NORDTEST method for experimental measuring of the moisture buffer capacity and defined a common unit, the moisture buffer value (MBV).

Similar to the NORDTEST method a recent Japanese industrial standard describes an experimental test method of ad/desorption performance of building materials to regulate indoor humidity (JIS A 1470-1, 2002).

The two experimental approaches to determine the MBV were compared by numerical simulation by Roels & Janssen (2006). The two methods are very similar but they use different definition of the specimen thickness, which Roels and Janssen found to be very important. The humidity cycle times were also found to have a major impact on the MBV, since dynamic response to short-term variations had less correlation to MBV, whereas long-term dynamic response similar to the NORDTEST protocol showed MBV to be a good indicator of the buffer capacity.

Moisture buffer performance is also part of an international research project of *Whole Building Heat, Air and Moisture Response*, which is Annex 41 of the International Energy Agency's (IEA) *Energy Conservation in Buildings and Community Systems Programme* (Hens 2003). As an IEA activity it is also the scope to illustrate how a better understanding of the overall hygrothermal behaviour of buildings can lead to better energy performance, e.g. by inventing optimized strategies for ventilating, heating and cooling that take the overall hygrothermal reality of buildings into account.

To summarize, it is clear that moisture buffer performance of whole buildings is influenced by the moisture buffer capacities of both constructions and furnishing elements. But there is still a need for both more experimental investigations of moisture properties for all kinds of materials. Such material data will be very useful for the development of hygrothermal models for whole building response.

2.3 Hygrothermal modelling

The whole issue of humidity in indoor environments has also been investigated numerically by use of hygrothermal models. It is common to distinguish between 3 key types of models:

hygrothermal building component models, addressing moisture/heat/air transport in single building parts (**HAM**). An application example is building component durability, which is primarily governed by the hygrothermal state

computational fluid dynamics models, focusing on air/heat(/moisture) transport in single building zones (**CFD**). An application example is thermal comfort of occupants in the indoor environment, which is largely affected by local air velocities and temperatures

whole building simulation models, aiming at heat/air(/moisture) transport in single buildings (**whole building**). An application example is energy use for building conditioning, which is mainly governed by conduction, ventilation and radiation flows

The specific focus area of each modelling tool is represented in adequate detail, while significantly simplifying the side areas. The development of the 3 model types is related to their use and application and therefore they remain poorly integrated. Recent developments in the field of building heat, air and moisture engineering do however, defy the borders between modelling approaches and call for an integrated modelling. The increased demand to reduce building energy consumption leads the evolution towards highly insulated buildings, which increases the relative contribution of ventilation in buildings' energy consumption. This points towards new strategies for ventilation since constant rate ventilation may be unnecessary. Another method is ventilation control based on indoor relative humidity levels since one of the main purposes of ventilation is to remove excess indoor humidity. However, ventilation must be ensured since it serves to ensure the physiologically necessary supply of fresh air and removal of indoor moisture production (mainly from human activities) and pollutant emission from occupants and materials.
The interior air humidity is affected by hygroscopic buffering of finishing materials and furniture elements, a process which in turn heavily depends on local surface moisture transfer coefficients. Reliable evaluation of relative humidity controlled ventilation with respect to energy consumption and occupant comfort thus calls for an integrated modelling of the heat, air and moisture behaviour of whole buildings, building zones, and building components.

Some first steps towards integration of CFD and HAM models are currently being taken, but the publications are limited. Steeman et al. (2006) implemented a simplified wall model for vapour transfer in a commercial CFD package for an analysis of surface moisture transfer coefficients in a ventilated room. The implementation also included both heat and moisture buffering of the walls, which is based on the moisture penetration depth. The wall based moisture buffering model was applied to a simplified test case that contains neither windows nor doors. The geometry was a rectangular box of 6 x 8 m² floor area and 2.7 m's height (external measures), which also contains a ventilation system and a moisture source. The data was partially validated by comparison of the simulated results from another program. An example of their results is given in Figure 2.3. The Figure shows the distribution of the relative humidity in the modelled wall layer defined by the penetration depth at the end of the day. For further details see Steeman et al. (2006). Their findings point out that the strength of CFD tools is their ability to simulate local effects and that proper application will provide accurate details.

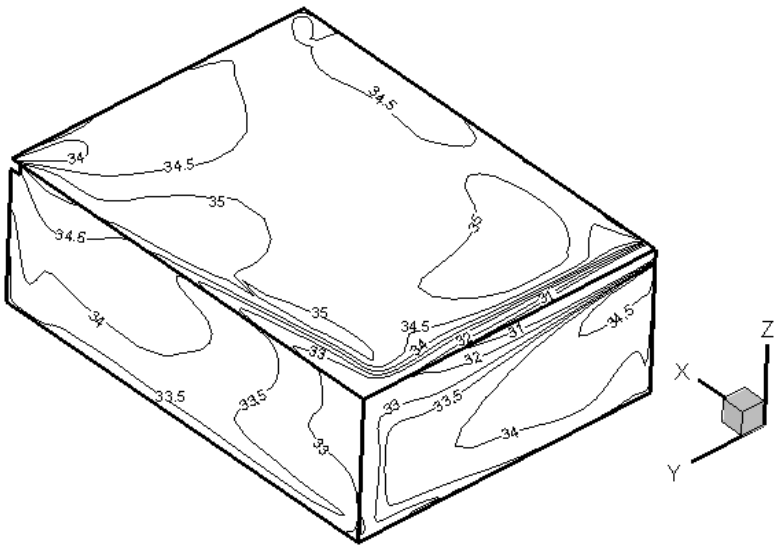

Figure 2.3 *Distribution of relative humidity (%) in the wall layer defined by penetration depth at t =24 hours, which is a representation of the moisture buffer effect of the walls. Printed with permission from the author (Steemans et al. 2006)*

Steeman et al. (2007) have also used CFD modelling to investigate the used analogy between heat and moisture transfer in building simulation. They found that similarity between boundary conditions is very important to avoid errors of local coefficients when heat and moisture analogy is applied.

In relation to simulation of moisture interactions by CFD Clarke et al. (1999) developed a model that could predict conditions leading to mould. Theodosiu et al. (2003) presented CFD modelling of heat air and moisture in a full scale room, with special focus on human comfort. Hohota (2003) expanded this work and showed, that CFD models can be used to predict condensation on surfaces. However, Hohota did not include sorption of walls. These works shows the potential of CFD tools in hygrothermal modelling but extension are necessary in order to model hygrothermal microclimates.

Paper III presents and partly validates an approach of using '*immobile fluids*' as walls that demonstrates how heat and moisture transport in solids can be directly implemented in a CFD environment.

The model used in the paper is implemented in a commercial CFD tool (Fluent 2003). The moisture in the air is represented as a perfect mixture of two perfect gases, dry air and water vapour, so that the water vapour properties as density or heat capacity are represented. As a first approach only heat conduction and vapour diffusion will be implemented.
Basically, there are two ways to represent moisture transfer in the envelope:

To use Fluent's existing model for heat transfer in a solid material and enhance it for moisture transfer. In this case vapour diffusion needs to be programmed by the user.

To use Fluent's existing diffusion equation. As diffusion is computed only in fluid domains, the walls need to be defined as fluids.

User programmed code will decrease the numerical performance of the numerical solver. This is the main reason for choosing a fluid wall approach. The wall construction can be given "fluid properties" that corresponds to normal building materials characteristics, so the thermal behaviour of the wall should be unaffected by the use of fluid walls. But the fluid walls enable modelling of moisture diffusion. A first test showed that in order to use the fluid walls, it is necessary to declare them as laminar zones with no velocities, because otherwise the fluid walls contain a turbulence equation that will give numerical errors. The CFD software is capable of treating thermal interactions between fluids but some first tests showed that there is no moisture transfer between fluids.

The explanation is that in the program, the two fluids, the room air and the wall, is regarded as being separated by a barrier so they are unable to interact unless specific functions are defined for the interaction. One could regard the boundary as being split in two halves: One that is in contact with the room air, and a shadow copy of this, which is in contact with the wall. The two faces, the real and the shadow, are placed at the same geometrical position but have no functional contact regarding moisture transfer. This is illustrated in Figure 2.4. That the two surface meshes have the same geometry does not mean that the cell volumes are identical.

A simple approach is used for the moisture transfer where the moisture content of cell c0 in the air is transported to the cell c0* in the wall. For a first approach it was decided to use a macro-modelling approach and neglect surface resistance. This allows that part of the moisture content in c0 can be transported to c0* in the wall or from wall to the air. To explain the principle it is assumed that the moisture flux will be from the air to the wall. The transport is based on the flux between c1 and c0 in the air. The distances between the cells is a measure that is related to the volume size and this is used to assure that a big amount of water is not transported immediately to a very small cell since this can cause divergence in the solver.

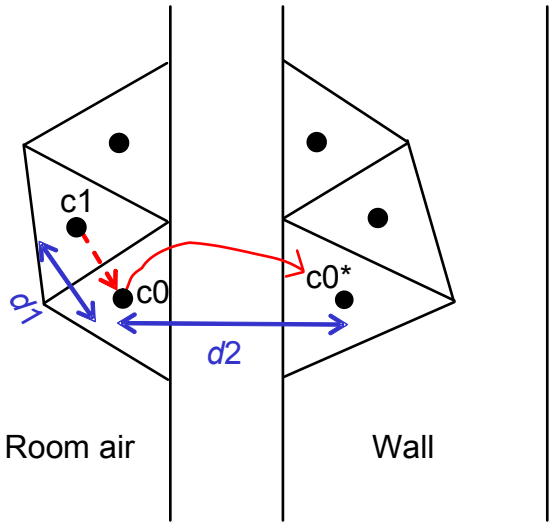

Figure 2.4 *A close-up of the face separating the two fluid zones, room air and wall. On each side of the face there are two meshes with same face geometry*

The transport is not based on any physical transport since in this first approach the simulation will only include steady-state simulation. In steady-state both vapour and heat distribution will be a linear based on the two surface contents, so the idea is just to make the fluids interact. An example of results obtained by use of the described immobile fluids is given in Figure 2.5. The Figure depicts a small room of 2 x 2 x 2 m^3 with 2 immobile fluid walls. The room includes a piece of furniture placed 2 cm from the wall and 5 cm from the floor. Due to both a moisture source and ventilation of the room different levels of humidity are observed in the middle of the room and in the air gaps near the furniture. The furniture is modelled as a solid and therefore it has no moisture content. The wall actually contains water, which is seen in the upper part of the left wall. The moisture content in the other part of the wall is out of the range and the moisture level is represented in form of relative humidity which is a little strange. The result clearly shows that the moisture distribution in the room is not evenly distributed so an assumption of fully mixed conditions can not be applied in the current case. For more results see **Paper III**.

The idea of using immobile fluid walls has proved that it is possible to implement HAM in a CFD environment. This is a fairly easy implementation method but there are of course ideas for improvement. At the moment 8 user-defined functions need to be programmed and applied in order to have two immobile fluid walls. The application is based on the id number the CFD software assign each surface, which is inconvenient because the code must be modified to call the right surface. The immobile fluid wall has a problem with air infiltration if it is not assured that the wall

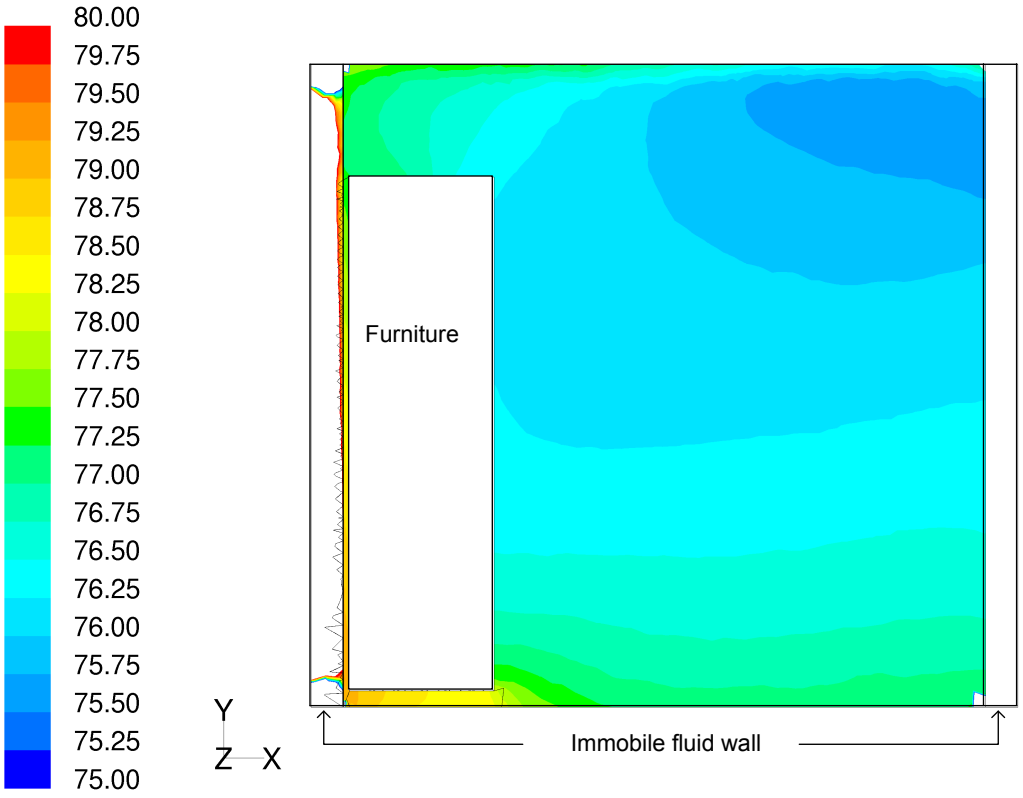

Figure 2.5 *Relative humidity distributions in a small room that contains moisture sources and is ventilated. Only relative humidities in the range 75-80% are shown*

section only contains immobile wall fluid and vapour. In the current application this is assured also by user-defined functions. An idea for improvement could be to declare the surface between the fluid and the wall as an interior boundary since across interior surfaces both heat and moisture interaction can take place.
Earlier investigations without use of CFD models have shown the potentials of inclusion of moisture buffering in hygrothermal modelling. A hygrothermal multi-zone model used by Plathner and Woloszyn (2002) showed that including sorption of internal surfaces in simulation gave much more realistic results for the indoor humidity compared to measurements.

Holm et al. (2003) developed a model based on hygrothermal simulations tools for building envelope components and expanded it with models for indoor air volumes and by making provision for simultaneous calculation of several building components. Alternatively, Rode & Grau (2003) presented a building energy simulation model, which already contained capabilities for making thermal analysis of whole buildings, but expanded it with models for transient moisture transport in the building components. Joint work of Chalmers University of Technology in Sweden and the Technical University of Denmark has lead to development of the International building Physics Toolbox (HAM-tools) that takes into account interactions between building structure, building services, climate and user behaviour (Kalagasidis, 2004 and Rode et al. 2002). Also the IEA Annex 41 has led to further focus of hygrothermal modelling by common exercises on moisture performance, where 13 sets of results were collected coming from 11 institutions from 9 countries using as much as 10 different programs (Woloszyn et al. 2005).

The development of hygrothermal models is an on-going process. It is clear that there is a need for integrated models in order to investigate local effects. This can lead to a better understanding of the problematic microclimates. The summation of previous work indicate that the step toward better understanding of hygrothermal microclimates may be seen with integrated modelling tools. Hopefully, this can lead the way to building design with more appropriate moisture conditions for the occupants.

2.4 Microclimates

Earlier in this chapter evidence was shown for that moisture has an impact on the indoor environment as well as on the constructions and furnishing. One of the most important concerns is, however, the critical areas where the problems may take place. The most severe conditions typically occur in the coldest parts of the indoor environment. Hence, these are most often the areas where mould growth or similar symptoms are seen. Therefore it is necessary to take a closer look at what happens in thee critical areas, for example in corners, near other thermal bridges or in places with limited airflow. Figure 2.6 shows an example of an office room that includes a microclimate behind the bookcase, but it is unknown if it is critical. In critical microclimates the airflow patterns may be very important since the air will transport both heat and moisture to and away from the area. The humidity is very temperature dependant so even small temperature changes can change the RH drastically. Figure 2.7 illustrate a critical microclimate in a corner with mould growth.

Figure 2.6 *A picture of an office with a large bookcase which may be a potential critical microclimate*

Therefore, the microclimatic conditions are the main issue in the present work and will be investigated in form of some boundary layer conditions and by numerical and experimental investigation of a case study, **Papers III, IV and V**.

Figure 2.7 *A picture of a critical microclimate in a corner, Foto Kristian Fog Nielsen, BioCentrum-DTU*

Chapter 3

Boundary layers

Generally a boundary layer is the part of a fluid that is adjacent to a solid surface in which, e.g. air will create a boundary layer close to a wall surface. The presence of shear stresses indicates that it is a boundary layer region. Both viscous and inertial forces are important in the boundary layer. The boundary layer is affected by heat, moisture or momentum transfer to or from the surface. The viscous forces of the boundary layer distort the nearby flow where the effect of viscosity is negligible. The viscous forces are related to the Reynolds number, which is used to distinguish between laminar and turbulent flows. The Reynolds number expresses the relation between the inertial forces and the viscous forces. The concept of boundary layers was first introduced by Ludwig Prandtl in 1904.

A normal approximation states that for sufficiently high Reynolds numbers, the flow over a surface can be divided into an outer region of inviscid flow unaffected by viscosity (the majority of the flow), and a region close to the surface where viscosity is important (the boundary layer). Thereby, the effect of viscosity is only important in the boundary layer, whereas outside the viscosity effect is negligible and the flow can be treated as inviscid. The size of the boundary layer is dependant on the viscosity of the fluid. The boundary layer disturbance thickness is usually defined as the distance from the surface to the point where the velocity is within 1 % of the free stream velocity (Fox and MacDonald, 1994).

The moisture interaction between furniture or construction and room air is influenced by the boundary layer. There is a lack of knowledge about the actual moisture interactions occurring in the boundary layers between construction and room air. Therefore, one of the purposes with the current project was to investigate further not only how the boundary layer affects the moisture exchange but also how the boundary layer is affected by full scale airflows. The natural convection in dwellings may be superimposed by forced convection from ventilation but in the microclimates natural convection may be dominant.

3.1 Moisture surface resistance

The moisture surface resistance expresses the vapour diffusion resistance of the external boundary layer between the material surface and the room air.

The water vapour permeability expresses a materials resistance to water vapour diffusion. The standard EN ISO 12572:2001 describes the experimental procedure for determination of water vapour transmission properties. The principle is to add a material sample to a test cup containing a desiccant or salt solution. The test cup is then placed in a temperature and humidity controlled test chamber. Due to differences in partial vapour pressure over the sample specimen a flow through the sample will occur. By regular weighing of the test cups the rate of water vapour transmission in steady state can be determined. The measured water vapour permeability of materials contains surface resistances, resistance of the air layer inside the cup and the resistance of the measured material. For most building materials the water vapour resistance of the material is much higher than the surface and air layer resistance, and therefore these are negligible. This may however not be the case for open lightweight materials such as insulation and some types of membranes. The air layer resistance and the internal surface resistance can be removed by use of inverted dry cups. The inverted dry cups hang upside down so the desiccant is in direct contact with the sample specimen and the lower surface is in contact with the air in the test chamber.

It is possible to assess the surface resistances experimentally by measurements on samples with different thicknesses as shown by Fanney et al. (1991) and Worch (2004). This method is also proposed in the Japanese standard JIS A 1470-1:2002. In the standard it is stated that the surface resistance can be found by using 2 cups with desiccant covered by 1 and 2 pieces of paper, respectively. The EN ISO 12572:2001 standard for determination of water vapour permeability prescribes mixed air to assure uniform conditions and the airflow velocity should be within the range 0.02-0.3 m/s above the sample. However, this relatively large span of airflow velocities could influence the surface transport coefficients.

The objective of **Paper II** has been to use the Japanese standard to reveal the surface resistances for a wide range of airflow velocities above the sample surfaces. The investigated airflow velocities were in the range 0.06 – 1.4 m/s.

The water vapour surface resistance, Z_{surf} can also be estimated by analytical investigation. The theoretical analysis is based on a relationship between the convective surface heat transfer coefficient, α_c and the surface coefficient of water vapour transfer, β. For fully turbulent flows Lewis has described the relationship as shown in Equation 1.

$$\beta = \frac{\alpha_c}{\rho \cdot c_p} \tag{1}$$

where ρ is the density and c_p is the heat capacity of air.

Nusselt (1930) derived a more general form of the relationship, which is shown in Equation 2.

$$\beta = \frac{D}{\lambda} \cdot \left(\frac{\lambda}{\rho \cdot c_p \cdot D} \right)^n \cdot \alpha_c = \frac{D}{\lambda} \cdot (\mathrm{Le})^n \cdot \alpha_c \tag{2}$$

where D is the diffusivity and n is a number between 0 or 1.

The coefficient n is 0 for laminar flows and 1 for fully turbulent flows. The vapour surface resistance Z_{surf} is found as the reciprocal value of the surface coefficient of water vapour transfer, β.

3.1.1 Dry cup experiments

A theoretical, experimental and modelling approach to determine moisture surface resistance is presented in **paper II**. The sample material used in the investigation is paper (190g/m²). The cup tests were performed in a specially designed cup test facility that consists of a closed duct system where air is circulated. The flow can be regulated and the temperature and humidity controlled. Figure 3.1 shows the principle of the placement of a cup and a picture of the cups in the test chamber, where the cups were installed and measured.

The flow in the duct was also measured above each sample surface by anemometers and it was found that the velocity differs for each cup position. The experiment tested 4 different levels of airflow velocity and in each test 10 cups where measured. For each of the 4 tests the 10 measuring positions were measured twice, with one layer of paper and with two layers of paper. The positions of the 10 cups are seen in Figure 3.1b. The cups were placed in the test facility with isothermal conditions of 22.6°C and a relative humidity of 54 %. The resulting diffusion rate of each cup was post-processed to give the surface resistance (see **Paper II**). The results can be seen in Figure 3.2.

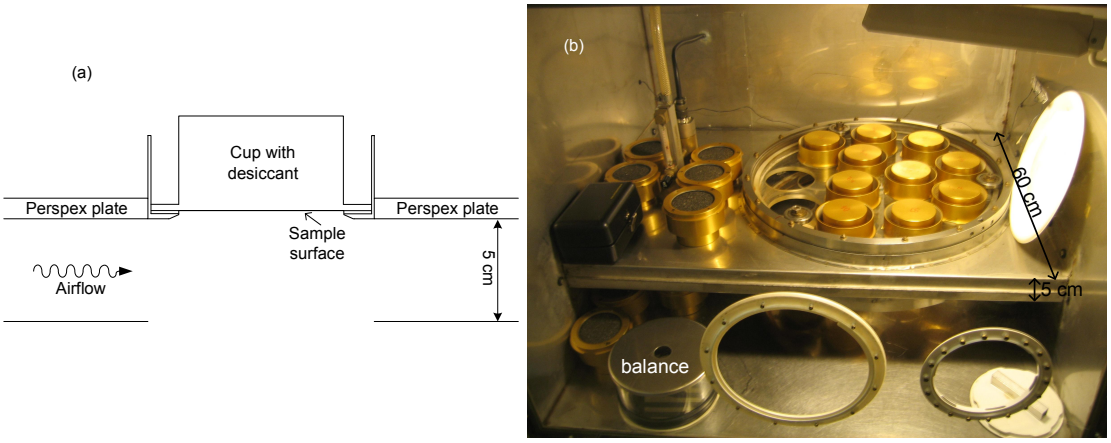

Figure 3.1 *(a) Principle of cup placement, (b) Picture of cups installed in the measuring chamber. The cups are weighed on the balance*

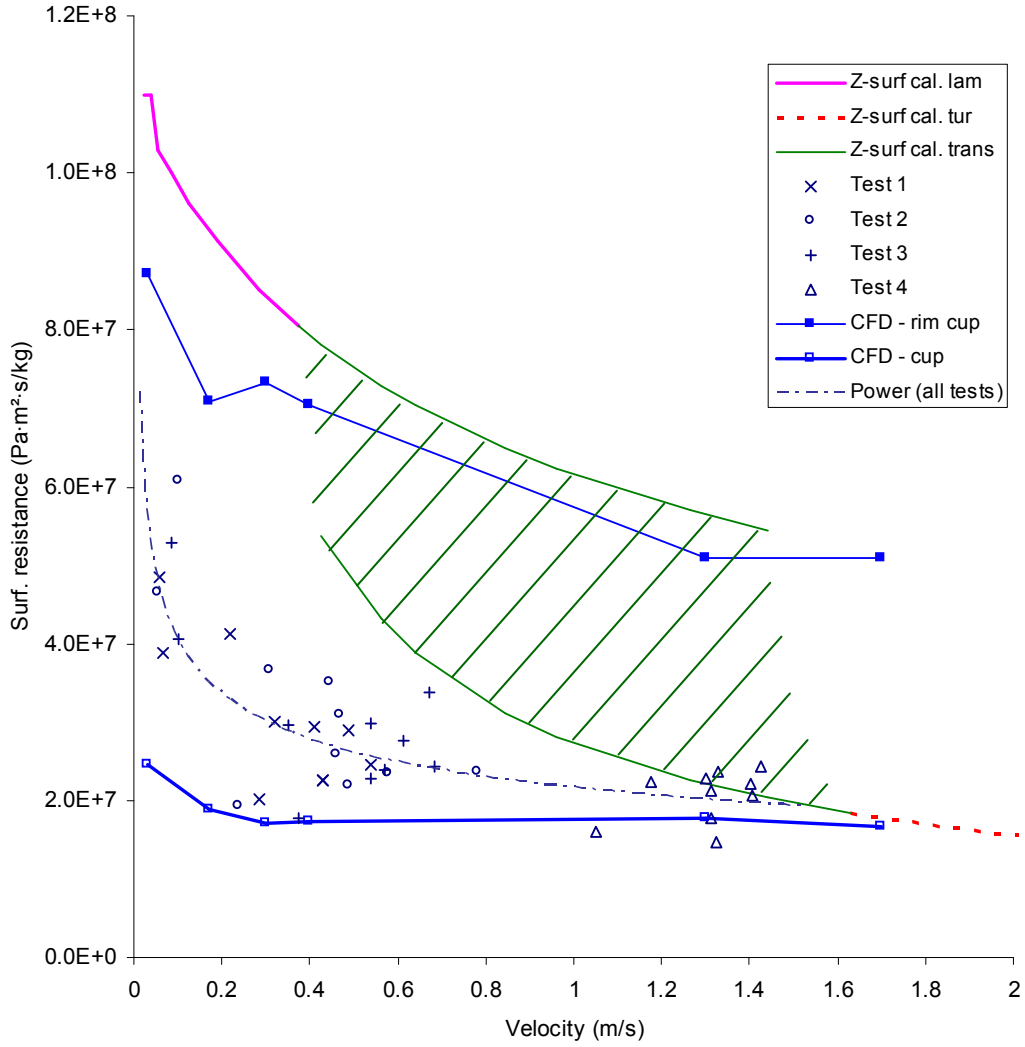

Figure 3.2 *Water vapour surface resistances, estimated, measured and simulated. The calculated theoretical values are separated in 3 parts, laminar, transition and turbulent. The transition part is hatched and between the laminar and turbulent boundary*

It was possible to determine the surface resistances of moisture transfer by measurements on samples with different thicknesses by use of dry cup experiments. The results showed that the surface resistances decrease for increasing airflow velocity above the boundary layer of the material surface. This was expected since the theoretically estimated surface resistances also show that the resistance increases with decreased airflow velocity. As seen in Figure 3.2 the surface resistances were also calculated based on numerical simulation of the surface heat transfer coefficients. The 3D model had the same geometry as the test cup facility. An example of the results is shown in Figure 3.3. The simulation showed that the velocities on the sample surfaces were dependant on the sample position because holes in the lower Perspex plate for wet cup positioning and a metal bar that separates the two Perspex plates disturbs the flow. The results in Figure 3.2 show that the measured resistances are somewhat smaller than the ones theoretical estimated but higher than the results of the CFD simulation. The measured and simulated results showed the same pattern. **Paper II** gives further details of the experiments and CFD simulation.

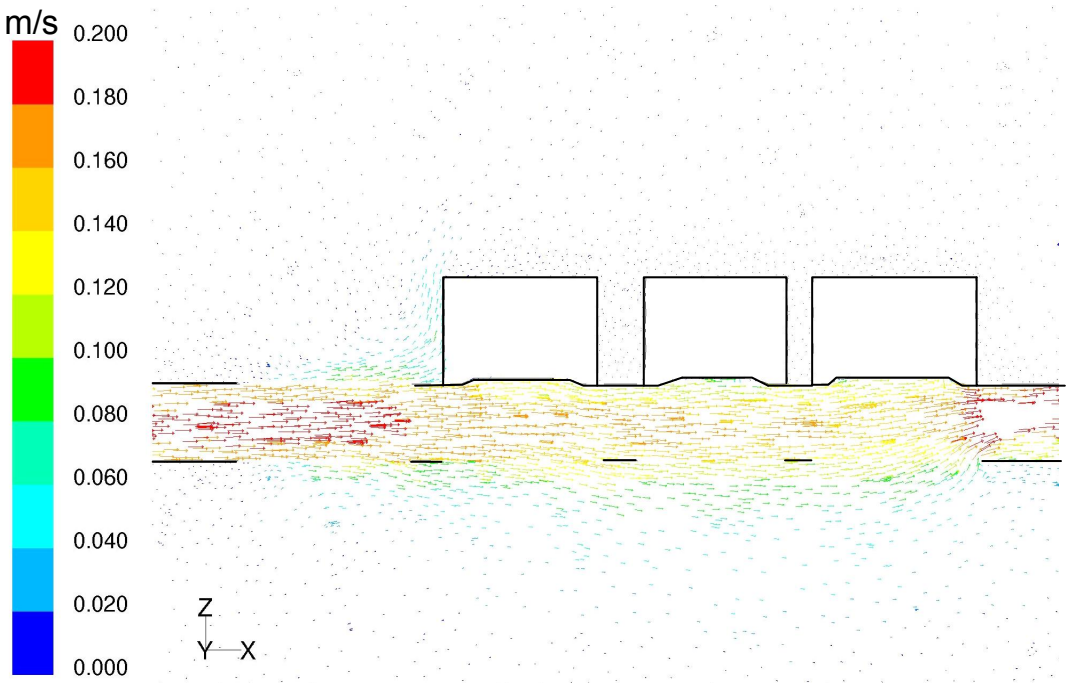

Figure 3.3 *Simulated airflow velocities in the duct when the inlet velocity is 0.17 m/s. The velocity is uniform until the cup area is reached*

3.1.2 Petri dish cups

The experiments were extended with the development of a Petri dish cup method for field measurements of surface resistances. The Petri dish cup tests are also described in **Paper II** and again the applied method was the one proposed in the Japanese standard JIS A 1470-1:2002. The Petri dish cup test concept should represent a method that can easily be performed in the field and can give reliable information of the water vapour surface resistances in microclimates. The idea is to have a simple applicable method that only requires a few basic materials, like a balance, Petri dishes, desiccant, desiccator for storage of the assembled Petri dish cup in until they are used. To test the concept some initial tests was performed in a controlled environment. The Petri dishes were filled with desiccant and closed with 1, 2 or 3 layers of paper that were taped firmly to the rim of the cup. The cups were then placed in a desiccator until they were installed in their measuring position. The Petri dish cups were set up in an experimental climate chamber as it is seen in Figure 3.4.

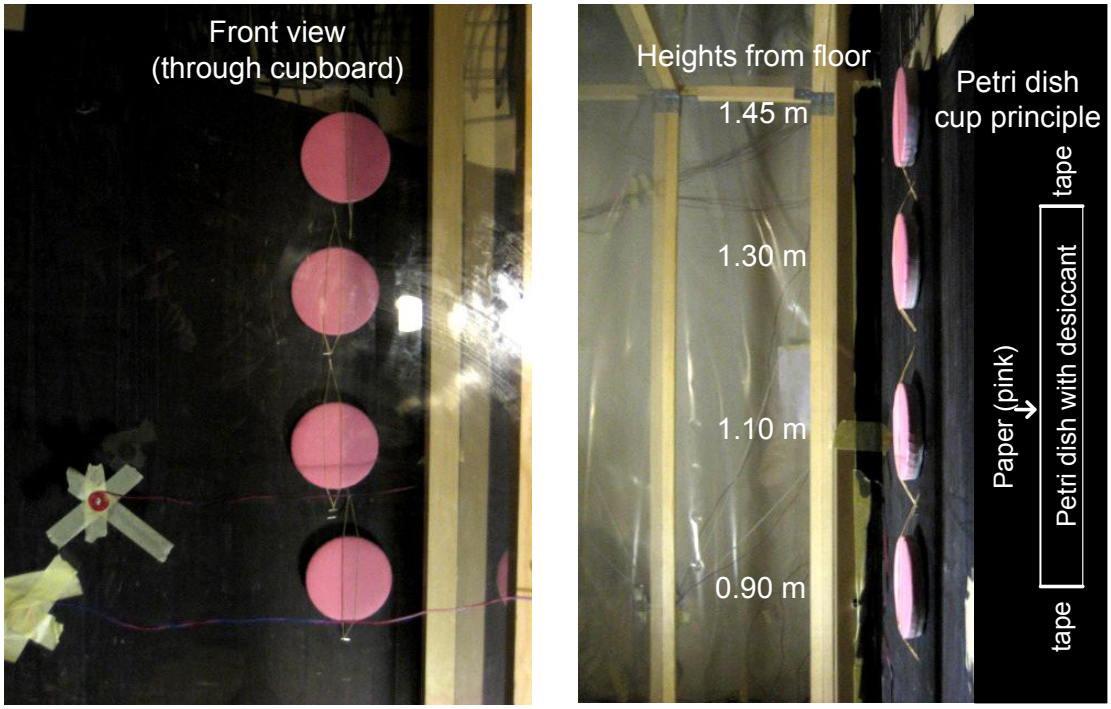

Figure 3.4 *Pictures of Petri dish cups placed vertically on the chilled wall with the paper facing the furniture (plexiglass box). The principle of the Petri dish cups can be seen at the right. The cup positions in terms of height from the floor is also provided*

The climate chamber was also used for the PIV measurements and thus more details of the room can be found in **Paper IV**. Inside the room there was a chilled wall that should imitate a poorly insulated exterior wall in a winter period and at a 5 cm distance to this wall an imitation of a cupboard is placed. The cupboard imitation was made from plexiglass sheets since the PIV measurements needed optical access. The narrow air gap behind the furniture represents a hygrothermal microclimate where the Petri dish cups were tested (see Figure 3.4). The cups were placed vertically on the chilled wall surface with the paper facing the furniture. Paper is relatively open to vapour diffusion and therefore the cups needed to be dismantled and weighed at minimum every hour to register the rate of diffusion. The high diffusion rate means that the measurements can be performed in a couple of hours, which is beneficial for field tests. The results of the initial test are given in Figure 3.5 where the diffusion resistance is plotted as a function of layers of paper. The surface resistances, Z_s are found as the intercept with no layers. It was found that the concept is promising but it needs to be developed and tested further.

3.1.3 Importance of moisture surface resistance

An investigation by Roels and Janssen (2006) illustrated a significant influence of the surface moisture transfer coefficient on the moisture buffering by materials. Their findings support the importance of knowing the actual surface resistances, which justifies the need for a field test method like the Petri dish cup method.

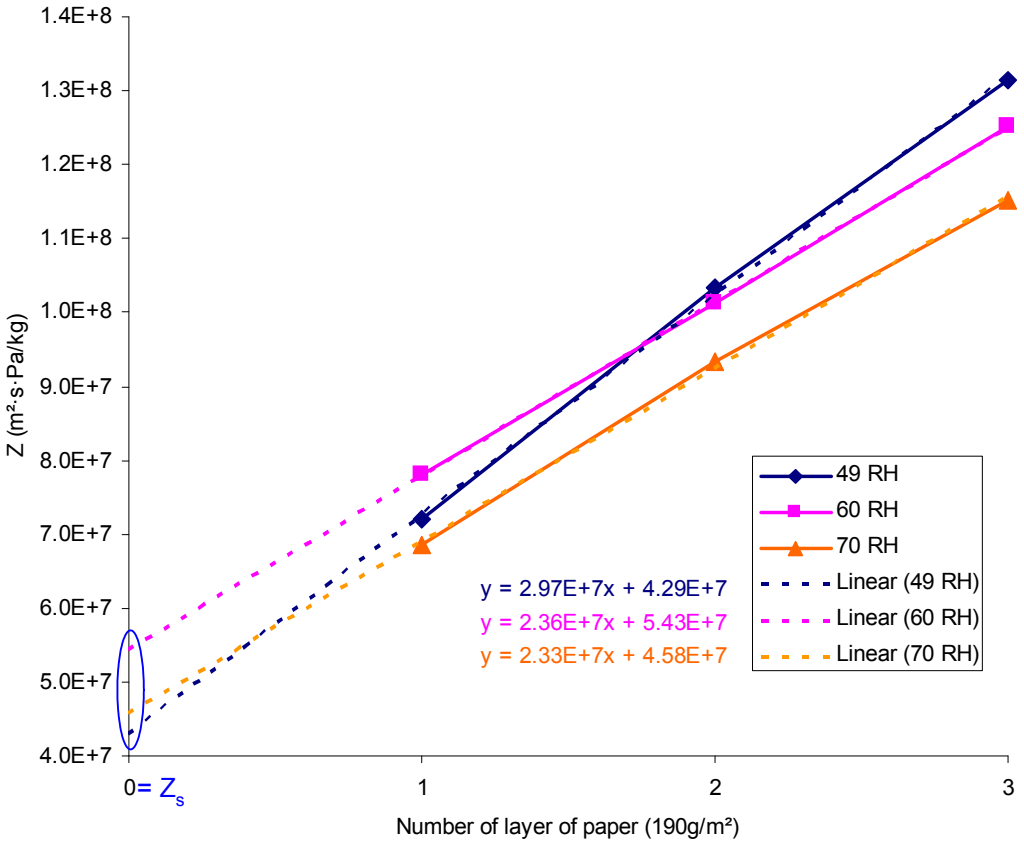

Figure 3.5 *Results of Petri dish cup tests. Diffusion resistances plotted as a function of the number of material layers. Data from 3 measurements are presented. The difference between the measurements is the relative humidity at the sample surface*

3.2 Natural convection

Buoyancy forces drive the flow when heated air rises. This is caused by density differences and gravitation. Flows driven by buoyancy forces are called natural convection, free convection or buoyant convection. The phenomenon of natural convection is experienced ubiquitously in daily life like rising cigarette clouds or campfire smoke. Density differences can also be caused by composition gradients and therefore moist air will rise due to lower density of the water vapour present in the air. The velocities associated with natural convection are relatively small and usually less than 2 m/s (Mills, 1995).

Natural convection is often found in dwellings. However, forced convection effects can be superimposed from ventilation by opening windows or fresh-air intakes. But this will not prevent the occurrence of natural convection in microclimates. This makes the determination of airflow patterns in room a difficult task. Another difficulty is imposed by turbulence characteristics, which evolve from the presence of surfaces. This poses a link between the airflow patterns in rooms and the surfaces that will affect the boundary layer conditions. Navier-Stokes equations must be solved to determine airflow patterns.

Computational Fluid Dynamics (CFD) models are characterised by solving the Navier-Stokes equations, which predict the airflow conditions in rooms. These are combined with conservation of mass, momentum and energy that give temperature, velocity and pressure fields. The benefit of using CFD models is that they can provide detailed information about the airflow patterns in the entire room. This also means that e.g. the surface heat transfer coefficients at walls will differ with the actual position. This is very important since microclimates are defined as local areas where the climate varies from that of surrounding areas due to a variety of influencing factors like surface heat transfer coefficients, temperature and humidity. In CFD models the internal surface conditions are usually given as boundary conditions. The CFD models are usually not used to predict heat and moisture conditions in the building envelope that surround the rooms. Therefore, part of this project is an attempt to model moisture transport in both room air and in adjacent constructions with a CFD approach. Where other models have focused on either air and moisture flows in rooms or on heat and moisture transfers in walls, the model described in **Paper III** is intended to combine the detailed modelling of both, i.e. to include the moisture transfers in both air and the surrounding building envelope.

3.3 Measurements

It is very difficult to measure boundary layer flow. The reason is that most techniques for measuring velocity have problems when applied in the vicinity of a wall. The proposed method is to use hot wire anemometers but special care is required for the use and calibration. The problem of using anemometers is that they intrude the flow and their response is influenced by cooling effects from the wall.

Another option is to use optical methods such as Laser-Doppler-Anemometry (LDA) or Particle Image Velocimetry (PIV).

LDA is a technique for measuring the direction and speed of fluids by crossing of two monochromatic laser light beams in the fluid flow. This method has not been used because it is not a scope of the project to measure the boundary layer flow but rather to investigate the general flow in a microclimate.

The principle of the PIV technique is to compare digital images of a fluid flow. Tracer particles are added to the fluid (air) and they will reflect light from an imposed laser light sheet.

These methods do not intrude on the flow, but their disadvantages are that they are non-continuous (so if there are fluctuations, the peak values may not be registered); they need an even distribution of seeding particles in the shear layer close to the wall; and the wall may reflect the laser light, which will corrupt the signal.

The PIV technique has been used in the current work but the purpose was not to measure the boundary layer but more generally to measure the airflow in a microclimate composed of a narrow air gap. The measurements are described in **Paper IV**, and the principle of the measurements will be described in Chapter 4, Case studies.

Chapter 4

Case studies

The numerical and experimental investigation in this work is based on case studies. Thus, it was important to choose a case study that characterise one of the many microclimates seen in ordinary dwellings. The case study must also represent a critical area in the indoor environment. Since mould growth is an easily recognizable indicator for critical microclimates this was used to select the considered options. It was found that mould growth is often caused by moisture from the foundation, in corners and near other thermal bridges and behind furniture filled with clothing and placed against an external wall. In the last mentioned case the occupant has a couple of possibilities to affect the microclimate merely by changing the furniture position, which made this case particularly interesting. Hence, it was chosen as a case study.

The chosen case study, with furniture placed close to a poorly insulated wall, is often observed in bedrooms in dwellings, where the moisture production during the night is relatively high due to respiration of occupants. The temperature of the internal wall surface can be 5-8 °C colder than the room temperature. The temperature difference has a huge impact on the RH level. If as an example a temperature difference of 6°C is assumed and the average room air humidity is 55 % RH at 22°C, then the RH in the microclimate will be 80 % RH at 16°C. This RH level could easily cause problems.

It is expected that the furniture limits the airflow near the wall, and the lack of warm room air near the surface will decrease the surface temperature even more, which can cause problems. This is combined with a high moisture production rate from sleeping persons during night and the concern is that it may lead to critical conditions. The lower temperature in the microclimate causes increased relative humidity and the outcome can be biological growth.

4.1 Initial CFD-studies

During the project the case study was first investigated by CFD. In the investigation the focus was on the airflow pattern near a cold wall caused by the placement of the furniture and the moisture distribution. In the study the size of the furniture was 0.45 x 1.0 x 1.6 m^3 in a room of 2 x 2 x 2 m^3, see Figure 4.1. The furniture was placed in the corner so 3D simulations were performed. First the impact of different boundary

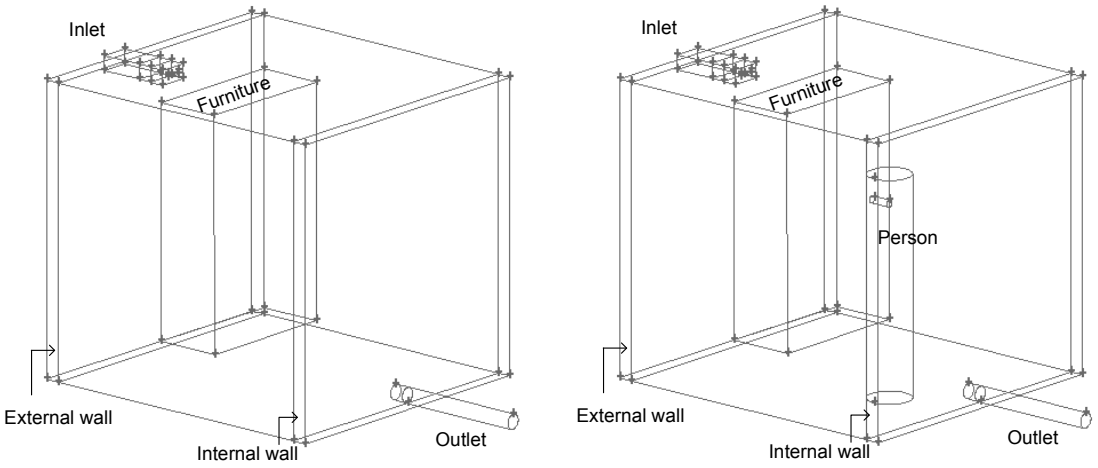

Figure 4.1 *The investigated geometries in the initial studies. The furniture is 50 mm above the floor The difference between the shown geometries is that in the right case a person is added as an extra moisture source.*

conditions was investigated and then the effect of having or not having a distance between the furniture and wall or floor.

The main purpose of the investigation was to see a combined effect of moisture and airflow changes in the microclimate behind the furniture. Figure 4.2 illustrates these results for one case in the set-up that includes a person as a heat and moisture source. In the shown case the furniture is placed directly on the floor.

The results in Figure 4.2 show that the moisture levels differ in the room. From the depiction of the velocity vectors it is seen that turbulence occurs near the surfaces. It also shows that even though the furniture is placed directly on the floor there will be a downwards flow caused by buoyancy. The downward flow is only possible if air flows out trough the sides of the air gap. Generally, it was found that different

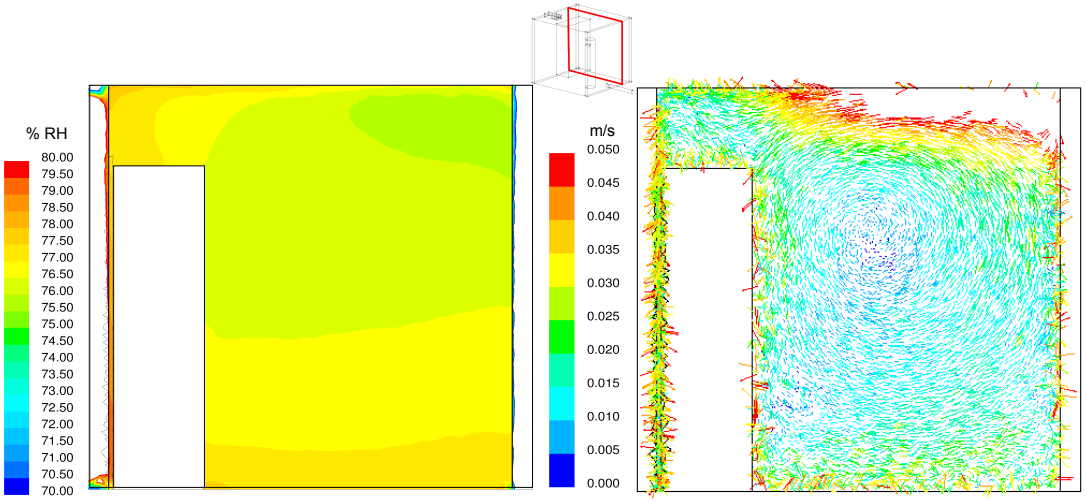

Figure 4.2 *Results planes for a case where the distance between the furniture and the wall is 2 cm and the furniture is placed directly on the floor. The left part show the relative humidities and the right show vector velocities*

placement of furniture near cold external walls may affect the relative humidities in the microclimate mainly due to temperature differences. Another finding was that the ventilation inlet conditions are important due to its controlling effect on the general airflow patterns in the room (**Paper III**).

4.2 Experimental investigation: Room with a chilled wall

The next step was to extend the examination of the case study with an experimental investigation. The main purpose of the experiment was to investigate the airflow pattern in the air gap behind the furniture. Particle Image Velocimetry (PIV) is an easy way to measure and visualize flows. Therefore, the PIV technique was used to capture instantaneous 2D vectors of the flow field by use of a laser and a special camera. As in the initial simulations several cases were studied with different air gap sizes between the furniture and wall or floor was investigated. The distance between the furniture and the floor was an imitation of furniture elevation from the floor by use of legs as support (**Paper IV**).

4.2.1 Principle of Particle Image Velocimetry

PIV can be used to obtain an instantaneous visualization of the measured flow field. The principle is to use a digital camera to take two images within a very short time period and compare them. The flow that needs to be measured must contain tracer particles that can reflect light. The reflections are caused by a laser light sheet that acts as a flash. The particle reflections will be seen as small spots that are brighter than the fluid they follow. The result is an image as shown in Figure 4.3.

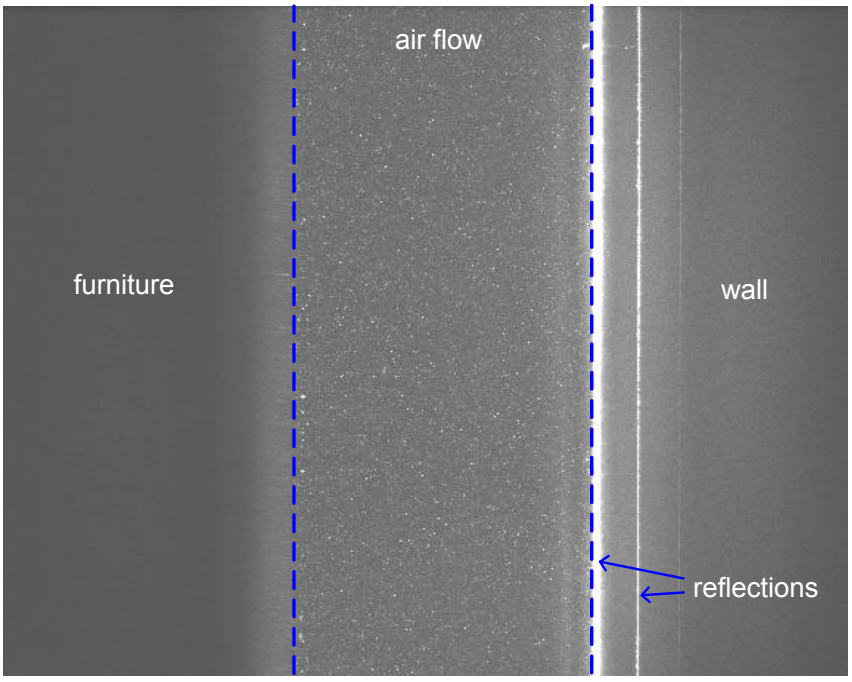

Figure 4.3 *Instantaneous image taken by PIV. All the spots are the reflections of the tracer particles. The white lines in the right are unintentional reflections from the wall surface*

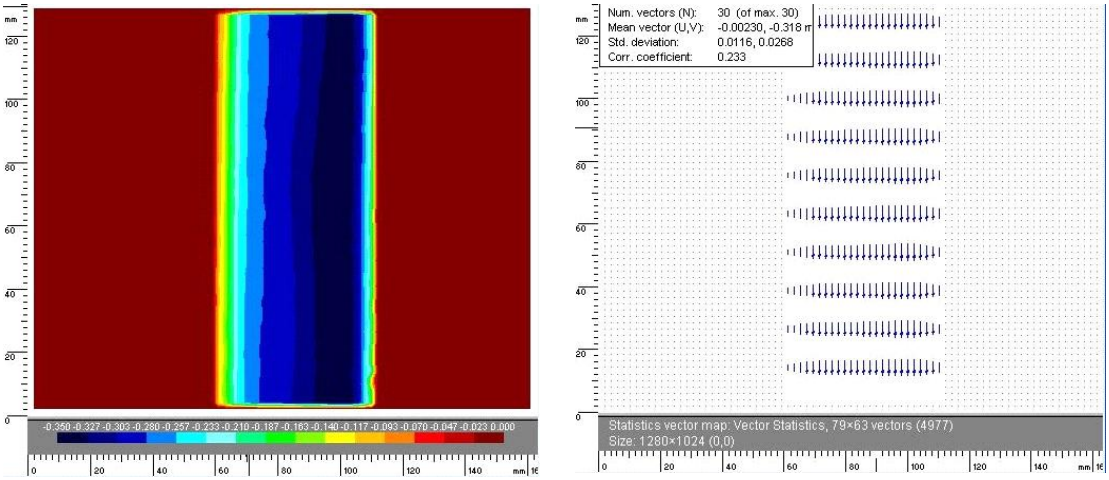

Figure 4.4 *Images after post-processing the instantaneous velocity vectors, vector statistics of 30 image pairs is used. The left part represent a scalar image where the velocities are shown by colours – the dark blue is the fastest. The right part depict average velocity vectors in the gap, only every 10th is shown*

The time interval between two images must be short enough to ensure that most of the particles recorded in the first image can be recovered in the second. A computer triggers both the camera and the laser so the camera is recording at the exact moment the laser sheet is illuminated and the time between two images is well defined. The information of the distance each particle travels between two images in combination with the time interval between the images provides velocity vectors.

The post-processing procedure includes masking of the images so velocity vectors are calculated only in the air gap where the flow evolves. Masking is also used to remove reflections since these will cause significant errors. The results are then cross-correlated in smaller sub-sections of the image to find the average value for the displacement that leads to a vector map of velocities. At last vector statistics is made from 30 image pairs. Figure 4.4 is given as an example of the vector presentation after post-processing of the images.

The PIV measurement technique is described in detail in **Paper IV**.

4.2.2 Experimental set-up

Inside a test chamber of 3.6 x 6.0 x 3.6 m³, a room was created with internal dimensions of 3.6 x 4.5 x 2.5 m³. A chilled internal wall was built in the chamber, and a plexiglass box was positioned against the chilled wall to imitate a piece of furniture standing at an external wall in a real building. An air gap behind the plexiglass furniture allowed room air to pass the chilled surface and this was meant to replicate a microclimate found in ordinary dwellings.

The imitation of the exterior wall was made of a wooden structure covered by plain gypsum board. The dimensions of the chilled wall were 2.3 x 0.5 x 2.5 m³. In the set-up the laser light sheet needs to pass the furniture, which therefore had to be transparent. Hence, it was made of plexiglass mounted on a wooden frame structure. The dimensions of the furniture were 1.5 x 0.46 x 2.0 m³ and it is shown in Figure 4.5.

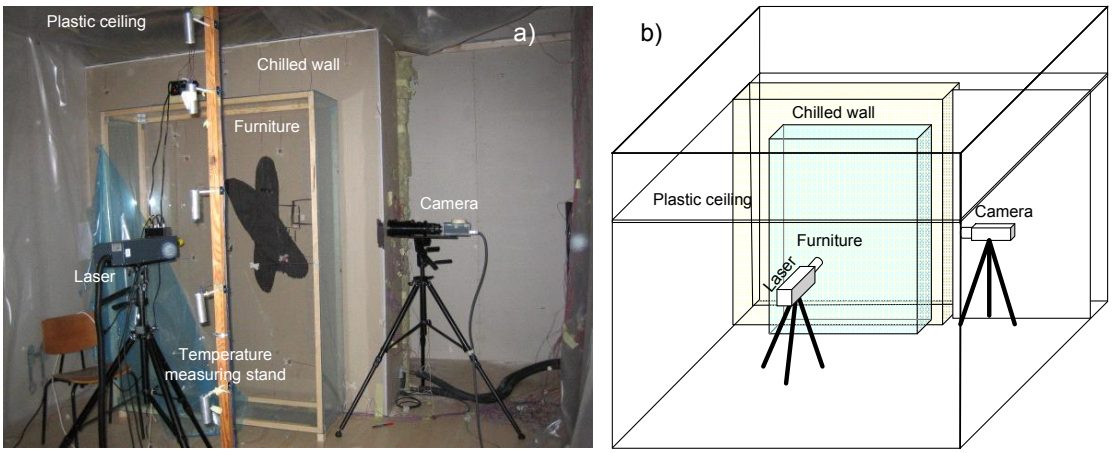

Figure 4.5 *The experimental set-up, where the camera points into the air gap between the chilled wall and the furniture and the laser sheet is pointed in through the plexiglass furniture. a) A picture of the experimental set-up. b) A diagram of the PIV set-up*

The measured cases have 2 different distances between the furniture and the wall in combination with 3 different distances between the furniture and the floor. The surface temperature of the chilled wall behind the furniture was constantly 16°C and the average room temperature was 22°C for all measurements. This presents a temperature difference of 6°C. In Table 4.1 the different distances between the furniture and floor or chilled wall are given. With a view from the laser the distance between the furniture and the wall was kept constant at 400 mm.

The two dimensional flow fields were measured from 7 different positions by the camera and the laser (A-G). The physical image height was on average 130 mm with a width of maximum 50 mm, which is the maximum gap size the flow was measured in. The positions of the camera and laser are absolute and described in Table 2 and illustrated in Figure 4.6.

Table 4.1 The different tested positions of the furniture.

Furniture position	Gap (mm) furniture - floor	Gap (mm) furniture - chilled wall
1	0	25
2	0	50
3	50	25
4	50	50
5	100	25
6	100	50
7	200	25
8	200	50

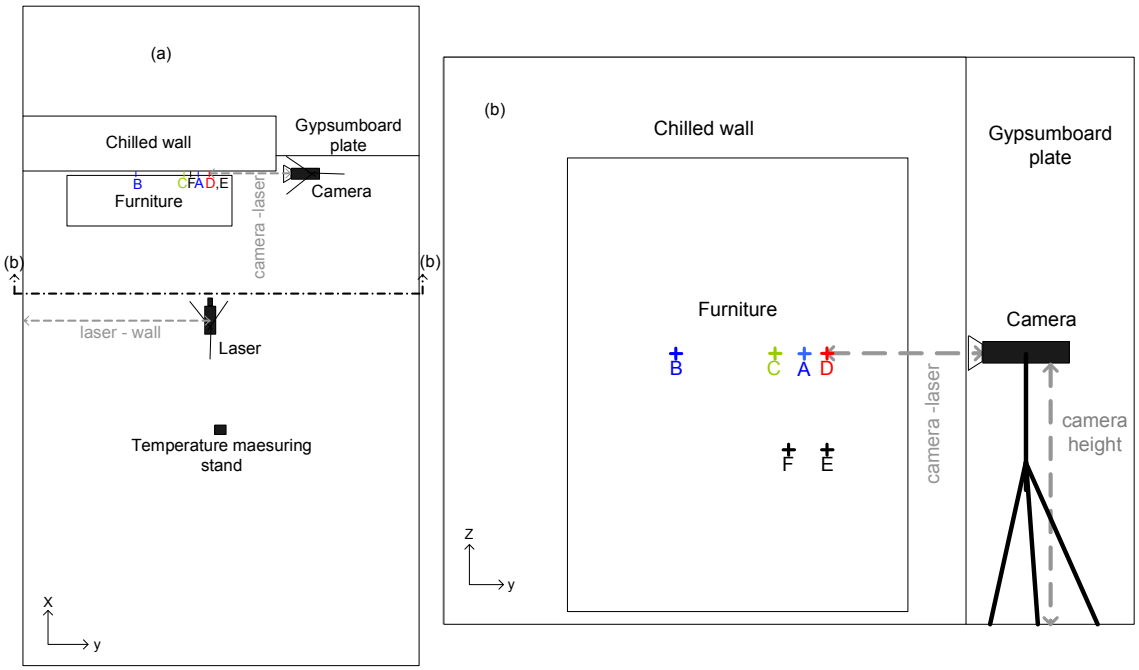

Figure 4.6 *Part (a) shows a plan of the measured PIV set-up and (b) shows a front view of the room. The letters A-F show the measuring positions given in Table 2. The distance between the camera and the laser sheet is shown for measuring position D*

Table 4.2 Description of different measuring positions with the PIV equipment. The physical image size changes with distance between camera and laser. The image widths are reduced to 25 or 50 mm depending on gap size.

Measurement position	Distance (mm) camera - laser	Image height (mm)	Camera height (mm)	Laser height (mm)	Distance (mm) laser – wall	Furniture positions investigated
A	1050	124	1183	1192	1570	1-8
B	1420	187	1183	1192	1000	3-4
C	1200	136	1183	1192	1440	3-6
D	920	106	1183	1192	1670	1-8
E	930	113	770	760	1670	3-4
F	1080	130	770	760	1500	1-8

4.2.3 Results of PIV experiments

The 2D PIV results showed that the flow rate is increased when the gap is expanded from 25 mm to 50 mm. Figure 4.7 shows an example of the results at measuring position A.

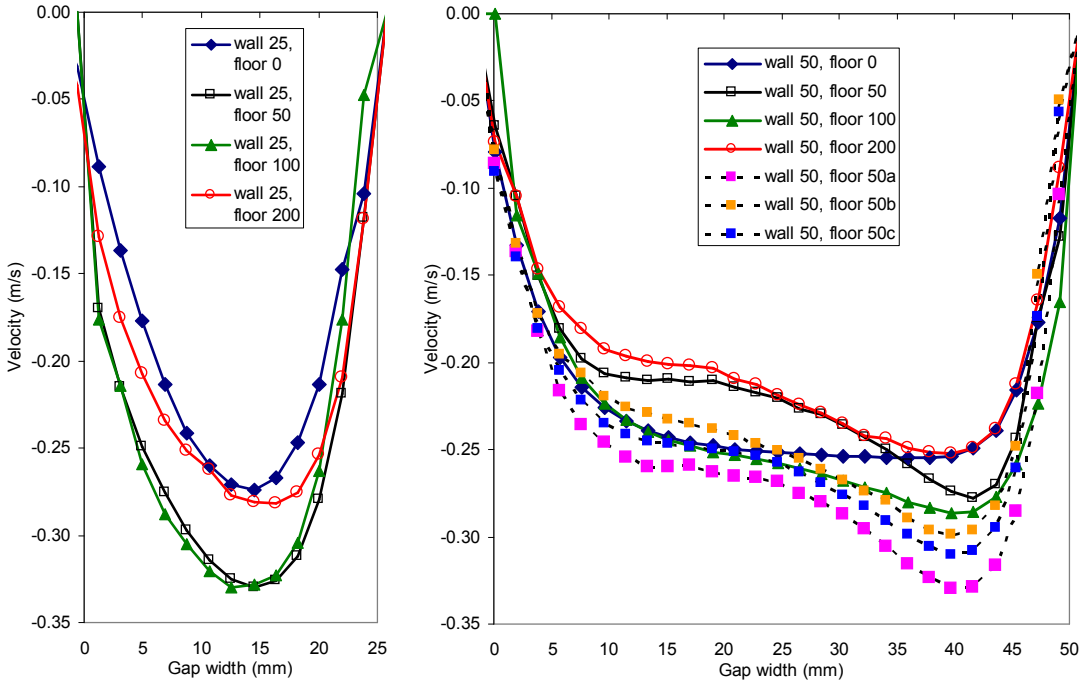

Figure 4.7 *Measured velocities at position A for the 8 furniture positions. The left part shows the odd furniture positions and the right the even positions. The velocities were measured 4 times for a distance of 50 mm to both chilled wall and floor. For both parts of the Figure the furniture is placed at x = 0 mm gap width*

The results show that the narrow gap of 25 mm has higher velocities than the 50 mm gap. But calculation of the flow rates (see **Paper IV**) showed that these were higher for the 50 mm air gap. The shape of the velocity profiles are not the same for the two gap widths. The 25 mm gap has a parabolic shape, which is similar to what Aung et al. (1972) have predicted analytically. In the 50 mm air gap the shape indicates that the density changes near the chilled wall is dominating the flow. Furthermore, there is an indication of higher flow rates if the furniture leg height is less than 200 mm but elevated from the floor (**Paper IV**).

4.3 Comparison of measured and simulated cases

The last investigation of the case study is performed by CFD simulations. A 3D model of the same setup as used for the PIV measurements is used for the simulations (**Paper V**). The simulations are made with a commercial CFD tool (Fluent, 2003). Obstacles as furniture in the indoor environment are known to cause turbulence and therefore the simulation includes a viscous turbulence model. The turbulence model was combined with an enhanced wall treatment because this two-layer model will assure that when the grid is fine enough, the laminar sub-layer will be solved and for walls with coarser mesh a blending between the viscosity affected region (boundary layer) and the outer region (free flow) is performed. The main interest was to investigate the flow behind the furniture, and by use of an unstructured mesh it is possible to create a denser grid in specific regions without adding extra cells in other

areas, and thus an unstructured grid was used for the discretization. A coarser mesh was used in the main part of the room (~400,000 cells) and this was refined behind the furniture (with extra ~700,000 cells), and especially at the measuring positions behind the furniture (an extra ~400,000 cells). Figure 4.8 gives an example of the comparison between the measured and simulated results.

When the results of the PIV measurements are compared to the CFD simulation, a good correlation has been found for a 50 mm air gap. The results from the narrower 25 mm gap are less convincing. The shape of the velocity profiles is fairly well predicted by the model but for the narrow air gap the velocity levels are significantly lower. When furniture is placed directly on the floor the airflow is also estimated as lower than the results of the PIV measurements showed. It is expected that the underestimated values for the narrow gap is due to influence from radiation between the surfaces. The simulations did not use a radiation model since initial tests showed that the influence was very little but the initial test were made for a 50 mm air gap. Therefore, it will be interesting to include radiation in the simulation. This will require that the discretization strategy is changed since the radiation models cannot be included when adaptation of the grid is used. The results are described in detail in **Paper V**.

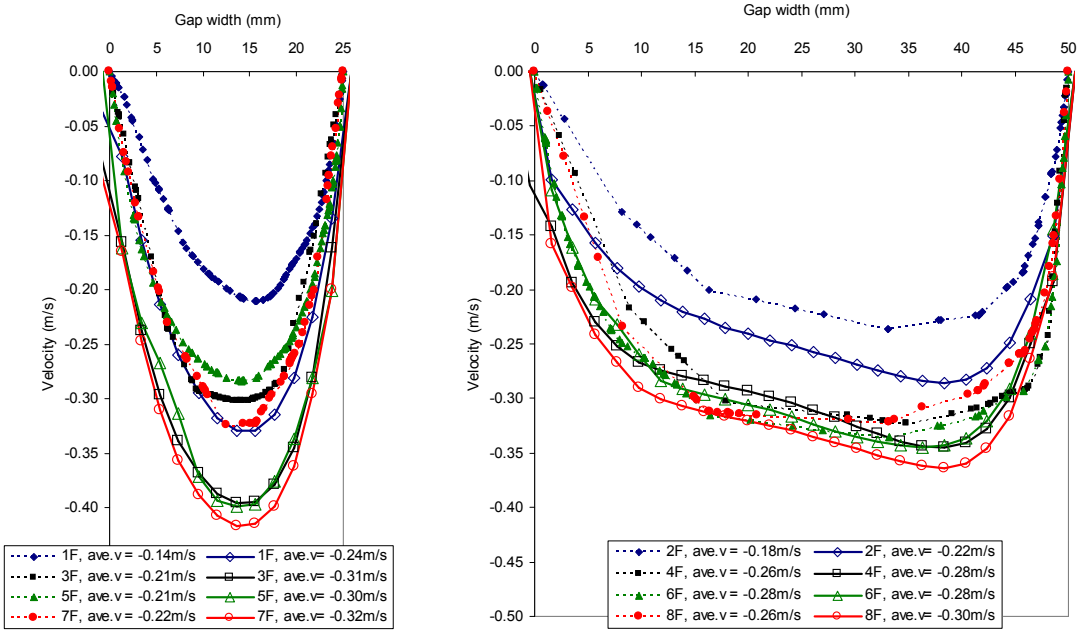

Figure 4.8 *Comparison of measured and simulated velocities in the 25 mm (left) and 50 mm (right) in measuring position F. The furniture surface is at x = 0 mm. The full lines are measured velocities and the dotted simulations. In the legend the calculated average velocity is given*

Chapter 5

Discussion

This thesis work has investigated microclimates based on two methods; experiments and numerical modelling. This chapter gathers and discusses the major findings and gives an outlook to the future on this research topic.

The purpose of the current work has been to investigate the hypothesis, that comprehensive moisture modelling can make it possible to predict the hygrothermal microclimatic conditions of surfaces in specific microclimates.

In the current project, microclimates are defined as local areas on internal surfaces of the building envelope. There is a lack of knowledge about, how these areas are affected by the overall airflows in rooms. The importance lies in how the coefficients for surface heat transfer and moisture exchange depend on the local airflow velocity at the surface. In this project the moisture surface resistances were examined experimentally, and the results showed that they increase for lower velocities, which was expected based on analytical investigations. However, it was found that the measured surface resistances were lower than those calculated theoretically. The measured values were also compared to results from numerical CFD simulations, where the surface heat transfer coefficients were converted to surface resistances, but these surface resistances were found to be even lower than the measured values. This indicates that the surface resistances may by overestimated theoretically, but it also shows that numerical CFD simulation may underestimate the effect.

The moisture surface resistance will influence the apparent moisture buffer capacity of materials, and thereby influence the hygrothermal conditions in microclimatic loci. As mentioned in Chapter 3, Roels & Janssen (2006) conducted a numerical sensitivity study of which factors influence the apparent moisture buffering capacity. They found that moisture buffering abilities will be affected by even small changes in moisture surface resistances, and that the proportions between the moisture buffer capacities of different materials may change. The surface resistances found in this project were in the range $1.5 – 6.0 \cdot 10^7$ Pa·m^2·s/kg. Roels and Janssen found that by varying the moisture surface resistance from 1.0 to $5.0 \cdot 10^7$ Pa·m^2·s/kg, the apparent moisture buffer capacity for a material like wood fibre board changed from 2.20 to 1.86 g/m²·%RH, and thus should be considered to be significant. It must be mentioned that the error of the cup measurements may be higher than the measured surface resistances, but due to the number of measurements that all show the same characteristic, the measured values seem significant. However, the findings still stress

that the moisture surface resistance may be an important factor that will be interesting to investigate in microclimates.

To investigate vapour surface resistances in microclimates in the field a Petri dish cup method was developed. Some first tests were performed but more results are needed to evaluate the performance of the design.

Another investigation in this work was the airflows in a microclimate that are also influenced by the overall room airflow. Particle Image Velocimetry (PIV) measurements were used to investigate the influence of different furniture positions on the airflow rates and velocities. The measurements were performed in an air gap behind a piece of furniture placed near a poorly insulated wall. In all 8 different furniture positions were measured and all results showed very streamlined downwards flow, which was expected due to buoyancy. The PIV measurements gave 2D velocity vectors of the airflow in the gap, and the horizontal velocities could also be found and they were merely 2 % of the vertical values. Evidence of amplified airflow rates was found when the furniture was elevated from the floor by legs and the flow increased even more if the width of the air gap was enhanced. Some measuring positions showed that too high furniture leg heights may decrease the flow rate. This result is interesting but further investigation is needed. Another aspect is the increased focus on modelling investigations where the airflow measurements will be very useful, since they provide data that can be used to validate models.

The modelling aspect was also a very important part of this project, so numerical modelling of the same geometrical set-up as used for the PIV measurements was performed. The results showed excellent conformity for a 50 mm air gap. For a 25 mm air gap width the shape of the estimated velocity profiles were similar to the measured, but the level of the velocities was about half. Currently, this difference cannot be explained, so further investigations are needed. One of the factors that may influence the results is the fact that no radiation model was used in the numerical simulation model.

As stated in the hypothesis the purpose of the project has been to investigate, if comprehensive moisture modelling can make it possible to predict the hygrothermal microclimatic conditions of surfaces in specific microclimates. These microclimates will be influenced by airflow conditions in room as already presented, this called for Computational Fluid Dynamics (CFD) modelling. Therefore, a commercial CFD code (Fluent, 2003) was used to implement vapour transport in walls, which is usually not included in CFD models. This was done by an immobile fluid wall approach.
Initial case study investigations were used to show, that CFD modelling can reveal detailed heat and moisture distributions in room. The differences between global and local values showed that there is a potential for using CFD models for microclimatic investigations in indoor environments and especially near internal surfaces. However, the results of the immobile fluid wall implementation, still needs to be validated by comparison of measured data.

5.1 Future work

The purpose of this thesis work was to provide new knowledge about hygrothermal interactions in microclimates. But to give final answers more questions need to be addressed.

Further investigations are recommended for use of CFD modelling of rooms with complex geometries as furnished dwellings, which may help to predict the hygrothermal conditions in microclimates. In the current work an approach to implement vapour diffusion in walls within the CFD domain is proposed. However, there is still a great need for further investigations and validation.

If the inclusion of vapour diffusion in walls can be validated, this can be expanded to include e.g. condensation and suction. It will also be interesting to include a radiation model because this should give more accurate modelling of temperatures in rooms in general. Humidity is very temperature dependant, so it may impact the moisture conditions in the microclimate. Investigation of other microclimates in rooms will also be interesting. This may include other cases in form of geometry, moisture sources and airflow conditions like different ventilation schemes. An import extension could be to perform transient simulations, which will give the opportunity to include moisture buffering.

The immobile fluid wall approach is integrated directly in a CFD environment, which may be very important for further development. The reason is that analysis on rough grids may be more efficient than coupling to external HAM models. This stresses that further development of the method is both promising and interesting for obtaining an efficient modelling tool that can predict hygrothermal conditions in microclimates.

In order to rely on model results, thorough validation is needed and the simulated results will never be better than the data supplied as boundary conditions. Therefore, there is still a great demand for further experimental investigation in a wide range of areas like material properties, advanced measurements of heat, air and moisture parameters in both small and full scale.

The developed Petri dish cup design will also need to be tested further to have a proper evaluation. The method should help to reveal vapour surface resistances in microclimates in field investigations.

Chapter 6

Conclusion

One of the main scopes of this thesis was to establish a model that can predict the hygrothermal microclimate on the interior surfaces of the building envelope. The complexity of indoor environments made this a difficult task. This was illustrated by humidity in buildings, which affects both the indoor air quality, mainly in form of relative humidity in the air, and the moisture content in surfaces of building materials, constructions and furnishing elements. These moisture interactions also affect the hygrothermal conditions in microclimates, so the presented model needed to predict different conditions in the room. While conventional HAM-models usually represent e.g. indoor air as one node, the strength of a CFD models is their ability to simulate local effects. Therefore, such a model was used. The numerical simulation studies were performed on two related case studies that represented critical microclimates.

A relationship between the airflow velocities at material surfaces and their effect on the moisture surface resistance were also investigated, both by experiments and numerical simulations. These results showed that the vapour surface resistance increases for low airflow velocities and that theoretical calculation overestimate the surface resistances. Opposed, numerical CFD simulation underestimates the surface resistance.

It was shown that a method of using immobile fluid walls can be implemented directly in the CFD environment. Numerical simulation confirmed that the method can be used to investigate microclimates on internal surfaces of the building envelope. However, validation of the approach is still needed but the results are promising. To gain better results, more development is also needed like implementation of a radiation model.

Another main scope of the thesis was to perform measurements that reveal airflow velocities near surfaces. Particle Image Velocimetry (PIV) was used to obtain 2D velocity vectors of the flow in an air gap between a poorly insulated external wall and furniture placed near it. It was found that the velocities were developing down through the air gap. The measured data constitute a basis for validation of airflows in microclimates estimated by numerical simulation.
The measured PIV data was used in comparison to numerical simulated results. This showed that numerical simulations can predict the airflow velocities in air gaps. The best estimation was found for a gap width of 50 mm whereas a more narrow 25 mm gap showed too low simulated velocities. The deviation is not accounted for, but may

be partly related to the fact that radiation was not included in the used model. This however, needs further investigation.

The general purpose of the PIV measurements was to study effects on the airflow from different furniture positions in a case study investigation. As expected, it was found that the velocities in the air gap were reduced when the furniture was placed directly on the floor. A wider 50 mm gap showed an increased airflow rate behind the furniture compared to a 25 mm gap. This result was replicated both in the measurements and the numerical simulation. In addition, it was found that the airflow velocity was higher for a narrow 25 mm gap in the measurements, while the numerical simulation did not show the same tendency. An interesting result of the measurements was that the flow velocity seemed to decrease when the furniture had legs of 200 mm height for two of the measuring positions. This could be due to increased turbulence but, this also needs further investigation.

The overall conclusion of the thesis is that it is possible to determine local airflow velocities and heat and moisture distributions in microclimates by numerical CFD modelling. However, further work is needed in form of validation to measured data and development of the model for it to account for other transport mechanisms. Development is also needed to have an easier implementation with less user-programming since this decrease the numerical performance of the numerical solver.

References

Andersen, I., Lundqvist, G.R., Jensen, P.L., Proctor, D.F. (1974). Human response to 78-hour exposure to dry air. Arch Environ Health 29, 319-324.

ASHRAE 2005 Handbook of fundamentals, SI Units, Atlanta: American Society of Heating, Refrigerating and Air-Conditioning Engineers, Inc.

Aung, W. (1972). Fully developed laminar free convection between vertical plates heated asymmetrically, International Journal of Heat and Mass Transfer 15, 1577-1580.

Bartak, B., Beausoleil-Morrison, I., Clarke, J.A., Denev, J., Drkal, F., Lain, M., Macdonald, I.A.., Melikov, A., Popiolek, Z. and Stankov, P. (2002). Integrating CFD and building simulation. Building and Environment, 37(8-9): 865-871.

Berglund, L. G. (1998). Comfort and humidity, ASHRAE Journal, 40 (8), 35-41

Bornehag, C.-G., Blomquist, G., Gynteberg, F., Järvholm, B., Malmberg, P., Nordvall, L., Nielsen, A., Pershagen, G. and Sundell, J., 2001, Dampness in building and health, review article, Indoor Air, 11 72-86.

Clarke, J A, Johnstone, C.M., Kelly, N.J., McLean, R.C., Anderson, J.A., Rowan, N.J. and Smith, J.E. (1999). A Technique for the Prediction of the Conditions Leading to Mould Growth in Buildings, Building and Environment, 34(4): 515-521.

Clausen, G., Rode, C., Bornehag, C.-G. and Sundell, J. (1999). Dampness in building and health. Interdisciplinary research at the International Centre for Indoor Environment and Energy, proceedings of the 5th Symposium on Building Physics in the Nordic Countries, Göteborg, Sweeden

Cunningham, M.J.(1996). Controlling dust mites psychrometrically - a review for building scientists and engineers, Indoor Air, 6(4), 249-258.

EN ISO 12572:2001. Hygrothermal performance of building materials and products – Determination of water vapour transmission properties. European committee for standardization. Brussels

Fang, L., Clausen, G., Fanger, P.O. (1998a). Impact of temperature and humidity on perception of indoor air quality during immediate and longer whole-body exposures. Indoor Air 8, 276-284.

Fang, L., Clausen, G., Fanger, P.O. (1998b). Impact of temperature and humidity on the perception of indoor air quality. Indoor Air 8, 80-90.

Fang, L., Clausen, G., Fanger, P.O. (1999). Impact of temperature and humidity on chemical and sensory emissions from building materials. Indoor Air 9, 193-201.

Fanger, P.O. (1983). Air humidity, comfort and health. Proceedings of XV International Congress of Refrigeration, Paris, Vol. V.

Fanger, P.O. (2006). What is IAQ?, Indoor air, 16 (5), 328-334.

Fanney, A.H., Thomas, W.C., Burch, D.M. and Mathena, L.R. (1991) Measurements of moisture diffusion in building materials, ASHRAE Trans. 97 (2) 99-113.

Fluent Inc. (2003). FLUENT® User's Guide, Lebanon, NH, USA: Fluent Inc.

Fox, R.W. and McDonald, A.T. (1994). Introduction to fluid mechanics, 4th edition, John Wiley & Sons, Inc., United States of America, chapter 9.

JIS A 1470-1:2002. Test method of adsorption/desorption efficiency for building materials to regulate an indoor humidity – Part 1: Response method of humidity. Japanese Industrial Standard, translated and published by Japanese Standard Association.

Harderup, L-E., 1998, Hygroscopic moisture of the indoor air considering non-stationary phenomena. Synthesis of publications for the period 1979-1998. In Swedish. Department of Building Physics, Lund University, Report TVBH-3033.

Hens, H., 2003, Whole building heat, air and moisture response (MOIST-ENG). Proposal for a new annex; International Energy Agency, EXCO Energy Conservation in Buildings and Community Systems. Department of Civil Engineering, KU-Leuven, Belgium.

Hohota R. (2003). Moisture modelling in a CFD code (low velocity in large enclosure). Comparison with experiments. (in French) PhD thesis, Laboratoire CETHIL INSA de Lyon, France

Holm, A. and Künzel, H.M. (2006). Experimental investigation of the hygric buffering capacity of wood based interior panelling, in proceedings of the 3rd International Building Physics Conference, Montreal, Canada, p. 3-9.

Holm, A., Künzel, H.M. and Sedlbauer, K. (2003). The Hygrothermal Behaviour of Rooms: Combining Thermal Building Simulation and Hygrothermal Envelope Calculation. Eighth International IBPSA Conference, Eindhoven, the Netherlands, p. 499-505.

Kalagasidis (2004), HAM-Tools - An integrated simulation tool for heat, air and moisture transfer analyses in building physics, PhD thesis, Chalmers University of Technology

Korsgaard, J. (1979). The effect of the indoor environment on the house dust mite. In: P.O.Fanger and O.Valbjørn (eds): Indoor Climate. Copenhagen, Danish Building Research Institute, 187-205.

Künzel, H. (1960). Die ‘‘klimaregelnde Wirkung’’ von Innenputzen, Gesundheits-Ingenieur, 81(7): 196–201.

Mills, A.F. (1995). Heat and mass transfer, Irwin, ISBN 0-256-11443-9 pp. 269-275.

Mitamura, T., Rode, C. and Schultz, J., 2001, Full scale testing of indoor humidity and moisture buffering in building materials, ASHRAE Conference, IAQ’01.

Mortensen, L. H., Rode, C. & Peuhkuri, R.(2005) Full scale tests of moisture buffer capacity of wall materials. Proceedings of the7th Nordic Symposium on Building Physics, Reykjavík, Vol. 2, 662-669.

Negrão, C.O.R. (1998). Integration of computational fluid dynamics with building thermal and mass flow simulation. Energy and Buildings, 27(2): 155-166.

Nusselt, W. (1930). Wärmeübergang, Diffusion und Verdunstung, Z. f. angew. Math. und Mech. Bd. 10, H. 2, 105-121.

Ojanen, T.and Salonvaara, M., 2003, A method to determine the moisture buffering effect of structures during diurnal cycles of indoor air moisture loads. Research in Building Physics,eds. Carmeliet, Hens & Vermeir , Lisse: Swets & Zeitlinger, ISBN 90 5809 565 7, pp.353-361.

Padfield, T., 1998, The role of absorbent materials in moderating changes of relative humidity, Department of Structural Engineering and Materials, Technical University of Denmark, Report R-054.

Peuhkuri, R., 2003, Moisture dynamics in building envelopes, Department of Civil Engineering, Technical University of Denmark, Report R-071.

Plathner P. and Woloszyn, M., 2002, Interzonal air and moisture transport in a test house. Experiment and modeling. Buildings and Environment, 37, pp. 189-199.

Reinikainen, L.M., Jaakola, J.J. K. (2003). Significance of humidity and temperature on skin and upper airway symptoms. Indoor Air 13, 344-352

Rode, C., 2003. Nordtest Workshop on Moisture Buffer Capacity –Summary Report. DTU, Lyngby, Denmark. August 21-22, 2003.

Rode, C. and K. Grau. Whole-building Hygrothermal Simulation Model. In: ASHRAE Transactions - American Society of Heating Refrigerating Air-Conditioning Engineers. 2003, 109 (1).

Rode, C., Gudum, C., Weitzmann, P., Peuhkuri, R., Nielsen, T.R., Kalagasidis, A.S. and Hagentoft C.-E. (2002) *International Building Physics Toolbox.* General report. R-02:4. Gothenburg: Chalmers University of Technology, Department of Building Physics. Available on www.ibpt.org

Rode, Carsten; Peuhkuri, Ruut Hannele; Mortensen, Lone Hedegaard; Hansen, Kurt Kielsgaard; Time, Berit; Gustavsen, Arild; Ojanen, Tuomo; Ahonen, Jarkko; Svennberg, Kaisa; Arfvidsson, Jesper; Harderup, Lars-Erik (2005). Moisture Buffering of Building Materials, in series: BYG Report (ISBN: 87-7877-195-1) pages: 78, Department of Civil Engineering, Technical University of Denmark.

Roels, S. and Janssen, H. (2006). A Comparison of the NORDTEST and Japanese Test Methods for the Moisture Buffering Performance of Building Materials, Journal of Building Physics, 30(2), 137-161.

Simonson, C.J., 2000, Tapanila ecological house, VTT Building technology, Technical research centre of Finland.

Simonson, C.J., Salonvaara, M. and Ojanen, T., 2001, Improving indoor climate and comfort with wooden structures, VTT Building and transport, Technical research centre of Finland.

Steeman, H-J., T'Joen, C., Willockx, A., De Paepe, M. and Janssens, A. (2006). CFD Modelling of HAM transport in buildings: Boundary conditions, in Proceedings of the third International Building Physics Conference. Research in Building Physics and Building Engineering / Ed. Fazio, P ; Ge, H ; Rao, J ; Desmarais, G. - The Netherlands : Taylor & Francis /Balkema, p. 535-542.

Steeman, H-J., Janssens, A., De Paepe, M. (2007). About the use of the heat and mass analogy in building simulation, in Proceedings of the twelfth Symposium for Building Physics, Dresden.

Svennberg, K. (2003). Determination of Moisture Properties for Materials Exposed to the Indoor Air, Report TVBH-3042 Lund 2003, Department of Building Physics - Licentiate thesis

Svennberg, K. and Harderup, L-E. 2002. Time-dependent moisture properties for plasterboard with surface coating. Indoor air 2002.

Svennberg, K., Lengsfeld, K., Harderup, L-E., Holm, A. (2007). Previous experimental studies and field measurements on moisture buffering by indoor surface materials, Journal of Building Physics 30 (3), 261-274.

Teodosiu, C., Hohota, R., Rusaouën, G. and Woloszyn, M. (2003). Numerical prediction of indoor air humidity and its effect on the indoor environment. Building and Environment 38(5): 655-664.

Toftum, J., Jørgensen, A.S., Fanger , P.O. (1998). Upper Limits for Indoor Air Humidity to Avoid Uncomfortably Humid Skin. Energy and Buildings 28, 1-13

Toftum, J. and Fanger, P.O. (1999). Air humidity requirements for human comfort, ASHRAE Trans., 105(2): 641-647.

Woloszyn, M., Peuhkuri, R.H., Mortensen, L.H. & Rode, C. (2005) IEA Annex 41, Subtask 1 - Modelling principles and common exercises, Proceedings for 26th AIVC conference, Brussels

Worch, A. (2004). The behaviour of vapour transfer on building material surfaces: The vapour transfer resistance, Journal of Thermal Envelope & Building Science 28 (2)187-200.

Wyon, D.P. , Fang, L., Meywe, H.W. , Sundell, J., Weirsøe, C.G., Sederberg-Olsen, N., Tsutsumi, H., Agner, T. and Fanger, P.O. (2002). Limiting Criteria for Human Exposure to Low Humidity Indoors. Proceedings Indoor Air

Zhia, Z., Chen, Q., Haves, P. and Klems, J.H. (2002). On approaches to couple energy simulations and computational fluid dynamics programs. Building and Environment, 37(8-9): 857-864.

Zhia, Z. and Chen, Q. (2003). Solution characters of iterative coupling between energy simulation and CFD programs. Energy and Buildings, 35(5): 493-505.

Bibliography

Journal papers

Mortensen, L. H., Wolozsyn, M., Rode, C. & Peuhkuri, R. (2007) Investigation of microclimate by CFD modelling of moisture interactions between air and constructions, Journal of Building Physics, 30 (4), 279-315, http://dx.doi.org/ 10.1177/1744259106075233

This paper combines the two conference papers concerning the same topic.

Mortensen, L. H., Rode, C. & Peuhkuri, R. (2007) Determination of Moisture Surface Resistance Using Cup Experiments, currently unpublished, submitted for publication

The publication is an expansion of the conference paper concerning the same topic. The extension concerns CFD modelling of airflows and Petri dish cup tests to reveal surface resistances in microclimates.

Mortensen, L. H., Rode, C. & Peuhkuri, R. (2008) Investigation of airflow patterns in a microclimate by Particle Image Velocimetry (PIV), Building & Environment, 43 (11), 1929-1938, http://dx.doi.org/10.1016/j.buildenv.2007.11.012

Presentation of PIV measurements performed at DTU in autumn 2005 in collaboration with a Belgium exchange Master student, Jeff Mertens. The measurements are taken in a microclimate between an exterior wall and a piece of furniture.

Conference papers

Svennberg, K., Hedegaard, L. & Rode, C. (2004). Moisture Buffer Performance of a Fully Furnished Room. *Proceedings of the 9th International Conference on Performance of the Exterior Envelopes of Whole Buildings.* Clearwater beach, FL, USA.

In collaboration with Kaisa Svennberg from Sweden and Carsten Rode we performed moisture buffer experiments in the Passys test cell at DTU. We wanted to mimic an office room since the size of the test cell corresponds to a single office. The test materials were ordinary office furniture sponsored by IKEA, Sweden with an expansion of curtains, books, paper piles and waste paper in the waste basket. The investigation provided knowledge of the moisture buffer performance of a fully furnish room. The experimental period ran from Dec. 2002 till Dec. 2003.

Mortensen, L. H., Rode, C. & Peuhkuri, R.(2005) Full scale tests of moisture buffer capacity of wall materials. *Proceedings of the7th Nordic Symposium on Building Physics, Reykjavík,* Vol. 2, 662-669.

This publication is a result of the interest in the moisture buffer capacity measurements that was performed as my Master project. These results had not been published in English before.

Mortensen, L. H., Wolozsyn, M., Peuhkuri, R. & Rode, C. (2005) Investigation of microclimate between wall and furniture with CFD. *Proceedings of the 7th Nordic Symposium on Building Physics, Reykjavík,* Vol. 2, 687-694.

This paper concerns the CFD modeling work done after the research stay in France. The moisture source in the room is now mimicked by a person.

Mortensen, L. H., Wolozsyn, M., Hohota, R. & Rusaouën, G. (2005) CFD modelling of moisture interactions between air and constructions, in proceeding of the *9th International Building Performance Simulation Association Conference, Montreal*, Vol. 2, 801-808.

This paper is a result of my research stay at CETHIL, Lyon, France. After the conference the authors were invited to expand it for a special issue of Journal of Building Physics.

Mortensen, L. H., Rode, C. & Peuhkuri, R. (2006) Effect of airflow velocity on moisture exchange at surfaces of building materials, in proceedings of the *3rd International Building Physics Conference, Montreal,* 187-191.

The basis of the current paper is water vapour permeability test performed in the cup test facility at DTU, summer 2005. The performed tests were dry cup experiments on 1 or 2 layers of heavy paper (190 g/m²), which can reveal the surface resistance.

Woloszyn, M., Peuhkuri, R.H., Mortensen, L.H. & Rode, C. (2005) IEA Annex 41, Subtask 1 - Modelling principles and common exercises, *Proceedings for 26th AIVC conference, Brussels*

The paper is based on the modelling exercises in IEA annex 41 where 2 of the co-authors are the subtask leaders.

Mortensen, L.H., Rode, C. & Peuhkuri, R. (2008) Impact of furnishing on room airflows, *Proceedings of the 8th Symposium on Building Physics in the Nordic Countries (C. Rode, editor)* Report R-189, Dept. of Civil Engineering, Technical University of Denmark, Kgs. Lyngby, Denmark, 2008, 323-330

This paper present a comparison of PIV measurements performed at DTU in autumn 2005 with numerical simulation of similar cases.

Other papers and publications

Peuhkuri, R., Rode, C., Padfield, T., Hansen, K.K., Hedegaard, L. (2003) *Moisture distribution in absorbent insulation.* Report SR-03-11. Department of Civil Engineering, Technical University of Denmark (in Danish)

When working as a research assistant in April 2003 my primary task was to prepare an extended summary in Danish for the above report for the Danish Energy Agency

Rode, C., Peuhkuri, R. & Hedegaard, L. (2003) *DTU Contribution to IEA Annex 41.* Start up meeting of IEA Annex 41 (Whole Building Heat, Air and Moisture Response MOIST-ENG), Leuven, Belgium

Shared presentation for all authors of the possible DTU contribution to IEA Annex 41.

Hedegaard, L., Rode, C. & Peuhkuri, R.(2004) *DTU PASSYS Facilities.* 1st working meeting of IEA Annex 41 (Whole Building Heat, Air and Moisture Response MOIST-ENG), Zurich, Switzerland

A short presentation of the Passys test facility at DTU. The facility can monitor the heat and moisture changes in an office size room, and imitate moisture production and ventilation.

Hedegaard, L., Woloszyn, M. & Rausaouën, G.(2004) *Moisture interactions between air and constructions modelled with CFD.* 2nd working meeting of IEA Annex 41 (Whole Building Heat, Air and Moisture Response MOIST-ENG), Glasgow, Scotland

A short presentation of the first try of CFD modelling with immobile fluids as walls.

Hedegaard, L., Rode, C. & Peuhkuri, R.(2005) *Effect of airflow velocity on moisture exchange at surfaces.* 4th working meeting of IEA Annex 41 (Whole Building Heat, Air and Moisture Response MOIST-ENG), Trondheim, Norway

A presentation of cup experiments performed at DTU, summer 2005. The purpose was to use different sample thicknesses to give the moisture surface resistance. Both wet and dry cup experiments were reported.

Hedegaard, L., Rode, C. & Peuhkuri, R.(2005) *Investigation of airflow patterns in microclimates with Particle Image Velocimetry(PIV).* 4th working meeting of IEA Annex 41 (Whole Building Heat, Air and Moisture Response MOIST-ENG), Trondheim, Norway

The experimental setup for PIV measurements was presented. This includes description of the exterior wall that is imitated by a cooled gypsum wall and a cupboard that was imitated by a plexiglass box so the transparency needed for the PIV equipment was achieved.

Rode, Carsten; Peuhkuri, Ruut Hannele; Mortensen, Lone Hedegaard; Hansen, Kurt Kielsgaard; Time, Berit; Gustavsen, Arild; Ojanen, Tuomo; Ahonen, Jarkko; Svennberg, Kaisa; Arfvidsson, Jesper; Harderup, Lars-Erik (2005). Moisture Buffering of Building Materials, in series: BYG Report (ISBN: 87-7877-195-1) pages: 78, Department of Civil Engineering, Technical University of Denmark.

The final report of the NORDTEST project, *Moisture buffering of building materials.* The report presents a developed definition of standardized quantity to characterize moisture buffering in form of a NORDTEST method.

Paper I

Moisture buffer performance of a fully furnished room

Svennberg, K., Hedegaard, L. and Rode, C. (2004)

Published in the *Proceedings of the 9th International Conference on Performance of the Exterior Envelopes of Whole Buildings.* Clearwater beach, FL, USA.

Moisture Buffer Performance of a Fully Furnished Room

Kaisa Svennberg **Lone Hedegaard** **Carsten Rode, Ph.D.**
Member ASHRAE

ABSTRACT

The moisture buffer capacity of hygroscopic materials can be used to moderate the relative humidity of indoor air as well as moisture content variations in building materials and furnishing. Since moisture plays a significant role in the development of many processes that affect the quality of the indoor air, such as growth of house dust mites, emissions from materials, and mold growth, it is anticipated that the moisture buffer effect can help to ensure healthier indoor environments.

Building materials, as well as furniture and other furnishing materials exposed to indoor air, will contribute to the moisture buffer capacity of rooms. Few studies have been made on the impact of furnishing materials in comparison with traditional building materials. This paper will present such a study conducted in a full-scale climatic test cell.

A series of experiments have been carried out in the test cell to show the moisture buffer performance of various furnishing objects. The objects will be exposed to cyclic humidity variations as in an inhabited indoor environment, and the response of the indoor humidity will be followed over time. It will be a step-by-step investigation starting with an empty room and going toward a fully furnished room. Comparisons are made with previous studies covering traditional building materials and calculations.

The study shows that the furnishings have to be included in the understanding of the moisture buffering performance of a room and that more material data in this area is needed.

INTRODUCTION

We spend most of our lives indoors and the primary purpose of designing buildings is to ensure good indoor environments for the occupants. This is obtained by interactions between the outdoor conditions, the building envelope, and the occupants. The thermal conditions are already recognized as being important, but moisture is still not considered to be an essential part of building design. In a hygrothermal approach, moisture buffer performance will play an important role. The interactions mean that the surface materials, which are capable of functioning as moisture buffers, are in contact with the indoor air. This study was initiated to increase the knowledge about the interaction between the indoor air and the moisture buffering surface materials. One reason for a growing interest in this topic is a widespread concern for indoor air quality, which to some extent is determined by the level and fluctuations of the humidity of the indoor air (Bornehag et al. 2001). The progress within hygrothermal and energy modeling is another reason for the growing interest in the moisture buffering issue. A literature survey conducted by Harderup (1998) has shown that in order to develop hygrothermal calculation models further, there is a need for a better understanding of the moisture buffer performance of a room, including furniture and furnishings, and more data are also needed concerning moisture properties of the surface materials used in the indoor environment.

Surface materials exposed to variations in the surrounding climate will absorb moisture when the relative humidity (RH) increases and desorb moisture when the RH decreases. This process is referred to as moisture buffering and is to a large extent due to the material composition and structure and to the surface treatment of the material. The moisture buffer capacity of the surface materials in the indoor environment

Kaisa Svennberg is a Ph.D. student in the Department of Building Physics at Lund Institute of Technology, Lund University, Sweden. **Lone Hedegaard** is a Ph.D. student and **Carsten Rode** is an associate professor in the Department of Civil Engineering and the International Center for Indoor Environment and Energy at the Technical University of Denmark.

will help to minimize the daily variations of RH in the air, which result from the activities of the occupants and the operation of HVAC systems. Both the surfaces of the inside of the building envelope, such as ceilings, floors, and walls, as well as the furniture and other furnishings, have an impact on the moisture conditions in the room. For example, Plathner and Woloszyn (2002) have shown that the correlation between simulated and measured moisture conditions of the indoor air is much better if the sorption of interior surface materials is taken into account.

One benefit of avoiding peaks of high RH is to decrease the risk of condensation on cold surfaces and thereby prevent biological growth. If the RH variations are held within 30% and 60% RH, the growth of allergenic or pathologic organisms can be minimized (ASHRAE 2001). Another advantage is that air with a lower relative humidity will be perceived as being fresher (Toftum and Fanger 1999) due to the increased cooling of the mucous membrane and thereby the increased well-being of inhabitants in the indoor environment. Moist air can also increase the pollutant emissions from materials in contact with indoor air, such as, for example, paints (Fang et al. 1999). These emissions should be avoided in order to keep a good air quality in the indoor environment since work efficiency decreases with rise in air pollution.

The moisture buffer performance is influenced by several material properties—e.g., moisture capacity, water vapor permeability, and the period time of the variations—and today there is no single parameter used to express the moisture buffer performance. A NORDTEST project to deal with this question has been initiated (Rode 2003) and work will be continued to define the moisture buffer performance and to develop standardized measuring methods.

Also, the ventilation and the microclimate influence the moisture buffering performance of the room. The impact of the ventilation depends on the ventilation rate and the vapor content of the indoor and outdoor air. If the ventilation rate is very high, it will control the RH of indoor air to a very high degree. If, on the other hand, the ventilation rate is low, the impact of moisture buffering in surface materials is larger (Christoffersen 1996). The ventilation rate will govern the mean level of RH in the indoor air, and the moisture buffer performance will affect the amplitude of the RH variations. It should be noted that moisture buffering in materials could never replace ventilation, since ventilation also removes heat and sensory and chemical pollution and provides clean air.

To understand the hygrothermal behavior of real rooms is a huge task, which requires a lot of field data and experience about how it can be modeled. Furthermore, the moisture buffer performance is of relevance in many countries worldwide and is much influenced by local climates, the building traditions, and how buildings are used and conditioned in different countries.

Previous research has also been concerned with the moisture buffer performance. In earlier studies the moisture buffer capacity of several materials has been investigated on a small scale (Padfield 1998; Mitamura et al. 2001; Svennberg and Harderup 2002; Peuhkuri 2003; Ojanen and Salonvaara 2003). In Finland, the moisture buffer capacity of a bedroom was studied in an ecological building without vapor retarder (Simonson 2000; Simonson et al. 2001). In the first investigation it was found that the highest peak humidity in the bedroom could be reduced by up to 20% RH, and the humidity during the winter months could be increased by up to 10% RH. The second investigation concerned the same room exposed to weather data from four different cities, and buffer materials were found to have most impact in a moderate climate such as Scandinavia, and, furthermore, the buffer effect of hygroscopic thermal insulation was strongly reduced when it was not directly exposed. In a comparison between calculations and measurements in a test house, Plathner and Woloszyn (2002) showed that taking into account the impact of the moisture buffering of the surface materials gave a better correlation between measurements and calculations.

The topic of moisture buffer performance has become a part of a newly started international research project, "Whole Building Heat, Air and Moisture Response," which is Annex 41 of the International Energy Agency's (IEA) Energy Conservation in Buildings and Community Systems Programme (Hens 2003). As an IEA activity, it also has the scope to illustrate how a better understanding of the overall hygrothermal behavior of buildings can lead to better energy performance, e.g., by inventing optimized strategies for ventilating, heating, and cooling that take the overall hygrothermal reality of buildings into account.

Most previous research have been conducted on unfurnished rooms, even if the furniture and furnishings of a room to a high extent cover the traditional building materials (Harderup 1998). The scope of this investigation has been to conduct a full-scale experiment with a fully furnished room under well-controlled conditions.

MATERIALS IN THE INDOOR ENVIRONMENT

Materials used in the indoor environment are a heterogeneous group of materials, from heavyweight concrete used in the building construction to lightweight textiles found in furniture and furnishings.

To ensure durability, facilitate cleaning, and/or for esthetical reasons, the materials of the indoor environment are often surface coated. The surface coatings are often based on polymers, e.g., latex paint, wax, and plastic films. In the indoor environment, surface coatings vary from sparse oil treatments to thick and almost impermeable enamel paints. The moisture resistance of a surface coating is dependent on the material used and the application. If there is a "heavy" surface coating on the top surface of furniture, e.g., a wooden table, usually the bottom will be untreated. The furnishing and furniture also hide the building materials of the building envelope. Therefore, an estimation of the accessibility of indoor air to the potential moisture buffer areas has to be included in an estimate of the moisture buffer performance.

In a preliminary study, Berggren and Skoog (2003) made an inventory of the surface materials present in a dwelling and an office. The comparison between the two buildings showed that in the office, a larger part of the surface materials had a surface coating, and in the dwelling, more untreated wood and textile materials were present (see Figure 1).

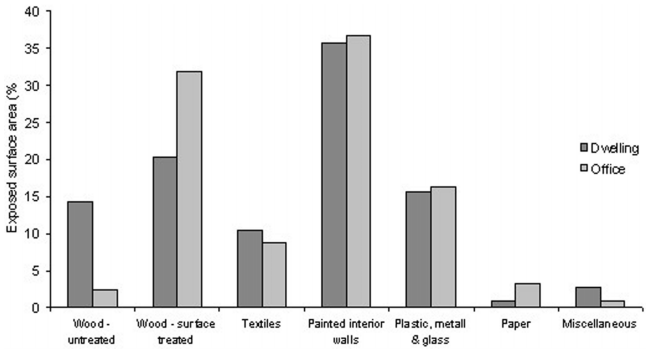

Figure 1 *Surface materials—a comparison between a dwelling and an office.*

In this study we have concentrated on furniture and furnishings. The materials present in the experiment, as listed in Table 1, were wood with different surface coatings, plastic, textiles, and paper.

TEST CELL AND EQUIPMENT

The experiments were performed in an airtight and moisture-tight test room. The test facility consists of a highly insulated steel box standing on pillars with an indoor floor area of 13.8 m^2 (149 ft^2) and room height of 2.75 m^2 (9 ft), giving a volume of 38.0 m^3 (1340 ft^3). The test cell consists of two rooms, a test room and a service room. The walls are insulated with 0.40 to 0.50 m (16 to 20 in.) of polystyrene and mineral wool and are covered with steel sheets on both the inside and the outside. An exception to this is the south wall, which is exchangeable. During the later experiments the south wall consisted of (from the outside) a wooden cladding, 0.30 m (12 in.) of mineral wool, 0.11 m (4.3 in.) of brick wall, and a polyethylene foil on the inside to provide a vapor-tight and non-absorbing interior surface. A picture and a diagram of the test cells are shown in Figures 2 and 3.

Table 1. Materials Present in the Experiment

Furnishing	Material	Surface Area m^2	Thickness m	Volume m^3	Weight kg
Writing desk	Melamine on all surfaces, except wood fiberboard on underside	2.56	0.034	0.041	10.24
Table legs	Wood	0.46		0.007	3.50
Room divider	Two thin sheets of wood fiberboard with 30 12 mm holes and an air cavity in between	1.04	0.038	0.018	4.12
Low plate on wheels	Wood fiberboard with melamine coating	0.42	0.022	0.004	2.64
Bookcase with 1 shelf	Wood with varnish	2.83	0.020	0.026	16.46
Book/accessory case on wheels	Wood with varnish	3.72	0.020	0.034	22.26
Office chair on wheels	Wool, foam plastic, plastic back, metal frame	0.30	0.050	0.015	7.50
Chair seat (for penetration measurements)	Wool, foam plastic, plastic back	0.19	0.050	0.010	
Carpet	Nylon on synthetic rubber backing	4.89	0.003	0.012	2.84
Curtain	Cotton	15.15	0.000	0.003	1.53
Books				0.046	37.20
Paper on desk and in waste basket					
Total		31.56		0.216	108.29

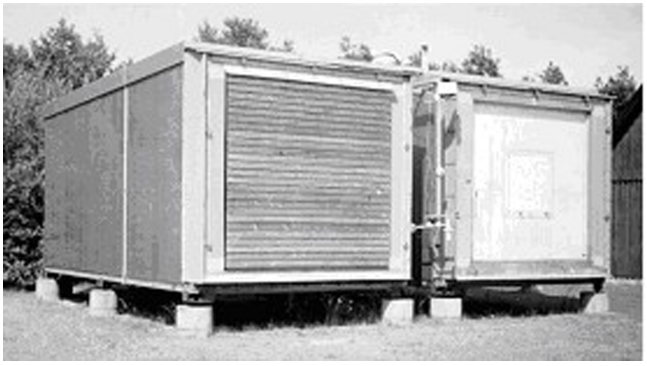

Figure 2 *Photo of the test cells.*

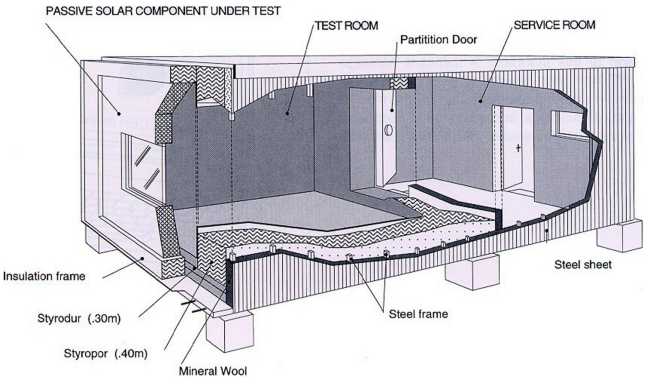

Figure 3 *Diagram of the test cells.*

The test room has an air distribution system connected to the cell's heating and cooling coils. A service room containing the cooling and control systems is placed at the northern end of the test cell. The cell is instrumented with sensors for measuring both the outdoor climate and the indoor conditions (air temperatures, surface temperatures, heating, power used by the cooling system and fans, heat fluxes, air infiltration rate, relative humidity, and air velocity). The indoor relative humidity is measured with capacitive moisture sensors with an accuracy of about ±2% RH. The data acquisition system is located in an adjacent building, from which the test cell can be controlled.

To measure the moisture buffering effect of the materials in this experiment, the room was subjected to controlled moisture variations. The idea was to mimic the exposure of moisture variations to interior surface materials in a common indoor climate, but in a controlled way. The moisture production was controlled, and the resulting RH variation within the test cell was registered.

The indoor humidification, which represents the moisture production of an inhabited room, was provided by evaporation of moisture from a reservoir of water heated by an electric coil. Humidity was withdrawn from the air by a dehumidifier draining into the same reservoir. The drying represents the removal of humidity from the room that would normally take place by ventilation.

The water reservoir was suspended in a load cell, and the rates of humidification and drying were controlled according to a predefined schedule. Padfield (1998) has used the principle in a small (0.5 m^3, 18 ft^3) test chamber in a laboratory. A schematic diagram of the apparatus is shown in Figure 4.

Another similar load cell, as for the water reservoir, was suspended in a rack from which a material specimen could be weighed continuously during the tests. The range and accuracy of the load cells was 10 kg±3 g (22±0.007 lb).

Two small fans were placed on the floor at both ends of the test cell to ensure a well-mixed airflow. The control system was set to save registered average data for a ten-minute period of measurements with sampling every thirty seconds.

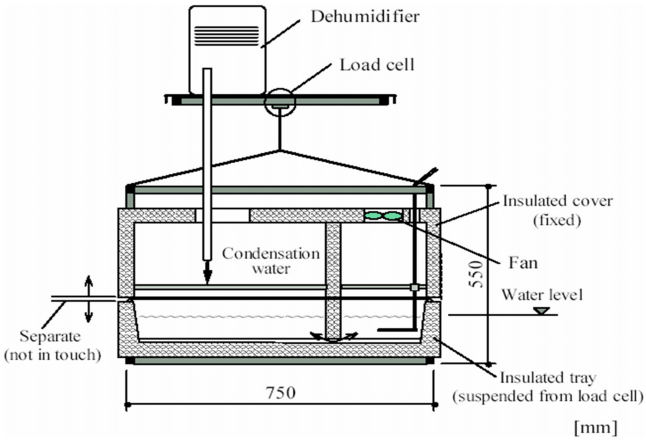

Figure 4 *A schematic diagram of the climatic control system of the test chamber.*

The air change rate of the test cell has been measured with tracer gas using the decay method and found to be about 0.20 h^{-1} at 50 Pa (0.015 in. Hg) pressure difference. Without pressurization the air change rate was about 0.007 h^{-1} (Mitamura et al. 2001).

MEASUREMENTS

This paper explains two sets of measurements in the test cell. The main experimental set presented for the purpose of this paper deals with the effect of furniture and other furnishing in a room to buffer the indoor humidity variations. For comparison, this is followed by a short presentation of a former study in the same equipment, where the moisture buffer effect of different interior wall systems was investigated.

Fully Furnished Room

In this investigation the relative humidity variation in an office was investigated. During the experiments the daily variation in the test cell was humidification and dehumidification moisture load of 33 g water per hour (1.2 oz per hour) and an isothermal temperature of 20.0±0.5°C (68±1°F).

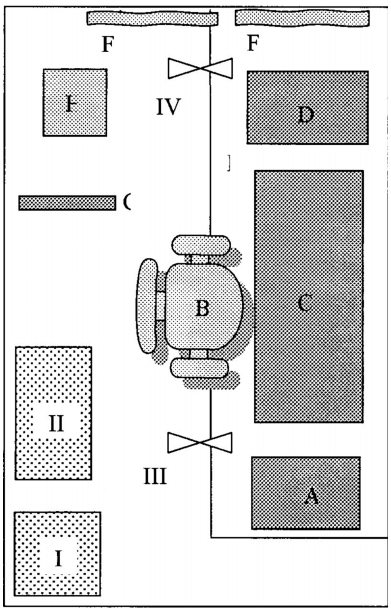

Figure 5 *A schematic diagram of the test cell.*

Figure 6 *Placement in the fully furnished test cell.*

The experiment concerned nine different cases. Cases 1 and 9 were both performed for the empty test cell as reference tests. Case 2 comprises the basic furniture of an office, with a desk, a room divider, an office chair and chair seat, a computer shelf, and a rolling shelf. In case 3 books were added in the shelves. A carpet was applied in case 4. Case 5 was a real office situation with papers in the wastebasket and spread over the table. Finally, a curtain was added to the test cell in case 6. The placement in the fully furnished test cell is shown in Figures 5 and 6.

The following cases were a gradual emptying of the test cell. In case 7 the curtain, the paper on the table, and the carpet were removed. In case 8 the books was removed, and in case 9 the test cell were empty except for the chair seat used for the penetration measurements.

Penetration Measurements

A chair seat was used for moisture penetration measurements. The chair seat was from an industrially manufactured chair and consisted of a 5 mm (0.2 in.) plastic board, 31 mm (1.2 in.) foam plastic, and a wool fabric as a cover. The plastic board was covered underneath with a nonwoven synthetic fabric.

Four combined temperature and relative humidity sensors were applied. The first sensor was placed between the plastic board and the foam plastic in the center of the seat. The second sensor was placed halfway down in the foam plastic and the third sensor on top of the foam plastic but under the wool fabric. The fourth and last sensor was placed on top of the wool fabric. The sensors were somewhat displaced so that interference from the other sensors was minimized.

The chair seat was suspended in the specimen load cell in the test room.

Interior Walls

A previous experiment (Hedegaard 2002) studied the moisture buffer capacity of an interior wall. In the setup the daily moisture load was set to evaporation at a constant rate of 25g/h (0.88 oz/h) for half a day followed by a similar period with condensation at the same rate. The experiments were performed under isothermal conditions of 21.0±0.5°C (70±1°F).

The inner wall consisted of a steel frame with insulation inside. The thickness of this basic part of the wall layer was 70 mm (2.8 in.). In cases 2 and 3 measurements were made with mineral wool as insulation or, alternatively, with loose fill cellulose insulation (65 kg/m^3, 4.0 lb/ft^3). A metal wire netting was added in order to keep the cellulose insulation in place. The following cases were only made with cellulose insulation. In case 4 untreated plasterboards were added on each side of the construction. The thickness of the plasterboard was 13 mm. In case 5 painted plasterboards replaced the untreated plasterboards. The painting consisted of two coats of latex wall paint. Finally, in case 6, a vapor retarder was added between the insulation and the painted plasterboards, although this is not normal to have in an interior wall. During all the experiments, moisture transport though the edges of the test walls was prevented by use of moisture proof tape. The exposed surface areas for each case are given in Table 3.

Table 2. Types of Furniture/Furnishing Exposed

Case	Furniture - Table - Chair - Room divider - Shelf 1 - Shelf 2	Books	Carpet	Paper on Table	Curtain
1 (empty)					
2	*				
3	*	*			
4	*	*	*		
5	*	*	*	*	
6 (fully furnished)	*	*	*	*	*

Table 3. Exposed Surface Areas

Case	Material	Exposed Surface Area, m^2
1	Empty test cell	0.0
2	Mineral wool in steel frame	15.38 (166 ft^2)
3	Cellulose insulation in steel frame	15.38 (166 ft^2)
4	Cellulose insulation in steel frame under untreated plasterboards	20.15 (217 ft^2)
5	Cellulose insulation in steel frame under painted plasterboards	20.24 (218 ft^2)
6	Cellulose insulation in steel frame under vapor retarder and painted plasterboards	20.24 (218 ft^2)

CALCULATIONS

The indoor humidity has also been modeled with a whole-building hygrothermal simulation tool (Rode and Grau 2003; Rode et al. 2001). The tool is capable of making transient prediction of the heat and moisture condition of materials in the building envelope and in indoor furnishings and simultaneous prediction of the humidity condition of the indoor air. Significant in this modeling is to see how the hygroscopic materials are able to moderate the variations of the indoor humidity. The scope of the modeling was to see if it could be possible to predict the effect of various items in indoor furnishing to act as moisture buffers and possibly to use the experimental results just presented to benchmark the model.

The calculation tool uses a finite control volume method and models the hygroscopic absorption of moisture in materials according to their sorption curve. In doing so, it also models the hysteresis that characterizes the difference between the sorption curves for absorption and desorption, and it models the so-called scanning curves that are followed in the transition between absorption and desorption. Moisture transport within the materials is modeled as vapor diffusion according to Fick's law. The heat and vapor transport coefficients at the surfaces of materials in the room are modeled with constant surface resistances: 0.13 m^2K/W (0.74 $ft^2 \cdot h \cdot °F/Btu$) for heat transfer and 5.1·107 $Pa \cdot m^2 \cdot s/kg$ (corresponding to a permeability of 340 perm) for vapor transfer.

To model the materials in indoor furnishings, e.g., an office chair or the books on a shelf, it is necessary to approximate these elements with planar construction surfaces, just like inner walls. Thus, it must be realized that even the relatively simple test chamber and furnishings that were analyzed in these tests can only be simulated using some rough approximations about how the materials should be represented in the model. It is not possible with the calculation model used to represent the real microclimatic conditions near the surfaces of the objects in the room. However, to get some indication of the influence of the boundary conditions in the interface between furnishing and indoor air, a simulation was also carried out for the fully furnished room when the surface resistance for vapor transfer was doubled to the value 1.02·108 $Pa \cdot m^2 \cdot s/kg$. This had the effect of increasing the amplitude of the daily indoor RH variation from about 21.6% RH to 22.8% RH, i.e., a relative increase in the order of 5%. This must be seen only as an indicative number since it depends on the choice of materials and their aerial configuration in the room. More research is needed into the importance of the surface mass transfer coefficient and the microclimatic conditions around indoor furnishings is needed.

Some simulation models were set up to predict the indoor humidity variation in different cases, from the empty test cell to the test cell fully furnished as an office with a desk with working papers, upholstered office chair, book cases with books on the shelves, a carpet, and curtains. The modeled

setting was the same as in the experiments described previously. The room was the well-insulated steel box, which is practically inert to moisture flow through its walls and is very airtight. A humidification of the room of 33 g/h (1.2 oz/day) was simulated for 12 hours followed by a dehumidification of the same magnitude for the other 12 hours per day. The indoor air temperature was modeled so it was constant at 20°C (68°F). The materials of the furniture were entered into the simulation model as multi-layered structures of homogenous material layers—sometimes down to a control volume thickness of around 0.1 mm (4 mil). The numerical grid was expanding, so the surface control volumes were thinner than control volumes deeper in the material. The calculations were carried out for one-week periods, where each day was calculated under identical assumptions. All materials started at a moisture content corresponding to a given initial relative humidity. This value was chosen to match as closely as possible the same conditions as in the experiments.

RESULTS

Comparison: Empty Room—Fully Furnished

The difference in the moisture buffer performance between the fully furnished test room and the empty test room can be seen in Figures 7 and 8. The two cases have approximately the same average RH (55% resp. 57% RH) but the fully furnished room has a smaller amplitude. A smaller amplitude indicates a larger moisture buffer capacity in the surface materials if the ambient conditions are similar in the cases compared, as in these experiments. For a one-day variation, the fully furnished room has a highest peak of humidity 10% RH lower than it was for the empty room, and the daily minimum value is 5% RH higher than for the empty room. Overall, this gives a less varying indoor climate. Comparing all the different cases (see Table 2 and Figure 8) it can be noted that the cases where lightweight organic materials, such as papers and textiles, are exposed have the lowest variation in RH for these weekly sequences of daily variations.

Penetration Measurements

The result of the measurement of moisture penetration into the chair seat that was used as a weighed specimen indicates that moisture penetration into the seat progresses almost instantaneously. Although there is a small time-delay for the moisture variation, it depends on the distance from the top surface. This is easiest to see when the change in RH is plotted as a function of time and at the lowest value for the moisture variation (see Figure 9). The upper half of the chair seat has a larger moisture variation.

It can also be noted that the effect of the disturbances, mainly from the control system of the humidification/dehumidification system, decreases with the distance from the top, as expected. In the bottom half of the chair seat, the sensors register almost no disturbances in comparison to the sensors on top of and just underneath the wool fabric.

Comparison Measurements and Calculations

Figure 7 shows the measured variation of indoor relative humidity for one typical day for the room without materials, as well as for the fully furnished room. For the empty room, the relative humidity varies between approximately 35% and 80% RH, while for the fully furnished room it varies between 40% and 70% RH. For the empty room, this corresponds to a variation in humidity ratio of the air between 5.1 g/kg and 11.7 g/kg (at 20°C, 68°F) and between 5.8 and 10.2 g/kg for the fully furnished room. The theoretical variation in indoor humidity ratio should be ±8.7 g/kg for the empty room when the as-planned 33 g/h (1.2 oz/day) of moisture are added to and withdrawn from the 38 m^3 (1340 ft^3) test cell in 12-hour periods. These results illustrate some deficits of the experimental configuration: The dehumidifier used to withdraw humidity from the air had some difficulty in desiccating the air significantly below 40% RH, so not all the planned humidity variation could be realized. Further, it may be possible that there was some hygroscopic absorption of moisture in the paint, polyethylene sheets, dust, and electrical wires in the otherwise empty room.

The same figure shows the results of the calculation of indoor humidity. The simulation result for the empty room shows a variation between 26% and 88% RH, while it varies between 45% and 66% RH for the fully furnished room.

Interior Walls

The results of indoor RH variation with inner walls as moisture buffers are shown for representative one-day periods in Figure 10. The experiments show that cellulose insulation has a very good buffering effect. In a small office with a 15 m^2 (166 ft^2) buffer wall of cellulose insulation the variation range of relative humidity can be reduced to half the variation in a similar room with non-absorbing materials. On the other hand, the moisture buffer capacity for mineral wool has been found to be very small. It was also found that if plasterboards cover the insulation in an interior wall, the moisture buffer capacity of the insulation is insignificant.

For the three cases with plasterboards it is hard to differentiate between the moisture buffer capacities. The curves for the two painted plasterboards are very similar. This seems reasonable since the penetration depth for the untreated plasterboard was less than the 13 mm (0.5 in.) thickness of the plasterboards so the test results were expected to be identical. The resulting error was 10% and thereby it seems fair that the two test series are alike. However, this also means that it is impossible to distinguish between the test with the untreated plasterboard and the tests with the painted plasterboards. The plasterboards have a moisture buffer effect somewhere between that of mineral wool and that of cellulose insulation.

DISCUSSION

The moisture buffer capacity of the surface materials of the indoor environment can be used to minimize the daily peak variations of relative humidity in the air and thereby avoid periods with both very high and very low relative humidity. As

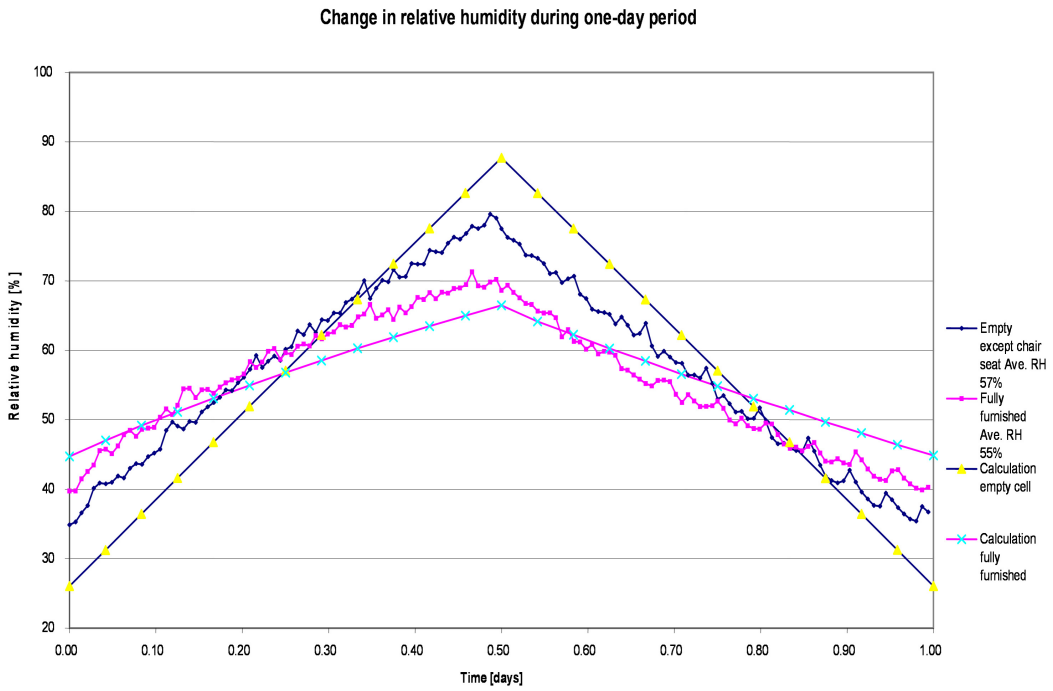

Figure 7 *Difference in the moisture buffer performance between the fully furnished test room and the empty test room.*

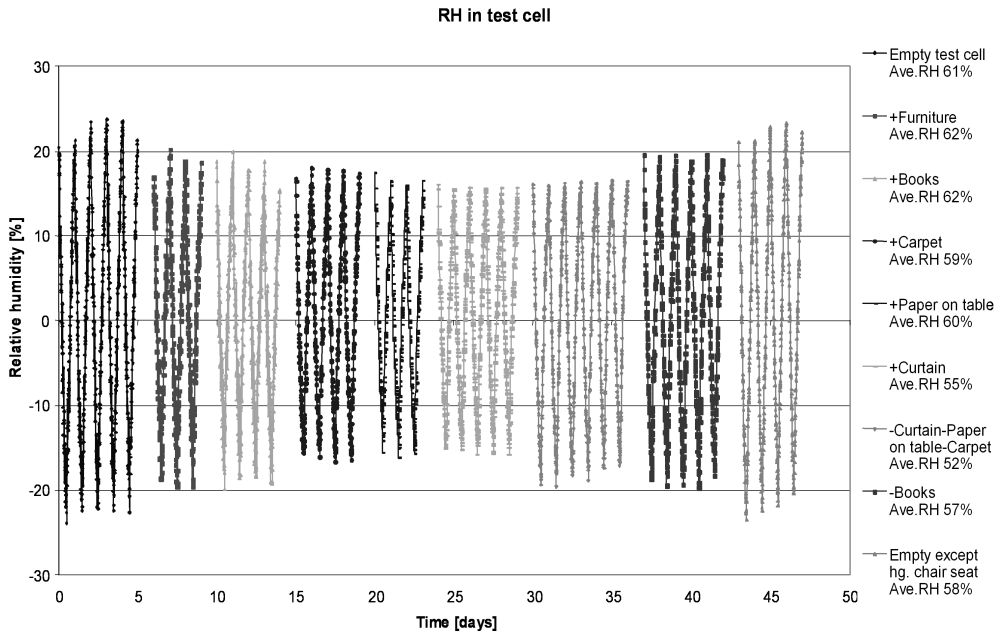

Figure 8 *The variation in RH for the nine different cases for the furnished room experiments.*

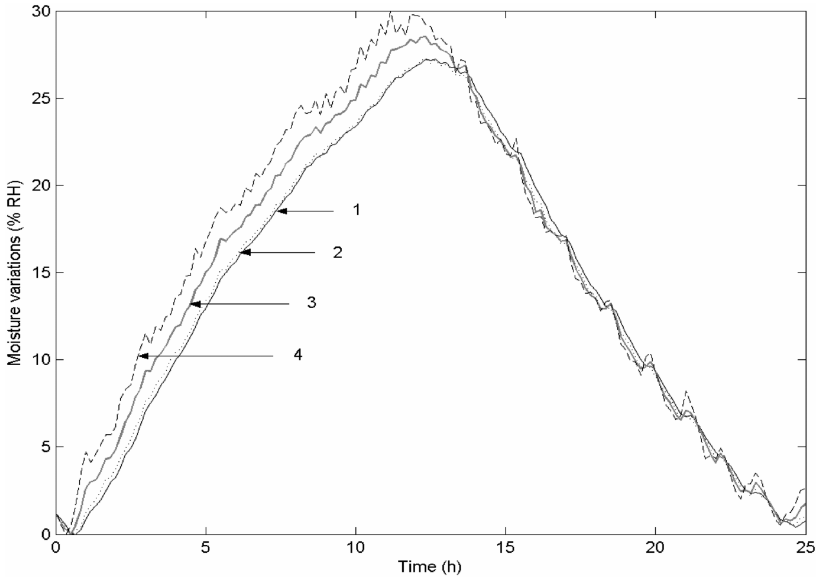

Figure 9 *The moisture variation in the chair seat.*

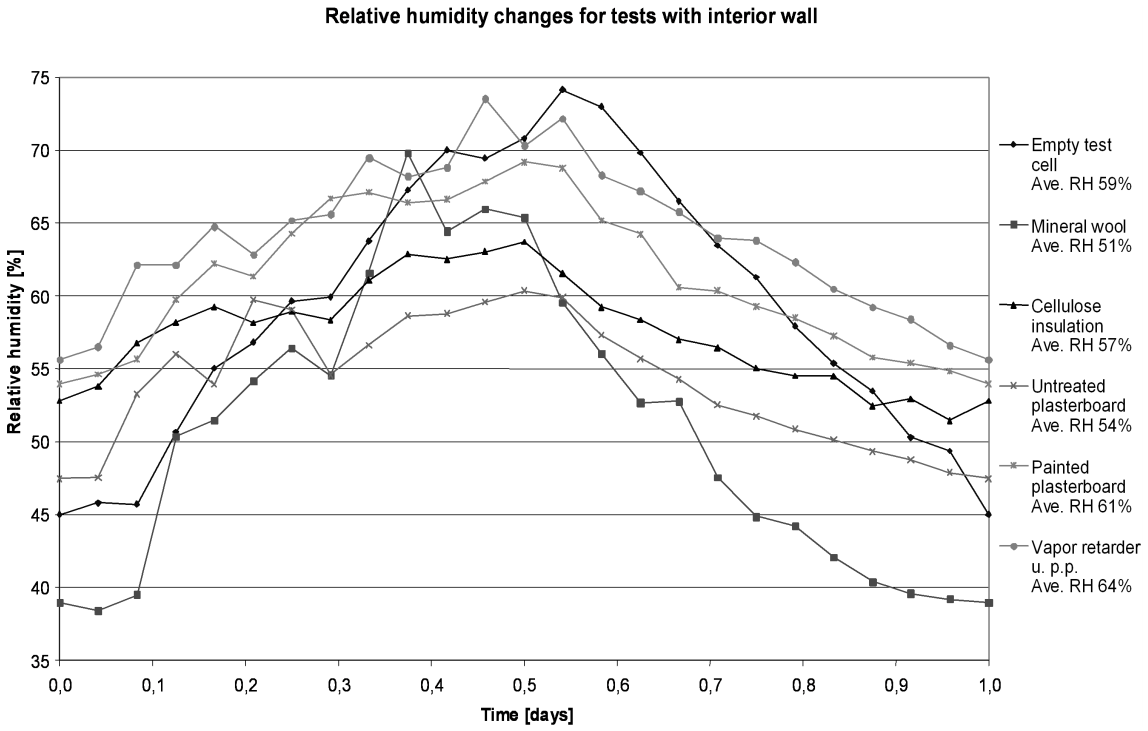

Figure 10 *The results of indoor RH variation with inner walls as moisture buffers are shown for representative one-day periods.*

mentioned in the introduction, there are many advantages. Reducing the highest appearing RH in the indoor air reduces the risk of condensation on cold surfaces and the number of emissions from surface treatments and causes the air to be perceived as fresher. The reduction of the high peak values is advantageous for both the constructions and the indoor air, since fungal growth and consequent deterioration and spread of spores are less likely to appear.

To play an active role in minimizing the daily peak variations, the materials in the indoor environment need to be relatively open and have a moisture buffer capacity together with a sufficient exposed area. In this experiment it has been shown that a fully furnished room has a better moisture buffer performance than a sparsely furnished room. Highly permeable and lightweight materials, such as papers and textiles, play an important role in moderating the hourly or daily variations, since to a high degree they cover other materials, such as surface-treated wooden book shelves or painted interior walls. There is a need for moisture properties for surface materials, both traditional building materials and materials for furnishing, and special interest should be paid to surface treatments such as lacquers and paint. The results from the experiment with the interior walls indicate that a further investigation in the field of paint coverings should be carried out. A larger survey of the materials present in the indoor environment is another topic for further research, which can be used to describe the indoor environment in a more precise way.

To model the indoor humidity of rooms while taking into account the moisture absorption in surfaces of the objects in the room requires detailed knowledge about the surface area, texture and topology of the surfaces, as well as knowledge about the material properties and the local surface coefficients for convective moisture flow at the different loci where humidity exchange takes place. Regarding these properties for real rooms with all their gadgets or even a simplified setup like the test cell investigated in this work, it is obvious that it will become an immense, or even impossible, task to achieve high precision in the provision of these data. The work illustrated in this paper has shown that it is possible to some extent to model the conditions in a room under simplified and idealized assumptions. By comparison of test cell and field test data, it should be possible to obtain good guidelines on how the complex layout of a room can be modeled in a way that merges all objects into a limited number of idealized surfaces. In addition, it should be possible by studying the microclimates in some characteristic material/air interfaces and analyzing these (e.g., with CFD calculation) to get a better understanding of the local mechanisms for heat and moisture exchange in such loci.

A large source of uncertainty in the experiments and calculations presented here is the surface moisture transfer coefficient, which to a high extent is governed by the microclimate at each location. We lack knowledge about the true microclimate and this has to be more carefully studied, as mentioned above. Also, the effective exposed surface areas introduce uncertainties into the experiments and calculations, and a methodology to determine the effective exposed surface area has to be carefully thought through.

The comparison between calculations and measurements as shown in the "Results" section and in Figure 7 illustrates some deficits of the experimental configuration. The dehumidifier used to withdraw humidity from the air had some difficulty in desiccating the air significantly below 40% RH, so not all the planned humidity variation could be realized. The possibility of some hygroscopic absorption of moisture in the paint, polyethylene sheets, dust, and electrical wires in the otherwise empty room poses another potential source of error.

The usefulness of this type of controlled full-scale measurement should still be considered very high, since it provides an important step between calculations and laboratory measurements on one hand and field measurements in real environments on the other hand. Especially this type of test cell with an exchangeable wall (see Figure 3) provides an advantage when future experiments can be done more realistically by conducting non-isothermal tests with a naturally varying indoor climate due to solar gain.

In the IEA Annex 41 project (described in the introduction) there will be activities that seek to gather as much field and test case information as possible from the different participating countries such that a broad knowledge base will be obtained. It is also anticipated that common exercises will be carried out where the modeling capabilities will be benchmarked and further developed. It appears obvious that the effect of furniture and other indoor materials to moderate the indoor humidity will be a part of this international study.

Altogether, it should be possible to establish a better empirical and analytical understanding of how a real room with all its furnishings performs to buffer the indoor humidity. The work presented in this paper may be seen as an early step on the path to improving this understanding.

CONCLUSION

The full-scale measurements of a fully furnished room have shown that moisture buffering needs to be more carefully studied since it has a notable impact on the moisture conditions in rooms. Calculation tools need to be modified to be able to handle, not only traditional building materials, but also furniture and other furnishing materials. There is also a lack of data for the moisture properties of the surface materials in the indoor environment. Also, a description of different surface materials present in normal indoor environments is needed. Alongside the task to find better descriptions of the materials, a better understanding and greater knowledge of the microclimate indoors is necessary.

ACKNOWLEDGMENTS

Support from IKEA is gratefully acknowledged. We thank J. Schultz, DTU, for valuable technical assistance and Dr. L. Wadsö, LTH, for experimental help. The work was carried out in part with support of the Technical Research Council of Denmark and FORMAS-The Swedish Research Council for Environment, Agricultural Sciences and Spatial Planning.

REFERENCES

ASHRAE. 2001. *ANSI/ASHRAE Standard 62-2001, Ventilation for acceptable indoor air quality.* Atlanta: American Society of Heating, Refrigerating and Air-Conditioning Engineers, Inc.

Bornehag, C.-G., G. Blomquist, F. Gynteberg, B. Järvholm, P. Malmberg, L. Nordvall, A. Nielsen, G. Pershagen, and J. Sundell. 2001. Dampness in building and health, review article. *Indoor Air* 11:72-86.

Berggren, T., and H. Skoog. 2003. Materials in the indoor environment—A preliminary study (in Swedish). Department of Building Physics, Lund University, unpublished report.

Christoffersen, L.D. 1996. ZEPHYR passive climate controlled respositories. Department of Building Physics, Lund University, Report TVBH-3028.

Fang, L., G. Clausen, and P.O. Fanger. 1999. Impact of temperature and humidity on chemical and sensory emissions from building materials. *Indoor Air* 9:193-201.

Harderup, L-E. 1998. Hygroscopic moisture of the indoor air considering non-stationary phenomena. Synthesis of publications for the period 1979-1998 (in Swedish). Department of Building Physics, Lund University, Report TVBH-3033.

Hedegaard, L. 2002. Moisture buffer capacity of building materials. M.Sc. thesis, Department of Civil Engineering, Technical University of Denmark.

Hens, H. 2003. Whole building heat, air and moisture response (MOIST-ENG). Proposal for a new annex; International Energy Agency, EXCO Energy Conservation in Buildings and Community Systems. Department of Civil Engineering, KU-Leuven, Belgium.

Mitamura, T., C. Rode, and J. Schultz. 2001. Full-scale testing of indoor humidity and moisture buffering in building materials. CD, *Conference Proceedings IAQ 2001, Moisture, Microbes, and Health Effects: Indoor Air Quality and Moisture in Buildings*. Atlanta: American Society of Heating, Refrigerating and Air-Conditioning Engineers, Inc.

Ojanen, T., and M. Salonvaara. 2003. A method to determine the moisture buffering effect of structures during diurnal cycles of indoor air moisture loads. *Research in Building Physics,*eds. Carmeliet, Hens, and Vermeir, pp. 353-361. Lisse: Swets & Zeitlinger, ISBN 90 5809 565 7.

Padfield, T. 1998. The role of absorbent materials in moderating changes of relative humidity. Report R-054, Department of Structural Engineering and Materials, Technical University of Denmark.

Peuhkuri, R. 2003. Moisture dynamics in building envelopes. Report R-071, Department of Civil Engineering, Technical University of Denmark.

Plathner, P., and M. Woloszyn. 2002. Interzonal air and moisture transport in a test house. Experiment and modeling. *Buildings and Environment* 37: pp. 189-199.

Rode, C. 2003. Nordtest Workshop on Moisture Buffer Capacity—Summary Report. DTU, Lyngby, Denmark.

Rode, C., and K. Grau. 2003. Whole-building hygrothermal simulation model. *ASHRAE Transactions* 109(1).

Rode, C., K. Grau, and T. Mitamura. 2001. Hygrothermal conditions in the envelope and indoor air of buildings. *Performance of Exterior Envelopes of Whole Buildings VIII* CD. Atlanta: American Society of Heating, Refrigerating and Air-Conditioning Engineers, Inc.

Simonson, C.J. 2000. Tapanila ecological house. VTT Building Technology, Technical Research Centre of Finland.

Simonson, C.J., M. Salonvaara, and T. Ojanen. 2001. Improving indoor climate and comfort with wooden structures. VTT Building and Transport, Technical Research Centre of Finland.

Svennberg, K., and L-E. Harderup. 2002. Time-dependent moisture properties for plasterboard with surface coating. *Indoor Air 2002*.

Toftum, J., and P.O. Fanger. 1999. Air humidity requirements for human comfort. *ASHRAE Transactions* 105(2): 641-647.

Paper II

Determination of Moisture Surface Resistance Using Cup Experiments

Mortensen, L. H., Rode, C. & Peuhkuri, R. (2007)

Unpublished

Determination of Moisture Surface Resistance Using Cup Experiments

Lone H. Mortensen[1*], Carsten Rode[1] and Ruut Peuhkuri[2]

[1]Department of Civil Engineering, Technical University of Denmark,
Brovej build. 118, DK-2800 Lyngby, Denmark.
[2]VTT Technical Research Centre of Finland P.O.Box 1000, FIN-02044 VTT.
**Corresponding author, phone +45 45251934, fax +45 4588 3282, loh@byg.dtu.dk*

Abstract
Moisture transfer between indoor air and constructions or furniture is affected by conditions at the boundary layer near the surfaces. The relation between surface resistance and airflow velocity near a material sample is investigated using dry cup experiments on paper samples. The experimental results are compared with CFD simulations in order to evaluate the influence of cup design. The results show that the surface resistances decrease with increasing airflow velocity above the material surface, but the measured resistances are somewhat smaller than those estimated theoretically. It is found that the cup design influences the local turbulence on sample surfaces.

Keywords
Boundary conditions, surface resistances, permeability measurements, CFD simulation, local turbulence.

Nomenclature

A	exposed surface area (m²)
A_c	cross-sectional area (m²)
c_p	heat capacity of air at constant pressure (J/kg·K)
D	diffusivity (m²/s)
D_h	hydraulic diameter, $4A_c/P$ (m)
G	stationary weight change per time (kg/s)
g	water vapour flux density (kg/s·m²)
k	constant (-)
L	length (m)
Le	Lewis number, $\lambda/\rho c_p D$ (-)
Nu	Nusselt number, $\alpha_c D_h/\lambda$ (-)
P	wetted perimeter (m)
Δp_v	water vapour pressure difference (Pa)
Pr	Prandtl number (-)
R_v	gas constant for water vapour (J/kg·K)
Re	Reynolds number, $\rho u D_h/\mu$ (-)
T	temperature (K)
u	air velocity (m/s)
x	entrance length (m)
$Z_{1\text{-layer}}$	total water vapour resistance of 1 layer of paper (Pa·m²·s/kg)
$Z_{2\text{-layers}}$	total water vapour resistance of 2 layers of paper (Pa·m²·s/kg)
Z_a	water vapour resistance of airlayer (Pa·m²·s/kg)
Z_m	water vapour resistance of sample material (Pa·m²·s/kg)
Z_{s1}	water vapour surface resistance, exterior side of sample (Pa·m²·s/kg)
Z_{s2}	water vapour surface resistance, interior side of sample (Pa·m²·s/kg)
Z_t	total water vapour resistance (Pa·m²·s/kg)
$Z_{1\text{-layer}}$	total water vapour resistance of 1 layer of paper (Pa·m²·s/kg)

Greek

α_c	convective surface heat transfer coefficient (W/m²·K)
β_p	surface coefficient of vapour transfer at constant pressure (kg/ Pa·m²·s)
λ	thermal conductivity of air (W/m·K)
μ	dynamic viscosity (kg/m·s)
ρ	density of air (kg/m³)

Subscripts

a	air layer
a	cross-section
D	hydraulic diameter
h	hydraulic
m	sample material
p	pressure
s1	surface, exterior
s2	surface, interior
t	total
v	water vapour

Superscript

n	number between 0 and 1

1 Introduction

The purpose of the investigation shown in this paper is to find the so-called surface resistances by use of cup measurements for determination of water vapour transmission. Moreover, we investigate how the surface resistance is affected by airflow velocity and cup design.

1.1 Background

Moisture interactions between room air, the surrounding constructions and furniture have a great influence on the indoor environment. The moisture transfer between air and construction are strongly dependant upon the boundary layer conditions close to the surface, which is influenced by the airflow patterns in the room. Thus, it is important to investigate the airflows carefully and to estimate their effect on the moisture transport. For instance,

small velocities will lead to an increased air layer resistance. Bednar & Dreyer [1] showed that it is possible to measure the surface transfer coefficients by use of small specimens with high liquid moisture conductivity. The surface resistance is a key parameter in understanding moisture interactions between room air and constructions, since the actual airflow velocities found in dwellings are relatively small.

The modelling development in hygrothermal building performance urges measurements of moisture parameters of building materials. A widely used method is the cup test but other methods have also been developed. Svennberg & Wadsö [2] invented a modified cup method that is best applicable for very permeable materials such as textiles and the method only requires very small sample sizes. Yet, another method was developed by Galbraith et al. [3] of low pressure permeability tests where the results can be obtained much faster. In addition Scheffler & Plagge [4] have designed a new type of equipment especially for drying measurements, which has the advantage that it can also produce data for the surface boundary of the material sample including surface resistances.

The effect of airflow velocities on material surfaces and how boundary layers relates to the moisture transfer rate is highly important in order to have better understanding of the moisture interactions between room air and constructions. Problems of mould growth are known to occur due to high relative humidities in microclimates e.g. between “cold” external walls and furniture. Therefore, the experiments in this study focus on determination of the surface transfer coefficients for moisture as a function of the airflow velocity above the boundary layer.

The surface resistances can be determined by measurements on samples with different thicknesses as shown by Fanney et al. [5] and Worch [6]. This corresponds well with the Japanese standard JIS A 1470-1:2002 [7]. In the standard it is proposed that the surface resistance can be found by using 2 cups with desiccant covered by 1 and 2 pieces of paper, respectively. The found resistances will be compared to the specifications of the EN ISO 12572:2001 standard [8] for determination of water vapour permeability. The standard prescribes mixed air to assure uniform conditions and the airflow velocity should be within the

range 0.02-0.3 m/s above the sample. However, this relatively large span of airflow velocities could influence the surface transport coefficients.

1.2 Outline of current paper

The purpose of these measurements is to gain information about the water vapour transport through a sample as a function of airflow velocity above the boundary layer of the exposed sample surface. Therefore, this paper presents permeability experiments with layers of paper as sample material extended with measurements of airflow velocity during the permeability experiments. Post processing the permeance results give the surface resistances. The permeability experiments use the inverted cup method and try to reveal differences in surface resistances due to changes in airflow velocities. The investigated airflow velocities are within the range stipulated in the EN ISO 12572:2001 standard [8], namely 0.02 – 0.3 m/s as well as higher velocities.

Additional experiments are performed in the laboratory to test the feasibility of using Petri dish cups as probes for field determination of the moisture surface resistance.

Furthermore, the surface resistances found by measurements are compared with numerical simulation. The numerical simulations are expanded to investigate local turbulence due to different cup designs, e.g. with and without rims. The numerical analysis of the laboratory experiments is based on the theory of flow in ducts.

2 Theory

The cup method principle for determining water vapour permeability is to have a cup with desiccant or a salt solution, to ensure a well known relative humidity (RH) that is covered by a sample and placed in a controlled environment. Then the cup is weighed regularly and the steady rate of weight gain or loss expresses the water vapour transfer transmission rate.

When the water vapour resistance, Z_t (total), for an entire sample of a building material is found by the cup test method the primary resistance is usually within the material itself, Z_m. However, there are also somewhat smaller resistances caused by surface resistances on

each side of the material, Z_{s1} and Z_{s2}. In addition, there can be an air layer resistance, Z_a, between the surfaces of the desiccant or the salt solution and the sample. In case of using the inverted dry cup method only Z_{s1}, the resistance on the exterior side of the sample of the cup exists. With these resistances and use of Fick's law the water vapour flux density, g can be described as in Equation 1.

$$g = \frac{G}{A} = \frac{\Delta p_v}{Z_t} = \frac{\Delta p_v}{Z_m + Z_{s1} + Z_{s2} + Z_a} \quad (1)$$

Equation 1 can be simplified to show the transport in case of inverted cup measurements and this is shown in Equation 2.

$$g = \frac{\Delta p_v}{Z_m + Z_{s1}} \quad (2)$$

Alternatively the surface resistances Z_{s1} and Z_{s2} can be found by use of the surface coefficient of water vapour transfer, β. In Equation 3 a general formula derived by Nusselt [9] is given.

$$\beta = \frac{D}{\lambda} \cdot \left(\frac{\lambda}{\rho \cdot c_p \cdot D} \right)^n \cdot \alpha_c = \frac{D}{\lambda} \cdot (\mathrm{Le})^n \cdot \alpha_c \quad (3)$$

In Equation 3 the exponent, n of the Lewis number is 0 for laminar flows and 1 for fully turbulent flows. For natural air movements in rooms the value, n should be 1/4 (Illig [10]). The surface resistance, Z_{s1}, is then found by the relation between the heat and moisture transfer coefficients.

$$Z_{s1} = \frac{1}{\beta} = \frac{R_v \cdot T}{\beta_p} = \frac{\lambda \cdot R_v \cdot T}{D \cdot \alpha_c \cdot \mathrm{Le}^n} = \frac{\rho \cdot c_p \cdot R_v \cdot T}{\alpha_c} \cdot \mathrm{Le}^{1-n} \quad (4)$$

The convective surface heat transfer coefficient, α_c depends on the airflow velocity, u, above the boundary layer but first some related properties have to be derived. These are Reynolds number, Re_D, hydraulic diameter, D_h, entrance length, x, and Nusselt number, Nu.

For forced flow in ducts and pipes the flow is laminar up till Reynolds numbers, $Re_D \cong 2300$ then there is a transition until turbulence is fully established when $Re_D > 10{,}000$. The Reynolds number is calculated by use of the hydraulic diameter as shown in Equation 5.

$$Re_D = \frac{\rho \cdot u \cdot D_h}{\mu} \quad (5),$$

where $D_h = \frac{4 \cdot A_c}{P}$

To estimate the mean Nusselt number the hydrodynamic entrance length, x must be found. For the laminar region the hydrodynamic entrance length, x is given by:

$$\left(\frac{x}{D_h}\right) \approx 0.05 \cdot Re_D \quad (6)$$

In the turbulent region the hydrodynamic entrance length, x is given by:

$$10 \le \left(\frac{x}{D_h}\right) \le 60 \quad (7),$$

here it will be assumed fully developed when $x/D_h > 10$.

The mean Nusselt number, Nu is constant when the flow is laminar and fully developed, this constant will be called, k. The constant, k is a correction factor for flows in ducts of differing cross-sections. For constant wall temperature the number is between 3 and 7.5. In the laminar developing region and for flow in ducts of various cross sections Mills [11] suggests calculation of the mean Nusselt number by use of an empirically derived equation:

$$Nu = k + \frac{0.03\left(D_h / L\right) \cdot \mathrm{Re}_D \cdot \mathrm{Pr}}{1 + 0.016\left[\left(D_h / L\right) \cdot \mathrm{Re}_D \cdot \mathrm{Pr}\right]^{2/3}} \quad (8)$$

In the turbulent region *Nu* is estimated as:

$$Nu = 0.023 \cdot Re_D^{0.8} \cdot Pr^{0.4} \quad (9)$$

By use of Nu the convective surface heat transfer coefficient, α_c is found by:

$$\alpha_c = \frac{Nu \cdot \lambda}{D_h} \quad (10)$$

More about forced convection in ducts can be found in e.g. Mills [11].

3 Experiments

3.1 The equipment for cup tests

To perform the permeability measurements a specially designed cup test facility has been used. It consists of a closed ventilation system where both temperature and relative humidity can be controlled and it passes through a test chamber. An outline of the facility is seen in Figure 1. The cup facility is combined with a data acquisition system where information about temperature, relative humidity, airflow velocity and pressure is recorded automatically, and the weight of the cups is entered at each weighing. Within the facility it is possible to test 12 ordinary cups and 12 inverted cups at the same time. In the test chamber the circulating air flows in a flat duct with 60 cm width and 5 cm height. Here, the samples are placed in contact with streaming air. This is seen in Figure 2 (a) where a picture of the test chamber is shown in and in part (b) a principle drawing is seen. The air circulation system ensures that both the humidity and the airflow velocity in the climate chamber duct can be controlled. Within the cup test facility it is possible to set different airflow rates. The air is circulated by a fan within the air circulation duct.

In the picture, Fig 2 (a) two openings are seen in the front plate and from these the samples are weighed on the balance seen in the bottom. Hansen [12] give a more detailed description of the used facility and equipment

3.1.1 Measuring methods

Airflow measurements

In theory the airflow velocity will influence the surface resistances. Hence, the airflow velocity is measured along with the permeability measurements.

The airflow measurements were performed with thermal anemometers. One of the advantages of thermal anemometers is their ability to sense very low velocities. Opposite, the limitations of hand-held and analogue electronic anemometers are that they must be carefully aligned with the airflow, they should be clean, and the readings can fluctuate in turbulent flows. In the current measurements, the fluctuating readings where smoothed by using time-integrated measurements. The airflow velocity measurements were performed in the middle of the 5 cm flat duct with around 2.5 cm distance to the sample surface. This means that the airflow velocities are assumed to have been measured in the free velocity field.

To have as low airflow velocity as possible the circulation fan inside the duct was set as low as possible. However, measurements showed that this gave results in the range 1.1 – 1.4 m/s. Since we wanted to test even lower velocities the air in the duct was slowed down by adding perforated rubber foam in the duct prior to the measuring area. With this foam it was possible to achieve velocities in a range of 0.06 to 0.78 m/s for 3 different settings of the ventilation fan. However, this span makes it important to measure each cup position as the velocities for the same ventilation fan setting have a large velocity span. It was found that the velocity measured at a specific cup position could be replicated, so the 3 fan settings each provide a group of 10 individually measured velocities.

For velocities in the range 1 - 2 m/s the measurements were taken twice for a 60 s time-averaged period and a 400 s time-averaged period with a Low Velocity Transducer, type 54R10 anemometer from Dantec (range 1-5 m/s). All 3 measurements were then averaged.

For velocities in the range 0 – 1 m/s the measurements were continued until the standard deviation was as low as possible with an Indoor Climate Analyser, type 1213 anemometer from Brüel & Kjær (range 0 - 1 m/s). In the actual measurements that gave standard deviations in a range of 0.04 – 0.15 m/s. The measurements were repeated another day and the results for both days were averaged.

Description of cup tests

Circular cups resistant to corrosion were used for the inverted cup measurements. Each cup consists of two parts that are screwed together with a rubber sealing ring on both sides of the sample. On top of the upper rubber sealing a Teflon ring was added to ensure smoother closing of the cup. The exposed sample area was circular with a diameter of 79.8 mm (5000 mm²). A picture of a cup is shown in Figure 3.

Due to the small sample size, a total of 5 samples were required according to the EN ISO 12572:2001 standard [8]. Hence, in each test 10 samples were tested but the airflow velocity above the boundary layer was not quite identical. The sample material was plain drawing paper with a weight of 190 g/m². Half of the cups had 1 layer of paper and the rest had 2 layers of paper.

Therefore, the results shown in this paper will consist of 4 groups of measurements with different airflow velocities each based on the measuring results from each cup. The measurements were performed in the described facility for cup tests. As dry cup desiccant, ($Mg(ClO_4)_2$, 0 %RH) was used. Four cases with different range of airflow velocities above the boundary layer were tested; Test 1 with range 0.06 – 0.54 m/s, Test 2 with range 0.06 – 0.78 m/s, Test 3 with range 0.09 – 0.69 m/s, Test 4 with range 1.04 – 1.40 m/s. The tested cases were actually measured twice, on day one they were performed with one layer of paper and the next day with two layers of paper. The tests 1-3 covered similar ranges of velocities but this is useful in order to assure repeatability of the measurements. During the tests the climate above the cups provided by the climate chamber was kept constant with temperature of 22.6°C ± 0.1°C and 54 %RH ± 1.5 %RH, according to the standard.

The results of the permeability experiments were post processed. The total water vapour resistance, Z_t, can give the surface resistance Z_{s1} by simple calculations:

$$\begin{aligned} Z_{1-layer} &= Z_{s1} + Z_{paper} \\ Z_{2-layers} &= Z_{s1} + 2 \cdot Z_{paper} \end{aligned} \quad \Rightarrow Z_{s1} = 2 \cdot Z_{1-layer} - Z_{2-layers} \quad (11)$$

Unfortunately, the inaccuracy of determining the surface resistance as proposed in Equation 11 will exceed the uncertainty of measuring the diffusion resistance of the individual cups.

3.2 Petri dish tests

Additional tests using Petri dishes as cups had two purposes; to see if the cup method would be applicable as a method to measure the moisture surface resistance under practical circumstances such as on interior building surfaces and to use the results to get an idea about the airflow velocity in the microclimate.

The concept could then be used as simple "field cup tests" to determine surface resistances in real microclimates. The idea was that only a precision balance and glass Petri dishes as cups were required. The method was tested under controlled conditions in a climatic chamber in the laboratory. In the chamber was built a chilled internal wall, and a Perspex box was positioned against that wall to imitate a cupboard standing at an external wall in a real building. An air gap behind the Perspex furniture allows room air to pass over the chilled surface. The room air temperature and relative humidity were kept constant at set values.

The Petri dish cups were placed vertically on the chilled wall with the paper-covered tops facing the room, see Figure 4. The glass cups were filled with desiccant and they were sealed with 1, 2 or 3 layers of paper (190 g/m²) of the same type as used in the experiments in the cup test facility. The used Petri dish cups had an exposed surface area of 7280 mm² (96 mm diameter). All tests were performed at a room temperature of 22.0°C ± 0.5°C but with 3 different relative humidities: 40, 50 and 60 %RH.

The temperature at the chilled wall surface, where the Petri dishes were located, was on average 18.2ºC giving 49, 60 and 70 %RH in the microclimate behind the cupboard. The

relative humidities and temperatures were measured both in the middle of the room and behind the cupboard.

During the measurements, the Petri dishes were dismantled from their positions and the weight was determined by use of a balance. The rate of weight increase together with knowledge of the difference of water vapour pressure over the cardboard specimens made it possible to determine the total water vapour resistance of the system of cardboard layers. The airflow above the Petri dish cups was not measured during these experiments.

4 Analytical investigation

The presented theory will be used to estimate the surface resistance in the cup tests based on the airflow velocities found in the measurements. Furthermore, numerical simulations of the airflows for the cup tests were performed. These were expanded with an investigation of changes due to cup design, e.g. with and without a rim.

4.1 Theoretical calculations for the cup tests

In Figure xx a calculation example is presented. The calculation represents an example of how theoretically estimated surface resistance can be estimated by use of Equations 4-10.

This example uses a velocity of 0.33 m/s, which is in the lower end of the measured velocity span for the experiments.

First the Reynolds number is found, which determines if the flow is laminar ($Re_D \leq 2300$) or turbulent ($Re_D > 10{,}000$).

$$D_h = \left(\frac{4 \cdot (0.05 \cdot 0.6) m^2}{2 \cdot (0.05 + 0.6) m} \right) = 0.0923 m$$

$$\mathrm{Re}_D = \frac{1.197 \, {}^{kg}/_{m^3} \cdot 0.33 \, {}^{m}/_{s} \cdot 0.0923 m}{1.7995 \cdot 10^{-5} \, {}^{kg}/_{m \cdot s}} = 2026$$

The found Re_D is in the laminar region. The laminar region will continue up till velocities of 0.37 m/s, then there is transition and when the air flow velocity exceeds 1.63 m/s it becomes turbulent.
To know if the flow is developing the hydrodynamic entrance length is calculated.

$$\left(\frac{x}{0.0923m}\right) \approx 0.05 \cdot 2026 \Rightarrow x \approx 9.35m$$

The length of the flat duct is 1.45 m so this is in the entrance region and the flow is laminar and developing. Calculations show that the laminar flow (u < 0.37 m/s) is only fully developed when the velocity is less than 0.05 m/s, whereas the flow is fully developed turbulent after an entrance length of 0.9 m. So when the flow is turbulent (u > 1.63 m/s) it is always fully developed after 0.9 m, which is when it reaches the sample area.
With the current information the mean Nusselt number can be calculated. The constant, k in Equation 8 is found by linear interpolation between correction factors with the current geometry, which gives k = 6.3.

$$Nu = 6.3 + \frac{0.03\left(0.0923m / 1.45m\right) \cdot 2026 \cdot 0.71}{1 + 0.016\left[\left(0.0923m / 1.45m\right) \cdot 2026 \cdot 0.71\right]^{2/3}} = 8.37$$

Then the convective surface heat transfer coefficient, α_c is then calculated.

$$\alpha_c = \frac{8.37 \cdot 0.02587\, {}^{W}\!/_{m \cdot K}}{0.0923m} = 2.35\, {}^{w}\!/_{m^2 \cdot K}$$

Finally, the water vapour surface resistance, Z_{s1} is found for the example by use of Equation 4.

$$\mathrm{Le} = \frac{0.0258\, {}^{W}\!/_{m \cdot K}}{1.197\, {}^{kg}\!/_{m^3} \cdot 1005.3\, {}^{J}\!/_{kg \cdot K} \cdot 2.5 \cdot 10^{-5}\, {}^{m^2}\!/_{s}} = 0.860$$

$$Z = \frac{1.197\,{}^{kg}/_{m^3} \cdot 1005.3\,{}^{J}/_{kg \cdot K} \cdot 461\,{}^{J}/_{kg \cdot K} \cdot 295.75K}{2.35\,{}^{W}/_{m^2 \cdot K}} \cdot 0.860^{1-0} = 8.13 \cdot 10^{7}\ {}^{Pa \cdot m^2 \cdot s}/_{kg}$$

In Table 1 an estimate of surface resistances based on the Equations 4-10 are shown. Velocities between 0.02 and 2.0 m/s give Nusselt numbers between 6.3 and 37.5, which is transformed to surface resistances between $1.08 \cdot 10^8$ and $1.56 \cdot 10^7$ Pa·m²·s/kg.

4.2 Airflow simulations with CFD

When investigating surface resistances it is important to know the precise surface conditions. The cups used in the permeability measurements are not exactly in plane with the flat duct surface. Therefore, a numerical simulation of the airflow development in the flat duct with the cups has been carried out. For the purpose a computational fluid dynamics (CFD) program [12] was used. The simulated geometry is shown in Figures 5 and 6.

An addition to the simulation of the current experiments presented in this paper is simulations of another variation of cup design with a 2 cm rim, see Figure 6. The idea is to study the effect of local turbulence due to cup design, which is of general importance for performing permeability tests using the cup method.

In the CFD simulation x m of the flat duct before the measuring area and x m after was simulated. These values correspond to the actual cup facility design. In the simulation a inlet velocity of x m/s and an isothermal temperature of x was used. The simulated fluid media was dry air.

The CFD calculations can provide the surface heat transfer coefficient for each sample surface and these will be compared both with measurements and with each other. The CFD software retrieves the surface heat transfer coefficient by use of xxx (formula)

5 Results

First the results of the permeability experiments are presented. Then the results of the airflow velocity measurements will be described. These results will be compared to the results

of the numerical simulations and the simulation results of other cup designs are presented. Finally, the Petri cup measurements are presented.

5.1 Results of dry cup experiments

For all the tested cases the measurements were continued until stationary weight loss or gain of the samples was achieved. The measuring period was typically around 7 hours with 1 weighing every hour. The results shown in this paper are based on at least 5 weighings where the weight change rate is constant within ± 5% of the mean value, which is required by the EN ISO 12572:2001 standard. However in most cases the weight change rate was constant within ± 2% of the mean value.

As an example of the results, the weight uptakes of the cups in test 1 are given in Figure 7. In the figure the numbers in the legend refer to the airflow velocity above the boundary layer of the material surface of the given cup. The slopes of the lines in combination with the exposed surface area and the water vapour pressure difference over the samples are used to calculate the total resistance of the samples. The slopes of the lines in Figure 7 are for 2-layers of paper. The calculated total resistances in this case are between $8.91 \cdot 10^7$ and $1.23 \cdot 10^8$ Pa·m²·s/kg. The lowest surface resistance is for the case with a velocity of 0.34 m/s and the highest value was measured at an airflow velocity of 0.06 m/s. These airflow velocities also have the steepest and the flattest slopes respectively in Figure 7.

By use of Equation 10 the surface resistances for each cup at every test have been found. The corresponding surface resistances as a function of the airflow velocity above the boundary layer of the four tests are shown in Figure 8. In the figure a trend-line is added which has been calculated by a least squares fit of all measurements according to a power function. The equation for the trend line is $Z_{s1} = 2.17 \cdot 10^7 \cdot u^{-0.273}$

Along with these measurements, the surface resistances estimated by Equations 3 - 9 are given together with the simulation results (described later).

5.2 Airflow measurements

In Table 2 the results are given of the performed airflow velocity measurements in the middle of the flat duct with 2.5 cm distance to the sample surface. The fan settings are 1 - 3 (1 is slowest) and the abbreviation PRF refers to perforated rubber foam, this gives average

velocities in the range 0.33 – 1.30 m/s. All results are time averaged as described in part 3.1.1.

5.3 Comparison of airflow measurements and simulation

The results of the simulation and the measurements are compared in Figure 8, where both the surface resistances of the actual cup used and a design with a 2 cm rim are given. The surface resistance of the sample surfaces are also compared at the actual position of each cup for both the simulation and the post processed permeability tests for an airflow velocity of 1.3 m/s in Figure 9.

5.4 Local turbulence due to cup design

In Figure 10 local airflow patterns due to cup design are shown. In part (a) the results of the simulation with the geometry of the cups actually used in the permeability tests are shown and in (b) results of the airflow pattern of a similar cup with a rim of 2 cm are shown. In Table 3 the calculated surface heat transfer coefficients for the two simulated cases are given.

5.5 Results of Petri cup test

The Petri cups were measured every hour for at least 8 hours and the results are based upon a minimum of 5 weighings. The results of the three tests with different relative humidities are given in Figure 11, where the resistance is plotted as a function of numbers of paper layers. The surface resistances are then found as the interception with no layers (intercept with y-axis). The found surface resistances where in the range 4.3 – $5.4 \cdot 10^7$ Pa·m²·s/kg.

6 Discussion

The measured results show a tendency of higher surface resistances for lower airflow velocities. This was expected since the theoretical values from Equations 4-10 also show that the surface resistance declines with increasing airflow velocity. However, if the surface resistances from the measurements are compared with the estimated theoretical surface resistances in Figure 8, it is found that the measured values are smaller than predicted. Apart from the general uncertainty of measuring the surface resistance, this could be a sign

that the true surface convection is stronger than assumed by the theoretical estimates of the air flow. In addition, the shape of the curves for measured and CFD simulated results are similar, but the simulated surface resistances are smaller, see Figure 8. For low velocities the simulated results are only about half the value of experiments but the distance between the two curves decreases with increasing airflow velocity.
For comparison, results from a drying experiment of a wet sample carried out by Bednar & Dreyer [1] have shown a moisture transfer coefficient, β_p of around $18 \cdot 10^{-5}$ kg/Pa·m²·h for a room with "still" air. This number corresponds to a surface resistance of $2.0 \cdot 10^7$ Pa·m²·s/kg. This resistance seems quite small compared to Figure 8 where both the estimated and the measured surface resistances for velocities less than 0.2 m/s are higher. However, as a drying experiment the conditions may not be quite comparable with those exerted in the cup experiments described in the present paper.

The results can also be compared to the cup tests by Fanney et al. [5] who found a surface resistance for a dry cup experiment in an environmental chamber at 23.6°C (44.7 %RH) of $13.3 \cdot 10^7$ Pa·m²·s/kg. This value was obtained by open cup (without an attached sample) experiments in "still air" inside desiccators and does not account for changes in temperature due to wetting of the desiccant.

The results of the Petri cup tests can also be compared to work by Janssens et al. [13]. They worked with prediction of water vapour transfer of spunbonded plastic films, which are highly permeable materials. They found that accurate measuring of the surface resistance was only obtained by permeance test on multiple material layers. In this work a surface resistance of $27.5 \cdot 10^7$ Pa·m²·s/kg for dry cup experiments was found, but for open cup measurements surface resistances of $4.6 \cdot 10^7$ and $4.9 \cdot 10^7$ Pa·m²·s/kg were found. In the current study of Petri cup test the resistances for multiple layers was also plotted. This resulted in surface resistances in the range $4.3 - 5.5 \cdot 10^7$ Pa·m²·s/kg, which corresponds well with the open cup results of Janssens et al. [13].

The measured and simulated airflow velocities below each cup can only be compared directly for the tests with an average airflow velocity of 1.3 m/s, due to the insertion of perfo-

rated foam plastic in the duct in the other 3 experiments. From Figure 9 it is found that the results are comparable but however simulation results alone show noticeable changes for the different airflow velocities so a comparison for lower airflow velocities could have been more interesting. The investigation of the airflow with CFD shows that there is great impact on the distribution of airflow velocities due both a metal bar separating the Perspex plates in the sample area and as seen in Figure 10 due to holes in the lower part of the Perspex plate/duct.

The simulations were extended to include an investigation of influence of cup design to study the influence of a rim. It was found that the airflow velocity at the sample surface is considerately lower when there is a rim resulting in bigger surface resistances. Even for turbulent airflow velocities the difference in surface heat transfer coefficients are > 65 %. However, the influence of the rim will still be negligible for most building materials, except for lightweight materials relatively open for water vapour.

The CFD simulated surface resistances were found to be slightly smaller than the measured. This may be due to the calculation of the surface heat transfer coefficient in the CFD program. We do not know exactly what is done e.g. at which distance from the surface is the velocity is evaluated. However the results are predicted quite well, so it is found that CFD simulation can be used to estimate expected surface resistances before any experiments are performed for airflow velocities in the range 0.1 – 1.4 m/s.

In the Petri cup tests the total resistance is plotted versus numbers of paper layers. Linear intercept with the y-axis (no layers) give the surface resistance as seen in Table 4. Here, the results show that the no layer intercept give almost the same value as if the surface resistance is found by Equation 11 modified to 1 and 3 layers of paper. This was expected since the intercept for plotting of 1 and 2 layers only gives the same results as subtracting 1 and 2 layers. It seems fairly simple to apply the Petri cup tests in practice however the idea needs some refining. From Figure 8 the airflow velocity corresponding to a surface resistance of $4.3 \cdot 10^7$ Pa·m²·s/kg (53% RH) is about 0.08 m/s for the cup test measurements. This number is very low and needs to be verified by other studies.

7 Conclusion

It has been found possible to determine the surface resistances of moisture transfer by measurements on samples with different thicknesses by using dry cup experiments as described in the Japanese standard JIS A 1470-1:2002 test method. The results show that the surface resistances decrease for increasing airflow velocity above the boundary layer of the material surface. This was expected since the theoretical estimated surface resistances also show that the resistance increases with decreased airflow velocity. The measured resistances are somewhat smaller than the ones theoretical estimated but higher than the CFD simulation results. The measured and simulated results show the same pattern.

The CFD simulations also compared cup designs. Two designs were tested one as used in the permeability experiments and a cup with a 2 cm rim. As expected, the rim has a significant influence on the airflow velocity above the exposed sample surface. The lower airflow velocities also give much lower heat transfer coefficients, which for open lightweight materials can play an important role. Thus CFD simulation can be used to give an idea about the expected surface resistances for velocities in the range 0.1 -1.4 m/s and it can provide useful information about the flow patterns so inconvenient design cup test facilities can be avoided.

The concept of using the Petri cup test for investigation of the microclimate in the field is promising but needs to be developed and tested further.

Acknowledgements

The work was carried out with support of the Technical Research Council of Denmark. This support is gratefully appreciated. Thanks are due to Associate Professor, PhD Kurt Kielsgaard Hansen for experimental help with use of the cup facility, and M.Sc. Jeff Mertens for performing the field cup tests.

References

[1] T. Bednar, J. Dreyer, 2003. Determination of moisture surface transfer coefficients under transient conditions, in: J. Carmeliet, H. Hens, G. Vermeir (Eds.) Research in Building Physics Proceedings of the Second International Conference on Building Physics, Leuven, Belgium, Swets & Zeitlinger, Lisse, ISBN 90 5809 565 7, 2003, pp. 233-236.

[2] K. Svennberg, L. Wadsö, A modified cup-method for lightweight and highly permeable materials, in: J. Carmeliet, H. Hens, G. Vermeir (Eds.) Research in Building Physics Proceedings of the Second International Conference on Building Physics, Leuven, Belgium, Swets & Zeitlinger, Lisse, ISBN 90 5809 565 7, 2003, p. 177-182.

[3] G. Galbraith, D.J. Kelly, R.C. McLean, Moisture permeability measurement under reduced barometric pressures, Materials and Structures 37 (2004) 311-317.

[4] G. Scheffler, R. Plagge, Defined drying behaviour measurement for building materials, in: J. Carmeliet, H. Hens, G. Vermeir (Eds.) Research in Building Physics Proceedings of the Second International Conference on Building Physics, Leuven, Belgium, Swets & Zeitlinger, Lisse, ISBN 90 5809 565 7, 2003, p. 23-30.

[5] A.H. Fanney, W.C. Thomas, D.M. Burch, L.R. Mathena, Measurements of moisture diffusion in building materials, ASHRAE Trans. 97 (2) (1991) 99-113.

[6] A. Worch, The behaviour of vapour transfer on building material surfaces: The vapour transfer resistance, Journal of Thermal Envelope & Building Science 28 (2) (2004) 187-200.

[7] JIS A 1470-1:2002. Test method of adsorption/desorption efficiency for building materials to regulate an indoor humidity – Part 1: Response method of humidity. Japanese Industrial Standard, translated and published by Japanese Standard Association.

[8] EN ISO 12572:2001. Hygrothermal performance of building materials and products – Determination of water vapour transmission properties. *European committee for standardization.* Brussels

[9] W. Nusselt, Wärmeübergang, Diffusion und Verdunstung, Z. f. angew. Math. und Mech. Bd. 10 (1930), H. 2, 105-121.

[10] W. Illig, Die Grösse der Wasserdampfübergangszahl bei Diffusionsvorgängen in Wänden von Wohnungen, Stallungen und Kühlräumen, Gesundheitsingenieur 73 (1952), H. 7/8, 124-127.

[11] A.F. Mills, Heat and mass transfer, Irwin, 1995, ISBN 0-256-11443-9 pp. 269-275.

[12] K.K. Hansen, Equipment for and results of water vapour transmission tests using cup methods, in: Heat and Mass Transfer in Building Material and Structure, *Sym*, J.B. Chaddock (*Ch*), Dubrovnik, 1989

[13] Fluent Inc. (1999). FLUENT® User's Guide, Lebanon, NH, USA: Fluent Inc.

[14] A. Janssens, H. Hens, Water vapour transfer properties of spunbonded plastic films, J. Thermal Insulation and Building Envelopes. 21 (1997) 202-220.

Figure captions

Figure 1. Drawing of the equipment for cup measurements. The air is circulated and conditioned within the equipment.

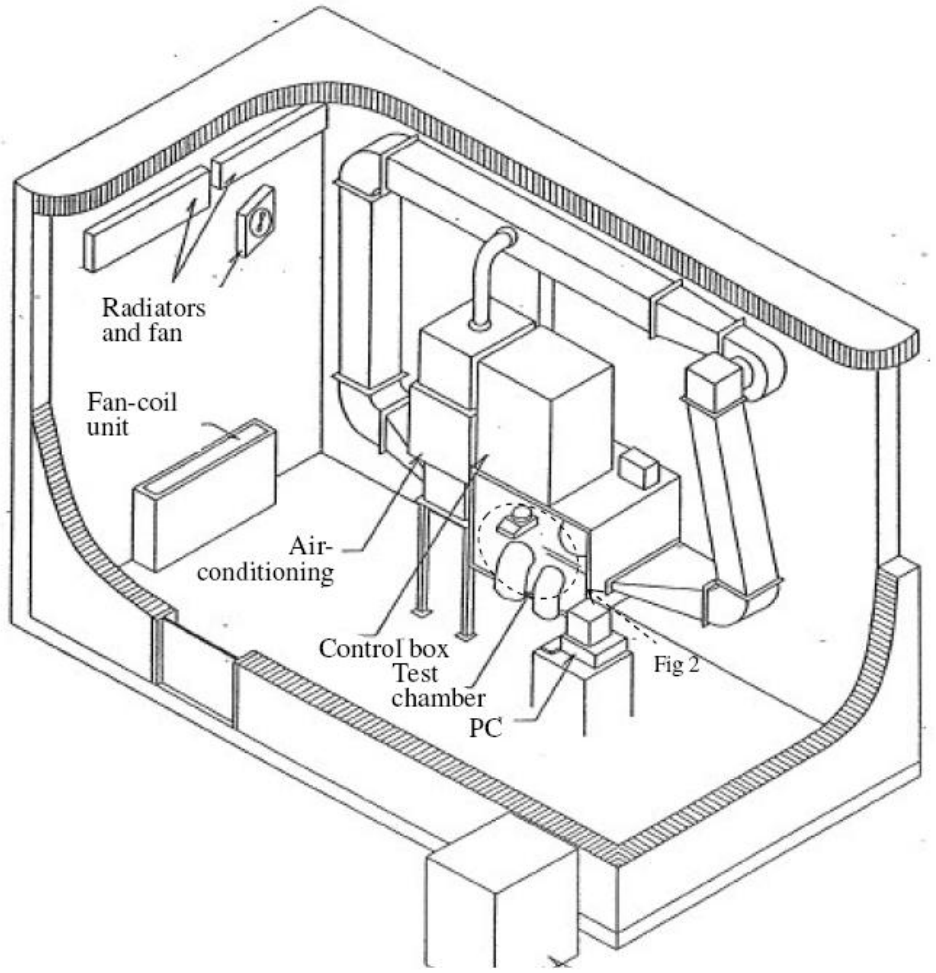

Figure 2. (a) Picture showing the actual test chamber. The inverted cup samples are positioned face down in holes in a Perspex plate. The air flows below the cups in the 5 cm high duct. (b) Principle drawing of a cup in the sample area. Note that part of the cup is actually in plane with the Perspex plate.

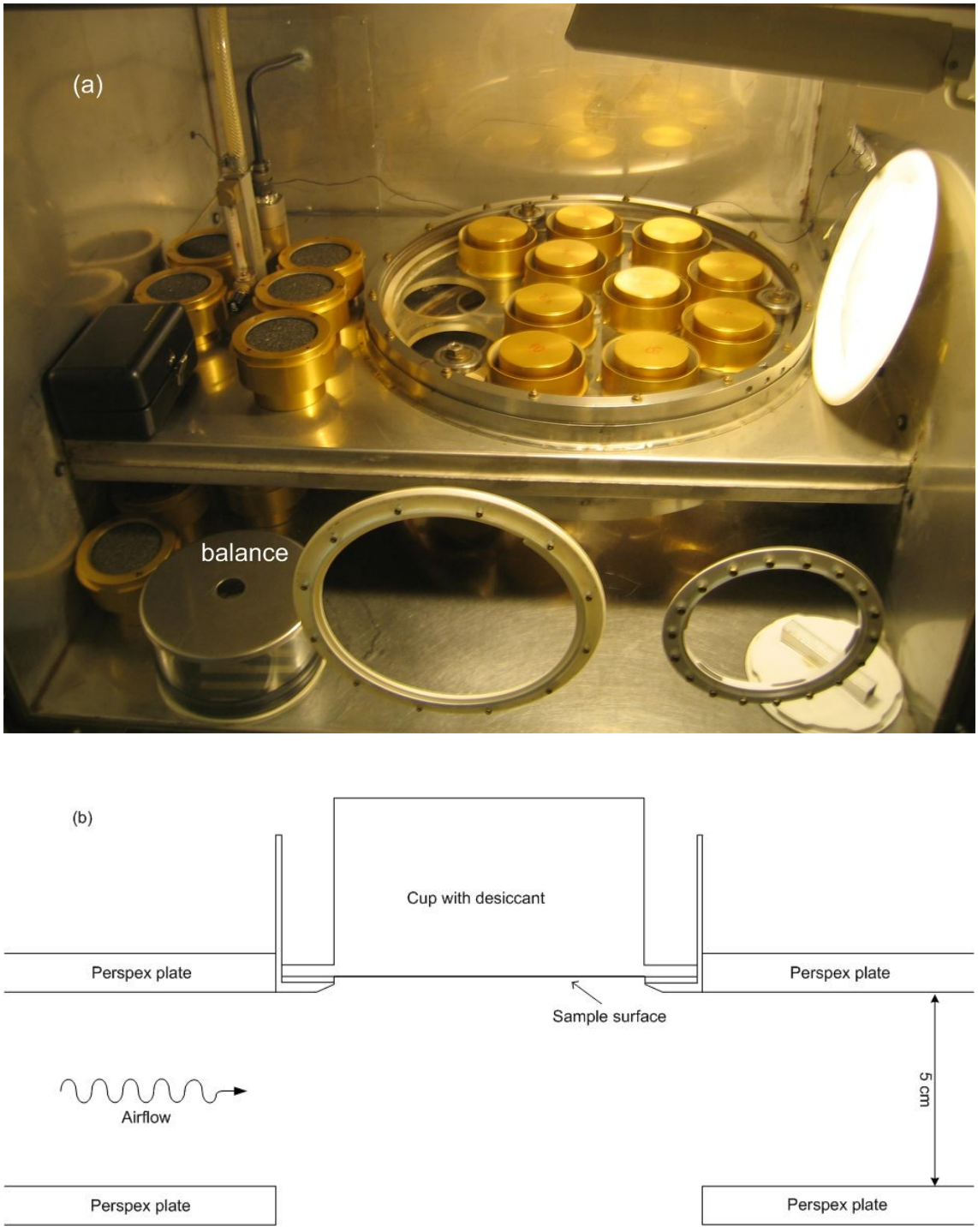

Figure 3. Picture of cup with half a piece of 1-layer sample paper (190 g/m^2) and without desiccant. The white ring above the sample is Teflon and the black ones above and below are rubber sealing rings.

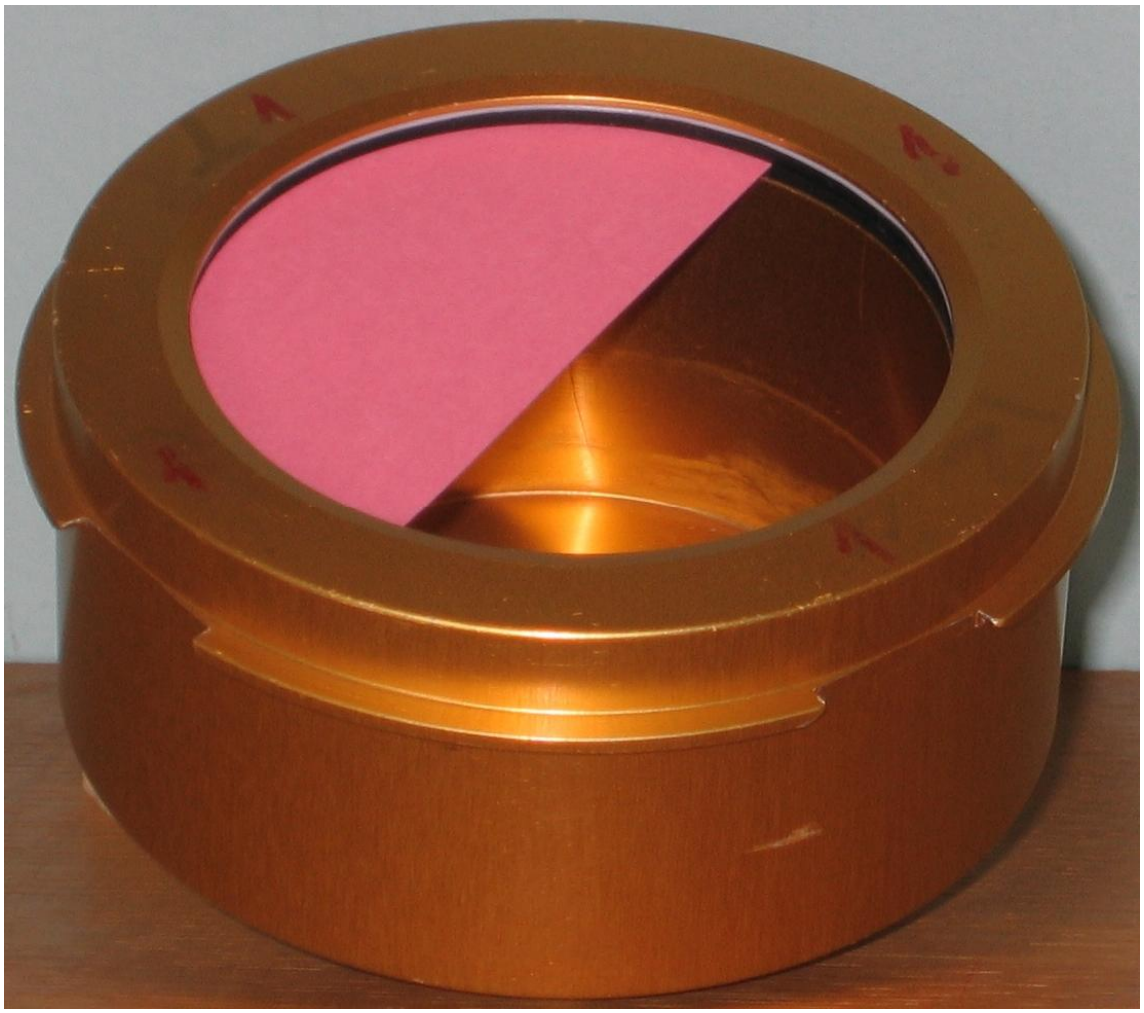

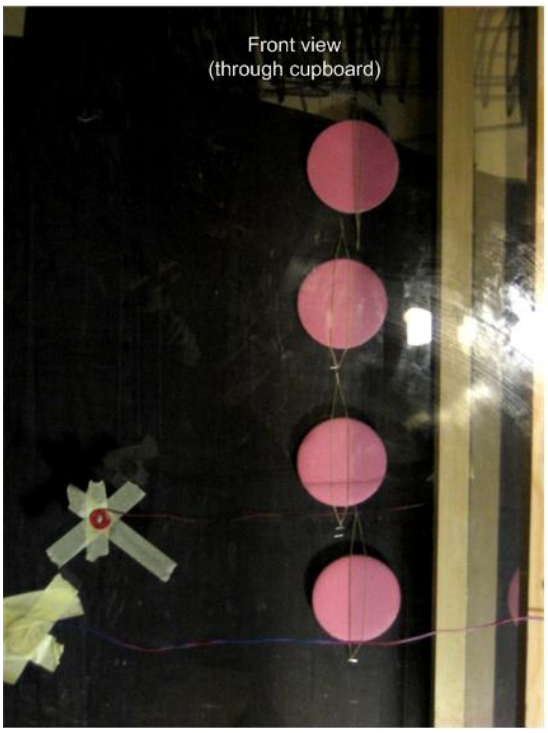
Front view
(through cupboard)

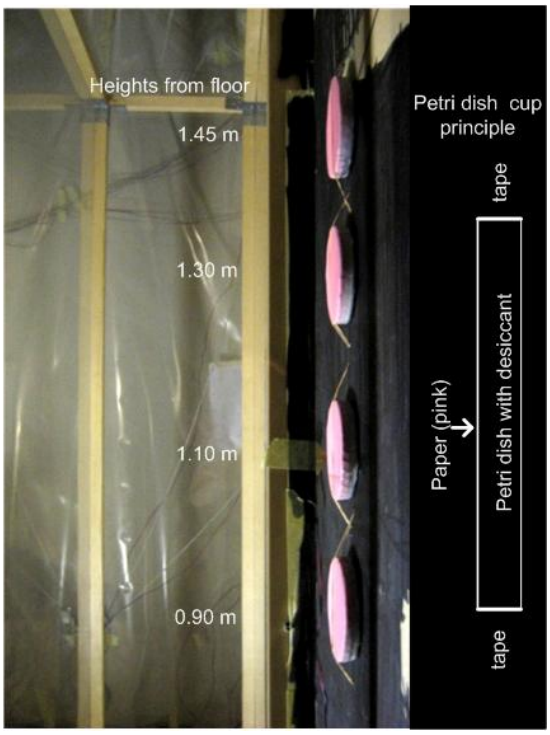
Heights from floor
1.45 m
1.30 m
1.10 m
0.90 m
Petri dish cup principle
tape
Petri dish with desiccant
Paper (pink)
tape

Figure 4. Picture of Petri dish cups placed vertically on the cold wall with the paper facing the room. The cupboard is made from Perspex plates so it is transparent. The principle of the Petri dish cups can also be seen as well as the heights the cups were placed in.

Figure 5. The figure shows the geometry of the simulated cases. Here the vector results for an airflow velocity of 0.17 m/s at the inlet are given in a plane, y = 0.25 m, which is 5 cm from the centreline. The inlet is at the end of the flat duct furthest away from the sample area, this ensures a uniform flow when the sample area is reached. The velocity vectors are coloured by the scale on the left in the range 0 - 0.2 m/s.

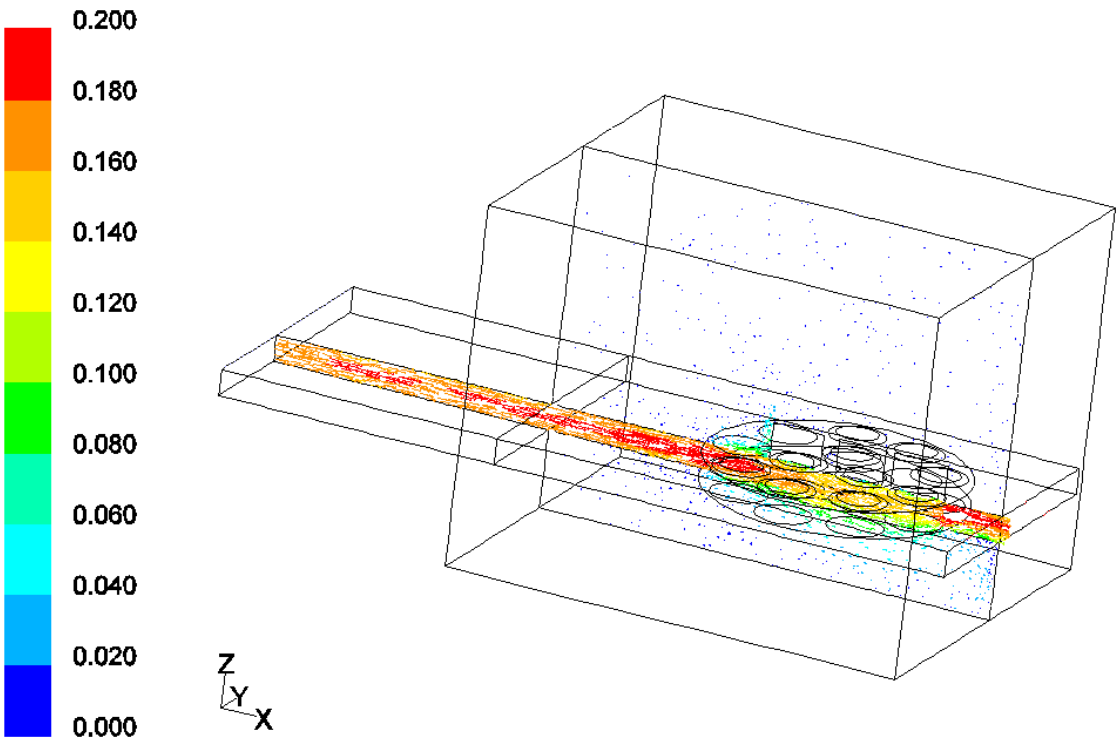

Figure 6. Geometry for CFD simulation of cup and cup with rim

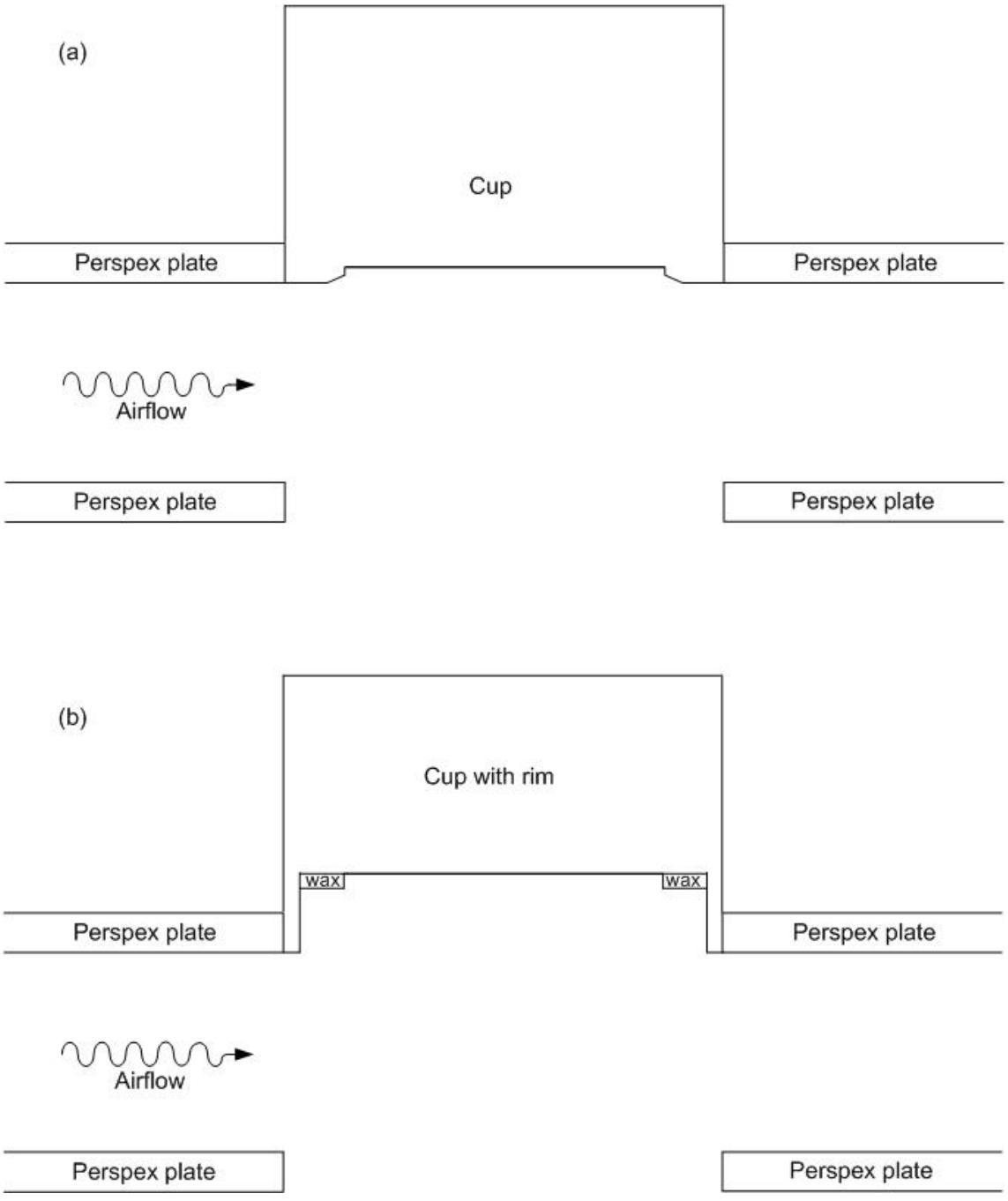

Figure 7. Dry cup weight changes in test 1 with 2-layers of paper. In test 1 the airflow velocity above the boundary layer of each of the cups is in the range 0.06 – 0.54 m/s.

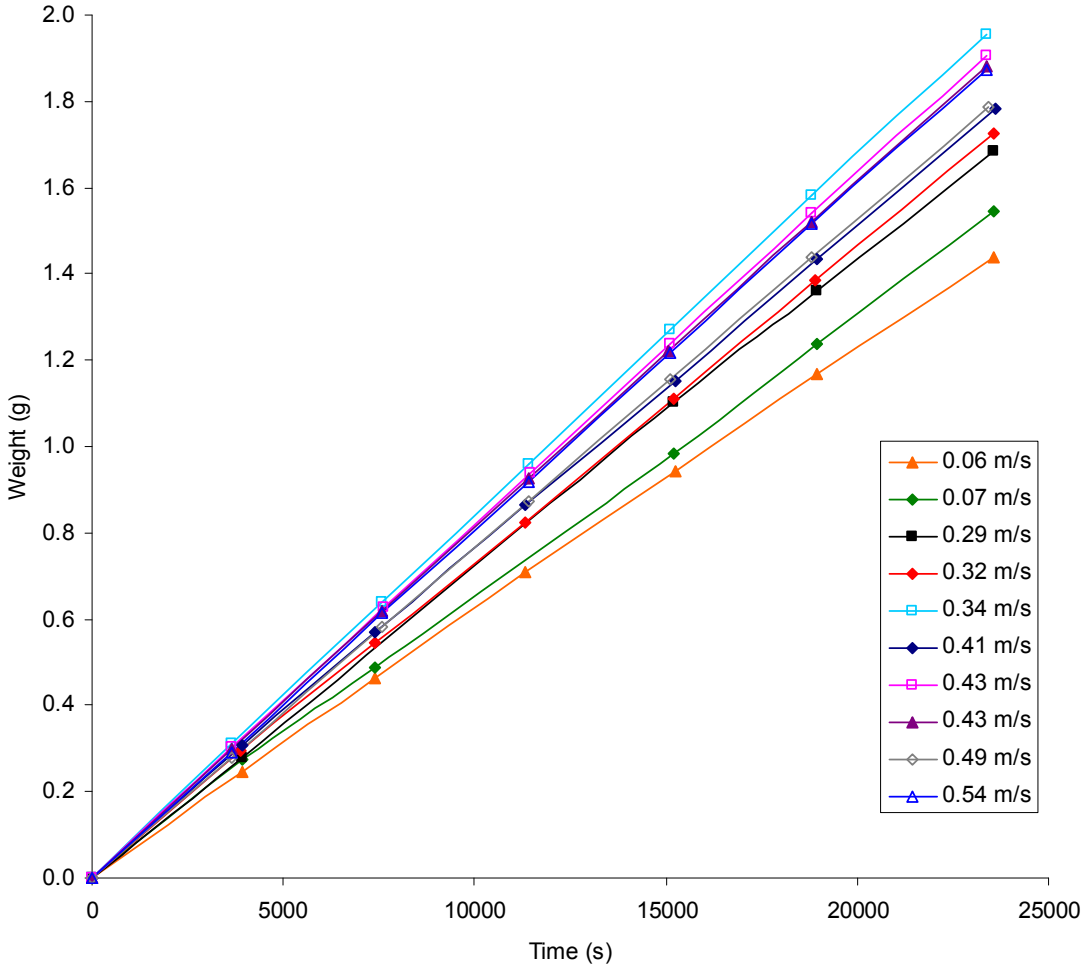

Figure 8. Water vapour surface resistances, estimated, measured and simulated. The calculated theoretical values are separated in 3 parts, laminar, transient and turbulent. The transient part is hatched and between the laminar and turbulent boundary.

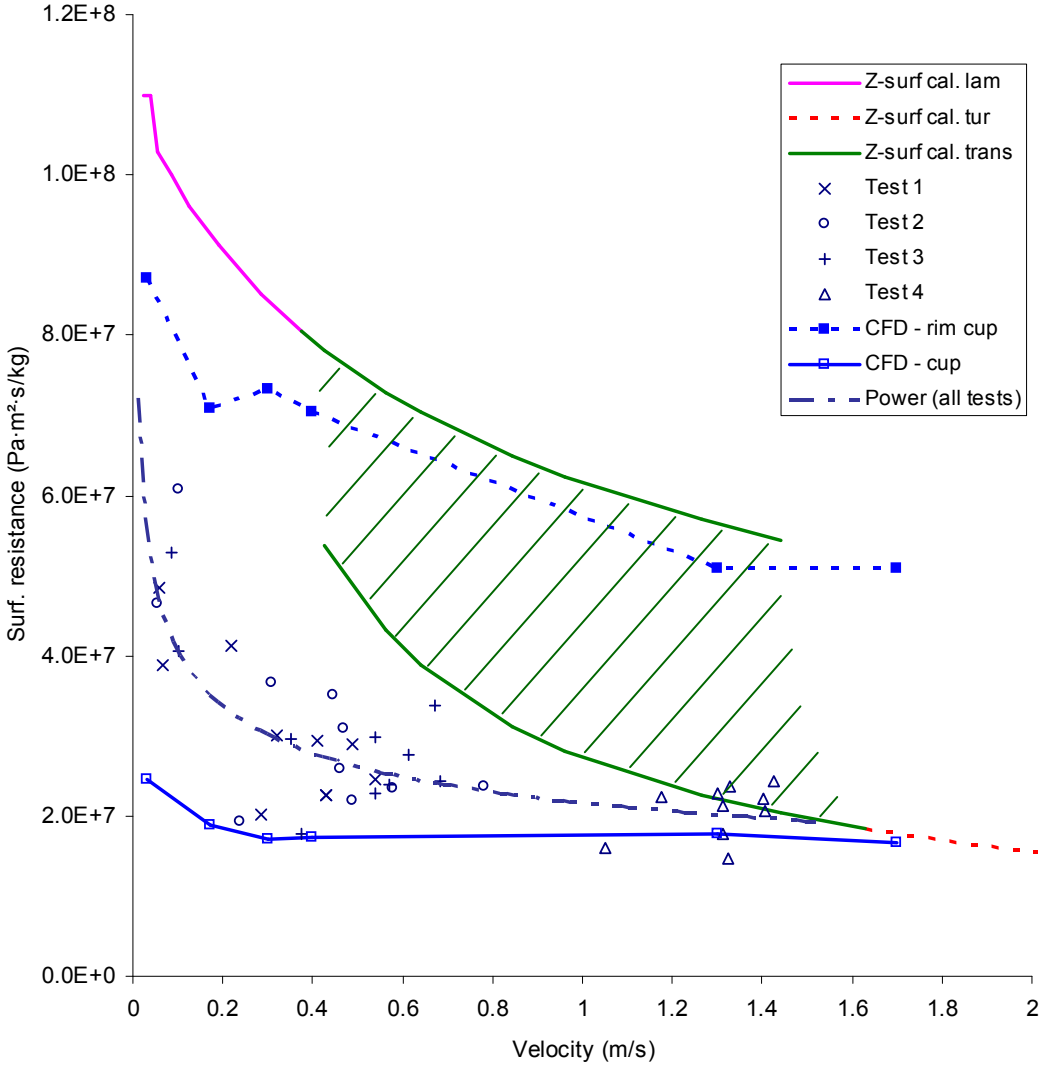

Figure 9. Examples of surface moisture resistances for each cup for an air velocity of 1.3 m/s (regime of transition). Results of cup experiment and numerical simulation are shown.

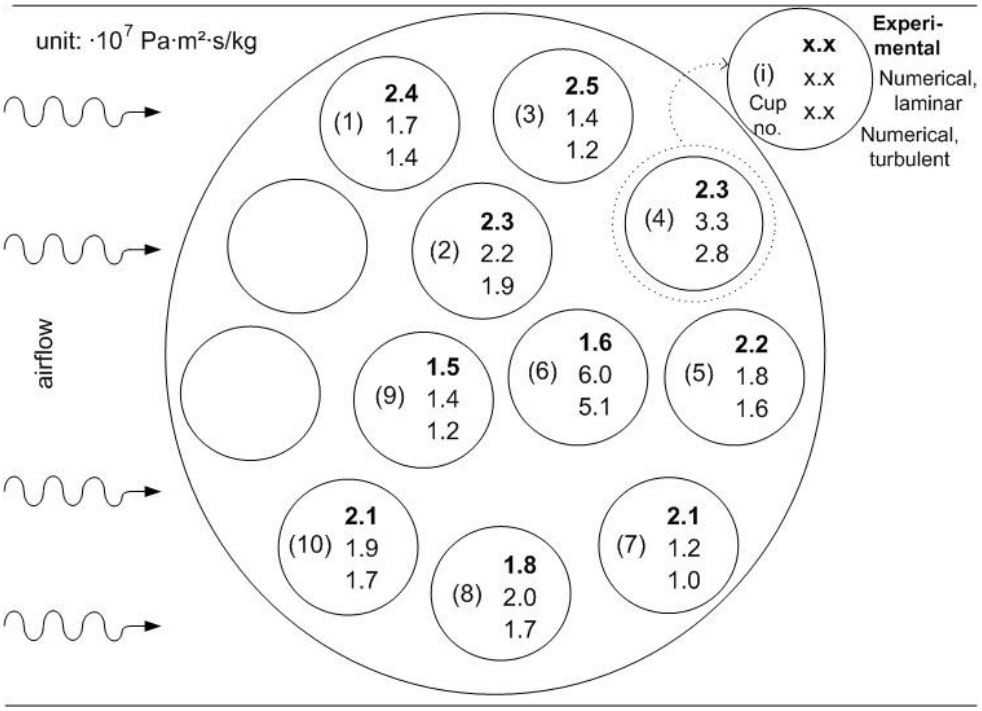

Figure 10. Airflow velocity distribution for inlet velocities of 0.17 m/s. The results are zoomed images of the result plane y = 0.25 and it is given for (a) the actual cup and (b) a cup with a 2 cm rim. The velocity vectors are given in the range 0 – 0.2 m/s.

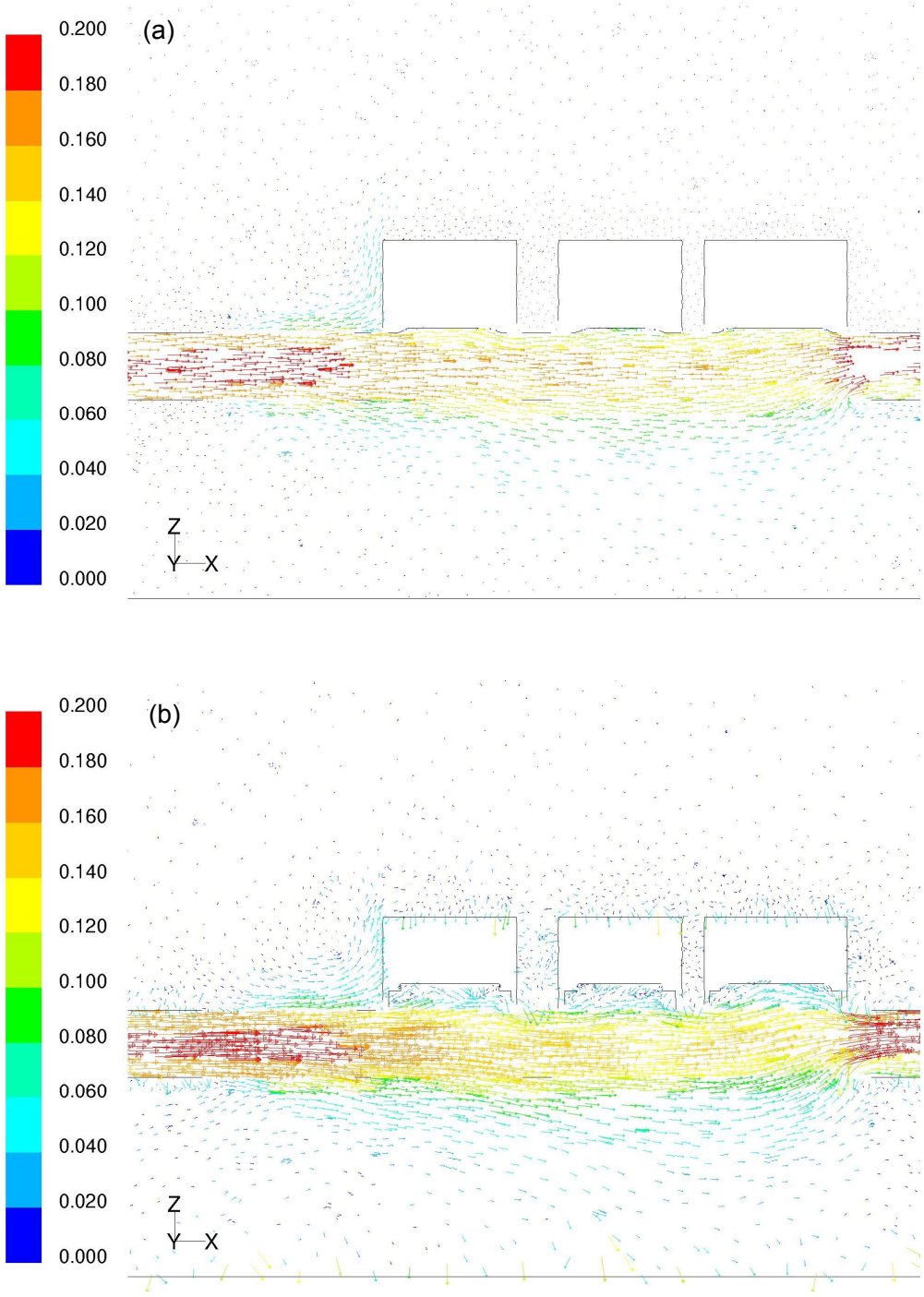

Figure 11. Results of Petri dish cup tests. Diffusion resistances plotted as a function of the number of material layers. Data from 3 measurements are presented. The difference between the measurements is the relative humidity at the sample surface.

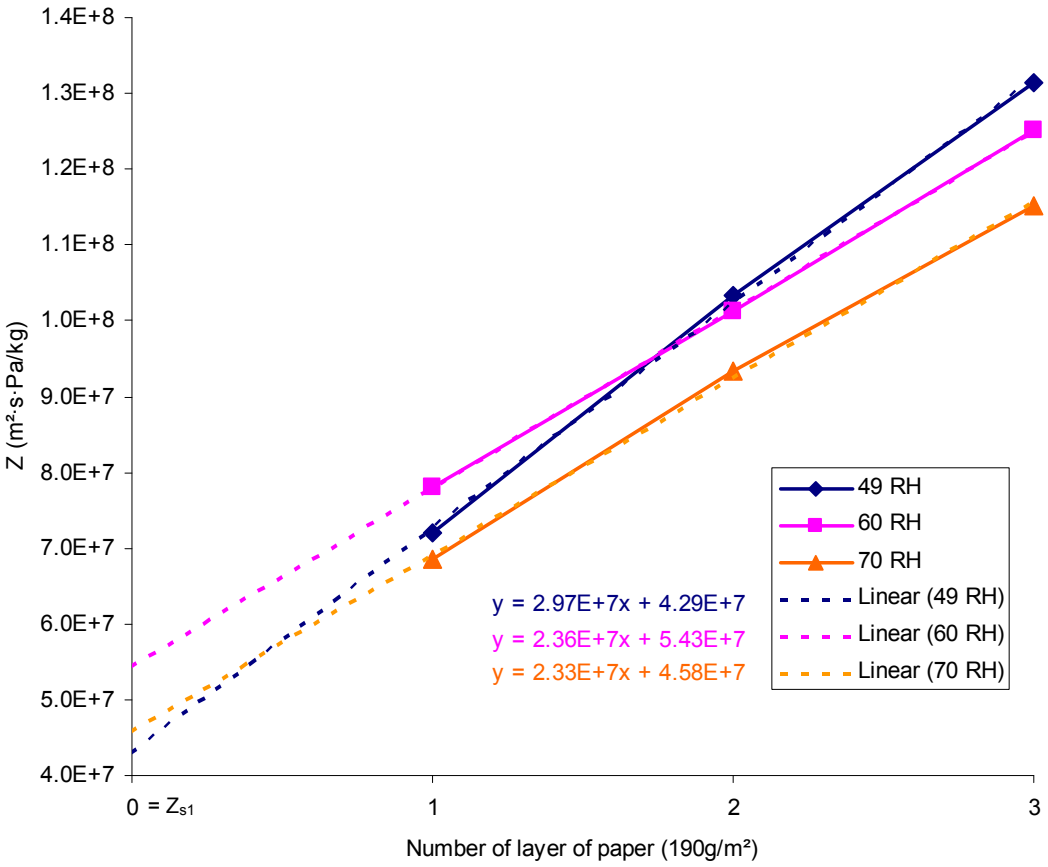

Tables

Table 1. Estimated surface resistances based on Equations 3-9. In the transition area values for both laminar (n = 0) and turbulent (n = 1) behaviour is calculated.

Airflow velocity	0.02 m/s	0.17 m/s	0.33 m/s	0.39 m/s	0.45 m/s	0.70 m/s	1.3 m/s	1.7 m/s	2.00 m/s
Nu (-)	6.3	7.5	8.4	8.7-10.1	9.0 - 11.3	10.1-16.2	12.3-26.5	32.9	37.5
α_c (W/m²K)	1.77	2.09	2.35	2.43-2.83	2.52-3.18	2.83-4.53	3.44-7.44	9.22	10.5
$Z\left(\frac{Pa \cdot m^2 \cdot s}{kg}\right)$	$1.1 \cdot 10^8$	$9.3 \cdot 10^7$	$8.3 \cdot 10^7$	$8.0 \cdot 10^7$-$5.8 \cdot 10^7$	$7.7 \cdot 10^7$-$5.2 \cdot 10^7$	$6.9 \cdot 10^7$-$3.6 \cdot 10^7$	$5.6 \cdot 10^7$-$2.2 \cdot 10^7$	$1.8 \cdot 10^7$	$1.6 \cdot 10^7$

Table 2. Measured airflow velocities, in the middle of the air circulation duct below each sample surface. The cup sample position can be seen in Figure 9. The abbreviation PRF is perforated rubber foam, which is used slow down the air. The number 1-3 are settings for the ventilation fan inside the cup test facility. The last column results are with the lowest fan setting and without the rubber foam to reduce the flow.

Measuring position	**PRF1** (m/s)	**PRF2** (m/s)	**PRF3** (m/s)	**1** (m/s)
Sample 1	0.22	0.31	0.35	1.33
Sample 2	0.41	0.45	0.54	1.30
Sample 3	0.06	0.10	0.10	1.43
Sample 4	0.07	0.06	0.09	1.18
Sample 5	0.32	0.47	0.67	1.40
Sample 6	0.43	0.49	0.57	1.05
Sample 7	0.49	0.46	0.62	1.31
Sample 8	0.54	0.58	0.69	1.31
Sample 9	0.29	0.24	0.38	1.32
Sample 10	0.43	0.78	0.54	1.40
Average	**0.33**	**0.39**	**0.45**	**1.30**

Table 3. Surface heat transfer coefficients for the two simulated cases, with and without rim.

Inlet velocities (m/s)	0.03	0.17	0.3	0.4	1.3	1.7
Cup, α_c (W/m²·K)	7.55	9.79	10.89	10.66	10.42	11.14
Rim, α_c (W/m²·K)	2.13	2.62	2.53	2.64	3.65	3.64
Difference %	71.8	73.2	76.7	75.3	65.0	67.3

Paper III

Investigation of microclimate by CFD modelling of moisture interactions between air and constructions

Mortensen, L. H., Wolozsyn, M., Rode, C. & Peuhkuri, R. (2007)

Published in: Journal of Building Physics, 30 (4), 279-315,
http://dx.doi.org/ 10.1177/1744259106075233

Investigation of Microclimate by CFD Modeling of Moisture Interactions between Air and Constructions

LONE H. MORTENSEN,[1,*] MONIKA WOLOSZYN,[2]
CARSTEN RODE[1] AND RUUT PEUHKURI[1]
[1]*Department of Civil Engineering, Technical University of Denmark Lyngby, Denmark*
[2]*CETHIL (Thermal Sciences Centre) UMR CNRS 5008 – UCBL – INSA Lyon, France*

ABSTRACT: There is a strong demand for accurate moisture modeling since moisture poses a risk for both the constructions and the indoor climate. This investigation has special focus on moisture modeling. This study describes a new model based on a CFD tool enhanced to include both detailed modeling of airflows in rooms and heat and moisture transfer in walls by applying them as fluid walls. The impacts of different boundary conditions and how these influence microclimates in rooms are investigated, in a 3D configuration. The studied microclimate is a piece of furniture placed near a cold exterior wall.

KEY WORDS: moisture modeling, CFD, boundary conditions.

INTRODUCTION

MOISTURE PLAYS A significant role in the development of many processes that are harmful to both the quality of indoor air and the conditions of the constructions in the building envelope. Therefore it is anticipated that moisture modeling can help to ensure design of healthier indoor environments and constructions. The focus of this investigation is on the multi-dimensional moisture interactions between constructions and the room air. The moisture flow between air and construction depends strongly upon the airflow conditions close to the surface, which is influenced by the airflow patterns in the room. Thus, it is important to investigate the airflows carefully and to estimate their influence on the moisture transport.

*Author to whom correspondence should be addressed. E-mail: loh@byg.dtu.dk
Figures 1–33 appear in color online: http://jen.sagepub.com

1744-2591/07/04 0279–37 $10.00/0 DOI: 10.1177/1744259106075233

In building simulation models it is common to consider just one node for the air in a room and to assume fully mixed conditions. If a more detailed analysis of the air distribution in the room is needed it can be obtained by use of computational fluid dynamics (CFD) simulations. The potential of using CFD for simulations is great, since it can provide detailed information on airflow patterns, temperature distribution, etc. CFD provides possibilities for developing new state-of-the-art models that provide easy visualization of the results, that can replace the very costly experiments, and after all the goal is to ensure better design of buildings. Other researchers have already tried to use the advantages of CFD for building simulation. Negrão (1998), Bartak et al. (2002), Zhia et al. (2002), and Zhia and Chen (2003) have all attempted to couple CFD and energy simulations of building envelopes. In relation to moisture interactions, Clarke et al. (1999) developed a model that could predict conditions leading to mold and recently Hohota (2003) has shown that CFD models can be used to predict condensation on surfaces.

Where other models have focused on either air and moisture flows in rooms or on heat and moisture transfers in walls, the model described in this study tries to combine the detailed modeling of both. The chosen approach is not to combine two existing models but to enhance an existing CFD model to include heat and moisture transport in walls. The main advantages of the chosen approach are the detailed description of the airflow patterns in the room and good numerical convergence, which can be difficult to obtain when two different codes are being combined. The aim of such a model is to obtain more information about what happens in microclimates that can be critical.

Hence, the enhanced CFD model including moisture transfers in both air and the surrounding building envelope is presented in the following sections. Then the model is used to study heat and moisture microclimate in the space behind a piece of furniture placed close to a cold external wall with limited airflow on the surface. The idea is to study how the diffusion and the airflows influence the vapor content at the internal surface. This is very important since it is in areas like this that mold growth can occur and it has a negative impact on the indoor climate.

MODEL

The detailed numerical model enabling the representation of both the moist airflow and its interactions with constructions is implemented in the commercial CFD tool FLUENT (version 6.1, Fluent, 1999). It is based on the finite-volume method using SIMPLE solving algorithm and a predictor-corrector approach (Patankar, 1980).

Moist Airflow Model

The velocity and temperature fields in a room are found from three basic CFD equations. They are the conservation equations for mass, momentum, and energy. The mass conservation is ensured by the continuity equation and the conservation of momentum is derived from Newton's second law and finally, the energy conservation equation is based on the first law of thermodynamics. Furthermore, CFD is based on Navier–Stokes equations for laminar flow which enables airflow modeling. In many cases these are expanded to include a turbulence model as well. More about computational fluid mechanics can be found for example, in Versteeg and Malalasekera (1995).

In the present study the realizable k–ε model developed by Shih et al. (1995) was used. This is an extension and improvement of a well-known standard k–ε model, proposed originally by Jones and Launder (1972). One of the main improvements is more accurate representation of boundary layer flows as shown by Shih et al. (1995) and Teodosiu (2001). This is very important in this case, as microclimates are highly dependent on boundary layer flows.

Moreover, the air layer close to the wall surface is represented using enhanced wall treatment. It is based on a two-layer approach that subdivides the region into a viscosity-affected and a fully turbulent region. This is done by a relation between the Reynolds number and the distance to the nearest wall. In the viscosity-affected region the one-equation model developed by Wolfshtein (1969) is employed. If the mesh in the near-wall region is too coarse a smooth blending of the laminar and turbulent wall law will be performed. Teodosiu (2001) showed that this model is suitable for building airflow studies, where air velocities are low.

Moist air is represented as a perfect mixture of two perfect gases: dry air and water vapor. Thus, the influence of water vapor on mixture properties, such as density or heat capacity, is represented.

Heat and Moisture Transfer in Walls

As the temperature and moisture conditions close to the walls are of main interest here, heat and moisture transfer in the walls is represented. For this first study, heat conduction and vapor diffusion in walls were modeled.

Existing CFD tools focus on airflow movement and have only some simple models of transfer phenomena in solids. Therefore, some extended modeling was needed in order to include both heat and

moisture transfer. Basically, there are two ways to represent moisture transfer in the envelope:

1. To use the existing model for heat transfer in a solid material and enhance it for moisture transfer. In this case, vapor diffusion needs to be programmed by the user.
2. To use the existing diffusion equation. As diffusion is computed only in fluid domains, the walls need to be defined as fluids.

The second approach was chosen, mainly because it limits the use of user-defined functions, which decrease the numerical performance of the numerical solver. The constructions are therefore modeled as immobile fluids with ordinary building material characteristics as material properties. This enables modeling of moisture diffusion within the walls. The diffusion model simply has two boundary vapor contents and then performs a linear regression between the values. To use the fluid walls, it is necessary to declare the walls as laminar zones with no velocities within them, because otherwise the fluid walls contain a turbulence equation that will give numerical errors.

It should also be noticed that a 'porous media' model, existing in some of the CFD codes cannot be used here, because in this case all fluid components (dry air and water vapor in this case) diffuse in the same way through the porous media. This representation is not suited for modeling of vapor diffusion only.

Heat and Moisture Interaction between Walls and Airflow

As stated earlier, the coupled heat, air, and moisture transfer model was implemented in the existing CFD software. It was originally designed to treat coupled heat and air transfers in fluids and solids, therefore the heat interaction between air and walls was automatically represented using existing standard models. However, first numerical tests showed that there was no moisture transfer between air and the wall. It should be recalled that the mass transfer in the air is modeled in detail with the airborne moisture transport and moisture diffusion in the air volume as well as in the boundary layer. The 3D vapor diffusion in the walls is also represented using the methodology described in the previous paragraph. However in the program, the two fluids, the room air and the wall, should be regarded as being separated by a barrier so they are unable to interact unless specific functions are defined for the interaction. One could regard the boundary as being split in two halves: one that is in contact with the room air, and a shadow copy of this, which is in contact with the wall. The two faces, the real and the shadow, are placed at the same geometrical position but have no functional contact regarding moisture transfer.

Introducing the moisture flow interaction between air and porous material is a difficult problem for both theoretical and numerical reasons.

Theoretically, the mass flow between air and material depends upon various parameters, such as surface painting, microstructure, etc. As the first approach it was decided to use a macro-modeling approach and neglect surface resistance. So it was assumed that the vapor content in the air at the surface was the same in the very first layer of material ($c0^*$) and the very first layer of the room air ($c0$). This is illustrated in Figure 1 where, for the purpose of illustration, the two parts of the boundary face are placed a small distance apart.

Numerically, a user-defined function was programmed and added to the existing model to represent the moisture flow through the boundary. However, it was found that if the identity of vapor content was imposed directly, by setting the content in both cells to be equal to the mean value at previous iteration, numerical divergence appeared. After several trials an iterative heuristic model was set up to describe the interaction between water vapor contents in the fluid cells on either side of the boundary and to respect mass conservation of vapor. The first step in the procedure is to perform a test to determine the direction of the moisture transfer. Then, on the basis of this information, the transfer of moisture is calculated. The principle of predicting the transfer is shown in Equation (1).

$$x_{c0} > x_{c0^*} \Rightarrow x^n_{c0^*} = x^{n-1}_{c0^*} + \frac{\left(x^{n-1}_{c1} - x^{n-1}_{c0}\right)}{d1} \cdot d2 \tag{1}$$

where x is the water vapor content in the air or pore air in wall (kg/kg);
c is cell and 0 refers to a cell next to the wall surface in the air;
$c0^*$ is the corresponding cell adjacent to $c0$ in the wall;
$c1$ is the cell next to $c0$; n is the iteration number;
$d1$ is the distance between the centers of $c1$ and $c0$ (m);
$d2$ is the distance between $c0$ and $c0^*$ (m).

The new water vapor content of mesh element $c0^*$ in the wall is calculated in an iterative way. If the water vapor content in the air $c0$ is higher than that in the wall then the transfer is from the air to the wall. In that case $c0^*$ at iteration level n is equal to its own value at the previous iteration level plus a gain determined by the amount that is coming to mesh element $c0$ in the air. The gain at cell $c0$ is proportional to the difference in vapor content between itself and its neighbor cell c_1 as evaluated in the previous iteration step. In order to avoid divergence of the procedure, it has proven useful to weigh the gain by the ratio of the distance between the centers of c_1 and $c0$ and the distance between $c0$ and $c0^*$. The ratio d_2/d_1 is similar to an 'under relaxation' coefficient used to stabilize the numerical iterations and to ensure numerical

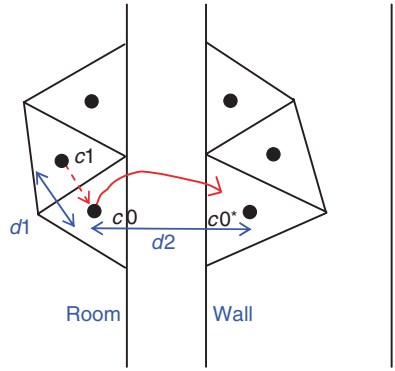

Figure 1. *A close-up of the face separating the two fluid zones, room air and wall. On each side of the face there are two meshes with the same face geometry.*

convergence. In addition to this moisture movement caused by Equation (1) the exactly same amount of water vapor is withdrawn from cell $c0$ in order to assure mass conservation. When the equations converged, the vapor contents in the fluid cells on either side of the boundary are equivalent.

CFD, Airflow Modeling, and Elements of Model Validation

The use of computer simulations to analyze the behavior of physical systems raises a difficult question of the validity of the results. To have confidence in the simulated results several possibilities can be used to validate the model. For example, comparisons with analytical solutions, intermodel comparison, and of course the comparison with experimental measurements. Of course, this last possibility is difficult to implement in practice, because of the difficulty in achieving the extensive amount of experimental data needed to validate a code in all possible configurations. In practice, it is admitted to validate some parts of the model and then to extend it to other situations.

The airflow model presented here is based on the work done by Hohota (2003). The same simulation tool was used (Fluent 6.1) with the same turbulence model and near-wall treatment, as described above. In addition, the moist air representation as a perfect mixture of two perfect gases is also taken from Hohota (2003). In the work of Hohota this numerical model was validated based on experimental measurements of temperature and velocity fields in a climatic chamber situated in CETHIL, Lyon (France).

The new ideas introduced in the model are the representation of mass flow between the wall and the air, which is done by using a ‘fluid wall’ approach. The thermal behavior of such a wall in 2 and 3D configurations was compared with an analytical solution, and the results are very similar.

The thermal part of the model approach with fluid walls has also been validated by a simulation where the temperatures found on the interior surface of the walls have been compared to experimentally obtained values. The experiments were performed by Hohota (2003). The comparison verified a good thermal coupling in the fluid wall approach where the measured temperatures on the internal surface of the wall were similar to the temperatures found by use of the model.

Additionally, a moisture balance was executed to verify the moisture model. Therefore the numerical results of the model seem to be of optimum quality. The moisture balance is shown later in this study in the description of the performed simulations.

Discretization

In large ventilated cavities air velocities are small and therefore the forces inducing the air movement are weak. In some cases the use of structured mesh results in artificial guidance of the airflow where the calculated flow follows the grid and not its physical path. The use of unstructured mesh avoids falling into a numerical problem and when the solution is converged the flow path results from physical driving forces and not from an artificial numerical grid.

Using an unstructured mesh is also better at dealing with corners and complex geometry than a structured mesh. Another advantage of the unstructured mesh is that it is much easier to refine in certain zones where more information on the flow or the distribution of temperature or moisture is valuable. This was a very important feature for this study, as the initial mesh was locally refined in the zone where the microclimate was the main interest. Therefore, unstructured mesh obtained using Delaunay circle test (Fluent, 1999) was used in all simulations.

However, the unstructured mesh can cause problems near the walls and this is compensated for by use of the so-called enhanced wall treatment (Teodosiu et al., 2003).

SIMULATIONS

The objective of the developed model was to investigate the relative humidity (RH) level in microclimates. In this study both the model and the microclimate in two cases are investigated. The two cases are quite similar, the difference between them is just the moisture source, which will be described later. The chosen case is just one example of an interesting microclimate that can provide some indication of what to expect in areas with reduced air circulation and/or in combination with cold surfaces.

Here it is chosen to use a simple room of $2 \times 2 \times 2\,m^3$, with an air inlet in one side and outflow of air on the opposite side. The two walls with the inlet and outlet are simulated as immobile fluid walls with thicknesses of 0.1m and modeled as described in the previous section. The geometry can be seen in Figure 2. The remaining wall boundaries are modeled as internal surfaces.

In real rooms or offices there are moisture sources in terms of persons, plants, and activities. So to mimic a room by simulation it is necessary to include some moisture sources. The inlet is a source but if all surrounding constructions are moisture tight the result is obvious and the room will have the same vapor content as the inlet air. For the sake of simplicity some 'wet walls' are chosen to be used as moisture sources. This means that the wall will have constant water vapor content and they will function as moisture sources or sinks depending on the moisture conditions in the room. Besides, to imitate also other moisture sources, a 'simple' person is modeled as a cylinder that also acts as a heat source.

Simulation Details

The simulations presented in this study are concerned with only 3D cases since they were non-symmetrical. The tested case was a simple room

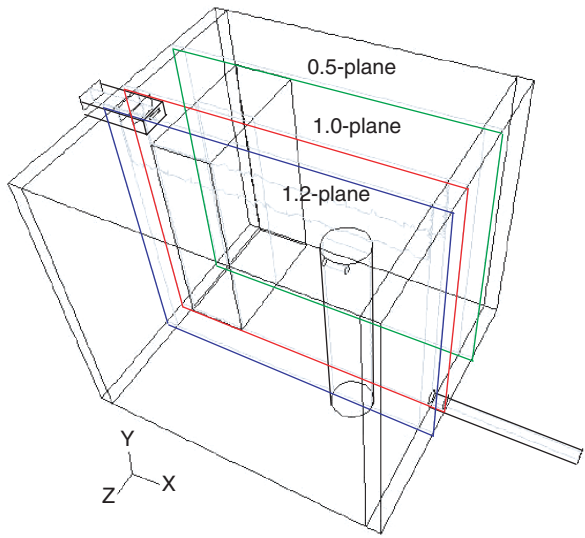

Figure 2. *Geometry of the 3D model also showing placement of result planes in the room. The numbering of the planes refers to their coordinate in the z-direction, the 0.5-plane goes through the furniture, while the 1.2-plane crosses the centre of the person. For cases with 'wet walls' as moisture sources the cylindrical 'person' is not included.*

of $2 \times 2 \times 2\,m^3$. The wall with the inlet is in contact with the outdoor air whereas all others are internal walls with a temperature of 22°C. The inlet is a rectangular duct with dimensions $0.2 \times 0.1\,m^2$ that continues 0.1 m inside the room where it ends in an orifice slit of $0.02 \times 0.05\,m^2$. The geometry is shown in Figure 2.

The immobile fluid walls are simulated with material properties of cellular concrete. More details about the used material properties for air and the fluid walls are given in Table 1.

Two series of simulations have been performed. The first series only has the walls as moisture sources and here the impact of different boundary conditions are tested. This series will be referred to as 'wet walls' and the five different cases are described in Table 3. The second series has both walls and a simple person as moisture sources and it concerns the impact of the geometry on a microclimate with two different air change rates. The six cases are referred to as 'person' cases and the details are given in Table 4. The floor and the two sides of the room are simulated with moisture tight surfaces and the remaining inlet and outlet walls as moisture sources/sinks with constant moisture content. The ceiling is also a moisture source in the cases with 'wet walls' but in cases with a person as moisture source the ceiling is moisture tight. The water vapor contents on the exterior surfaces of both the inlet and outlet walls is kept constant, but at different levels. The inlet is another moisture source in the room for both series. The inlet has the same water vapor content as the outdoor air but this is heated to 20°C in order to avoid modeling of heating systems in the model.

Table 1. Material properties for air and walls. Note that the air density changes with moisture content.

Material properties for air and fluid walls	
Air	
Density, ρ (dry)	$1.225\,kg/m^3$
Heat capacity, c_p	1006 J/kg·K
Thermal conductivity, λ	0.0242 W/m·K
Dynamic viscosity, μ	$1.79 \cdot 10^{-5}$ kg/m·s
Fluid walls	
Density, ρ	$400\,kg/m^3$
Heat capacity, c_p	960 J/kg·K
Thermal conductivity, λ	0.10 W/m·K
Dynamic viscosity, μ	1.0 kg/m·s
Wood furniture (solid)	
Density, ρ	$700\,kg/m^3$
Heat capacity, c_p	2310 J/kg·K
Thermal conductivity, λ	0.17 W/m·K

In Figure 2 it can be seen that a $0.45 \times 1.0 \times 1.6\,m^3$ piece of furniture is placed in the corner near one of the side walls and the inlet wall. The furniture is included in the case in order to create and analyze the microclimate behind it. The furniture is modeled as a wooden solid with ordinary heat conduction. The air gap between the furniture and constructions is 0.02 m and between the furniture and the floor it is 0.05 m for cases with 'wet walls'. For cases with the 'person' as a moisture source a combination of the same distances and the lack of distance are investigated. The analysis of the microclimate behind and below the furniture includes a detailed study of the effect of the airflows and the impact on the water vapor content in both air and constructions.

The mesh used in the simulation contains ≈1,000,000 tetrahedral elements in the first part of the simulation where the general airflow is determined. In the second part the mesh is refined in the area between the furniture and the wall so the amount of elements is increased by ≈20%. The approximate number of cell layers in the region is 5–8.

Simulations – Cases with Wet Walls as Moisture Sources

The moisture source for the first simulations is 'wet walls'. Five cases are simulated in order to provide information about the model sensitivity to changes in boundary conditions as humidity, temperature, and velocity. The reference case has boundary conditions as shown in Table 2 and all variations from reference are listed in Table 3. The importance of the inlet parameters; humidity, temperature, and velocity, is tested in Cases 2–4. The effect of a change in temperature on the outside surface of the inlet wall is studied in Case 5 with a higher temperature. In all cases, the inlet wall is a sink and the outlet wall and the ceiling are sources. The total net moisture load from the walls is 37 g/h except from Cases 3 and 4. In Case 3 the higher moisture load of the inlet reduces the moisture from the wall to almost nothing (1 g/h) and opposite the higher air change rate in Case 4 causes the walls to emit more vapor corresponding to 64 g/h.

Simulations – Cases with a Person as Moisture Source

These simulations have been performed in order to study the effect of changes in the microclimate near the furniture for different geometries. A total of six cases have been tested and they are listed in Table 4. Cases A–C used an air change rate of $1.5\,h^{-1}$ as used in the simulations with the wet walls and Cases D–F are similar apart from having an air change rate of $0.5\,h^{-1}$ corresponding to an inlet velocity of 0.056 m/s. The air gap between the walls and the furniture is 0.02 and 0.05 m between the furniture and the

Table 2. Imposed boundary conditions for simulated cases. The boundary conditions are for the inlet air and the external side of the walls for Case 1 and A.

	Boundary conditions
Inlet air	
Velocity, v	0.167 m/s, air chg. rate 1.5 h^{-1}
Temperature, t_{air}	20°C
Vapor, H_2O	4 g/kg – 27%RH (wet walls)
Vapor, H_2O	7 g/kg – 48%RH (person)
Temperatures	
Inlet wall	0°C External side (wet walls)
Inlet wall	10°C External side (person)
Outlet wall	22°C External side
Other walls	22°C
Person	180 W/m^3 Heat source
Vapor content, H_2O	
Inlet wall	4 g/kg (100%RH) (wet walls)
Outlet wall	10 g/kg (60%RH) (wet walls)
Ceiling	8 g/kg (48%RH) (wet walls)
Inlet wall	7 g/kg (92%RH) (person)
Outlet wall	6 g/kg (36%RH) (person)
Person	28 g/h Mouth zone release

Table 3. The five simulated cases with wet walls as moisture sources. Note that in Case 3 the higher inlet humidity is due to a lower temperature. The inlet wall is a sink and the ceiling and outlet walls are sources.

	Cases – wet walls (H_2O-source)			
	Inlet humidity (g/kg) (RH)	**Inlet temp (°C)**	**Inlet velocity (m/s)**	**Outs. inlet wall temperature (°C)**
Case 1	4 (27%)	20	0.167	0
Case 2	8 (54%)	20	0.167	0
Case 3	4 (74%)	5	0.167	0
Case 4	4 (27%)	20	0.333	0
Case 5	4 (27%)	20	0.167	10

floor for Cases A and D. For Cases B and C and corresponding E and F a combination of the same distances and the lack of distance between furniture and wall or floor is investigated.

The moisture source in these six cases A–F is a 'person' mimicked by a solid cylinder with a fluid mouth zone that evaporates water. The dimension of the solid part of the 'person' is a cylinder 1.5 m high and 0.30 m diameter. Since solids cannot evaporate water, a small cylinder (0.15 m long, 0.05 m

Table 4. The six simulated cases with a person as moisture source. Cases A–C have air change rate of 1.5 h^{-1} and Case D–F have 0.5 h^{-1}. The inlet and outlet walls have constant water vapor content.

Cases – Person (H_2O-source)			
	Dist. wall-furniture (cm)	**Dist. floor-furniture (cm)**	**Inlet velocity (m/s)**
Case A	2	5	0.167
Case B	0	5	0.167
Case C	2	0	0.167
Case D	2	5	0.056
Case E	0	5	0.056
Case F	2	0	0.056

diameter) is cut from the solid to represent a mouth. The small fluid area representing the mouth zone is set up to release water vapor at a rate of 28 g/h. Besides this moisture source, the inlet and outlet walls have constant water vapor contents on the external side and thus they will function as either sinks or sources depending on the moisture content in the room air. The given moisture sources and case geometry gives a moisture balance as set up in Equation (2), where the magnitude of the average RH is estimated on the basis of an assumed room air temperature of 22°C.

$$x_i = x_o + \frac{G}{n \cdot V \cdot \rho_{\text{air}}} = 0.007\ \text{kg/kg} + \frac{0.028\ \text{kg/h}}{0.5\ \text{h}^{-1} \times 8\ \text{m}^3 \times 1.225\ \text{kg/m}^3} = 0.0127\ \text{kg/kg} \tag{2}$$

where x_i is the water vapor content in the indoor air [kg/kg];
x_o is the water vapor content in the incoming outdoor air (kg/kg);
G is themoisture production (kg/h);
n is the air change rate (h^{-1});
V is the room volume (m^3); and
ρ_{air} is the density of the air (kg/m^3).

$$p_i = P\frac{x}{0.62198 + x} = 101{,}325 \cdot \frac{0.0127}{0.62198 + 0.0127}\ \text{Pa} = 2028\ \text{Pa}$$

where p_i is the water vapor pressure of the air (Pa)
P is the standard atmospheric pressure (101,325 Pa at 0 m altitude).

$$\text{RH} = \frac{p_i}{p_s(22^\circ\text{C})} \cdot 100\% = \frac{2028\ \text{Pa}}{2643\ \text{Pa}} \times 100\% \cong 76\%\text{RH}.$$

The calculated example is for Cases D–F. In the example the equation does not take into account the moisture released from or absorbed by the inlet and outlet walls but for Cases D–F the estimated RH of the room will be a little lower since both walls will function as sinks. Note that the density of dry air is used. The same is expected for Cases A–C since the moisture balance of the room will lead to ≅54%RH.

RESULTS

All simulations have been continued for 3300 iterations where the last 300 iterations are done with a refined mesh in the region behind/under the furniture. After the iterations the residuals found for the continuity are in the range $6.88 \cdot 10^{-5}$ to $2.38 \cdot 10^{-4}$, which is low and hence convergence is assumed reached.

The focus of the results is on the microclimatic conditions behind the furniture and more specifically on the moisture conditions. All results except the general velocities in the room are given in planes. The placement of the planes is shown in Figure 2.

Results – Cases with Wet Walls as Moisture Sources

The results of Cases 1–5 are all compared with the reference, Case 1. To start with, the results of this reference case are shown in Figures 3–8. In Figures 3 and 4 the moisture distribution in the room is shown in values of RH in the 0.5-plane. The average RH and temperature of the air in the entire room is 44%RH, 20.9°C (6.7 g/kg). On the entire internal surface of the inlet wall RH average is 46%, 20.7°C (7.0 g/kg) but where it faces the furniture it has 47%RH and 20.3°C (6.9 g/kg). So the furniture has an influence on the moisture and together with the temperature the differences from behind the furniture to its front side is 3%RH. The higher moisture content behind the furniture and at the inlet wall is explained by the moisture emitting ceiling that constantly has 8 g/kg. The airflow pattern near the inlet wall is that the air flows down behind the furniture and thus brings the moist air with it.

The temperature distribution is given in Figure 5. The average air temperature in the entire room is 20.9°C. The average temperature of the furniture is 20.7°C. It should be noted that there is a linear temperature distribution through the inlet wall.

The airflows in the room for Case 1 are shown in Figure 6. It can be seen that the airflow follows the ceiling and spreads out on the opposite wall.

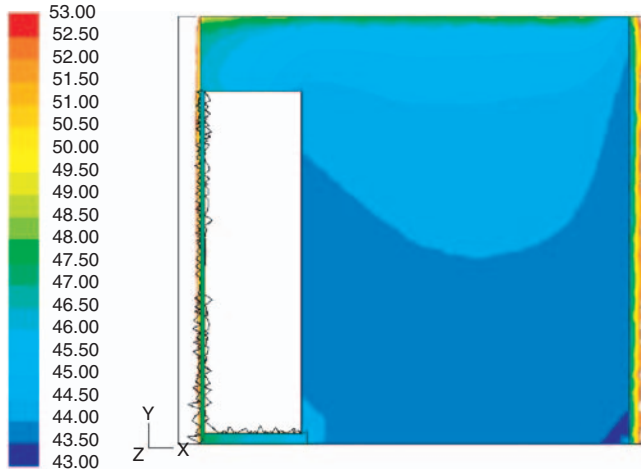

Figure 3. *RH distributions at the 0.5-plane in the room (Case 1). The white area in the left wall indicates that the moisture level is out of scale. The scale of RH is from 43% in the room to 53% at the external wall.*

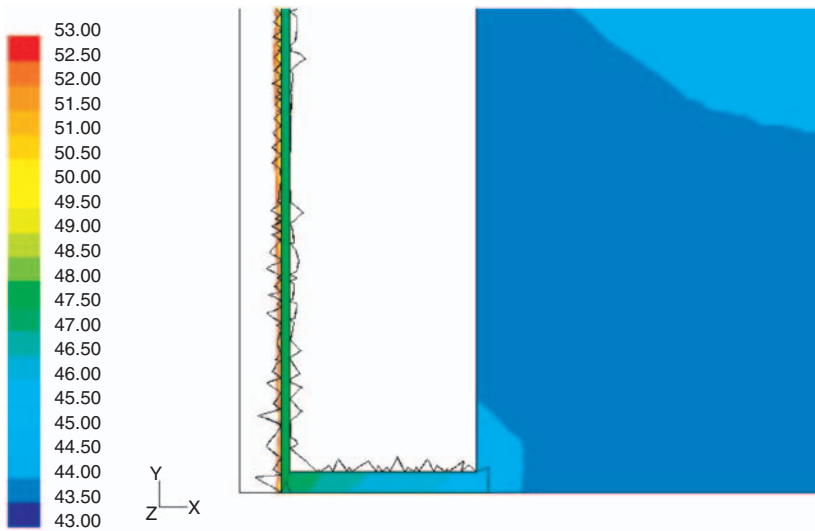

Figure 4. *Close-up of the RH distributions at the 0.5-plane (Case 1). The RH behind the furniture is 47%. Under the furniture the RH is also 47% (7.0 g/kg) in the corner and decreases slowly to 44% (6.7 g/kg) in the room.*

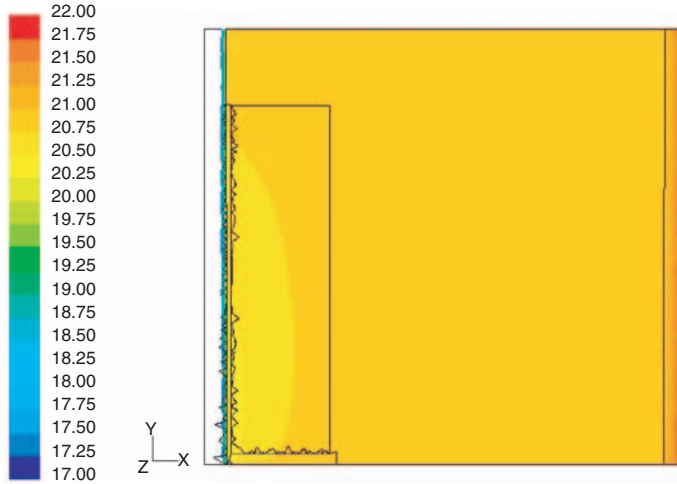

Figure 5. *Temperature distributions in the 0.5-plane (Case 1). The shown range is 17–22°C. In most of the room air the temperature is slightly <21°C.*

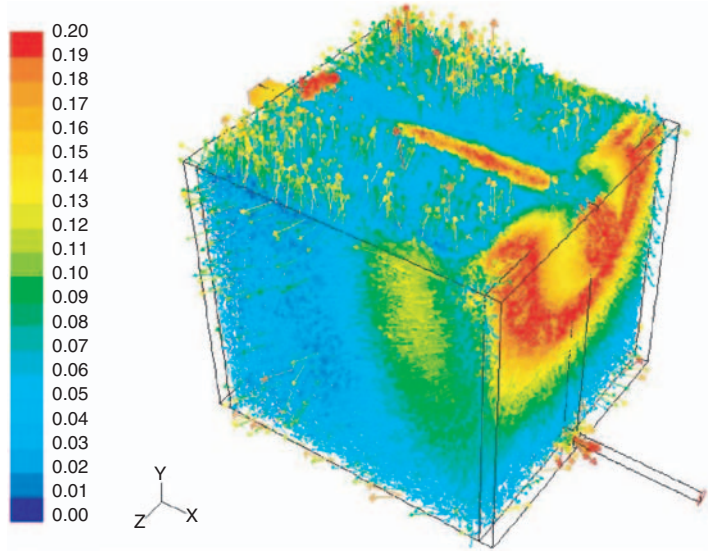

Figure 6. *Vector plot of the velocities in the room for Case 1. The highest velocities are from the inlet and near the ceiling and on the outlet wall where the jet spreads out. Note that only velocities in the range 0–0.2 m/s are shown.*

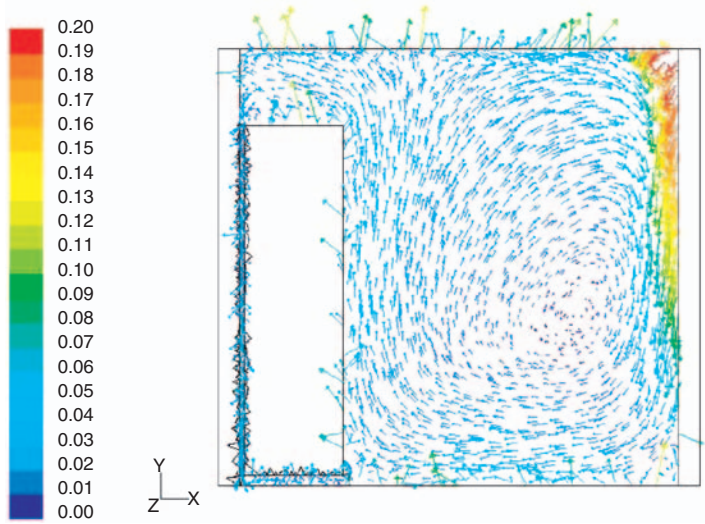

Figure 7. *Vector plot of the velocity distribution in 0.5-plane (Case 1). The highest velocities are at the outlet wall where the inlet jet has spread out. The range is 0–0.2 m/s.*

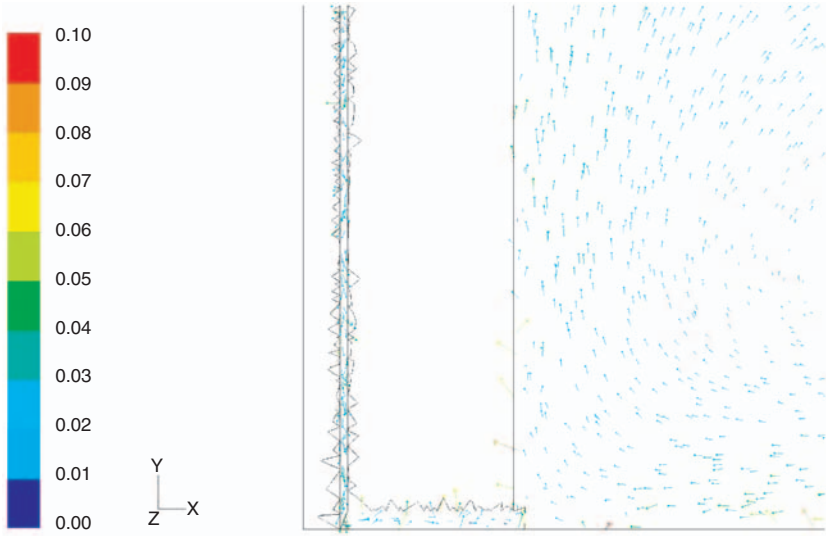

Figure 8. *A close-up of corner with furniture in the 0.5-plane in Case 1. The vectors indicate the direction of the air flow. The range is 0–0.1 m/s.*

The velocities in the rest of the room are very low and most are in the range 0.02–0.03 m/s. The maximum velocity is 2.4 m/s at the inlet.

Figure 7 shows the velocities at the 0.5-plane. The average velocity of the room air in the 0.5-plane is 0.025 m/s. The airflow velocity behind the furniture is slightly higher than the average in the 0.5-plane with a range is 0.03–0.04 m/s. To gain more information about the airflow pattern behind the furniture a close-up is shown in Figure 8. In this figure it is possible to see the direction of the airflow behind the furniture. The flow falls to the floor between the wall and the furniture and rises on the face turning to the outlet wall.

In Case 2 the moisture load in the inlet air was 8 g/kg at 20°C corresponding to air with 54%RH. The main difference between Cases 1 and 2 is that the moisture level in the room is increased. There is no difference in the temperatures and the velocity distributions in the room. In the room air there is an average of 52%RH (8.0 g/kg) and on the internal surface of the inlet wall the average is 53%RH (20.7°C). On the wall behind the furniture there is 54%RH hence again there is a difference from the room level.

In Case 3 a lower inlet temperature of 5°C was applied. In this test the inlet jet drops to the floor as expected. In the room air the averages are 47%RH and 19.5°C (6.6 g/kg). On the internal surface of the inlet wall there is an average of 47%RH (19.7°C). The distribution of temperatures in the room is shown in Figure 9. The falling inlet jet causes a new distribution of the velocities in the room, where the airflow between the wall and the furniture as well as on the other side of the furniture is streaming up. This is shown in a close-up of the 0.5-plane in Figure 10.

In Case 4 the inlet velocity is doubled to 0.333 m/s corresponding to an air change rate of $3\,h^{-1}$. This results in an average temperature of 20.8°C and RH of 42%RH. On the internal surface of the inlet wall RH average is 43%RH (20.6°C). These values are all lower than in Case 1. The airflow distribution in the room has also changed and this is shown in Figure 11. The airflow follows the ceiling from the inlet and spreads on the outlet wall. Then the air is pressed down and it follows the floor until it reaches the furniture where it rises again. Between the wall and the furniture the airflow drops to the floor and the velocity is in the range 0.01–0.03 m/s. Between the floor and the furniture the velocity range is 0.02–0.1 m/s, which indicates that the air is more turbulent.

The last variation, Case 5 had increased temperature on the exterior side of the inlet wall (from 0 to 10°C). The result is an average temperature and RH in the room air of 20.9°C and 44%RH, respectively, and on the internal surface of the inlet wall the average is 46%RH (20.8°C). These results are almost the same as in Case 1. However, there is a change in the temperature

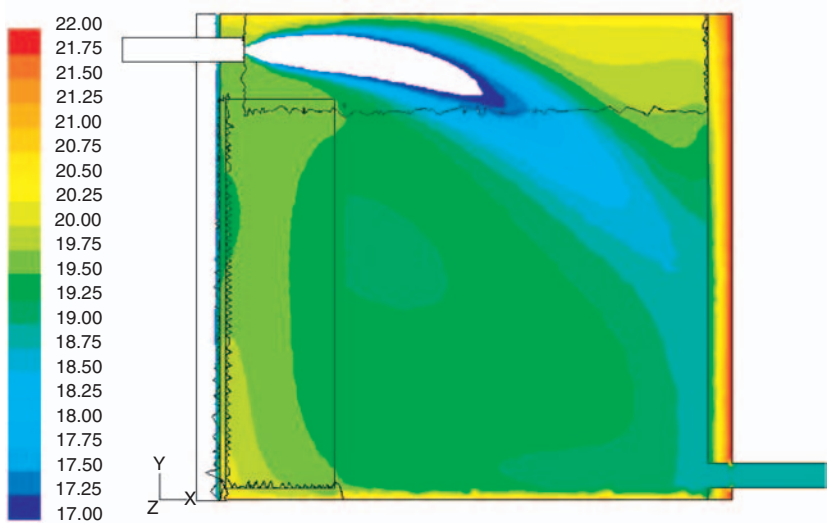

Figure 9. *Temperature distributions in the 1.0-plane for Case 3. Note that the inlet jet drops as seen by the temperatures. The shown range is 17–22°C.*

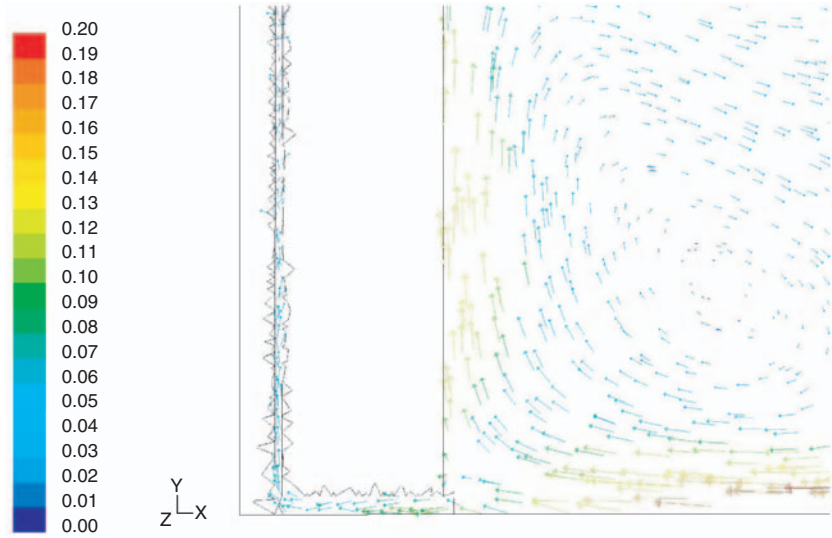

Figure 10. *A close-up of the velocities around the furniture for Case 3. The values under the furniture are in the range 0.07–0.09 m/s while the range is 0.04–0.06 m/s behind it. The shown range is 0–0.2 m/s.*

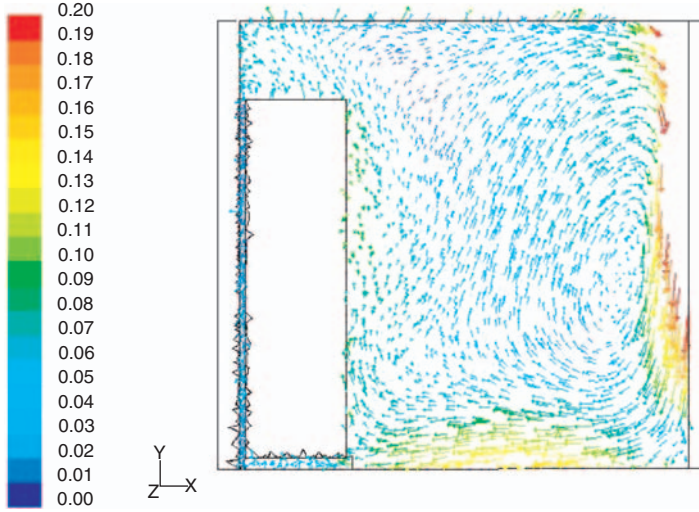

Figure 11. *Velocity distributions in the 0.5-plane for Case 4. The highest velocities are at the outlet wall and the lowest behind the furniture. The shown range is 0–0.2 m/s.*

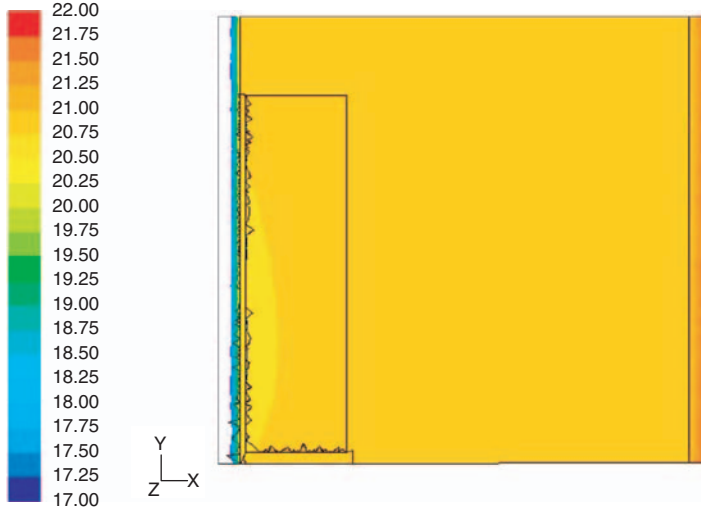

Figure 12. *Temperature distributions for Case 5 with an external temperature of 10°C (inlet wall). The shown range is 17–22°C.*

distribution in the room as can be seen in Figure 12. The average temperature of the furniture is 20.8°C. The room velocities are similar to Case 1 but are slightly higher. Between the furniture and floor the range of velocities is 0.01–0.09 m/s.

Results – Cases with a Person as Moisture Source

The focus of the investigation is on the moisture conditions in the microclimate and hence the moisture distributions are shown first. The RH distribution in Cases A, B and D, E are given in Figures 13–16, respectively. In Case C the RH distribution in the room was similar to that of Case B except under/behind the furniture. In both Cases A and B the average is 54.3%RH in the room air and for Case C it is 54.2%RH. For Cases D–F it is higher due to the lower air change rate with 76.3%RH for Cases D and E and 76.5%RH for Cases E and F.

Since the microclimate was of special interest close-ups of the RH distribution for all cases are given in Figures 17–22. It can be seen that the highest RH in the microclimate is found in Case A behind the furniture (55.7%RH), in Case B under the furniture with 54.9%RH, and in Case C the highest value behind the furniture, 55.6%RH. The same pattern is found for the corresponding Cases D–F with RHs of 79.3%RH in Case D, 77.8%RH in Case E, and for Case F it is 79.6%RH.

The RH is strongly temperature dependent so the temperatures are also very important. The temperature distribution for Cases A and E are shown in Figures 23 and 24. It can be seen that the temperature distributions are almost the same for both cases. In Case E the higher temperature close to the outlet wall is caused by a combination of the heat producing person and the lower ventilation rate of $0.5\,h^{-1}$. The average temperatures in the room for the six cases are 22.2°C for Case A, 22.3°C for Cases B and C, and 22.4°C for Cases D–F.

Figure 25 shows the velocities for Case A in the 1.0-plane, and since the placement of the furniture only has little impact on the overall velocities in the room the results of Cases B and C are very similar. For all three cases the inlet jet turns to the corner at the outlet wall opposite of the furniture because of the free convection around the person on the other side of the centerline in the room. In Figure 26 the velocities for Case D are shown, which are similar for Cases E and F. The main difference between Figures 25 and 26 are that the lower air change rate makes the slightly colder inlet air detach from the ceiling and fall down in Figure 26. In Cases A–C the maximum velocity at the inlet is 2.4 m/s whereas the maximum for Cases D–F is only 0.8 m/s. Owing to the free convection around the person the air rises in the part of the room closest to the outlet wall. The free convection plume around the person is shown in Figure 27.

To gain more information about the airflow pattern behind and below the furniture, close-ups of all the three cases are shown in Figures 28–33. In the figures, it is possible to see the direction of the airflow behind the furniture. The flow falls to the floor between the wall and the furniture. Under the

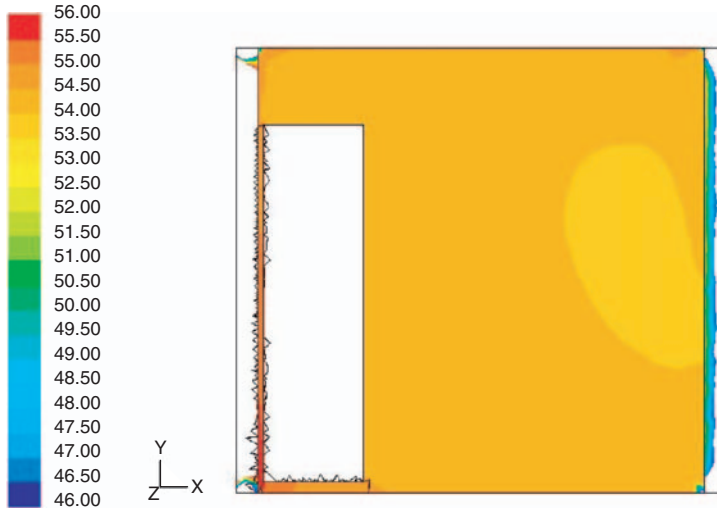

Figure 13. *RH distributions at the 0.5-plane in the room for Case A. The scale of RH is from 46 to 56% white areas are levels out of scale.*

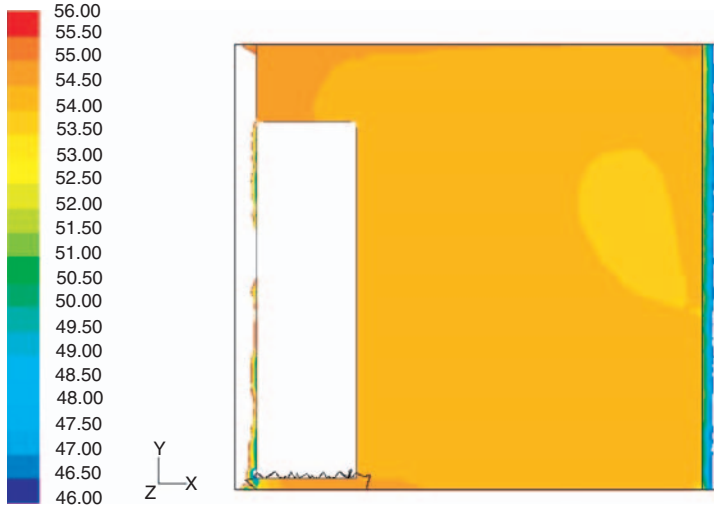

Figure 14. *RH distributions at the 0.5-plane in the room for Case B. The scale of RH is from 46 to 56%.*

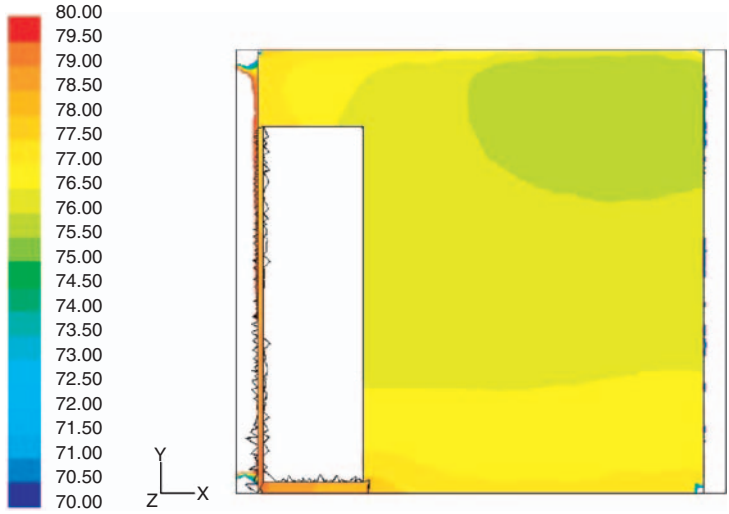

Figure 15. *RH distributions at the 0.5-plane in the room for Case D. The scale of RH is from 70 to 80%.*

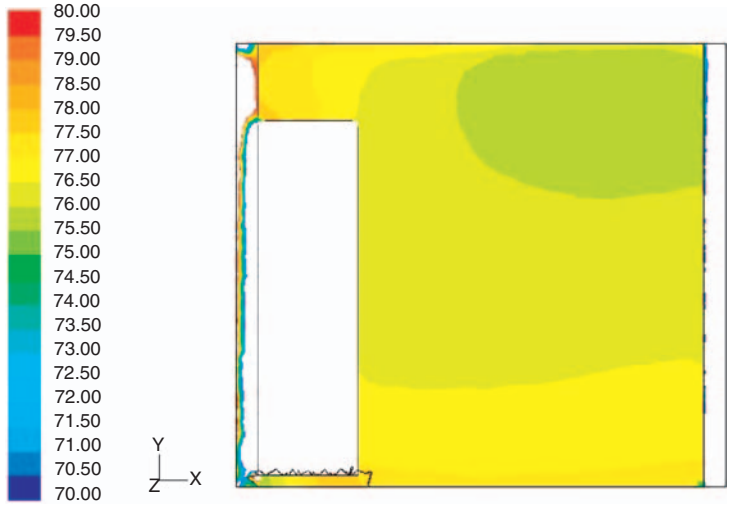

Figure 16. *RH distributions at the 0.5-plane in the room for Case E. The scale of RH is from 70 to 80%.*

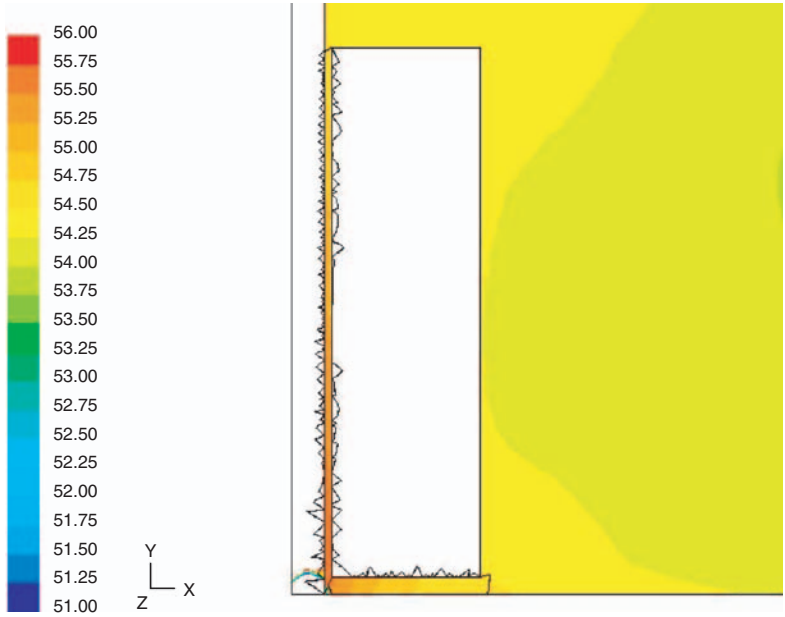

Figure 17. *RH distributions at the 0.5-plane for Case A. Range of RH is 51–56%.*

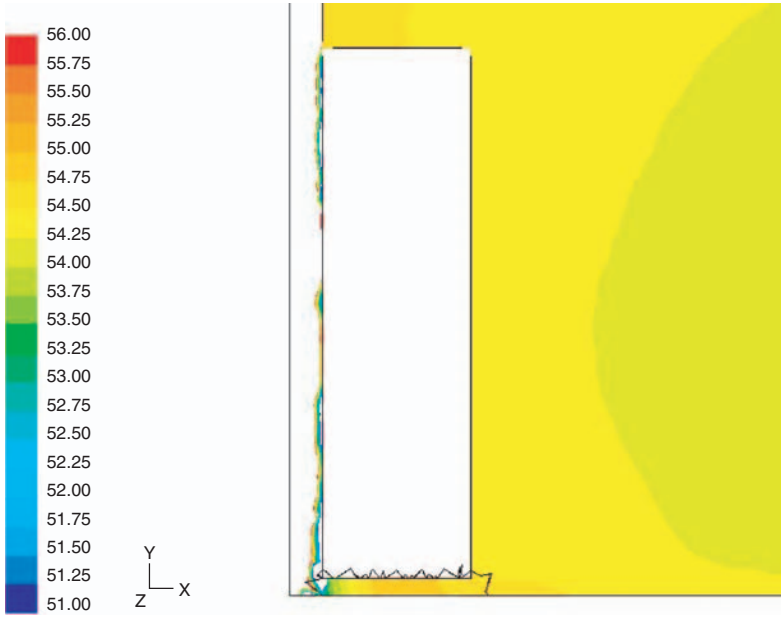

Figure 18. *RH distributions at the 0.5-plane for Case B. Range of RH is 51–56%.*

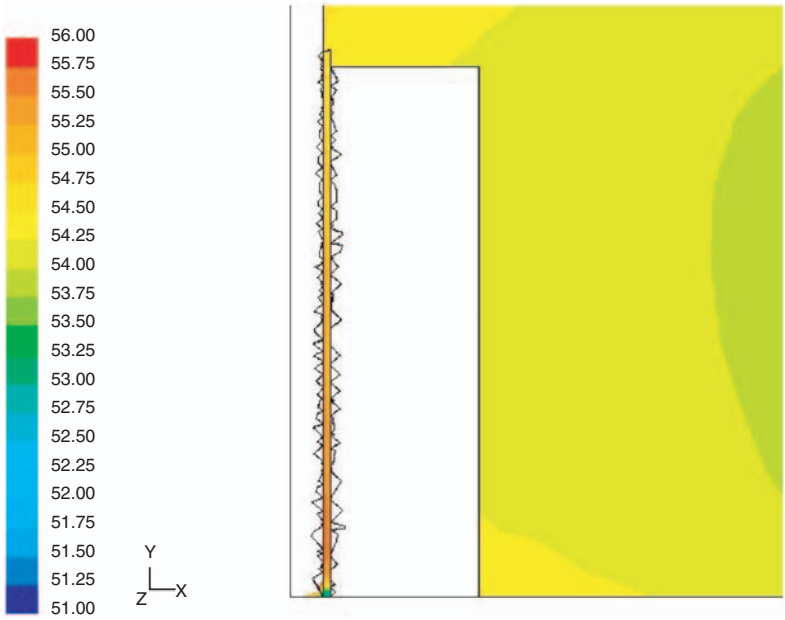

Figure 19. *RH distributions at the 0.5-plane for Case C. Range of RH is 51–56%.*

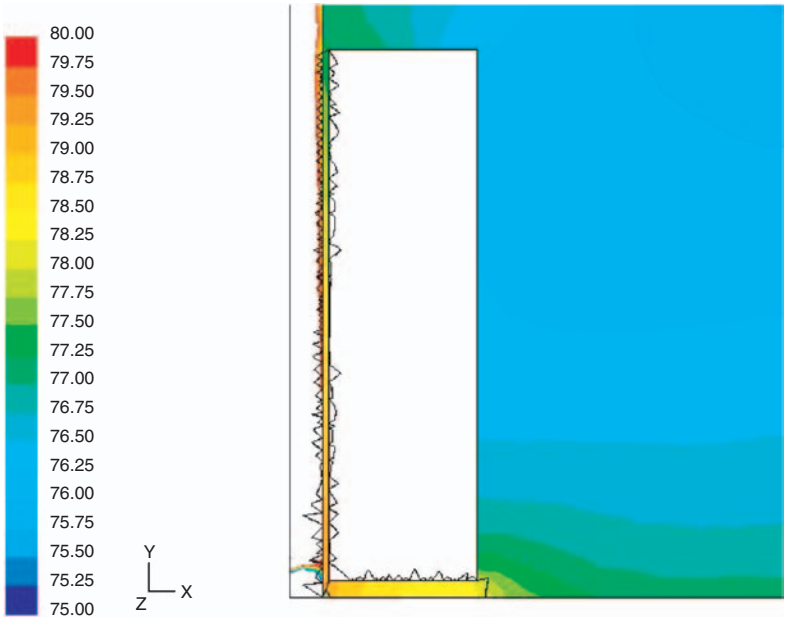

Figure 20. *RH distributions at the 0.5-plane for Case D. Range of RH is 75–80%.*

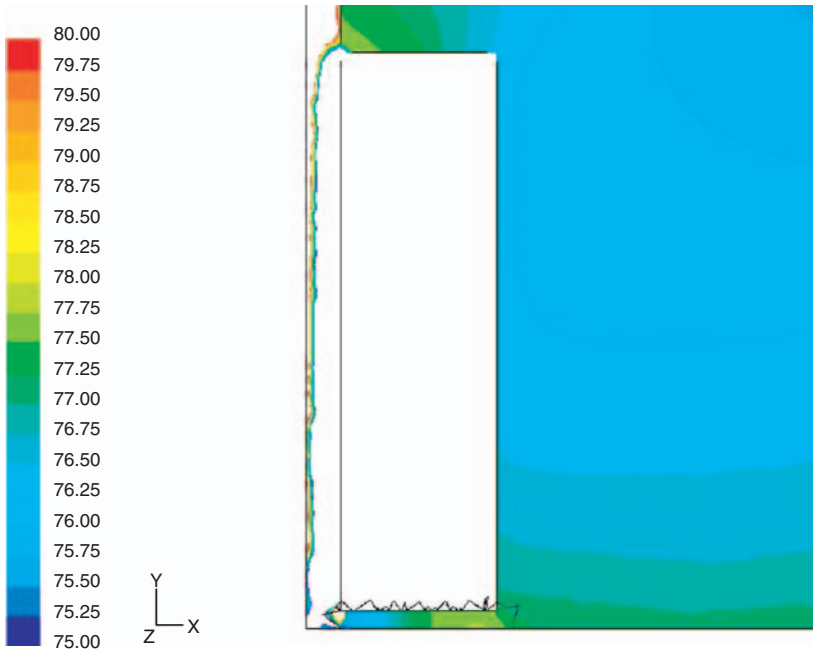

Figure 21. *RH distributions at the 0.5-plane for Case E. Range of RH is 75–80%.*

furniture, the airflow is more turbulent, which is indicated by the longer arrows that seem to go into the furniture, but this is due to scaling of the velocity vectors. In Figures 29 and 30, and 32 and 33 for Cases B, C, E, and F the air seems to go to dead ends because of the 2D plots but in reality it flows out to the sides.

DISCUSSION

Cases with Wet Walls as Moisture Sources

Generally the results are as expected since the airflow patterns in the room follow the ceiling and there is an almost isothermal condition in the room.

The simulation of Case 1 showed that the conditions in the room were very much as expected on the basis of the setup and the boundary conditions for the resulting RH, temperature, and airflow patterns. On the internal surface of the inlet wall, where it faces the furniture, the conditions are 47%RH and 20.3°C (7.0 g/kg), while on the side of the furniture facing the room they are 44%RH and 20.9°C (6.7 g/kg). So the furniture has an

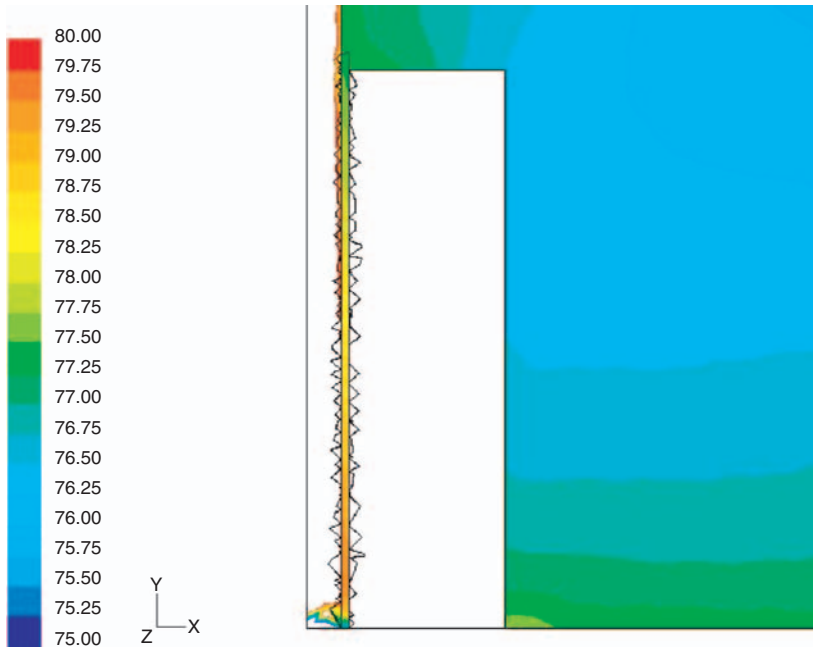

Figure 22. *RH distributions at the 0.5-plane for Case F. Range of RH is 75–80%.*

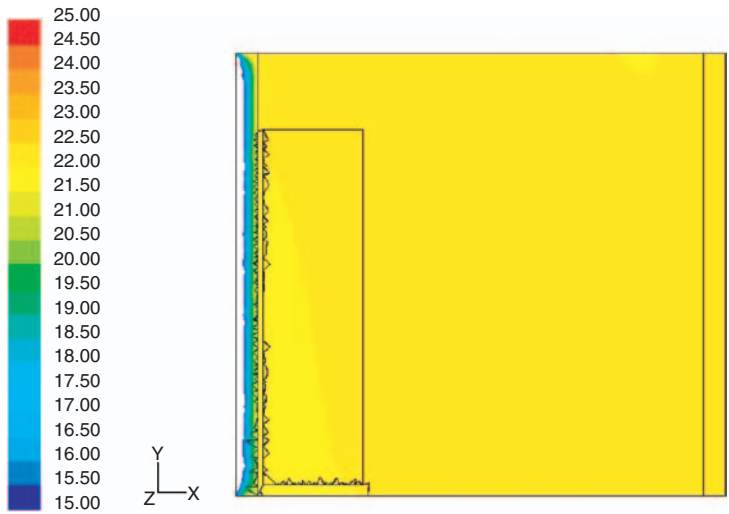

Figure 23. *Temperature distributions at the 0.5-plane in the room for Case A. The range is 15–25°C.*

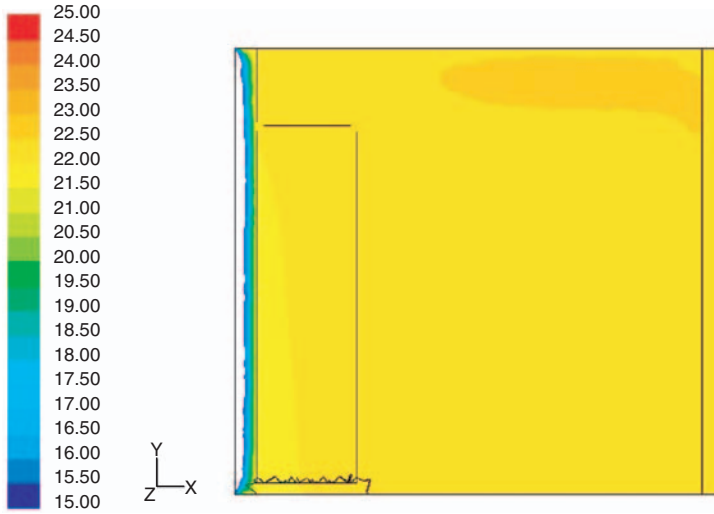

Figure 24. *Temperature distributions at the 0.5-plane in the room for Case D. The range is 15–25°C.*

influence on the moisture conditions of the microclimate. In this case it is not a problem but in more severe cases the influence of the furniture on differences in moisture levels might be highly interesting.

In the reference case the air change rate of $1.5\,h^{-1}$ ensures air velocities in the room below 0.2 m/s except at the ceiling in front of the inlet and on the top part of the outlet wall. In the rest of the room the velocities are very low and most are in the range 0.02–0.03 m/s. These low values would not cause drafts in an indoor environment and therefore they seem reasonable. Behind the furniture the airflow velocity is also low and in the range 0.03–0.04 m/s. This means that the flow behind the furniture is slightly higher than in the room in general and it must be explained by the flow along the room surfaces and almost still air in the areas just a little away from the construction surfaces. The flow behind the furniture falls to the floor and rises on the face of the furniture turning toward the outlet wall.

The variation with doubled moisture content in the inlet air gave almost the same results as the reference case but the moisture level in the room air is increased to an average of 52%RH (8.0 g/kg). This was obvious since a bigger moisture load should lead to higher relative humidities but it is still not a risk for the indoor climate.

A lower inlet temperature of 5°C causes the inlet jet to drop to the floor because the density of cold air is higher than warm air. The falling inlet jet

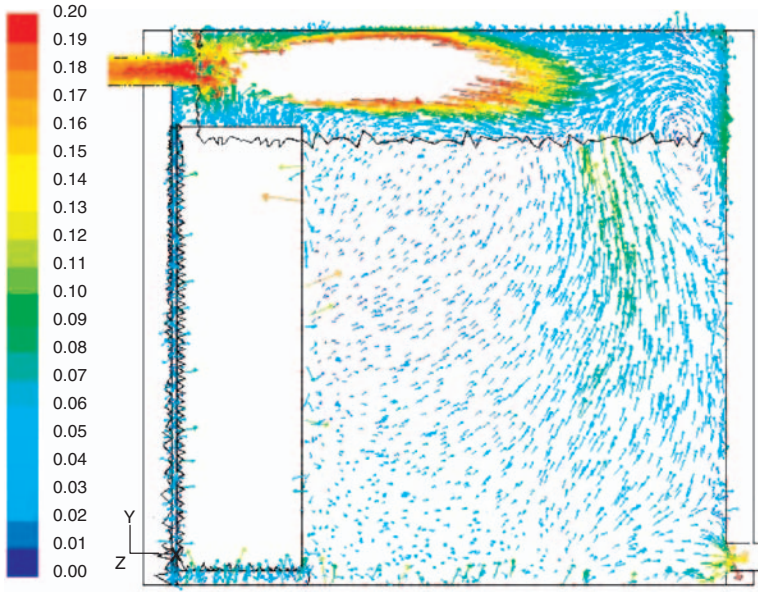

Figure 25. *Vector plot of the velocities in the room for Case A at the 1.0-plane. Note that only velocities in the range 0–0.2 m/s are shown.*

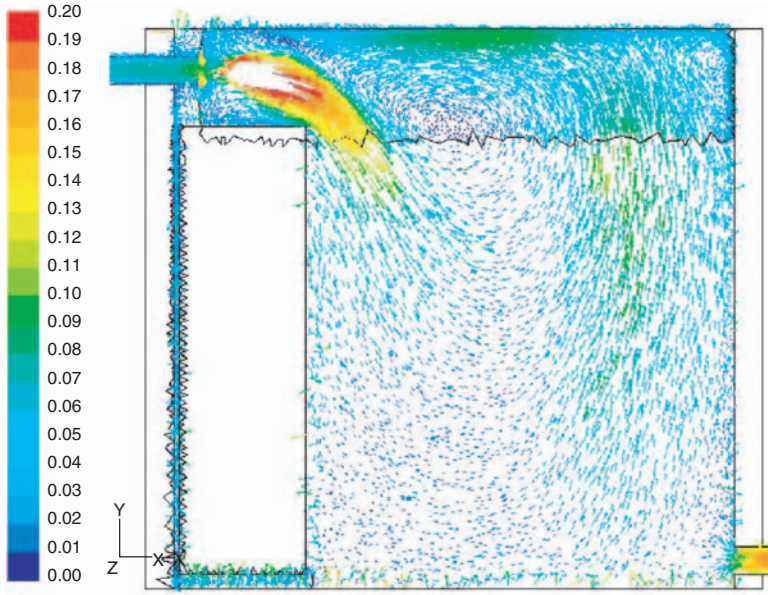

Figure 26. *Vector plot of the velocities in the room for Case D at the 1.0-plane. Note that only velocities in the range 0–0.2 m/s are shown.*

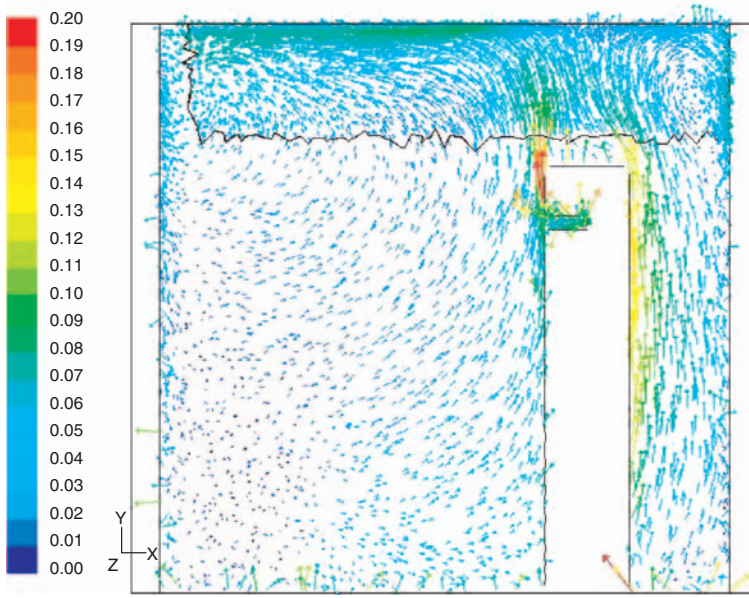

Figure 27. *Vector velocities for Case A at the 1.2-plane. Note the free convection around the heat producing person causing a rising plume above it. The range is 0–0.2 m/s.*

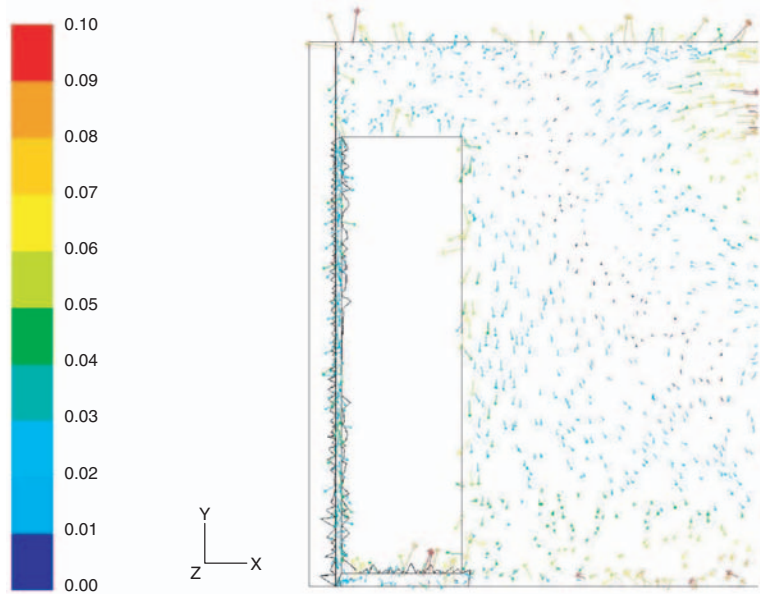

Figure 28. *Vector velocities for Case A at the 0.5-plane. The air drops behind the furniture and moves out into the room under it. The range is 0–0.1 m/s.*

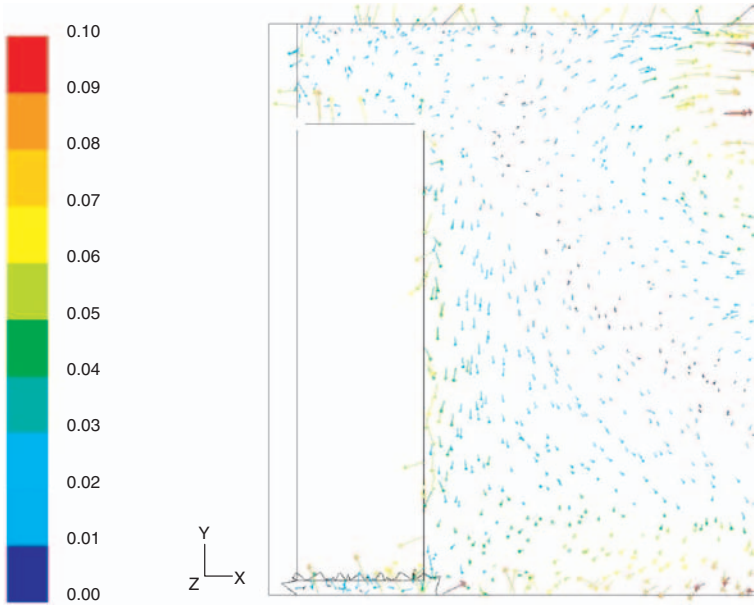

Figure 29. *Vector velocities for Case B at the 0.5-plane.The airflow under the furniture is quite turbulent and seems to be rising. The range is 0–0.1 m/s.*

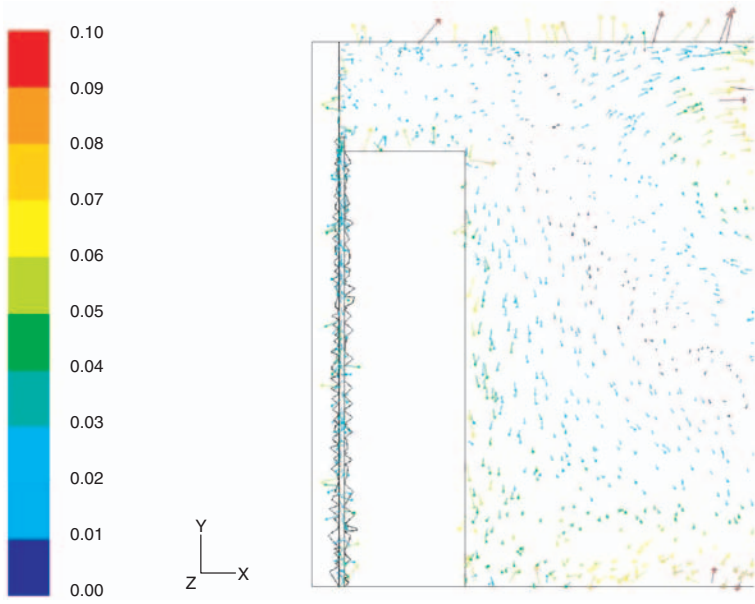

Figure 30. *Vector velocities for Case C at the 0.5-plane. The air falls down between the furniture and the wall. The range is 0–0.1 m/s.*

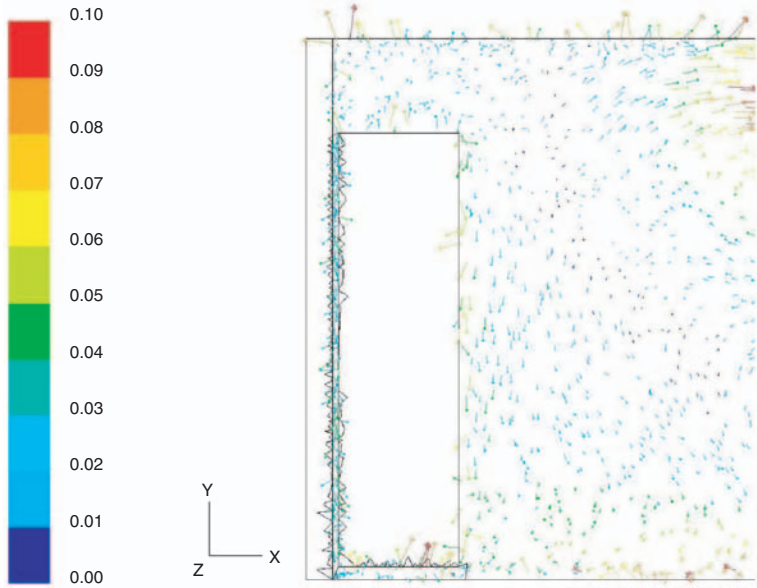

Figure 31. *Vector velocities for Case D at the 0.5-plane. The air drops behind the furniture and moves out into the room under it. The range is 0–0.1 m/s.*

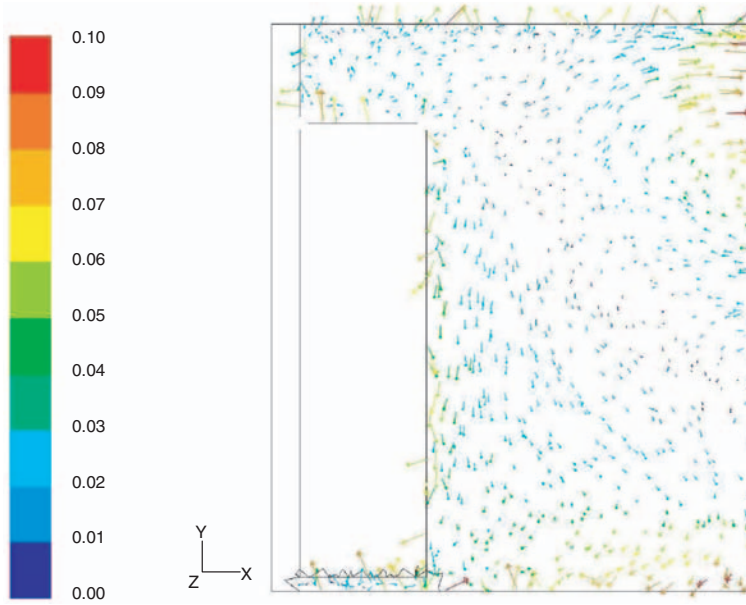

Figure 32. *Vector velocities for Case E at the 0.5-plane.The air flows under the furniture is quite turbulent and seems to be rising. The range is 0–0.1 m/s.*

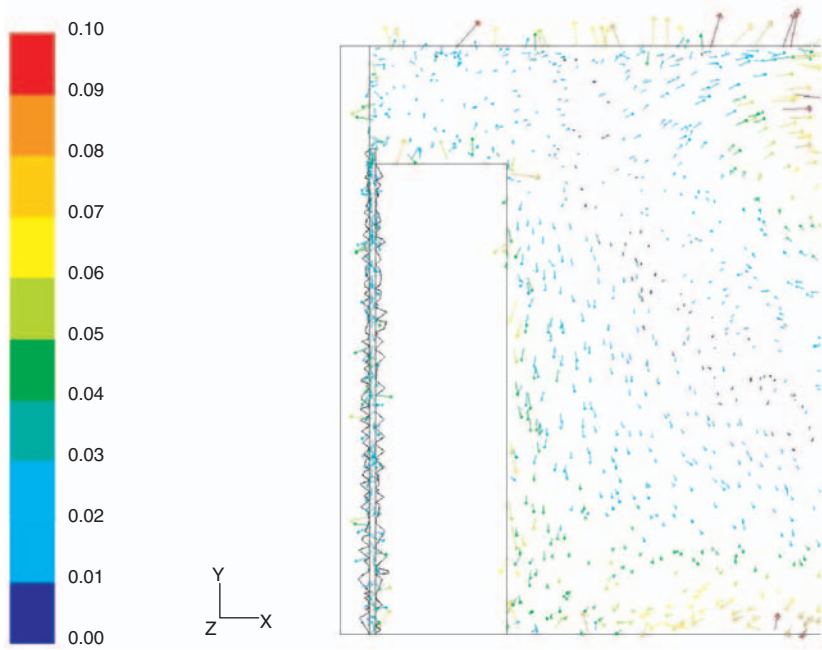

Figure 33. *Vector velocities for Case F at the 0.5-plane. The air falls down between the furniture and the wall. The range is 0–0.1 m/s.*

affects the airflow distribution in the room. The impact is that the air is moved up on both sides of the furniture. The average RH and temperature for the room air was 47% and 19.5°C. Because of the highly temperature dependent RH it is reasonable that a lower temperature gives a higher RH for a given vapor content.

The test with doubled inlet velocity of 0.333 m/s corresponding to an air change rate of $3\,h^{-1}$ (Case 4) gave temperatures and RHs that are lower than for Case 1 but the result is obvious since the air coming in is quite dry (27%RH, 4.0 g/kg) and when the air change rate is increased from 1.5 to $3\,h^{-1}$ the equilibrium vapor content must be lower. The increased air change rate also cools the room air because more air of 20°C replaces the warmer air. However, this should have the opposite effect on the RH, which should be increased by lower temperatures but the much drier air entering the room dominates this effect. The airflow distribution in the room also changed. It follows the ceiling from the inlet and spreads on the outlet wall and then it is moved down and follows the floor until it reaches the furniture where it rises again. Behind the furniture the airflow drops to the floor.

In the last variation (Case 5) the temperature on the exterior side of the inlet wall was changed from 0 to 10°C. The average results were the same as in Case 1. However, the temperature distribution in the room changed a little and, for example, the average temperature of the furniture was 0.1°C warmer than for Case 1. The change is realistic since the exterior wall was warmer and this affects the furniture, which is placed near the wall.

Discussion – Cases with a Person as Moisture Source

With the focus on the microclimate, the highest RH is found for Case F with 79.6%RH at 21.7°C (12.8 g/kg), which was expected since the furniture on the floor was likely to limit the airflow. The limited airflow gives lower surface temperature on the internal side of the inlet wall and hence the RH is higher. The lowest maximum value for the RH in the microclimate is found in Case B where it is 54.9%RH at 22.0°C (9.0 g/kg). The reason is that in Case B the furniture is hanging directly on the wall, which removes the cold air dropping down along the cold wall surface. Furthermore, the warmer floor gives higher temperatures and thereby lowers the RH. The found RH levels in the room all seem reasonable compared to the values estimated by the simple moisture balance for the room in Equation (2).

Generally the results of the airflow patterns in the room seem reasonable. In Cases A–C the inlet jet starts in the centerline and follows the ceiling and slowly turns to the corner at the outlet wall opposite of the furniture because of the free convection around the person placed on the other side of the centerline in the room. In Cases D–F the effect of the lower inlet velocity is that the jet drops to the floor just after entering the room and rises again near the outlet wall due to free convection around the person. The overall velocity patterns in the Cases A–C are generally very similar and the same is seen for Cases D–F, but in the microclimate behind and below the furniture some differences have been found. Here the corresponding placements of the furniture seem to dominate the effect of the changed airflow rate. There is no indication of difference between the airflows behind the furniture whether it is placed directly on the floor or not. Behind the furniture, the airflow velocity is also low and in the range 0.02–0.05 m/s. In the four cases A, B and D, E the velocity under the furniture is in the range 0.01–0.12 m/s. This indicates a more turbulent airflow pattern under the furniture. The temperature of the furniture is influenced by the colder inlet wall and therefore the temperature under the furniture is slightly < 22°C, and this can help to explain the rising airflow under it, since the boundary condition is a floor temperature of 22°C. This means that the air near the floor will be warmer than that under the furniture, and it will rise because of buoyancy.

General Discussion

For all the cases described in this study there is a linear stratification in the fluid walls for both the temperature and the moisture distribution.

The RH values found for the simulated Cases 1–5 are all low, between 42 and 52%RH. The found levels seem reasonable but the model results should be compared to measured values in order to assure validation. The found low range means that the moisture does not pose a risk to either the indoor climate or the constructions. On the internal surface of the inlet wall the worst case (double inlet moisture load) gave an average of 53%RH (20.7°C), which should not cause problems.

For Cases A–F the placement of the furniture near the exterior wall seems to influence the temperatures and the RH most. In Cases A–F the highest RH was found for the case where the furniture is placed on the floor with a small distance to the wall and with the lowest air change rate as expected. For Cases D–F behind or below the furniture the RH values are in the range 77.8–79.6%RH, which are high enough to be able to cause moisture problems. However, the room air itself is also quite humid with average values of 76.2–76.3%RH, so the indoor air will not provide sufficient cooling of the mucous membrane when breathing and thereby the air will be perceived as uncomfortable and stuffy (Toftum and Fanger, 1999).

It was unexpected that the effect of elevating the furniture from the floor seems to be relatively small, since the air should be able to move more freely and thus more warm air passing should heat the wall more and thereby decrease the RH. Therefore, it would be interesting to simulate different distances to the wall and floor and also study the effect of changing the floor temperature.

The airflow in the room is found to influence the airflow direction behind the furniture. This means that the placement of inlet and outlet in modeling of microclimates is very important and it could change the flow patterns completely.

Yet, another thing that can influence the microclimate that has not been taken into account is the moisture interaction with the furniture. This might not be that far from the truth since furnishing often have varnished surfaces, which are quite moisture tight. However, in many real situations the backside of furnishing is vapor permeable because it is untreated and in that case it will interact more with the vapor content in the surrounding air.

FUTURE WORK

In this simplified case study no radiation model was used. It would therefore be very interesting to include this in the model in the future.

It is quite common to neglect radiation in the first approach of using the program in a nonstandardized way, as done here by use of fluid walls for simulation of moisture transfer in walls. Including radiation in the model should give more accurate modeling of temperatures in the room in general and thus, it may have a considerable impact on the moisture conditions in the microclimate.

To be sure that the results obtained by use of this model are correct it is necessary to validate it by comparison between simulations and experimental data of a given case. Therefore, in future work the model described in this study will be compared to particle image velocimetry (PIV) experiments. The experiments will be designed to reveal the airflow patterns between a cold exterior wall and a piece of furniture placed with different distances to the wall and the floor. The case for comparing simulation with experiments will include natural convection within the room cavity, and the simulation will be expanded to include radiation between surfaces as well. The experimental configuration is currently being developed at Technical University of Denmark (DTU).

If the model can be validated the idea is to use it on more realistic cases in the future and thereby gain a better understanding of heat and moisture transfers in microclimates.

It would be interesting to simulate other cases with for example, more realistic geometry size and moisture sources. Realistically the moisture load from a person standing still should be around 61 g/h according to Koch et al. (1986).

CONCLUSIONS

In this study, it has been shown that it is possible to make investigations of microclimates in rooms with the described CFD model, which simultaneously calculates temperature, moisture, and airflow fields. This has been done by simulation of two particular cases with different moisture sources. By use of these cases it was found that it is possible to obtain information about both the water vapor content and heat distribution in both air and constructions. Furthermore, the model can provide detailed information about the airflow distributions patterns also in small gaps with limited airflows.

It was found that the simulations gave reasonable results. This is important, because here the CFD model is used in a nonstandardized way (e.g., use of fluid to represent solid wall behavior) and their correct behavior in the situation needed to be confirmed.

For all the tested cases with a relatively high air change rate of $1.5\,h^{-1}$ the results showed an inlet jet that follows the ceiling and spreads out on the

opposite outlet wall except for a case with decreased inlet temperature where the increased density of the air made the jet fall toward the floor. For Cases D–F with an air change rate of $0.5\,h^{-1}$ the airflow detached from the ceiling and fell down. It was found that the airflow patterns in the room are of great importance for the flow direction behind the furniture. Therefore accurate modeling of both inlet and outlet is very important.

In all cases except Cases D–F the low RH found in the microclimate behind the furniture for the studied cases does not cause moisture problems but the furniture does influence the moisture levels, so for more severe cases this type of investigation can be interesting. For Cases D–F with a low air change rate the results show RH levels higher than 78%, which can cause moisture problems in the indoor environment. It is also found that the model is able to calculate the moisture level and the results seem reasonable compared to expected results from a moisture balance calculation. However, the model needs to be validated by comparison with experimental data. As the airflow pattern in the room has a strong influence on the microclimate, such an experiment should include detailed description of the airflow as the CFD based model presented here.

A disadvantage of using a CFD model is that it is only suitable for steady-state predictions. The explanation is the long computational time needed, so an in-stationary simulation would be too time consuming.

ACKNOWLEDGMENTS

The work was carried out with the support of the Technical Research Council of Denmark. Thanks are due to Gilles Rusaouën, Associate Professor (CETHIL - UMR CNRS 5008, INSA de Lyon, UCBL) and Raluca Hohota, Assistant Professor (Faculty of Building Services and Equipment, Technical University of Civil Engineering Bucharest – UTCB, Romania) for their help with creating the model.

REFERENCES

Bartak, B., Beausoleil-Morrison, I., Clarke, J.A., Denev, J., Drkal, F., Lain, M., Macdonald, I.A., Melikov, A., Popiolek, Z. and Stankov, P. (2002). Integrating CFD and Building Simulation, *Building and Environment*, **37**(8–9): 865–871.

Clarke, J.A., Johnstone, C.M., Kelly, N.J., McLean, R.C., Anderson, J.A., Rowan, N.J. and Smith, J.E. (1999). A Technique for the Prediction of the Conditions Leading to Mould Growth in Buildings, *Building and Environment*, **34**(4): 515–521.

Fluent Inc. (1999). FLUENT® User's Guide, Fluent Inc., Lebanon, NH, USA.

Hohota, R. (2003). Moisture Modelling in a CFD Code (Low Velocity in Large Enclosure), Comparison with Experiments (in French), PhD Thesis, Laboratoire CETHIL INSA de Lyon, France.

Jones, W.P. and Launder, B.E. (1972). The Prediction of Laminarization with Two Equation Model of Turbulence, *Int. J. Heat Mass Transfer*, **15**(2): 301–314.

Koch, A.P., Kvisgaard, B., Larsen, J.G. and Nielsen, T. (1986). Moisture Production in Dwellings, *Moisture in Dwellings* (in Danish), **1st edn**, p.11, Teknologisk Instituts Forlag, Tåstrup, Denmark.

Negrão, C.O.R. (1998). Integration of Computational Fluid Dynamics with Building Thermal and Mass Flow Simulation, *Energy and Buildings*, **27**(2): 155–166.

Patankar, S.V. (1980). *Numerical Heat Transfer and Fluid Flow*, Hemisphere Publishing Corporation, Washington.

Shih, T.-H., Liou, W.W., Shabbir, A., Yang, Z. and Zhu, J. (1995). A New k-ε Eddy Viscosity Model for High Reynolds Number Turbulent Flows, *Computers & Fluids*, **24**(3): 227–238.

Teodosiu, I.C. (2001). Modelling of Technical Systems in the Field of Building Equipment Using CFD Codes (in French). PhD Thesis. Laboratorie CETHIL INSA de Lyon, France.

Teodosiu, C., Hohota, R., Rusaouën, G. and Woloszyn, M. (2003). Numerical Prediction of Indoor Air Humidity and its Effect on the Indoor Environment, *Building and Environment*, **38**(5): 655–664.

Toftum, J. and Fanger, P.O. (1999). Air Humidity Requirements for Human Comfort, *ASHRAE Trans.*, **105**(2): 641–647.

Versteeg, H.K. and Malalasekera, W. (1995). *An Introduction to Computational Fluid Dynamics, the Finite Volume Method*, John Wiley & Sons Inc., New York.

Wolfshtein, M. (1969). The Velocity and Temperature Distribution of One-dimensional Flow with Turbulence Augmentation and Pressure Gradient, *International Journal of Heat & Mass Transfer*, **12**(3): 301–318.

Zhia, Z., Chen, Q., Haves, P. and Klems, J.H. (2002). On Approaches to Couple Energy Simulations and Computational Fluid Dynamics Programs, *Building and Environment*, **37**(8–9): 857–864.

Zhia, Z. and Chen, Q. (2003). Solution Characters of Iterative Coupling between Energy Simulation and CFD Programs, *Energy and Buildings*, **35**(5): 493–505.

Paper IV

Investigation of airflow patterns in a microclimate by Particle Image Velocimetry (PIV)

Mortensen, L. H., Rode, C. & Peuhkuri, R. (2008)

Published in: Building & Environment, 43 (11), 1929-1938,
http://dx.doi.org/10.1016/j.buildenv.2007.11.012

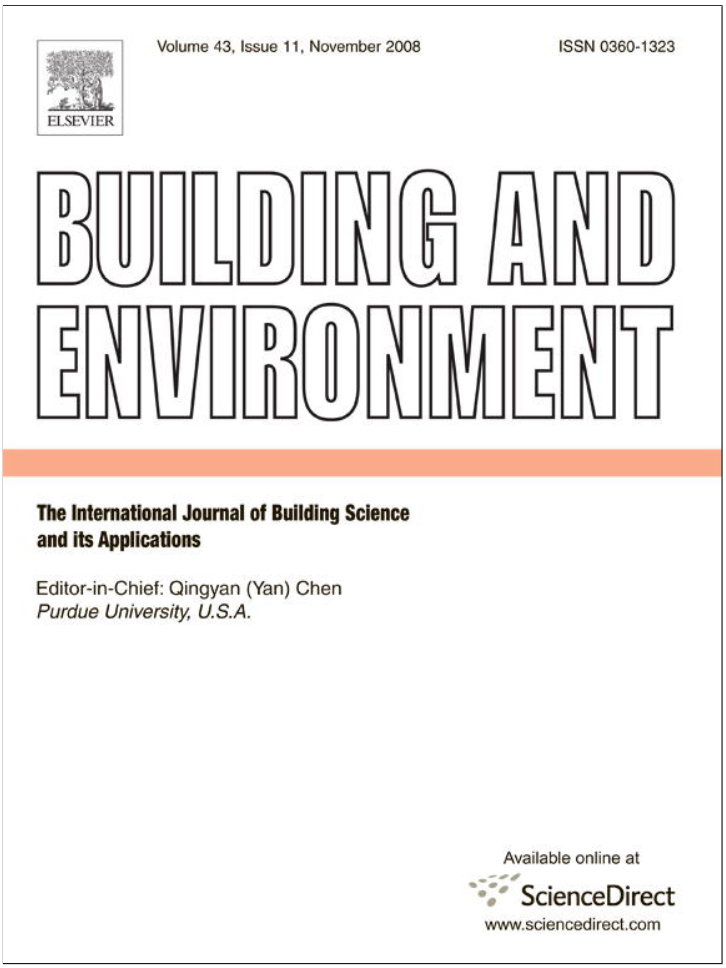

Available online at www.sciencedirect.com
ScienceDirect
Building and Environment 43 (2008) 1929–1938
BUILDING AND ENVIRONMENT
www.elsevier.com/locate/buildenv

Investigation of airflow patterns in a microclimate by particle image velocimetry (PIV)

Lone H. Mortensen[a,*], Carsten Rode[a], Ruut Peuhkuri[b]

[a]Department of Civil Engineering, Technical University of Denmark, Brovej Building 118, DK-2800 Lyngby, Denmark
[b]VTT Technical Research Centre of Finland, P.O. Box 1000, FIN-02044 VTT, Finland

Received 2 April 2007; received in revised form 22 November 2007; accepted 23 November 2007

Abstract

Problems with mould growth in dwellings usually occur in bedrooms in the microclimate behind closets placed next to exterior walls with poor insulation. It is anticipated that the problems are caused by lack of airflow behind the furniture in combination with a colder surface temperature and a high moisture production. The lack of air circulation decreases the surface temperature, which can cause problems. A particle image velocimetry (PIV) investigation was performed of the airflow patterns in such a microclimate. This paper describes the experimental set-up and the results. The results indicate that the flow rates behind the furniture will increase with increased distance between the closet and the wall, and even higher airflow rates are seen when the furniture is elevated by legs.

Keywords: PIV; Boundary conditions; Airflow velocity; Measurements; Natural convection

1. Introduction

1.1. Background

Moisture interactions between room air and the surrounding constructions and furniture have a great influence on the indoor environment. High moisture production or cold areas can cause high relative humidity (RH), which can lead to mould growth. This is undesirable in the indoor environment due to concerns of indoor air quality. A review study of humidity in dwellings has been performed by Bornehag et al. [1] and their advice is to avoid moist buildings.

The critical areas in dwellings typically occur in bedrooms, where problems may appear in microclimates behind furniture placed next to exterior walls without or with poor insulation. In dwellings with problems, the surface temperature of the exterior wall is typically 5–8 °C colder than the room temperature. It is assumed that the furniture limits the airflow near the wall and the lack of warm room air near the surface will decrease the surface temperature even more, which can cause problems. When this is combined with a high moisture production rate from sleeping persons during the night, the lower temperature in the microclimate causes increased RH, and the outcome can be biological growth. However, to be able to quantify the microclimatic effect on the indoor environment, there is a lack of knowledge of the airflow velocities behind furniture in dwellings.

In the present investigation the focus has been on the airflow pattern near a cold wall caused by the placement of furniture. An earlier investigation by computational fluid dynamics (CFD) showed that different placement of furniture near colder external walls may affect the RH in the microclimate and that the highest values were found when the furniture was placed directly on the floor and had a small distance to the wall [2]. There is a lack of empirical data of flow patterns behind furniture. Therefore, a number of different cases were used here: combination of the distance between the furniture and the wall, the distance between the furniture and the floor. The distance between the furniture and the floor was an imitation of furniture elevation from the floor by use of legs as support.

*Corresponding author. Tel.: +45 4525 1934; fax: +45 4588 3282.
E-mail address: lomo@alectia.com (L.H. Mortensen).

0360-1323/$ - see front matter © 2007 Elsevier Ltd. All rights reserved.
doi:10.1016/j.buildenv.2007.11.012

The investigation was performed by particle image velocimetry (PIV). The results will provide empirical data of expected airflow velocities in such situations, and may be used as validation of numerical CFDs simulations. The aim of the current paper is to provide knowledge about the airflow patterns behind furniture placed in the vicinity of walls.

1.2. Particle image velocimetry

PIV is a fairly easy way to visualize fluid flows by the use of tracking particles. The method is non-intrusive apart from the particles and thereby it is ensured that the actual flow field is determined. However, to use the technique it is necessary to have optical access.

The PIV technique works by comparing the image frames of a flowing fluid containing tracer particles. A laser creates a light sheet and the scattering particles on it reflect the light. Then a digital charge-coupled device (CCD) camera is used to capture the instant placement of particles. The camera is connected with the laser and so an image frame is recorded when the laser pulse is triggered. When a double laser pulse is fired the reflection of light from the particles is saved in two different images. Hence, two frames are taken with minute intervals, and then it is possible to rediscover the particles of the first frame in the second frame. The particle movement between two frames gives a visualization of the flow pattern. However, the size of the tracking particles is very important when PIV is used. The reason is that small particles follow the fluid flow well whereas larger particles are better at reflecting the light, which is needed by the camera for the recording. Therefore, the size of the scattering particles is a compromise between a size that is small enough to follow the fluid and a sufficient size to reflect the needed light. Another factor that influences the amount of light recorded by the camera is the numerical aperture (F-number). A low F-number allows more light to enter the camera and this can reduce the required laser power. The F-number is usually set as low as possible in order to ensure enough recorded light to detect the particles. The particle images are sampled by the CCD camera and is characterized by the pixel pitch. The lens is an analogue filter before the digitization of the image and so the filter frequency must be lower than the sampling frequency to avoid aliasing. The diffraction-limited spot diameter should be twice the size of the pixel pitch and for most cameras this corresponds to an F-number between 8 and 16. Therefore, the Nyquist sampling theorem will be violated by small values of the F-number impacting the measurement accuracy [3].

The replacement of the particles and the time delay between two laser pulses give the velocity vectors, which more accurately are derived from sub-sections of the target area, which are called interrogation areas. It is assumed that there is a uniform displacement within an interrogation area.

To obtain high-quality PIV records a scattering particle concentration of 15 particles within each interrogation area is needed [4]. A scale factor is used to establish a relation between the displacements in pixels to metric displacements. In Eq. (1) the determination of the flow velocity is shown:

$$v = \frac{\Delta x}{\Delta t}, \tag{1}$$

where v is the velocity, Δx is the common displacement and Δt is the time between two laser pulses.

After recording, the images need to be post-processed. Within all recorded images the different interrogation areas are cross-correlated with each other to find the average value for the displacement that leads to a vector map of velocities. One of the correlation methods is an adaptive correlation [5,6], which avoid most errors in the flow field by comparing every vector with the average of the surrounding vectors. If the processed vector is more than 90% different from the surrounding average the vector is removed. There can, of course, still be errors if there are at least two errors very close to each other.

PIV has been used for more than 20 years and during this time it has evolved drastically as summarized by Adrian [7]. Adrian particularly highlights the development of double-pulsed laser systems and CDD cameras. PIV has been used for numerous applications from aerodynamics of aircrafts, cars, buildings and other structures in air to velocity measurements of water in pipe flows. The technique has even been extended so that it is able to measure microscale flows. Investigation of airflows in a whole room is almost impossible with PIV due to a limited field of view area, which is roughly $0.5 \times 0.5\,\mathrm{m}^2$ for common equipment. To overcome this problem Zhao et al. [8] invented a new PIV system for full-scale rooms but further research is needed to improve the technology. Another method is to use scale models as done by Posner et al. [9] in a study of the influence of how obstructions influence airflows in a room. When using scale models it might even be more convenient to use water as working fluid instead of air since this decreases the velocities. The approach of using water as the fluid medium has been used and has shown good agreement with numerical simulations for air by Adeyinka and Naterer [10]. An earlier application of PIV in building physics by Lee et al. [11] concerned ventilation flows inside a 1/1000 scaled factory building. They used air as the medium and found that the airflow was dependent on the location and size of opening vents, building arrangement and the outdoor direction and speed of wind.

The air gaps that are investigated in this paper can be assumed to be comparable with flow between asymmetrically heated parallel plates, which is closely related to natural convection flows in open-ended channels. Aung [12] and Aung et al. [13] studied natural convection flows in channels with asymmetric heating both numerically and experimentally but not with PIV. Habib et al. [14] used PIV

to investigate airflow between both symmetrically and asymmetrically heated vertical plates of 125 mm height with a gap width of 40 mm. They found that an asymmetrically heated channel 10 °C higher and lower than ambient temperature yielded an upward flow near the hot plate and it had a wider boundary layer than the cold plate with downward flow. With the same equipment Ayinde et al. [15] studied turbulent natural convection in a symmetrically heated channel also by PIV and found an indication of significant diffusion rates of the normal Reynolds stresses towards the centre of the channel.

1.3. Outline of the current paper

The objective of the present study is to clarify the behaviour of natural convection in microclimates between the external wall and furniture with a special focus on airflow patterns and velocities. To obtain the highest resolution of the investigated air gap of only 25 or 50 mm it was chosen to use PIV in a full-scale room. Air was used as the fluid medium and to ensure the right natural convection pattern caused by buoyancy effects, and so an entire room was needed. The instantaneous velocity vectors in a two-dimensional flow field were measured with PIV, while the temperatures at the surrounding boundaries were measured by thermocouples. Before it was chosen to use a PIV system it was considered to use hot-wire measurements but because of a combination of practical difficulties of placing hot-wire probes in the narrow air gap behind the furniture, and the fact that it is an intrusive method, which will disturb the flow, the hot-wire method was disregarded. This paper presents an investigation of natural convection behind furniture in dwellings, which was investigated by different cases of distance between the furniture and the wall in combination with different furniture leg heights. Furthermore, the measurements were performed at different heights and different distances between the camera and the laser sheet.

2. Facilities and equipment

To investigate the airflow pattern near the surface due to natural convection, it has been necessary to create a chilled wall surface where the temperature is evenly distributed and can be controlled. The PIV experiments were performed in a laboratory where the external wall was imitated by use of a lightweight construction of a chilled wall.

2.1. Test room

An ordinary room with internal dimensions of $3.6 \times 4.5 \times 2.5\,m^3$ was created. The room was created inside a test facility of $3.6 \times 6.0 \times 3.6\,m^3$. In the chamber a chilled internal wall was built, and a plexiglass box was positioned against that wall to imitate a closet standing against an external wall in a real building. An air gap behind the plexiglass furniture allows room air to pass over the chilled surface and this imitates microclimates found in ordinary dwellings.

The imitation of an exterior wall was made from a wooden structure covered by a plain gypsum board. Fans inside the wall circulated the air, which was cooled by a cooling pipe system at the back of the wall. The fans ensured an evenly distributed temperature on the external surface of the wall. The incoming temperature and velocity of the cooling fluid was controlled. The dimension of the chilled wall was $2.3 \times 0.5 \times 2.5\,m^3$. Fig. 1 shows a picture of the chilled wall during the construction. In Fig. 2 an overview can be seen of the experimental set-up. The width of the room is 3.6 m and since the chilled wall is only 2.3 m wide it is not large enough to close off the last part of the room. This is done with a single layer of gypsum board with a width of 1.3 m. The reason for this configuration was that the camera and tripod take up some space just at the end of the wall and otherwise the camera would not have been able to capture the flow near the chilled wall (see Fig. 2).

The plexiglass cupboard is a fairly good approximation of reality. The thermal resistance between room and the surface of the chilled wall is estimated to be $0.58\,m^2\,K/W$, which corresponds well with the IEA Annex 14 report [16] that recommends use of $2\,W/m^2\,K$ as the surface film coefficient behind a cupboard. The plexiglass ensures transparency, which is needed by the laser to create a light sheet in the air gap between the furniture and the chilled wall where the airflow patterns were investigated. The dimensions of the furniture were $1.5 \times 0.46 \times 2.0\,m^3$ (width × depth × height) and it is shown in Fig. 2.

2.2. Thermocouples

Supplementary measurements of the temperature distributions were made to assure that all PIV measurements

Fig. 1. Chilled wall set-up without a front plate. The cooling pipes cool the air in the wall cavity and fans mix the air to provide an evenly distributed temperature on the internal surface of the "external wall".

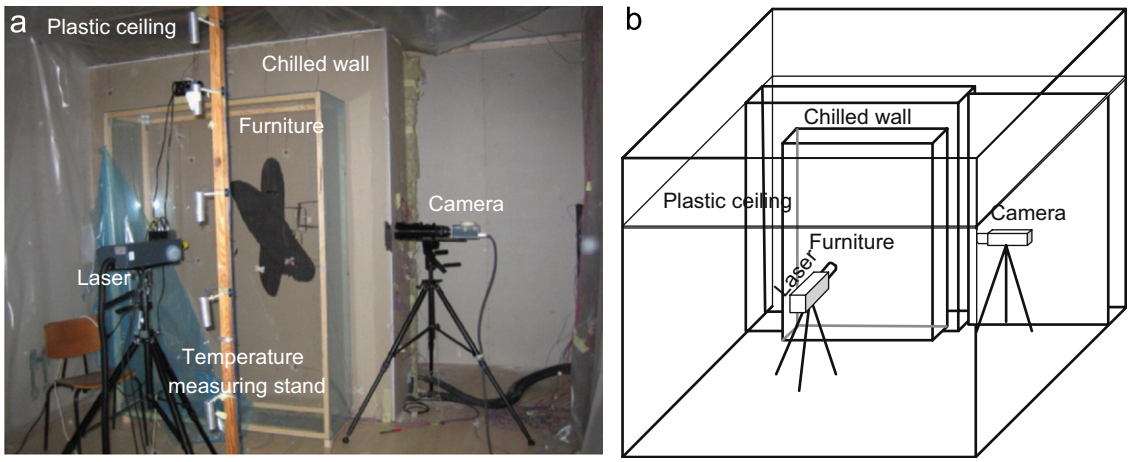

Fig. 2. The experimental set-up, where the camera points into the air gap between the chilled wall and the furniture and the laser sheet is pointed in through the plexiglass furniture: (a) a picture of the experimental set-up, (b) a diagram of the PIV set-up.

were performed at the same temperature and thus natural convection conditions. The temperature measurements were taken with copper-constantan thermocouples with an accuracy of 0.5 K. Furthermore, the temperature distribution on the chilled wall was measured in order to check that the temperature distribution actually was uniform. The surface temperatures of the furniture were also registered.

2.3. PIV equipment

The two-dimensional flow field was measured using a smoke of small oil droplets (glycol 0.1–1.0 μm) as tracers, and their motion was captured by a CCD camera (Dantec HiSense camera, 1024×1280 pixels). The tracer particles were illuminated by a light sheet of (about 3 mm in thickness) discharged from a water-cooled double-pulse Nd:YAG laser system (100 mJ/pulse).

An external processor unit triggers signals to the camera and the laser, and coordinates the transportation of data from the camera to the computer processor.

3. Measurements

The measurements were performed in the described facility. The purpose of the measurements was to gain information about the airflow distribution patterns in small air gaps between cold exterior walls and furniture placed near it. Fig. 2 shows a picture and a perspective projection of the experimental set-up.

During the measurements two different distances between the furniture and the wall were tested in combination with three different distances between the furniture and the floor. The surface temperature of the chilled wall behind the furniture was constantly 16 °C and the average room temperature was 22 °C for all measurements (giving a temperature difference of 6 °C). Table 1 gives the different distances between the furniture and floor or chilled wall.

Table 1
The different tested positions of the furniture

Furniture position	Gap (mm)	
	Furniture—floor	Furniture—chilled wall
1	0	25
2	0	50
3	50	25
4	50	50
5	100	25
6	100	50
7	200	25
8	200	50

The two-dimensional flow fields were also measured from different positions of the camera and the laser. The distances between the camera lens and the image plane were in the range 0.9–1.4 m. The physical image height was on average 130 mm with a maximum width of 50 mm, which is the maximum gap size the flow was measured in. The positions of the camera and laser are absolute and described in Table 2 and illustrated in Fig. 3.

First, a short distance between the camera and the laser sheet was tested, and since this was most likely to provide useable results, this is referred to as position A. Next in position B the distance between the laser and the camera was increased because this would provide a larger image. The instantaneous vector visualizations were bad due to too many particles, between the camera and the laser. In position C the laser was moved closer to the camera again. The immediate vector results were still not good, partly due to several reflections from the chilled wall and the plexiglass. Therefore the laser was moved even closer to the camera with a distance of less than 1 m. Here, in position D, all the furniture positions were measured. The next idea was to measure in a lower position of both the camera and the laser, position E. The instant vector results were not good and the effect was assumed to be caused by a small distance the corner of the furniture. Therefore, the

Table 2
Description of different measuring positions with the PIV equipment

Position	Distance (mm) camera–laser	Image height (mm)	Camera height (mm)	Laser height (mm)	Distance (mm) laser–wall	Measured furniture position
A	1050	124	1183	1192	1570	1–8
B	1420	187	1183	1192	1000	3–4
C	1200	136	1183	1192	1440	3–6
D	920	106	1183	1192	1670	1–8
E	930	113	770	760	1670	3–4
F	1080	130	770	760	1500	1–8

The physical image size changes with distance between camera and laser. Only image width of maximum 50 mm is used; the rest is masked out.

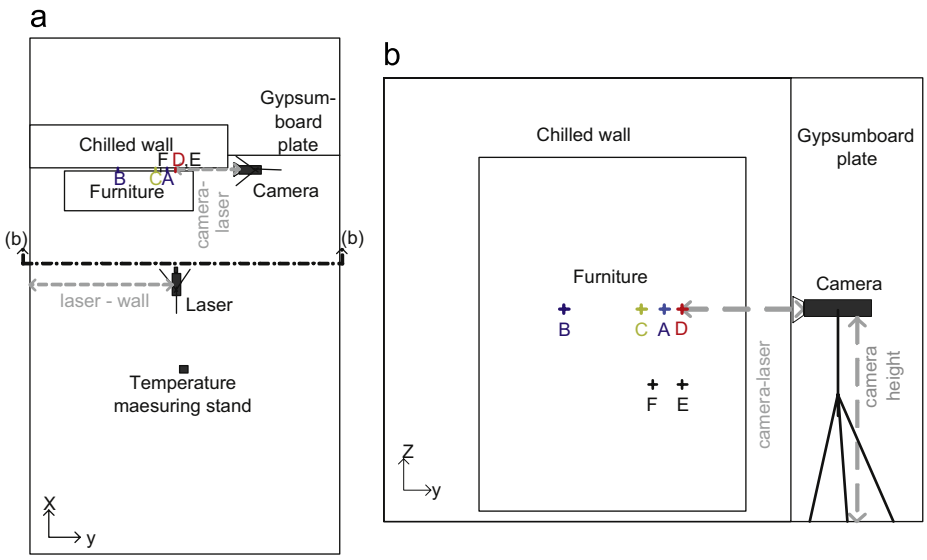

Fig. 3. (a) A plane of the measured PIV set-up and (b) a front view of the room. The letters A–F show the measuring positions given in Table 2. The distance between the camera and the laser sheet is shown for measuring position D.

laser was moved so that the distance between the laser and the camera was increased slightly to position F. Here it was possible to take measurements of all the positions of the furniture.

The focus of the investigations was on the natural convection caused by the chilled wall in the room, but it was impossible to keep the tracer particles locally distributed behind the furniture and thus they needed to be distributed evenly in the entire room. For most cases this was achieved by emitting a burst of smoke and leaving the room to stabilize for approximately 15 min before the measurements were taken. It proved slightly difficult to control the amount of smoke emitted and hence sometimes more or less time was needed for the room to stabilize.

The time interval between two pulses was set to 3500 μs, except for measurement of position B, where 5500 μs was used. The local displacements were calculated using an adaptive correlation method with interrogation areas of 32×32 pixels and a 50% overlap both horizontally and vertically. This gives around 15 interrogation areas for the 25 mm gap and approximately 28 for 50 mm.

For every measuring positions A–F a calibration was made that determined the scale factor and so the real vector velocities were obtained. With every run of the PIV equipment 3 series of 10 recordings were taken. Every recording contains two images, one for each of the double-laser pulse.

All recordings were post-processed but first the images were masked so that only the flow field in the actual air gap was evaluated. Then an adaptive correlation was performed for each of the 30 recordings. These data were used to obtain average vector statistics of all recordings in every series resulting in just one velocity vector map.

During the experiments the temperature distribution in the room was also measured. The temperature was measured in 22 positions on the chilled wall to ensure an equal temperature distribution. The temperatures were also measured in the middle of the room, underneath the furniture, on the floor under the furniture and at the surface of the furniture facing the room air.

4. Results

Only the vertical velocities in the vertical air gap will be shown and discussed, since the horizontal velocities are very small. The horizontal velocities (x-direction in Fig. 3)

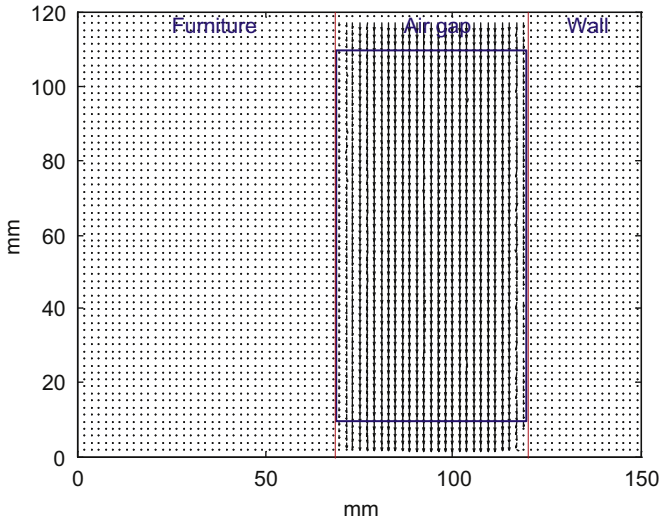

Fig. 4. Average velocity vectors based on 30 images for position 4A (Tables 1 and 2). The frame marks the numbers of vectors used in the averages shown in Figs. 4 and 5.

are in the order of magnitude of 2% of the vertical velocities in the air gap between the furniture and the chilled wall. The measured velocity field is set to be positive upwards (z-direction in Fig. 3).

The results of the tested cases are divided into two parts depending on the distance between the chilled wall and the furniture with either a 25 or 50 mm air gap. First, the results are presented for the furniture position with odd numbers (see Table 1), followed by even-numbered furniture positions. In the figures with results the absolute camera position is given by its letter (see Table 2), and in most cases the measurements were taken after a stabilization time for the smoke in the room of 15 min. If the stabilization was longer this is given by a number after the camera position. All the presented results are based on average velocity vector maps. An example is given in Fig. 4 of an average velocity vector map for position 4A. These results are averaged again for every velocity vector position in the height of the air gap except for the top 5 and bottom 5, because these may be influenced by the physical limits of the image size as shown by the frame in Fig. 4 (see also

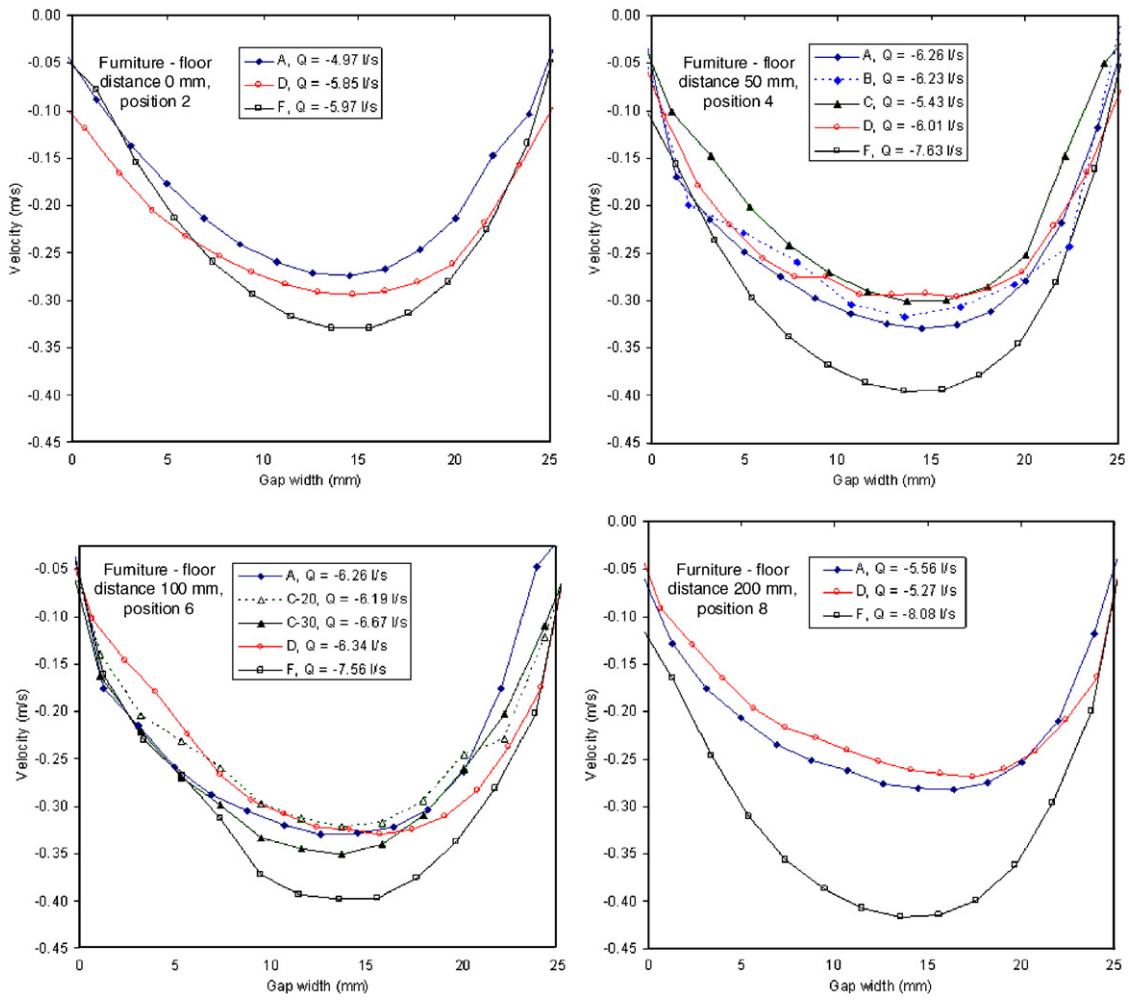

Fig. 5. Measured velocities and flow rates (in legend) for the air gap of 25 mm between the chilled wall and the furniture. The letters A–F refer to different positions of the camera and laser (Table 2). The surface of the furniture is at a gap width of 0 mm and the chilled wall at 25 mm gap width.

Fig. 7). Therefore, the results are shown as single velocity curve profiles for every measuring position. By integrating the velocity profiles over the gap width, the local flow rates per width of the furniture have been calculated. The flow rate is given in the legends of the result figures.

4.1. Results of 25 mm air gap

The results of all the measured velocities for the air gap of 25 mm between the furniture and the chilled wall are presented in Fig. 5.

Generally, the shape of the velocity profiles seems to be only slightly dependent on both the measuring positions A–F and the distance between the floor and the furniture. The maximum velocities are reached closer to the chilled wall ($x = 25$ mm) than the surface of the furniture. It is also noticeable that the velocities are always the highest for position F.

A general pattern of lower maximum velocity is seen when the furniture is placed directly on the floor, than if the furniture is elevated by legs of 50 or 100 mm, and the flow rates are also smaller. An increase of the furniture leg height from 50 to 100 mm gives slightly higher maximum velocities and flow rates in most positions.

The highest maximum velocity in the air gap is 0.42 m/s for measuring position F, when the distance between the floor and the furniture is the highest, 200 mm. This also gives the highest flow rate. However, for 200 mm furniture leg height the maximum velocities for measuring positions A and D are only 0.28 and 0.27 m/s, respectively, which is almost the same as when the furniture is placed directly on the floor. For position A the maximum velocity is 0.27 m/s when the furniture is placed on the floor and for position D it is 0.29 m/s. The flow rates for A and D with 0 mm or 200 mm furniture leg heights are both smaller than when the furniture height is 50 or 100 mm.

4.2. Results of 50 mm air gap

Fig. 6 gives the results of an air gap of 50 mm between the furniture and the chilled wall for all measuring positions, A–F.

A slightly dependence is observed for the general shape of the velocity profiles on both the measuring positions

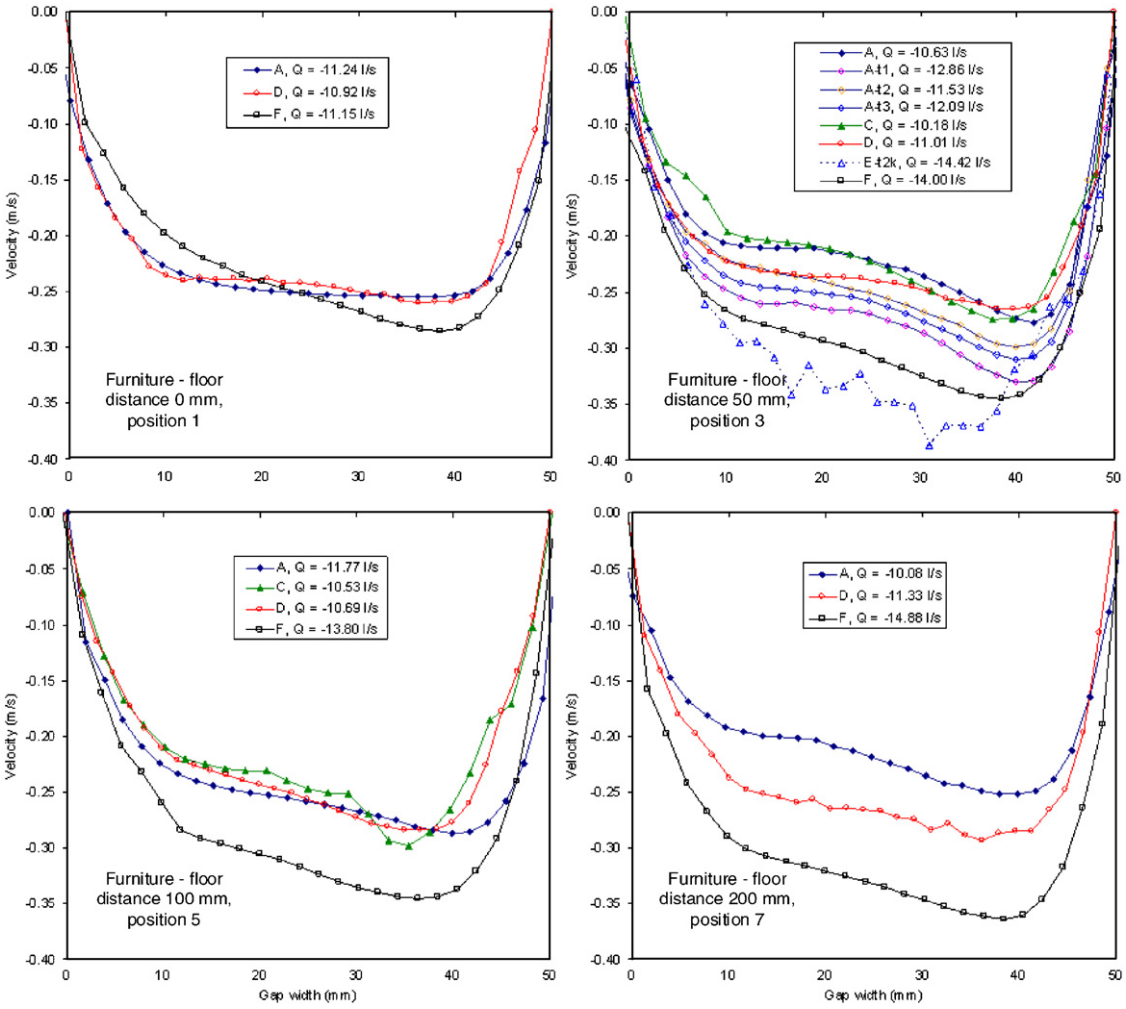

Fig. 6. Measured velocities and flow rates (in legend) for the air gap of 50 mm between the chilled wall and the furniture. The letters A–F refer to different positions of the camera and laser. The surface of the furniture is at a gap width of 0 mm and the chilled wall at 50 mm gap width.

A–F and the distance between the floor and the furniture for a 50 mm air gap. However, another velocity profile shape was found when the furniture was placed directly on the floor for positions A and D. In all the other positions it is even more obvious than for the 25 mm gap that the velocities are higher near the chilled wall ($x = 25$ mm) than near the surface of the furniture.

The highest maximum velocity in the air gap is 0.36 m/s for measuring position 8F (leg height 200 mm), but for a furniture leg height of 50 and 100 mm in position F are 0.35 and 0.34 m/s, respectively. In position F the maximum velocity is almost independent of the leg height, but the flow rate for a 200 mm leg height is around 2 l/s higher. For positions A and D a furniture leg height of 50, 100 and 200 mm gives velocities in the range 0.25–0.33 m/s and flow rates of 10–12 l/s.

Four measurements for position A were performed with a furniture leg height of 50 mm, one ordinary run and three tests. The first two tests, t1 and t2, were tests of the time interval between pulses, the two results in the graph is for 3500 μs, which was also used in ordinary runs. The last-presented test, t3, is a test to see the influence of the F-number of the camera, and so here in t3 an F-number of 4.0 was used, while the ordinary runs used 2.8 (camera minimum) was used. The results from position 4A are very similar, and the maximum velocities are in the range 0.28–0.33 m/s and the flow rate ranges are 10.6–12.1 l/s.

4.3. Comparison of 25 and 50 mm gap widths

If Figs. 5 and 6 are compared it is observed that the shape of the velocity profile is different for the two gap widths. The velocities in the air gap between the furniture and the chilled wall are the highest for a narrow 25 mm gap than for a wider 50 mm gap with maximums of 0.42 and 0.36 m/s in both cases for a furniture leg height of 200 mm but the flow rates are the highest for the wider gap with 15 l/s compared to 8 l/s. The maximum velocity for both gap widths is found within the 15 mm closest to the chilled wall and in most cases just around a 10 mm distance.

Both the maximum velocity and the flow rate increase when the furniture is elevated 50 or 100 mm, in contrast, for positions A and D the effect disappears when the leg height is 200 mm.

Generally, the results for measuring positions A and D are very similar, whereas the velocities in general are higher for position F for both gap widths. Similar results are observed when the furniture is placed directly on the floor the results in position F as when 100 mm furniture leg heights are used in positions A and D.

4.4. Temperatures

The room temperature and the surface temperatures of the chilled wall and the furniture were registered during all the PIV measurements. The average temperature in the room during the experiments was $21.6 \pm 0.7\,^{\circ}C$. The registered temperatures of the chilled wall proved that the wall temperature was almost uniform, and that it was almost constant at $16 \pm 0.4\,^{\circ}C$.

5. Qualitative errors

The biggest source of errors is due to laser light reflections from both the chilled wall and the plexiglass furniture. Most reflections from the chilled wall were removed by painting it black (see the black cross in Fig. 2) but, the problems were not solved completely. The reflections are pronounced when the chilled wall, the furniture and the laser sheet are not aligned perfectly. There may even be reflections from within the plexiglass furniture. The screws used to assemble the plexiglass furniture also caused some reflections. The reflection errors in the images were removed by use of a mask.

The global distribution of smoke also caused some errors since smoke was distributed globally, in the whole room and in the air gap. The reason is that the amount of smoke particles between the camera and the laser sheet are increased with enhanced distance between the camera and the laser. The tracer particles that are not actually in the laser sheet image plane reduce the camera visibility.

A key factor in obtaining useable PIV results is the focus of the camera. A defocused camera will record images, which gives inaccurate data. The scale factor of the measurements is related to the focus of the camera. In the presented measurements the scale factor was between 20 and 30. This means that any inaccuracy caused by defocused images will be magnified.

The masking of the images in combination with the adaptive correlation also imposes an error. This error is caused by the overlapping interrogation areas. In the masked area of the images the velocities are 0 m/s and when an interrogation area is near the mask edge the adaptive correlation tries to smooth the results. This causes the gap width to seem larger than the actual 25 or 50 mm. However, this will not affect the results a short distance from the gap edges (furniture and wall). Fig. 7 shows the standard deviation for vector statistics performed on 30 images. The image is comparable to Fig. 4, which shows the vectors of a single image. The worst errors are seen in the bottom (120 mm). They are caused by particles leaving the image and this is the reason for disregarding the top and bottom five vectors.

Basically, PIV is efficient for measurement of the main flow. However, it is difficult to measure the velocities perpendicular to the main flow since these much smaller velocities would require different setting of the equipment like reduced time between laser pulses and smaller interrogation areas. Thus, this is yet another reason for not going into detail with the horizontal velocities in the x-direction.

To summarize, some of the factors in the resolving error are particle and image size, interrogation area, velocity

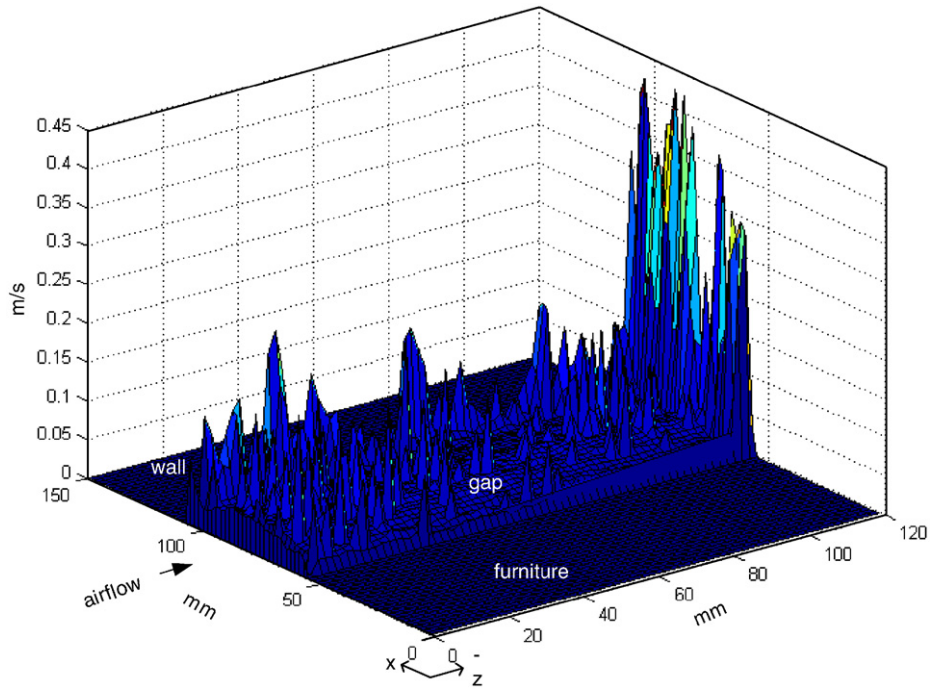

Fig. 7. Standard deviation of average velocity vectors based on 30 images for position 4A (Tables 1 and 2).

gradients, number of particles, instrumentation performance and computational errors like rounding and truncation.

6. Discussion

A good repeatability of the results is found since the four measurements taken in position A with a 50 mm distance to both the chilled wall and the floor all have the same velocity shape pattern. In position 4A the velocities are within a band of 0.05 m/s and the flow rates in the range 10.6–12.1 l/s. The temperatures were also monitored and controlled in order to provide the same surrounding conditions for all taken measurements, and with only small fluctuations these are not assumed to influence the natural convection in the PIV measurements.

The objective of the current study was to investigate the natural convection between an exterior wall and a piece of furniture next to it with PIV.

All the measured velocity profiles for the different measuring positions seem to follow the same pattern. The maximum velocity and the highest flow rate always occur at measuring position F for both gap widths and for all four heights of the furniture (0–200 mm). Therefore, a fully developed flow is not assumed at least not for positions A and D. The flow rates for measuring position F are always higher than the other positions, and this indicates that air from the side of the furniture must be drawn in.

For a small air gap of 25 mm the height of the furniture is considerably larger than the width of the air gap and thus the flow behaves like a flow between vertical plates heated asymmetrically, as shown by Aung [12].

Another pattern is seen for the air gap of 50 mm in Fig. 6, except for positions A and D when the furniture is placed directly on the floor. The velocity increases with distance to the furniture, followed by an almost linear increase of velocity until the maximum velocity is reached and then it decreases again getting closer to the chilled wall. This is similar to the results of Habib et al. [14] who investigated asymmetrically heated plates where the cold plate and hot plate had a temperature difference of 10 °C from the ambient air. They found a downward flow near the cold plate and a higher maximum velocity near the bottom of the plate than found at the top.

For both gap widths the maximum velocities are found closest to the chilled wall. This indicates that the boundary layer near the chilled wall dominates the flow, which is reasonable since the cold wall chills the air and the higher density makes it fall downwards.

When the furniture is placed directly on the floor the velocity profile generally seems to reach a lower maximum velocity than if the furniture is elevated by legs of 50 or 100 mm and the flow rates are also lower. For the 50 mm gap the shape of the air velocity profile is different for positions A and D when the furniture leg height is 0 mm, where the velocity grows with increased distance to the furniture until the maximum is reached. The maximum is around 0.25 m/s and from this point a constant velocity continues till it starts to decrease near the chilled wall. The air must exit through the sides behind the furniture in a three-dimensional flow path since it cannot flow out underneath the furniture but this was not recorded by the camera since the velocity measurements taken were two dimensional. For the narrow 25 mm gap the maximum furniture leg height of 200 mm gives lower velocities

for positions A and D. Again, the only reason is a three-dimensional effect, which needs to be investigated further, but it may be due to increased turbulence in the region under the furniture. This could indicate that there is a limit to the effect of the furniture leg height if the goal is to ensure as a high velocity or flow rate behind the furniture as possible.

The lowest maximum velocity at 0.25 m/s was found for the 50 mm air gap at position A with leg heights of 0 or 200. Even the lowest maximum velocity is high enough to cause draught and so the furniture does not actually significantly limit the airflow behind it. The assumed concern that furniture limits the airflow cannot be confirmed. Furthermore, the results indicate that there may be a linear correlation between the gap width behind furniture and flow rates.

Generally, the two-dimensional PIV results of the airflow in the microclimate behind furniture placed near a cold exterior wall indicate that the flow rate will increase when the distance between the wall and furniture is enhanced, and the effect is even better when the furniture is elevated from the floor by legs. However, the results indicate that the leg height should be less than 200 mm.

7. Conclusion

This paper presents an investigation of the airflow pattern in a small air gap between a chilled wall imitating an exterior wall and a piece of furniture placed next to it using PIV. The results provide empirical data for the velocities behind furniture in dwellings. These data can be useful for comparison to numerical simulation of airflow behind furniture.

The most difficult part of the measurements was to ensure a good global distribution of the tracer particles, since this has a major impact on visibility between the camera and the laser sheet. Furthermore, the focus of the camera and alignment of both laser and camera to reduce reflections has proven to be difficult, but the obtained results suggest that the actual flow field of the air gap was visualized.

The measured and analysed two-dimensional results indicate, that the flow in the air gap was not fully developed. The results were also found to be repeatable. The two investigated gap widths of 25 and 50 mm showed different patterns of velocities, but they both seem to be dominated by the boundary flow near the chilled wall. For all the tested measuring positions it was found that the flow rate is increased when the gap is expanded from 25 to 50 mm. Furthermore, there is an indication of higher flow rates if the furniture is elevated from the floor when the leg height is less than 200 mm. However, this needs further investigation.

Acknowledgements

The work was carried out with support of the Technical Research Council of Denmark. This support is gratefully appreciated. Thanks are due to M.Sc. Jeff Mertens, who helped perform the PIV measurements.

References

[1] Bornehag C-G, Blomquist G, Gynteberg F, Järvholm B, Malmberg P, Nordvall L, et al. Dampness in buildings and health. Nordic interdisciplinary review of the scientific evidence on associations between exposure to "dampness" in buildings and health effects (NORDDAMP). Indoor Air 2001;11(2):72–86.

[2] Mortensen LH, Rode C, Peuhkuri R. Investigation of microclimate by CFD modelling of moisture interactions between air and constructions. Journal of Building Physics 2007;30(4):279–313.

[3] Westergaard CH, Madsen BB, Marassi M, Tomasini EP. Accuracy of PIV signals in theory and practice. In: Fifth international symposium on particle image velocimetry, Busan, Korea, 2003.

[4] Melling A. Tracer particles and seeding for particle image velocimetry. Measurement Science and Technology 1997;8(12):1406–16.

[5] Westerweel J, Dabiri D, Gharib M. The effect of a discrete window offset on the accuracy of cross-correlation analysis of digital PIV recordings. Experiments in Fluids 1997;23(1):20–8.

[6] Scarano F, Riethmüller ML. Iterative multigrid approach in PIV image processing with discrete window offset. Experiments in Fluids 1999;26(6):513–23.

[7] Adrian RJ. Twenty years of particle image velocimetry. Experiments in Fluids 2005;39(2):159–69.

[8] Zhao L, Zhang Y, Wang X, Riskowski GL, Christianson LL. Measurement of two-dimensional air velocities in a full-scale room using particle image velocimetry. ASHRAE Transactions 2001; 107(2):434–44.

[9] Posner JD, Buchanan CR, Dunn-Rankin D. Measurement and prediction of indoor air flow in a model room. Energy and Buildings 2003;35(5):515–26.

[10] Adeyinka BO, Naterer GF. Particle image velocimetry based measurement of entropy production with free convection heat transfer. Transactions of the ASME 2005;127:614–23.

[11] Lee SJ, Lim HC, Kim HB. Improvement of ventilation flow inside a large factory building using PIV velocity field measurements. Journal of Visualization 2002;5(1):67–75.

[12] Aung W. Fully developed laminar free convection between vertical plates heated asymmetrically. International Journal of Heat and Mass Transfer 1972;15(8):1577–80.

[13] Aung W, Fletcher LS, Sernas V. Developing laminar free convection between vertical flat plates with asymmetric heating. International Journal of Heat and Mass Transfer 1972;15(11):2293–304.

[14] Habib MA, Said SAM, Ahmed SA, Asghar A. Velocity characteristics of turbulent natural convection in symmetrically and asymmetrically heated vertical channels. Experimental Thermal and Fluid Science 2002;26(1):77–87.

[15] Ayinde TF, Said SAM, Habib MA. Experimental investigation of turbulent natural convection flow in a channel. Heat and Mass Transfer 2006;42(3):169–77.

[16] ECBCS Annex Publications-Annex 14. Condensation and energy: source book, vol. 1. Belgium: KU Leuven, Laboratory for Building Physics; 1991.

Paper V

Impact of furnishing on room airflows

Mortensen, L. H., Rode, C. & Peuhkuri, R. (2008)

Published in*: Proceedings of the 8th Symposium on Building Physics in the Nordic Countries (C. Rode, editor)* Report R-189, Dept. of Civil Engineering, Technical University of Denmark, Kgs. Lyngby, Denmark, 2008, 323-330

Impact of furnishing on room airflows

L.H. Mortensen, Ph.D.,
ALECTIA A/S;
lomo@alectia.com

C. Rode, Associate Professor, Ph.D.,
Department of Civil Engineering, Technical Univeristy of Denmark;
car@byg.dtu.dk

R. Peuhkuri, Senior Research Scientist, Ph.D.,
Technical Research Centre of Finland;
ruut.peuhkuri@vtt.fi

KEYWORDS: *Boundary conditions, natural convection, PIV measurements, CFD simulation.*

SUMMARY:
In building simulation it is common to use idealized empty rooms for simulation. However, furnishing elements may cause local microclimates. These microclimates can be critical for instance if furniture is placed close to poorly insulated external walls in Nordic countries, where the external temperatures in the winter season may lead to condensation or high relative humidity on the internal side of the building envelope. Therefore it was important to investigate the influence of furniture on the airflow patterns in rooms and on the local airflow behind the furniture. The current paper presents an investigation of the airflow patterns behind a piece of furniture placed near a cold external wall. The investigation is based on a combination of Particle Image Velocimetry experiments and Computational Fluid Dynamics. The main topic of the investigation is to highlight the effect of increasing the distance between the wall and the furniture as well as between the wall and the floor. As expected the results showed that increased gap widths give increased airflow rates. Comparison of measurements and simulations indicated a good predictability for the cases, where radiation played a minor role.

1. Introduction

1.1 Background

Moisture interactions between room air and surrounding constructions and furniture have a great influence on the indoor environment. High moisture production or cold areas can cause high relative humidity, which can lead to mould growth. This is unwanted in the indoor environment due to concern for the indoor air quality. A review study of humidity in dwellings has been performed by Bornehag et al. (2001) and their advice is to avoid moist buildings. Typically, the critical areas in dwellings occur in insufficient ventilated bedrooms in microclimates behind furniture placed next to exterior walls with poor insulation, The surface temperature of the exterior wall is typically 5-8 °C colder than the room temperature in dwellings with problems. It is assumed that the furniture limits the airflow near the wall and the lack of warm room air near the surface will decrease the surface temperature even more, which can cause problems. When this is combined with a high moisture production rate from sleeping persons during night, the lower temperature in the microclimate causes increased relative humidity and the outcome can be biological growth. However, to be able to quantify the effect of such a microclimate on the indoor environment, there is a lack of knowledge about the airflow velocities behind furniture in dwellings.

Conventional building energy simulations tools can calculate temperatures in walls whereas the room air is represented by just one node. For overall energy performance this simplification is reasonable but for microclimatic investigations more details are needed. The local airflow patterns will influence the microclimate due to changes in the surface heat transfer coefficient and temperature differences. Computational fluid dynamics (CFD) solves the Navier-Stokes equations, which provides both global and local airflow patterns. Many earlier investigations of airflows in rooms have been done with CFD (Nielsen 1998; Murakami & Kato1989; Gan 1995; Teodosiu et al. 2003; Kuznik et al. 2007). The CFD technique is widely used, but the reliability of obtained quantitative information obtained from CFD remains difficult to determine. Therefore experimental validation is usually required.

Several people have used CFD numerical simulation of airflow pattern in full scale rooms and compared them to measured PIV data (Zhao et al. 2001; Sun et al. 2004, Posner et al. 2003). However, Posner used a scaled model for the PIV measurements. Also, numerous studies of airflow patterns in indoor environments have been performed, but in most cases the rooms are idealized empty rooms. Therefore, in the current investigation the room contained a piece of furniture. An earlier investigation by computational fluid dynamics (CFD) showed that different placement of furniture near colder external walls may affect the relative humidities in the microclimate (Mortensen et al., 2007a). In this study the main focus is on the airflow behind the furniture.

1.2 Paper outline

The objective of the present study is to clarify the behaviour of natural convection in microclimates between an external wall and furniture with special focus on airflow patterns and velocities. The natural convection behind furniture in dwellings was investigated by different cases of distance between the furniture and the wall in combination with different leg heights of the furniture. The investigation was performed with a commercial CFD code (Fluent, 2003) and the simulation results were compared to PIV measurements of the same cases.

The PIV measurements of the different cases provide 2D images of the airflow in a few given positions. The numerical 3D model of the room provides a clearer view on the natural convection in the entire test room. The idea was that the numerical simulation could help understand the measurements better since this would reveal 3D effects.

2. CFD model

Obstacles in rooms are known to cause turbulence and most room airflows are turbulent. Therefore, a viscous turbulence model is used. The dilemma is to choose the most appropriate turbulence model because a wide selection is available. The simplest and most widely used is the standard k-ε model, or modifications of it like the Realizable or RNG k-ε models. The presented CFD simulations were performed with the Realizable k-ε viscous model for turbulence, which have been found to predict well the airflow velocities in a room (Teodosiu et al. 2003;Kuznik et al. 2007). However, a comparison of 6 turbulence models by Sun et al. (2004) found indications that the RNG k-ε model would generally be preferred for airflow in full-scale rooms, but also their investigation showed good results with the Realizable k-ε model, and therefore it was used in the current study. The advantage of the Realizable k-ε model proposed by Shih et al. (1995) is that the model satisfies some constraints on Reynolds stresses that are consistent with physics of turbulent flows, which is neither the case for the standard k-ε model nor the RNG k-ε model. The turbulence model was used in combination with enhanced wall treatment.

The enhanced wall treatment is a near-wall modelling method that combines a two-layer model with enhanced wall functions. When the near-wall mesh is fine enough (typically y+ ~1, $y+ \equiv \rho \cdot u_T \cdot y/\mu$, ρ is density, u_T is friction velocity, y is distance to wall and μ is fluid viscosity) the laminar sublayer will be resolved by the traditional two-layer zonal model. However, the enhanced wall treatment does not require all walls to have fine meshes because a blending function combines the viscosity affected region with the outer region (Fluent 2003). Kuznik et al. (2007) found that better flow predictions are obtained when the k-ε model is combined with a two-layer near-wall treatment.

The main focus of the present investigation concerns natural convection caused by buoyancy effects in the air gap near the chilled wall. Therefore the simulations were performed using the Boussinesq approximation, which is given in Equation 1.

$$\rho = \rho_0 \left(1 - \beta \cdot \Delta T\right) \qquad (1)$$

where ρ is the actual density at a given position, ρ_0 is the operating density, β is the thermal expansion coefficient and ΔT is the temperature difference between the actual temperature and the operating temperature.

When the density changes are small, the approximation in Equation 1 is accurate enough.

3. PIV measurements

The Particle Image Velocimetry (PIV) measurements provided 2D velocity vector fields of the flow in the air gap behind the furniture.

3.1 Test Room

A test room was set-up for PIV-measurements on furniture near a colder external wall. An ordinary room with internal dimensions of 3.6 x 4.5 x 2.5 m³ was created inside a larger test facility. A chilled internal wall was built in the chamber, and a plexiglass box was positioned against that wall to imitate a cupboard placed next to an external wall in a real building. The plexiglass box was used because it provides the transparency that is needed in PIV measurements. An air gap behind the plexiglass furniture allows room air to pass over the chilled surface, and this imitates the microclimates found in ordinary dwellings, see Figure 1. The dimensions of the furniture were 1.5 x 0.46 x 2.0 m³ (width x depth x height).The set-up of the test room can be seen in Figure 2. Further details of the experimental set-up can be found in Mortensen et al. (2007b).

3.2 PIV Equipment

The two-dimensional flow field was measured by using a smoke of small oil droplets (glycol 0.1 – 1.0μm) as tracers and their motion was captured by a CCD camera (Dantec HiSense camera, 1024 x 1280 pixels). The tracer particles were illuminated by a light sheet of (about 3 mm in thickness) discharged from a water cooled double pulse Nd:YAG laser system (100 mJ/pulse).

An external processor unit triggers signals to the camera and the laser, and coordinates the transportation of data from the camera to the computer processor. Further description of the equipment and measurements can be found in Mortensen et al. (2007b).

4. Description of cases

The purpose of the investigation was to gain information about the airflow distribution patterns in small air gaps between cold exterior walls and furniture placed near it. Figure 1 shows a picture and a perspective projection of the experimental set-up, the same geometry was studied by numerical simulation.

The study involved 2 different distances between the furniture and the wall in combination with 4 different distances between the furniture and the floor. In one of these the furniture is placed directly on the floor. The surface temperature of the chilled wall behind the furniture was constantly 16°C. During the measurements the average room temperature was 22°C (giving a temperature difference of 6°C) but in the numerical simulation the air temperature was slightly smaller, 21.2°C. This lower temperature was caused by the chilled wall together with the temperatures of the other surfaces of the room that were set to 22°C. Table 1 gives the different cases and their distances between the furniture and floor or chilled wall. The absolute camera and laser positions are described in Table 2 and illustrated in Figure 2. Position F is used to compare simulations and measurements.

4.1 Simulations

The simulation model has the same geometry as the measurements.The discretization of the computational domain was accomplished with an unstructured mesh consisting of tetrahedral elements. The advantage of the unstructured mesh is that it can easily be refined in specified areas without addition of unnecessary cells in other parts. This advantage was used in the air gap between the furniture and the wall to obtain a better resolution of the obtained flow velocities. However, the unstructured mesh can cause problems near the walls and this is compensated for by use of the so-called enhanced wall treatment (Teodosiu et al., 2003).

The simulations were split in two parts; first simulations were performed with a rough grid (~400,000 cells) for the entire room to resolve the overall flow pattern, then adaptation of the grid was added in the air gap behind the furniture (>1,100,000 cells) and further iterations were performed to resolve the airflow velocities in the air gap. Even further adaptation was made in the area of the measuring positions to ensure y+~1.

The simulations focused only on the airflow in the room so energy and viscous airflow models were used. In the material database, the air properties were set as dry air at 22°C and a boussinesq density. The cold wall was set to 16°C and the other walls 22°C except the gypsum board wall that extends the chilled wall to reach the side wall (behind the camera in Figure 2). This wall was assumed adiabatic. The measuring positions A-G of the PIV equipment are given in Table 2. Here only results from position F will be compared for different furniture position cases (see Table 1).

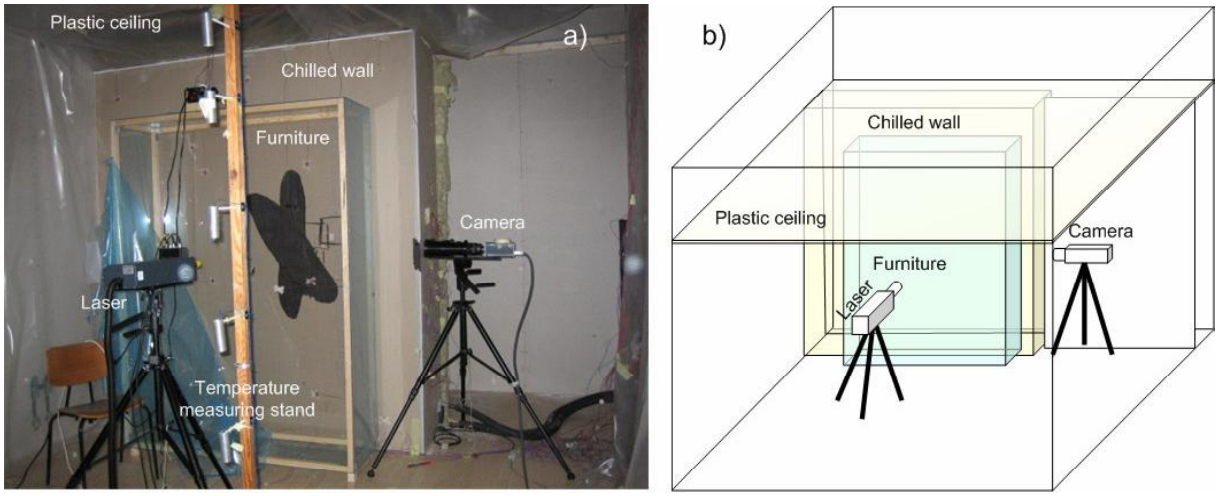

FIG. 1: The experimental set-up, where the camera points into the air gap between the chilled wall and the furniture and the laser sheet is pointed in through the plexiglass furniture. a) A picture of the experimental set-up. b) A diagram of the PIV set-up.

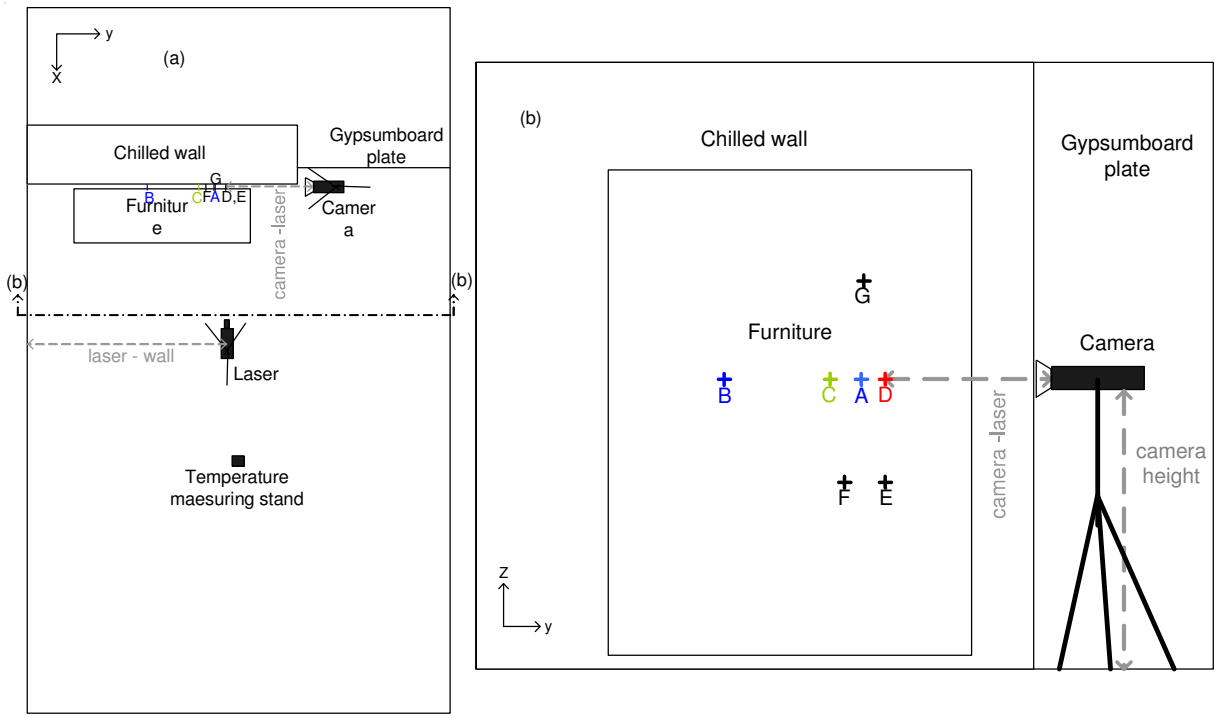

FIG. 2: Part (a) show a plane of the measured PIV set-up and (b) show a front view of the room. The letters A-F show the measuring positions given in table 2.

TABLE 1: The different tested positions of the furniture.

Furniture position	Gap (mm) furniture - floor	Gap (mm) furniture - chilled wall
1	0	25
2	0	50
3	50	25
4	50	50
5	100	25
6	100	50
7	200	25
8	200	50

TABLE 2: Description of PIV measuring positions. The physical image size changes with distance between camera and laser. Only image widths of maximum 50mm is used; the rest is masked out.

Posi-tion	Distance (mm) camera - laser	Image height (mm)	Camera height (mm)	Laser height (mm)	Distance (mm) laser – wall	Measured furniture position
A	1050	124	1183	1192	1570	1-8
B	1420	187	1183	1192	1000	3-4
C	1200	136	1183	1192	1440	3-6
D	920	106	1183	1192	1670	1-8
E	930	113	770	760	1670	3-4
F	1080	130	770	760	1500	1-8
G	970	119	1595	1570	1580	4

5. Results

Only the vertical velocities in the vertical air gap will be shown and discussed, since the horizontal velocities are very small. The horizontal velocities (x-direction in Fig. 2) are in the order of magnitude of 2 % of the vertical velocities in the air gap between the furniture and the chilled wall. The velocity field is set to be positive upwards (z-direction in Fig. 2). In the current paper, PIV measurements results will be presented in form of comparison to numerical simulations.

5.1 Simulation Results for the Entire Room

Figure 3 illustrate the airflow pattern of the room. The highest airflow velocities are seen in the air gap behind the furniture and the velocities behind the furniture increases all the way to the bottom of the air gap.

5.2 Comparison of measurements with CFD

In Figure 4 a comparison is shown between the PIV-measurements and the numerical simulation of the airflow in a gap between the chilled wall and the furniture. The average velocity is calculated and shown in the legend. The figure shows that the shape of the velocity profile is the same for the cases with different distance to the floor but at different velocity levels. However, the shape of the velocity profile changes when the gap is increased from 25 mm to 50 mm. The comparison of the simulation results and the measured data shows that the general shape of the velocity profiles is fairly well predicted by the simulation. The simulated velocities are about half of the measured values for the 25 mm air gap. Opposite to this, the velocity levels are predicted quite well for the cases with a 50 mm air gap, except for the case where the furniture is placed on the floor. The calculated average velocities confirm that the simulation underestimates the velocities. The model predicts the velocities for the 50 mm air gap very accurately but there are some minor differences. For instance, the maximum velocity is underestimated since the measurements found the maximum velocities near the chilled wall at x ~ 40 mm, whereas the simulation have maximum at x~35 mm.

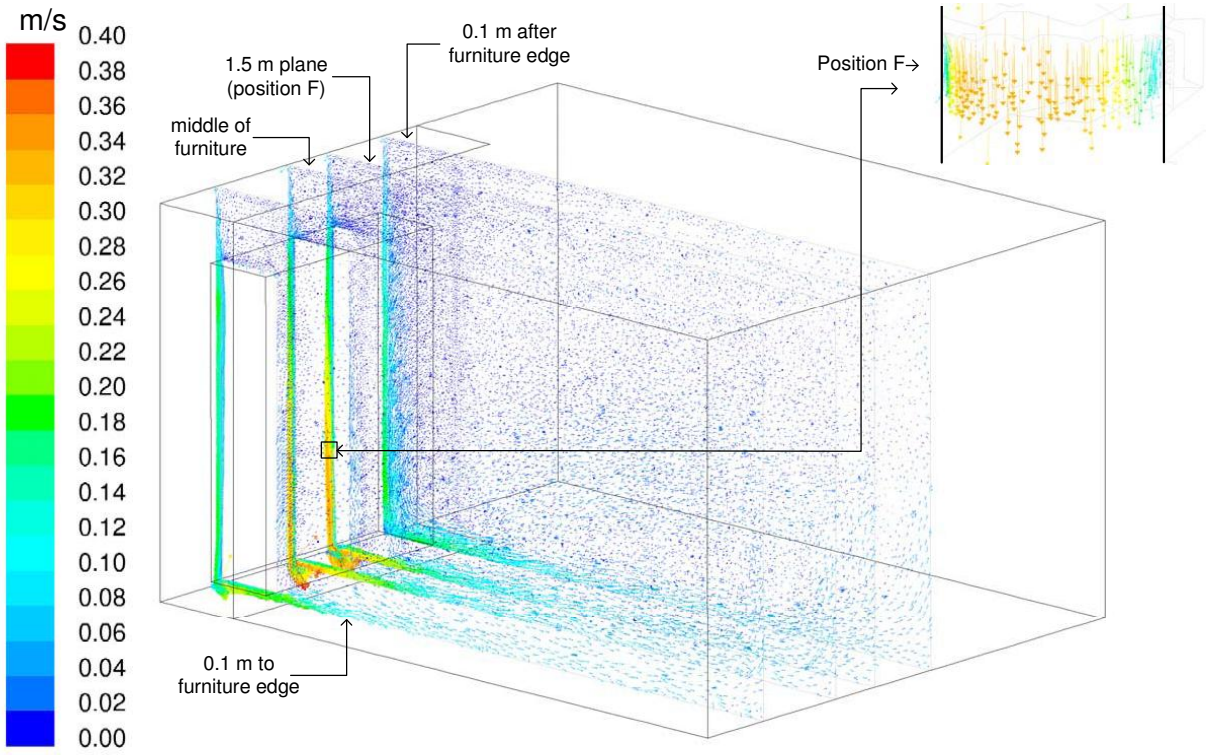

FIG. 3: Airflow patterns are presented as vectors in 3 planes.

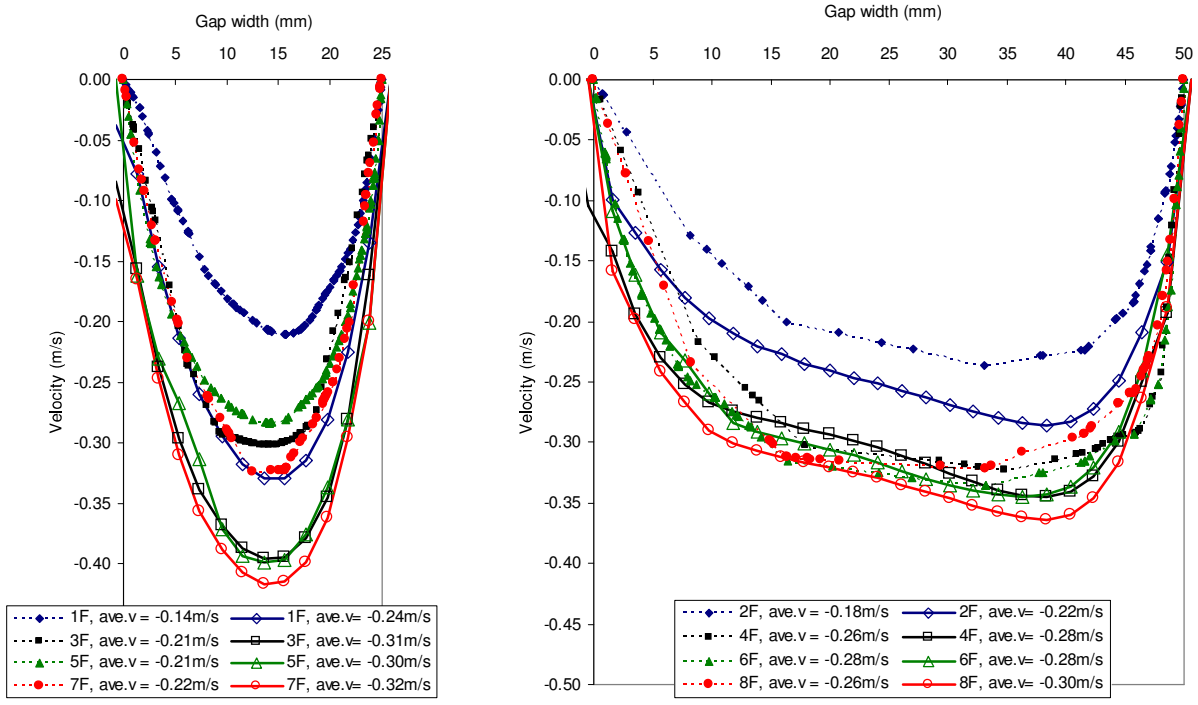

FIG. 4: Comparison of measured (solid) and simulated (dashed) results for position F for a gap width of 25mm and 50mm, furniture surface at x = 0 mm. In the legend the calculated average velocity is given.

6. Discussion

The objective of the current study was to investigate the natural convection between furniture and an exterior wall. The measured data have been compared to simulated data for a similar geometrical setup. The highest air-flow velocities in the room are found in the air gap behind the furniture as seen in Figure 3. Two gap widths of 25 and 50 mm have been investigated. The highest measured and simulated velocities were found closest to the chilled wall, see Figure 4. This confirms that density changes dominate the flow by air-cooling in the gap. Both simulations and measurements also confirm that elevation of the furniture will increase the flow behind the furniture. Whether the effect will be enough to avoid problems with condensation or humidity levels suitable for mould growth has not been investigated in this study.

In Figure 3 it is clearly seen that the velocities are highest at the bottom of the airgap, which is a 3D effect as air must have entered from the sides of the furniture. This effect was actually confirmed by the PIV measurements in the other measuring positions as shown in Mortensen et al. (2007b).

In Figure 4 it is seen that the predicted shape of the velocity profiles seem similar to the measured. Especially the simulation results for the 50 mm air gap match the measured data very well. This clearly indicates that CFD simulations can be used to predict airflow velocities in microclimates. However, the model underestimates the velocities in the narrower 25 mm air gap. The profile is predicted well but the velocity level is only about half the measured value. This may be explained by influence of radiation between the surfaces of the wall and furniture, which was not included in these simulations. The velocity of the airflow in the gap is very temperature dependent as the denser cold air will fall towards the floor. This can explain why the narrow gap is highly underestimated as radiation between the surfaces of the chilled wall and the furniture surface may be more pronounced for the 25 mm gap than for the wider 50 mm gap where the distance between the surfaces are twice as wide. For the 50 mm air gap a preliminary test with radiation showed that it had little influence on the results, and since the radiation model cannot be used in Fluent in combination with mesh adaptations, no radiation model was used in the simulations. This implies that for narrow air gaps, initial simulations must be performed in order to investigate what is the influence of radiation, and only if the influence is neglible, the unstructured mesh combined with adaptations can be used to zoom in on a small microclimate.

The good results of the comparison between the simulated and measured data suggest that CFD simulation can be used to accurately calculate the surface heat transfer coefficient which again can be used to predict the water vapour surface resistance. Therefore, this implies that the CFD simulation can be a useful tool for investigation of hygrothermal microclimates in dwellings. However, one should be cautious when radiation plays an import role in the heat transfer in the microclimate, because this might influence the simulated airflow velocities.

This investigation has shown that further analysis should be made where the CFD simulations include radiation in order to see what effect it will have on the prediceted airflow velocities in the air gap.

The starting point for this investigation was the moisture interactions in rooms and particularly the relative humidity in microclimates. However, it is not expected that the airflow velocities in the gap behind the furniture will be affected by moisture in the air as the moisture driven convection potential is much smaller than the buoyancy driven convection. Even though the airflow velocity is properly not influenced by moisture in the air there may still be RH variations behind the furniture compared to the general average in the room as shown in Mortensen et al. (2007a). The narrow air gap has higher airflow velocities but the total volume flow rate is smaller than for the wider 50 mm gap, so less moisture can be transported away from the air gap and a lower airtemperature generally gives higher RH, which may be critical.

7. Conclusion

An investigation was performed using PIV and CFD of the airflow pattern in a small air gap between a chilled wall imitating an exterior wall and a piece of furniture placed next to it. The two investigated gap widths of 25 and 50 mm showed different patterns of velocities but they both seem to be dominated by the boundary flow near the chilled wall, since the maximum velocity was found closest to this wall. The study also confirms that the airflow behind the furniture will increase if the furniture is elevated from the floor.

For a 50 mm air gap the simulated and measured results were rather uniform, which indicates that CFD models can be used to predict airflow velocities in local microclimates. However, the differences between the measurements and the simulations of the narrow 25 mm gap cannot be fully accounted for.

8. Acknowledgements

This work was supported by the Technical Research Council of Denmark. The support is gratefully appreciated.

9. References

Bornehag C.-G., Blomquist G., Gynteberg F., Järvholm B., Malmberg P., Nordvall L., Nielsen A., Pershagen G., Sundell J. (2001). Dampness in buildings and health. Nordic Interdisciplinary Review of the Scientific Evidence on Associations between Exposure to "Dampness" in Buildings and Health Effects (NORDDAMP), *Indoor Air*, Vol. 11, No. 2, 72–86.

Fluent (2003). FLUENT® User's Guide, Lebanon, NH, USA: Fluent Inc.

Gan G. (1995). Evaluation of room air distribution systems using computational fluid dynamics, *Energy and Buildings,* Vol. 23, No. 2, 83-93.

Kuznik F., Rusaouën G., Brau J. (2007). Experimental and numerical study of a full scale ventilated enclosure: Comparison of four two equations closure turbulence models, *Building and Environment*, Vol. 42, No. 3, 1043–1053.

Mortensen L.H., Woloszyn M., Rode C., Peuhkuri P. (2007a). Investigation of microclimate by CFD modelling of moisture interactions between air and constructions, *J. of Building Physics*, Vol. 30, No. 4, 279-315.

Mortensen L.H., Rode C., Peuhkuri R.(2007b). Microclimate investigation of airflow patterns by Particle Image Velocimetry (PIV), Accepted for publication in *Building and Environment*, doi: 10.1016/j.buildenv.2007.11.012

Murakami S., Kato S. (1989). Numerical and experimental study on room airflow-3-D predictions using the k-ε turbulence model, *Building and Environment,* Vol. 24, No. 1, 85-97.

Nielsen P.V. (1998). The Selection of Turbulence Models for Prediction of Room Airflow, *Ashrae Transactions,* Vol. 104, No. 1B, 1119-1127.

Posner J.D., Buchanan C.R., Dunn-Rankin D. (2003). Measurement and prediction of indoor air flow in a model room, *Energy and Buildings,* Vol. 35, No. 5, 515-526.

Shih T.-H., Liou W.W., Shabbir A., Yang Z., Zhu J. (1995). A new k-ε eddy viscosity model for high Reynolds mumber turbulent flows. *Computers & Fluids*, Vol. 24, No. 3, 227-238.

Sun Y., Tan Z., Zhang Y., Zhao L. (2004). Comparison of six CFD models for room airflow study with PIV measurement data, *ASAE Annual International Meeting*, 5239-5259.

Teodosiu C., Hohota R., Rusaouën G., Woloszyn M. (2003). Numerical prediction of indoor air humidity and its effect on the indoor environment, *Building and Environment,* Vol. 38, No. 5, 655-664.

Zhao L., Zhang Y., Wang X., Riskowski G.L., Christianson L.L. (2001). Measurement of two-dimensional air velocities in a full-scale room using particle image velocimetry, *Ashrae Trans.,* Vol. 107, No. 2, 434-444.